Functional networks in Parkinson's Disease

Ashwani Jha

UCL

Sobell Department of Movement Neuroscience

UCL Institute of Neurology

Submitted for the degree of Doctor of Philosophy in the fields of Neurology and Neuroscience

i) Declaration

I, Ashwani Jha, confirm that the work presented in this thesis is my own. Where information has been derived from other sources, I confirm that this has been indicated in the thesis.

Signed:……..

Date:……..…….

ii) Abstract

Parkinson's Disease (PD) is a common neurodegenerative condition characterised pathologically by progressive dopaminergic cell loss in the substantia nigra pars compacta, dopamine depletion and resulting cortico- basal ganglia circuit dysfunction. There is a considerable variation in symptoms and treatment response *between* patients and therefore a need to individualise treatments, such as dopamine replacement therapy, and deep brain stimulation (DBS). We therefore require a better understanding of how different motor and non-motor symptoms emerge from the cortico-basal ganglia dysfunction characteristic of PD. In this thesis, I investigated the hypothesis that distinct symptoms in PD may be due to the dysfunction of distinct cortico-basal ganglia circuits.

I characterised cortico-basal ganglia coupling by simultaneously recording cortical activity with magnetoencephalography (MEG) and basal ganglia activity from intracranial electrodes placed during DBS surgery for PD. Coupling was measured in terms of coherence – a frequency specific measure of coupling.

I found that resting cortico-basal ganglia networks had distinct cortical topographies at different frequencies. Frontal regions coupled to both the subthalamic nucleus (STN) and the pedunculopontine nucleus region (PPNR) in the beta frequency band whilst temporal, parietal and cerebellar areas coupled in the alpha range. I hypothesised that activity in the frontal beta network may relate to executive function, and found that local synchronisation in two frontal cortical hubs was related to stopping an on-going movement – a crucial executive function. In a related experiment in PD patients, transient frontal – basal ganglia coupling was again apparent during motor inhibition, but how this is related to behavioural performance needs further investigation.

These results are useful in highlighting how cortico-basal ganglia networks can be separated both spatially and spectrally and how the function and dysfunction of these networks can be interrogated in PD patients. Future work should determine how different stimulation parameters differentially affect these distinct circuits.

iii) Contents

i) Declaration 2
ii) Abstract 3
iii) Contents 4
iv) List of Tables 12
v) List of Equations 12
vi) List of Figures 12
vii) Publications related to the thesis 15
viii) Acknowledgements 16
ix) Abbreviations used in the text 17

1. Introduction 21
1.1 Scope 21
1.2 Clinical aspects of Parkinson's Disease 22
1.2.1 Diagnostic Criteria 22
1.2.2 Epidemiology 23
1.2.3 Genetic and environmental risk factors 25
1.2.4 Pathology 27
1.2.5 Motor Symptoms 28
1.2.6 Non-Motor Symptoms 29
1.2.7 Medical Treatments and side effects 30
1.2.8 Deep Brain Stimulation 31
1.3 The pathophysiological basis of Parkinsonian symptoms: function and dysfunction of the cortico-basal ganglia network 35
1.3.1 The firing rate model of cortico-basal ganglia connectivity 35
1.3.1.1 Parallel, partially segregated, partially closed circuits 35
1.3.1.2 The striatum and the origin of the direct and indirect pathways 38
1.3.1.3 The rate model explains movement and movement disorders 38

1.3.2 Revisions to and limitations of the rate model 39
1.3.2.1 The topography and organisation of cortical connections to the basal ganglia 39
1.3.2.2 The subthalamic nucleus and the hyperdirect pathway 40
1.3.2.3 Complex connectivity between the striatum, GPe and GPi/SNr 42
1.3.2.4 The pedunculopontine nucleus 43
1.3.3 Developing concepts of basal ganglia function 44
1.3.4 The pattern model of movement disorders 46
1.3.4.1 Limitations of the rate model and emergence of the pattern model 46
1.3.4.2 Beta oscillations and their relation to movement, dopamine and DBS 47
1.3.4.3 Theta-alpha oscillations and their relation to dystonia and dyskinesias 48
1.3.5 Characterising cortico- basal ganglia circuit activity in humans with PD 49
1.3.5.2 Functionally distinct circuits are spatially segregated 49
1.3.5.3 Cortico - basal ganglia circuits are frequency specific and dopamine sensitive 50
1.4 Quantifying cognitive functions: a psychological perspective 53
1.4.1 Response interference and inhibition 53
1.4.1.1 The stop –signal paradigm 54
1.4.1.2 The horse-race model 56
1.4.1.4 Different methods to estimate SSRT 57
1.4.2 Factors modulating the stop-signal reaction time 59
1.4.2.1 The effect of stimulus characteristics 59
1.4.2.2 The effect of response characteristics 60
1.4.2.3 The effect of subject characteristics 61
1.4.3 Modifications to the stop-signal task 62
1.4.3.1 The stop-change task 62
1.4.3.2 The LATER model 64
1.4.4 Strategic adjustments in reaction time 64
1.5 The neural correlates of response inhibition 66
1.5.1 Lesion studies 66

1.5.2 Single-cell activity 67
1.5.3 Human neurophysiology 68
1.5.4 Pathophysiology in Parkinson's Disease 71
1.6 Summary and thesis objectives 73

2. Methods 75
2.1 Subjects and Operative Procedure 75
2.1.1 Subject baseline clinical and psychological data 75
2.1.2 Surgical procedure 76
2.2 Electrophysiological Data Acquisition 77
2.2.1 Magnetoencephalography 77
2.2.2 Intracranial electrode recordings 79
2.3 Pre-processing 79
2.3.1 Sampling rate 79
2.3.1 Filtering 80
2.3.2 Artefact rejection 80
2.3.3 Frequency transformation 81
2.4 Connectivity Metrics 82
2.4.1 Coherence 82
2.4.2 Granger causality 83
2.5 Source localisation 84
2.5.1 The basis of the electromagnetic signal recorded by EEG and MEG 84
2.5.2 The inverse problem and its solutions 85
2.5.3 Beamformers 85
2.6 Statistical analysis 86
2.6.1 General Linear Model as applied to images 86
2.6.2 Event-related convolution analysis 87
2.7 Summary of Limitations 88
2.7.1 Phenotypic variation and lesion effects 88

2.7.2 Variation in surgical practice and MEG systems 88
2.7.3 Artefacts in the MEG signal 89

3: Resting cortico-subthalamic nucleus connectivity in Parkinson's Disease 90
3.1 Introduction 90
3.2 Methods 91
3.2.1 Participants and surgery 91
3.2.2 Simultaneous STN-LFP and MEG recordings 94
3.2.3 Data pre-processing and beamformer approach to localisation of coherent sources 94
3.2.4 Characterisation of coherent sources within a single patient 95
3.2.5 Characterisation of effect of dopaminergic medication and frequency on coherence topography across patients 97
3.3 Results 99
3.3.1 Clinical features 99
3.3.2 Contact location 99
3.3.3 Individual patients display spectrally and spatially restricted sensor-level patterns of cortico-subthalamic coherence 100
3.3.4 Spatial location of cortical sources coherent with STN is consistent across patients 102
3.3.5 Topography of cortical activity coherent with STN activity is frequency dependent across patients 107
3.3.6 Dopaminergic medication has an effect on topography of cortico-subthalamic coherence in the beta frequency band 110
3.3.7 Relationship between cortical activity, STN activity and coherence 113
3.3.8 Effective direction of cortico-subthalamic connectivity 113
3.3.9 Correlation between effect of dopaminergic medication on source activity and clinical variables 116
3.4 Discussion 116
3.4.1 Supremacy of the cortical drive to the STN area 117
3.4.2 Frequency of subthalamo-cortical coherence 118

3.4.3 Is subthalamo-cortical coherence at rest due to default brain networks? 118

4: Resting cortico-pedunculopontine nucleus region connectivity in Parkinson's Disease . 121

4.1 Introduction 121

4.2 Methods 122

4.2.1 Participants and surgery 122

4.2.2 Simultaneous PPNR-LFP and MEG recordings 127

4.2.3 Data pre-processing, artefact rejection, and head localisation 127

4.2.4 The beamformer approach to coherent source localisation 128

4.2.5 Characterisation of effects of dopaminergic medication, frequency and electrode height on coherence topography across patients 129

4.2.6 Directionality 130

4.3 Results 131

4.3.1 Intracranial electrode recordings correspond to activity of the PPN and neighbouring regions. 131

4.3.3 Networks involving the PPNR are frequency specific 132

4.3.4 Networks involving the PPNR are modulated by dopamine in a frequency-specific manner 135

4.3.5 Coherence is topographically modulated within the PPNR in a frequency and dopamine dependent manner 138

4.3.6 Variation in the effective direction of coupling with height of electrode 141

4.3.7 Assessment of the impact of ferromagnetic electrode artefact and the use of different MEG systems on sensor and source level coherence. 143

4.4 Discussion 145

5. Functional roles of the pre-SMA and right IFG during stopping in healthy controls 150

5.1 Introduction 150

5.2 Methods 152

5.2.1 Subjects and paradigm 152

5.2.2 Behavioural analysis 154

5.2.3 Magnetoencephalographic data acquisition and pre-processing 158
5.2.4 The convolution model for magnetoencephalographic data..... 159
5.2.5 Analysis of time-frequency images..... 161
5.3 Results 161
5.3.1 Subject task performance..... 161
5.3.2 Primary task reaction time depends on task complexity and the previous trial... 165
5.3.3 Complexity affects the slope of the inhibition function but not the stop-signal reaction time 168
5.3.4 Beamforming adequately separates cortical sources involved in the stop/change process 170
5.3.5 The convolution model extracts time-frequency data typical of basic responses 172
5.3.6 Stop/change signals are associated with a rapid, global theta/alpha synchonisation 172
5.3.7 Stop signals are followed by changes in beta activity in frontal structures 175
5.3.8 Task complexity modulates go signal related activity. 179
5.4 Discussion: 180
5.4.1 Pre-SMA gamma and modulation of context 180
5.4.2 Global theta/alpha responses in a spatially diffuse ‘stopping network’ 181
5.4.3 Right IFG theta/alpha corresponds to stopping efficiency..... 182
5.4.4 Beta changes selective to stopping only..... 183
5.5 Conclusion 183

6. Dynamic cortico-basal ganglia connectivity during response inhibition in PD 185
6.1 Introduction..... 185
6.2 Methods 186
6.2.1 Participants and surgery..... 186
6.2.2 Experimental Paradigm 189
6.2.3 Behavioural analysis 190
6.2.4 Simultaneous STN-LFP and MEG recordings 192
6.2.5 Data pre-processing, artefact rejection, and head localisation..... 192

6.2.6 Beamformer source extraction 193
6.2.7 Time-frequency analysis and epoching 193
6.2.8 The convolution model for magnetoencephalographic data 194
6.3 Results 196
6.3.1 Subject behavioural data 196
6.3.2 Beamforming adequately separates cortical sources involved in the change process 203
6.3.3 Epoched data shows that event-related oscillatory responses can be visualised individually in the majority of subjects 205
6.3.4 Group level theta and beta dynamics in the contralateral STN during a change signal 211
6.3.5 Coherence between the motor cortex and STN cannot be seen consistently in individual subjects. 213
6.3.6 Group level network coherence dynamics during the change task 213
6.4 Discussion 217
6.4.1 Signal Fidelity 218
6.4.2 Amplitude responses of cortical and subthalamic regions during the change-of-plan task 218
6.4.3 Dynamic coherence responses during the change-of-plan task 219
6.4.4 Conclusions and further directions 220

7. Discussion 222
7.1 Simultaneous MEG and basal ganglia LFP recording – a new model for studying cortico-basal ganglia oscillations 222
7.1.1 Limitations 223
7.2 Cortico-basal ganglia networks at rest 224
7.2.1 The cortico-basal ganglia alpha network 224
7.2.1.1 Potential functions of the alpha network 224
7.2.1.2 Clinical correlation with alpha activity 225
7.2.2 The cortico-basal ganglia beta network 227

7.2.2.1 Are beta networks pathological? 228
7.2.2.2 Is there more than one beta network? 229
7.2.3 Directionality within the resting networks 229
7.2.3.1 The STN 229
7.2.3.2 The PPNR 230
7.3 Dynamic cortico-basal ganglia activity during executive function 230
7.3.1 Theta activity and the cortical response to a stop-signal 231
7.3.2 Pre-SMA gamma activity and the modulation of context 232
7.3.3 Beta changes selective to stopping only 233
7.3.4 Cortico-subcortical interactions during stopping – a 'proof-of-principle' 233
7.4 Summary 234

8. References 236

iv) List of Tables

Table 1: UK Parkinson's Disease Society Brain Bank clinical diagnostic criteria. 24
Table 2: Summary of current practice for STN Vs GPi DBS. 34
Table 3: Clinical features of patient cohort. 93
Table 4: Clinical details of the study participants 124
Table 5: Brain regions where a significant condition effect or an interaction between condition effects was detected. 134
Table 6: Trial numbers and reaction time data for each subject and condition. 156
Table 7: Clinical details of the study participants 189
Table 8: Descriptive statistics of change-of-plan task in patients. 199

v) List of Equations

Equation 1: Mathematical Formalisation of the horse-race model. 58
Equation 2: Continuous Fourier Transform. 81
Equation 3: Coherence. 83
Equation 4: The beamforming spatial filter. 86
Equation 5: The General Linear Model. 87

vi) List of Figures

Figure 1: Simplified diagram of the basal ganglia circuit.. 37
Figure 2: Distribution of afferents into the STN. 41
Figure 3: The inhibition function. 55
Figure 4: The horse-race model. 58
Figure 5: Spiking neurons in the pre-supplementary motor area (pre-SMA) of a rhesus monkey during switching. 68
Figure 6: Brain networks activated during the stop-signal task. 69
Figure 7: The CTF MEG system in London.. 78
Figure 8: Example analysis representing beta frequency coherence referenced to a bipolar left STN DBSE channel in one patient. 101
Figure 9: Topographical maps of coherence. 103
Figure 10: Frequency distribution of potential cortical sources. 104
Figure 11: The variation in location and peak frequency of significant cortical sources coherent in the 5-45 Hz frequency range. 105

Figure 12: Independence of peak alpha and beta coherence within individual hemispheres. 106
Figure 13: Mean of the normalised DICS images. 108
Figure 14: SPMs showing differences in the relative topography of alpha and beta band coherence between cortex and subthalamic region. 109
Figure 15: SPMs testing for the effect of dopaminergic medication on coherence. 111
Figure 16: Simple effect of dopaminergic medication on beta frequency coherence was not due to local changes in cortical power. 112
Figure 17: Relationship between cortical activity and cortico-subthalamic coherence. 114
Figure 18: Effective direction of coupling between cortex and subthalamic region.. 115
Figure 19: Variation in theeffective direction of coupling between cortex and subthalamic region according to cortical location.. 115
Figure 20: Localisation of contact locations within the brainstem, represented in Montreal Neurological Institute (MNI) space (sagittal view). 126
Figure 21: Mean beamformer images of coherence with PPNR activity. 133
Figure 22: SPMs testing for the main effect of frequency on coherence with the pedunculopontine region.. 135
Figure 23: SPMs testing for an interaction between the effects of dopamine and frequency on coherence with the pedunculopontine region. 136
Figure 24: SPMs testing for an interaction between the effect of height (of electrode relative to PM line) and other effects of interest. 137
Figure 25: Mean unnormalised coherence between the PPNR and significant peak voxels from the SPM analysis, plotted as a function of electrode height (mm). 139
Figure 26: Individual subject mean log source power and source-PPNR coherence data. 140
Figure 27: The effective direction of coupling. 142
Figure 28: Sensor level analysis. 144
Figure 29: Paradigm details. 153
Figure 30: Behavioural data examples.. 162
Figure 31: Inhibition functions for each subject and condition. 164
Figure 32: GO reaction time and trial history. 167
Figure 33: Post stop/change trial go only reaction times adjusted for the previous go only reaction time. 168
Figure 34: Effects of stimuli type (< or |) and response (stop or change) on the slope of the inhibition function. 169
Figure 35: Regions of interest. 171
Figure 36: Estimated event-related activity from the convolution models of cortical activity. 173

Figure 37: Time-frequency SPMs triggered to the stop/change signal. 174
Figure 38: Timing of significant theta/alpha and beta RMS amplitude changes induced by the stop/change event. 176
Figure 39: Peak rate of theta/alpha rise in different cortical locations. 177
Figure 40: Time-frequency SPMs and beta RMS amplitude plots showing the interaction between the success and response in the pre-SMA and the right IFG. 178
Figure 41: Time-frequency SPMs and RMS amplitude plots showing the effect of complexity on the induced response to the Go signal in the pre-SMA. 179
Figure 42: Inhibition functions for each subject and condition. 201
Figure 43: Regions of interest in the OFF medication condition. 204
Figure 44: Regions of interest in the ON medication condition. 205
Figure 45: Individual time-frequency images of left M1 activity during a right go signal. 206
Figure 46: Individual time-frequency images of left M1 activity during a right button press. 207
Figure 47: Individual time-frequency images of left STN activity during a right go signal. . . 209
Figure 48: Individual time-frequency images of left STN activity during a right button press. 210
Figure 49: Experimental effects on the induced response to the change signal in STN and M1. 212
Figure 50: Coherence between the left M1 and left STN during a right button press. 214
Figure 51: Average group-level coherence between the left M1 and left STN during the change task. 215
Figure 52: Average group-level coherence between the pre-SMA and left STN during the change task. 216
Figure 53: Average group-level coherence between the right IFG and pre-SMA during the change task. 217

vii) Publications related to the thesis

Litvak V, Jha A, Flandin G, Friston K (2012) Convolution models for induced electromagnetic responses. Neuroimage 64C:388-398.

Litvak V, Eusebio A, Jha A, Oostenveld R, Barnes G, Foltynie T, Limousin P, Zrinzo L, Hariz MI, Friston K, Brown P (2012) Movement-related changes in local and long-range synchronization in Parkinson's disease revealed by simultaneous magnetoencephalography and intracranial recordings. J Neurosci 32:10541-53.

Litvak V*, Jha A*, Eusebio A, Oostenveld R, Foltynie T, Limousin P, Zrinzo L, Hariz M, Friston K, Brown P(2011) Resting oscillatory cortico-subthalamic connectivity in patients with Parkinson's disease. Brain 134:1578-88.

Litvak V, Eusebio A, Jha A, Oostenveld R, Barnes GR, Penny WD, Zrinzo L, Hariz MI, Limousin P, Friston KJ, Brown P(2010) Optimized beamforming for simultaneous MEG and intracranial local field potential recordings in deep brain stimulation patients. Neuroimage 50:1578-88.

Thevathasan W, Mazzone P, Jha A, Djamshidian A, Dileone M, Di Lazzaro V, Brown P (2010) Spinal Cord stimulation failed to relieve akinesia or restore locomotion in Parkinson Disease. Neurology 20: 1325-7

Jha A, Brown P (2010). Paradoxes in Parkinson’s Disease and other Movement Disorders. In Kapur N, Pascual-Leone A, Ramachandran VS, editors. The Paradoxical Brain. Cambridge University Press.

*Both authors contributed equally to this work

viii) Acknowledgements

I am immensely grateful to both my supervisors Professor Peter Brown and Vladimir Litvak. It was thanks to Peter's work that I first became interested in basal ganglia electrophysiology. Because of his crucial input we secured funding in the form of a fellowship from Parkinson's UK, allowing me to study this area further. Always approachable, involved and with the keenest understanding of the data, I could not have asked for a wiser or more patient guide. If I have developed any skill with magnetoencephalographic data analysis, it is entirely thanks to Vladimir's expert tutelage, and to his robust approach to programming. Always supportive, and always with an answer to my questions, I have been exceptionally fortunate to work directly with the originator of much of the software used for this thesis.

I am also indebted to Professor Masud Husain for guiding the cognitive aspects of this thesis, and also to Parashkev Nachev who not only clarified my understanding of the stop-signal paradigm, but also introduced me to the potential philosophical pitfalls of cognitive neuroscience.

This thesis could not have been completed without a lot of support from the functional neurosurgical teams that I worked with. In London I am grateful to Tom Foltynie, Patricia Limousin, Ludvic Zrinzo, Marwan Hariz and Joseph Candelario – not only for their support with patients but for their experimental ideas and their help in providing clinical data and anatomical electrode locations. In Oxford I am grateful to Jonathan Hyam, Alexander Green, Tipu Aziz and especially Wesley Thevathasan for clinical support, especially with chapter 4.

I am grateful to many colleagues for practical help including David Bradbury and Sven Braeutigam who helped run the MEG experiments, Al Reid and Spencer Neil for their engineering advice, and Atbin Djamshidian, Alex Pogosyan, Huiling Tan and Louise Gaynor for their time in the lab. I am also grateful to the people at Parkinson's UK for their continued support and funding.

I would also like to register a debt of thanks to Gareth Barnes for imparting his enthusiasm for magnetoencephalography, Professor Andrew Lees for teaching me what I know about Parkinson's and to Professor Karl Friston who helped me to understand experimental design and statistics.

Finally I am grateful to my brother Alok, and my mum and dad for their continued support and guidance.

ix) Abbreviations used in the text

AAL	Automated Anatomical Labelling
AC	Alternating Current
ACC	Anterior cingulate cortex
ANOVA	Analysis of Variance
ANCOVA	Analysis of Covariance
CMA	Cingulate motor area
CT	Computed Tomography
CTC	Communication-through-coherence
DBS	Deep Brain Stimulation
DC	Direct Current
DDS	Dopamine Dysregulation Syndrome
DICS	Dynamic Imaging of Coherent Sources
DTF	Directed Transfer Function
DTI	Diffusion tensor imaging
ECD	Equivalent Current Dipole
EEG	Electroencephalography
EMG	Electromyogram
EOG	Electro-oculogram
EPSP	Excitatory Post-Synaptic Potentials
ERD	Event-related Desynchronisation
ERF	Event-related Field
ERP	Event-related Potential
ERS	Event-related Synchronisation

FDI	First Dorsal Interosseus
FOGQ	Freezing of Gait Questionnaire
FT	Fourier Transformation
GABA	Gamma-aminobutyric Acid
GAD	Glutamic Acid Decarboxylase
GBA	Glucocerebrosidase mutations
GCI	Glial Cytoplasmic Inclusion
GFQ	Gait and Falls Questionnaire
GLM	General Linear Model
GPe	Globus Pallidus externa
GPi	Globus Pallidus interna
fMRI	Functional Magnetic Resonance Imaging
ICD	Impulse Control Disorder
IFG	Inferior frontal gyrus
IPL	Inferior Parietal Lobule
IPSP	Inhibitory Post-Synaptic Potentials
LATER	Linear Rise to Threshold
LCMV	Linearly Constrained Minimum Variance
LFP	Local Field Potential
LRRK2	Leucine Rich Repeat Kinase 2
M1	Primary motor cortex
MEG	Magnetoencephalography
MPTP	1-methyl-4-phenyl-1,2,5,6-tetrahydropyridine
MRI	Magnetic Resonance Imaging

MSA	Multiple Systems Atrophy
MCMC	Markov Chain Monte Carlo
MNI	Montreal Neurological Institute
MSN	Medium Spiny Neurons
MTG	Medial Temporal Gyrus
PD	Parkinson's Disease
PDC	Partial Directed Coherence
PET	Positron Emission Tomography
PFC	Prefrontal Cortex
PM	Pontomesencephalic line
PPNR	Pedunculopontine Nucleus Region
Pre-SMA	Pre-supplementary Motor Area
PRP	Psychological Refractory Period
PSP	Progressive Supranuclear Palsy
PUT	Putamen
REM	Rapid Eye Movement
RMS	Root Mean Squared
RSN	Resting State Network
RT	Reaction Time
SQUID	Superconducting Quantum Interference Device
SMA	Supplementary Motor Area
SNP	Single Nucleotide Polymorphism
SNc	Substantia Nigra pars compacta
SNr	Substantia Nigra pars reticulata

SOA	Stimulus Onset Asynchrony
SPM	Statistical Parametric Mapping
SSD	Stop Signal Delay
SSRT	Stop-signal reaction time
STG	Superior Temporal Gyrus
STN	Subthalamic Nucleus
TAN	Tonically Active neuron
TMS	Trans-cranial Magnetic Stimulation
UPDRS	Unified Parkinson's Disease Rating Scale
VTA	Ventral tegmental area

1. Introduction

1.1 Scope

This thesis concerns the identification and functional interrogation of distributed neural activity in Parkinson's Disease (PD). In practice, such functional research has traditionally been hindered by several obstacles which may be useful to highlight at the start.

Firstly, only humans get PD and accessing neural activity *in vivo* is difficult. An 'ideal' experiment would involve the use of invasive neurophysiological recording devices in healthy humans and those that suffer from PD, but this is clearly unethical. Researchers have therefore traditionally circumvented this obstacle in two ways: either by losing fidelity of the neurophysiological signal (by using non-invasive techniques such as PET, fMRI, EEG or MEG) or by approximating the diseased system (the use of animal models of PD). In this thesis, we rely on a small subgroup of PD patients who have high-fidelity recordings made possible via intracranial electrodes implanted for deep brain stimulation therapy.

Secondly, some symptoms in PD can only be objectively measured indirectly. Classically, PD is thought of primarily as a movement disorder, and as such provides directly observable behavioural parameters with which brain activity can be correlated. For example, motor physiologists have made great progress in associating pathological rhythmic activity in the basal ganglia with bradykinesia (the slowing and shrinking of movements) in humans, and representative behaviour in rodents (Hammond et al., 2007). However, PD patients can also develop cognitive and psychiatric complications including distortion of their memory, mood and decision-making capabilities. These are usually assessed subjectively, for example with questionnaires, and as such cannot be dynamically related to neurophysiological measurements in an experimental setting. However, although cognitive processes cannot be measured directly, they can be *inferred indirectly* as hidden variables in an objective model of behaviour. For example, although we cannot directly test the strength of a subject's memory, we can assume that stronger memories are recalled quicker and more accurately. Therefore in an appropriate experimental design, the directly observed *objective* behavioural parameters of reaction time and error-rate can be used to infer the strength of a memory, given a model linking memory, reaction time and error-rate. Such behavioural models fall within the realm of psychologists, who have successfully uncovered a range of insights into the diversity of human behaviour. However traditionally, and some may argue entirely appropriately, such researchers have regarded the brain as a 'black box', developing complex architectures of human behaviour with only brief regard to their neural

instantiation. In contrast, more recent developments in functional imaging have allowed such psychological models to be tested empirically in the field of cognitive neuroscience. In later chapters of this thesis, we will also depend on behavioural models, namely the horse-race model of response inhibition. The advantage of such models is that we can use them to *translate* the subjective cognitive symptoms of PD into objective measurable parameters appropriate to be related to neurophysiological measurements. However, we must always be aware that the hidden or inferred parameters that psychological models rely on may not in turn be the same parameters that the brain uses to generate that behaviour.

Thirdly, the Parkinsonian brain is *not* a homunculus of symptoms. If we want to correlate neural activity with behaviour, we would presumably start by identifying brain regions where behavioural modulations correlated with neural activity. This approach assumes that regions of the brain are functionally specialised to undertake different functions. Indeed we will rely on this sort of comparison in our introductory review. However, when trying to understand symptoms, rather than separately modelling different brain regions, we may be better served by modelling behaviour as an emergent property of the functional relations (i.e. connectivity) between regions (Friston, 2002). Similarly dysfunctional brain circuitry may better correspond to behaviour if the activity of functionally connected compensatory regions is also taken into account. In this thesis, we weight our analyses towards measurement of cortico-basal ganglia *coupling* to address this issue.

However, before proceeding, we will first carefully review the clinical features of PD, psychological models which may give insight into the cognitive symptoms of PD, and the anatomical and physiological basis of current neural models explaining these symptoms.

1.2 Clinical aspects of Parkinson's Disease

1.2.1 Diagnostic Criteria

Idiopathic PD is a common neurodegenerative condition characterised by basal ganglia dysfunction due to progressive dopamine depletion (Lees et al 2009). The clinical syndrome was first described by the surgeon and apothecarist, James Parkinson in 1817 who saw 6 patients (including some seen in the street, and not formally examined) with a 'shaking palsy' (Parkinson, 1817; Kempster et al., 2007). The condition was later named after Parkinson by Jean Martin Charcot. Currently PD is viewed as a heterogeneous clinico-pathologically defined syndrome, the cause of which remains unknown. The clinical diagnosis is based on the presence of reduction in amplitude and speed of repeated alternating movements

(bradykinesia) in combination with either tremor, stiffness of passive movement around a joint (rigidity) or postural instability. Additionally, a good response to dopaminergic treatment is also supportive (Gibb and Lees, 1988). *Parkinsonism* refers to idiopathic PD and other aetiologies which may mimic the symptoms of PD including Progressive Supranuclear Palsy (PSP), Multiple System Atrophy (MSA), and cerebrovascular disease. The most influential diagnostic criteria were formalised in 1986 as the Queen Square Brain Bank Criteria (see **Table 1**). In addition to the symptoms described above, these criteria list symptoms and signs (such as cerebellar signs) that effectively rule out idiopathic PD (Gibb and Lees, 1988).

1.2.2 Epidemiology

The lifetime risk of developing PD is 2% for men and 1.3% for women (Elbaz et al., 2002), with a median age of onset of 60 years (Lees et al., 2009). The age standardised prevalence of PD in the UK lies between 105-169 per 100000 (Wickremaratchi et al., 2009). This changes with age rising from 9.9 per 100000 in those aged 40-49, 272 per 100000 in those aged 60-69 and 1297 per 100000 in those aged over 80 years old (Wickremaratchi et al., 2009). A study from Rochester, USA found the overall incidence of PD to be 10.8 per 100000 person-years. Incidence increased with age, with rates of 17.4, 52.5, 93.1 and 79.1 per 100000 person-years in those aged 50-59, 60-69, 70-79 and 80-89 respectively (Bower et al., 1999). Incidence rates have been stable over time (arguing against an environmental aetiology) and men are consistently more affected than women (Bower et al., 1999; Rocca et al., 2001) with a male to female ratio around 1.5 (Wooten, 2004). However a recent meta-analysis of incidence studies placed the overall incidence of PD higher than previously thought at 16-19 per 100000 person-years (Twelves et al., 2003). The death rate in those on dopaminergic replacement therapy is between 5.86 - 6.17 per 100 person-years (Katzenschlager et al., 2008), with a median duration from diagnosis to death of about 15 years (Lees et al., 2009).

STEP 1: Diagnosis of PARKINSONIAN SYNDROME:
BRADYKINESIA (slowness of initiation of voluntary movement with progressive reduction in speed and amplitude of repetitive actions).
And at least one of the following:
a. Muscular rigidity
b. 4-6Hz rest tremor
c. postural instability not caused by primary visual, vestibular, cerebellar or proprioceptive dysfunction.
STEP 2. Exclusion criteria for Parkinson's Disease
History of repeated strokes with stepwise progression of Parkinsonian features
History of repeated head injury
History of definite encephalitis
Oculogyric crises
Neuroleptic treatment at onset of symptoms
More than one affected relative
Sustained remission
Strictly unilateral features after three years
Supranuclear gaze palsy
Cerebellar signs
Early severe autonomic involvement
Early severe dementia with disturbances of memory, language and praxis
Babinski sign
Presence of cerebral tumour or communicating hydrocephalus on CT scan
Negative response to large doses of levodopa (if malabsorption excluded)
MPTP exposure
STEP 3: Supportive prospective criteria for PARKINSON'S DISEASE.
Three or more required for diagnosis of definite Parkinson's disease.
Unilateral onset
Rest tremor
Progressive disorder
Persistent asymmetry affecting the side of onset most
Excellent response (70-100%) to levodopa
Severe levodopa-induced chorea
Levodopa response for 5 years or more
Clinical course of 10 years or more

Table 1: UK Parkinson's Disease Society Brain Bank clinical diagnostic criteria.

Adapted from Gibb and Lees (1988) *with permission from BMJ Publishing Group Ltd.*

1.2.3 Genetic and environmental risk factors

The underlying cause of PD is unknown, but many risk factors have been investigated. Of these, one of the most important is older age (Bower et al., 1999; Rocca et al., 2001). Evidence for other risk factors is less convincing. A systematic review determined that people who smoked tobacco were half as likely to get PD (Allam et al., 2004). Caffeine consumption also reduces PD risk in men but not, on average, in women. This later discrepancy may be confounded by the effect of oestrogens – for example if women on postmenopausal oestrogen replacement are excluded, then the remaining female coffee drinkers have a reduced incidence of PD, just like their male counterparts (Ascherio, 2004). But such risk factors may not *cause* PD per se – rather such behaviour may be a result of early subclinical disease. For example it is likely that the lower incidence of smoking and drinking coffee may be explained by lower sensation-seeking rates in patients with PD (Evans, 2005).

Risk from environmental causes is low. In 1983, four people developed chronic Parkinsonism after illicitly injecting a drug containing 1-methyl-4-phenyl-1,2,5,6-tetrahydropyridine (MPTP) (Langston et al., 1983). MPTP has a molecular structure close to the herbicide paraquat and so these case reports prompted investigation into the risk of exposure to herbicides and pesticides (Elbaz and Tranchant, 2007). A meta-analysis revealed odds ratios for developing idiopathic PD were 1.56 for rural residence, 1.26 for well water use, 1.42 for farm exposure and 1.85 for pesticide exposure (Priyadarshi et al., 2001). Cyanide, carbon disulphide and toluene toxicity can also cause an extrapyramidal syndrome similar to PD (Lees et al., 2009). There is continued debate whether head injury is also a risk factor. Parkinsonism can also be iatrogenic (drug-induced Parkinsonism) usually due to long-term use of anti-psychotic drugs such as chlorpromazine as well as a miscellany of other drugs such as metoclopramide, sodium valproate, flunarizine and herbal remedies such as kava kava and Indian snake root (Lees et al., 2009). REM sleep behaviour disorder – the tendency to shout or kick out in one's sleep – is also a strong predictor of PD. Although properly controlled cohort data are lacking, prospective studies have suggested that 5 years after diagnosis of REM sleep behaviour disorder, 19-38% of patients also develop PD or PD dementia, and at 10 years, this figure rises to 40-65% (Postuma et al., 2010).

Several genetic mutations can cause a syndrome clinically indistinguishable from idiopathic PD (**Table 2**). The commonest of these are leucine rich repeat kinase 2 (*LRRK-2*) mutations, which have a total frequency of 1% in sporadic PD and 4% in hereditary (with an affected first-degree relative) PD. However this is highly geographically variable, being most common in north African Arabs (hereditary 36%, sporadic 39%) and Ashkenazi Jews

(hereditary 28%, sporadic 10%) (Healy et al., 2008). These mutations are dominantly inherited and the commonest mutation (Gly2019Ser) confers a 28% risk of developing parkinsonism before the age of 60 years increasing to 74% by the age of 79 years (Healy et al., 2008).

Recessive mutations in parkin, *DJ-1*, *PINK1*, and *ATP13A2* genes cause Parkinsonism with an earlier onset, but more benign course, characteristically presenting with leg tremor, dystonia and early behavioural symptoms. Hyposmia is unusual in this cohort (Lees et al., 2009).

Gene	Pathology	Comments
	Parkinsonism	
Parkin	Substantia-nigra degeneration but usually no Lewy bodies	Recessive, young onset
PINK1	Data on only one subject, showing Lewy bodies	Recessive, young onset, psychiatric features
DJ-1	No data	Recessive, young onset
ATP13A2	No data	Recessive, young onset
	Parkinson's Disease	
Alpha-synuclein	Lewy bodies, sometimes GCIs and Tau inclusions.	Dominant point mutations (PARK1) and duplications/triplications (PARK4). Rapid motor progression; frequent dementia.
LRRK-2	Usually Lewy bodies in commonest mutation	Dominant mutations, variable clinical features
GBA	Lewy bodies	Dominant loss of function mutations increase risk

Table 2: Genes associated to L-dopa-responsive parkinsonism. *GCI: Glial cytoplasmic inclusions; GBA: Glucocerebrosidase mutations. Adapted from* Lees et al. (2009) and Poulopoulos et al. (2012) *with permission from Elsevier.*

Additionally, genetic risk may be due to the combined effect of many mutations (rather than the monogenic forms discussed above). In such cases, several single nucleotide polymorphisms (SNPs) confer the genetic risk. A recent genome wide association study found 11 loci where polymorphisms were associated with PD (Nalls et al., 2011). However, the odds ratio of the highest at risk quintile of disease was only 2.51, suggesting that these genetic loci may not yet be useful as a clinical prediction tool (Klein and Ziegler, 2011).

1.2.4 Pathology

The pathological hallmark of PD is dopaminergic cell loss in the substantia nigra pars compacta (Hassler, 1938; Damier, 1999), progressively spreading more medially and rostrally as the disease progresses (Damier, 1999). However cell loss can also be found in the locus coeruleus, dorsal nuclei of the vagus, raphe nuclei, nucleus basalis of Meynert and the pedunculopontine nucleus. In addition to cell loss, intraneural 8-30 micrometre inclusions of hyaline can be seen can be seen and are termed Lewy bodies. Lewy bodies stain strongly for alpha-synuclein, an abnormal post-translationally modified, aggregated protein (Spillantini et al., 1997). Although very sensitive to the diagnosis of PD, Lewy bodies can also be found in other conditions, including those without extrapyramidal features and even in normal aging (Parkkinen et al., 2005). Much research has tried to relate the Lewy body burden in particular cases to their symptomatology. However, this is confounded by the observation that the *number* of nigral Lewy bodies does not change with disease length or severity (Greffard et al., 2010) suggesting rather that they are accumulated and degraded constantly. Lewy bodies appear in the brainstem and cortex and similarly the *topography* of Lewy body spread has also been related to clinical features. Braak and colleagues have suggested that Lewy Body pathology spreads from the olfactory nuclei and the gastric autonomic plexus of Meissner and the olfactory nerve endings through the brainstem to the cortex as the disease progresses (Braak et al., 2003). This theory has been partially confirmed in a subset of younger patients with PD, with slowly progressive disease, however, the same study characterised another group of older patients, with shorter survival and more immediately diffuse Lewy bodies pathology (Halliday et al., 2008). Indeed, although it remains highly influential, up to 15% of post-mortem examinations do not conform to the Braak progression (Kalaitzakis et al., 2008). Cortical Lewy bodies most commonly appear in the frontal, parietal, insular, cingulate and entorhinal areas, although work trying to correlate regional cortical Lewy body load and symptoms is unclear. Lewy bodies do not correlate with the degree of motor symptoms (Parkkinen et al., 2005) although one study did

find less Lewy bodies in a group of younger tremor-dominant subjects (Selikhova et al., 2009). The relationship between cortical Lewy body load and frank dementia is also unclear although some reports suggest that cases with dementia have higher diffuse cortical loads of Lewy bodies (Hurtig et al., 2000; Apaydin, 2002; Halliday et al., 2008). More promising clincopathological correlations occur between the presence of dementia in PD and cortical beta-amyloid deposition (Jellinger and Attems, 2008) and the correlation between cognitive function in life (as measured by the MMSE) and the degree of cortical B-amyloid deposition (Braak et al., 2005).

1.2.5 Motor Symptoms

The cardinal symptoms of PD are bradykinesia, rigidity, tremor and later on in the condition, postural instability. Symptoms are usually unilateral at onset. Bradykinesia and rigidity usually present with loss of hand dexterity or with dragging of a foot, although first recollections may be of finding it easier to sit still or tending to swim in circles (Lees et al., 2009). Friends may notice that their facial expressions are less marked, their blink rate is reduced or that their writing has changed (becomes smaller as they write) or that their speech is quiet or monotonous. Bradykinesia, can be elicited on examination as a reduction in amplitude and speed of alternating hand movements. Some patients also develop more sustained, stereotyped and painful increases in tone, termed dystonia, often in their feet.

A subgroup of patients also present with a 4-6Hz unilateral pill-rolling tremor of the upper limb, which is most apparent at rest. Older (>70 years old) patients may also present with jaw, chin, lip and tongue (but not usually head) tremor.

Later in the disease, patients can develop slurred and accelerating (festinant) speech, sudden arrests of movement termed ‘freezing’ (especially triggered by visual cues such as doorways whilst walking) and falls. Patients can have difficulty turning in bed and eventually with chewing and swallowing food, sometimes needing feeding through percutaneous gastrostomy in the late stages (Chaudhuri et al., 2006; Lees et al., 2009).

Progression of motor symptoms in PD can be assessed using part III of the Unified Parkinson’s Disease Rating Scale (UPDRS) - an objective motor score, administered by a trained physician or nurse (Goetz et al., 2008). UPDRS part III score increases on average by 2.24 points per year in successfully medicated patients (Evans et al., 2011).

Although the Queen Square Brain Bank criteria are highly specific for the diagnosis of PD, they fail to convey the heterogeneity of PD symptoms in practice. It is clear that not all

patients develop all symptoms and some patients undergo much more rapid progression than others. Zetusky reported that the presence of tremor resulted in more benign progression, whilst the presence of postural instability resulted in a more rapidly progressive disease (Zetusky et al., 2012). Lewis et al. used a data-driven approach to identify PD sub-syndromes in 120 cases of PD. Cases were segregated into four groups: those with earlier disease onset (25%), those that were tremor dominant (31%), those that had minimal tremor but cognitive impairment and depression (36%) and those with rapid disease progression without dementia (8%). This classification scheme was partially supported by a retrospective analysis of the symptoms of 242 pathologically proven cases of PD, which identified increased cortical Lewy body and amyloid deposition in the rapidly progressive group with dementia and no tremor (Selikhova et al., 2009).

1.2.6 Non-Motor Symptoms

Although motor symptoms have received the greatest interest from researchers into PD, non-motor symptoms such as depression and cognitive impairment contribute significantly to patients' quality of life (Schrag, 2000) . A UK survey of 163 patients showed that in addition to difficulties with balance - sleep disturbance, memory symptoms and dribbling were rated as most disabling (Chaudhuri et al., 2006).

The commonest symptoms later on in the condition are those related to autonomic dysfunction including constipation, postural hypotension, erectile dysfunction, urinary urgency and pain. All these may require appropriate pharmacological intervention, additionally sometimes needing urinary catheterisation (Chaudhuri et al., 2006; Lees et al., 2009).

Critically non-motor symptoms can predate motor symptoms by years, and close study could allow for earlier identification of Parkinson's patients. Current opinion is that the earliest non-motor sign is usually hyposmia, although it is rarely declared as a symptom without prompting. Although it is difficult to study the epidemiology of non-motor symptoms of PD, hyposmia in a relative of a PD patient conveys a 10% increased risk of that relative developing PD (Ponsen et al., 2004). Patients may also suffer from fatigue and stiffness years before the characteristic motor symptoms of PD become recognisable (Chaudhuri et al., 2006; Lees et al., 2009).

Approximately one third of PD patients develop rapid eye movement (REM) sleep behaviour disorder (Gagnon et al., 2002) and sometimes years before the diagnosis of PD is made (Olson et al., 2000). In this condition, the patient suffers from vocalisations and sometimes

violent movements during sleep, occasionally waking up with scratches, or being unknowingly violent to a bed partner (Lees et al., 2009). Other difficulties with sleep are also common including sleep apnoea, difficulty turning in bed due to nocturnal stiffness and vivid dreams. Poor sleep at night, associated dementia and dopaminergic medications can all lead to daytime somnolence, sometimes with abrupt and unexpected episodes of sleep in the daytime (Chaudhuri et al., 2006).

Depression occurs in 2.7 – 70% of patients with PD (Burn, 2002) again often before the diagnosis of PD has been made. It is thought to occur not only because of the effects of motor disability on quality of life, but also as the result of multiple neurotransmitter imbalances that occur in PD. Patients can also suffer from anxiety and apathy.

Patients suffer from a degree of cognitive impairment which in some may lead to frank dementia, taking a mean of 6.2 years (Evans et al., 2011). PD dementia is characterised by fluctuating alertness, visuospatial difficulties and sometimes visual hallucinations, although up to 40% of patients have minor psychotic symptoms or visual hallucinations in the absence of formal dementia. Williams-Gray et al. used a 5 year longitudinal follow-up to disambiguate cognitive symptoms and the risk of developing dementia in 126 patients with PD. At the time of diagnosis, 62% of patients had some evidence of mild cognitive dysfunction on extensive neuropsychological testing. Five years after diagnosis, 10% of patients had developed dementia and a further 57% showed evidence of mild cognitive impairment. The authors suggested that cognitive impairment in PD could be subdivided into a rapidly progressive global syndrome, i.e. dementia, or a relatively stable frontal dysexecutive pattern of cognitive impairment. They identified three factors which predicted dementia at the time of diagnosis: age>72 years, semantic fluency <20 in 90s and inability to copy pentagons (Williams-Gray et al., 2007).

1.2.7 Medical Treatments and side effects

There is currently no cure for Parkinson's Disease, and there are no disease modifying agents. However there are many available preparations to manage the motor symptoms (Lees et al., 2009; Fox et al., 2011). The most common and most effective treatment for PD remains dopamine replacement therapy with levodopa. It is administered in combination with a peripheral dopa decarboxylase inhibitor in order to reduce the systemic side-effects of the dopamine pro-drug. Most symptoms improve within weeks of starting treatment, although tremor can sometimes take much longer to improve. Side-effects include lightheadedness, hypomania, delirium, and daytime somnolence although it is well tolerated in the majority.

In addition it is thought that continued levodopa therapy precipitates periods of excessive choreiform movements that are known as dyskinesias, and rapidly fluctuating excessive and reduced movements which are known as motor fluctuations. Evans et al. reported that the median time to develop dyskinesias was 6.6 years from disease onset, and 4.8 years from onset of levodopa therapy (Evans et al., 2011). Estimates of the prevalence of dyskinesias at 10 years are up to 90% (Vlaar et al., 2011). It is speculated that this may be due to poor absorption of levodopa later in the disease, neuroplastic effects of continued, but pulsatile, levodopa therapy or the reduced capacity of middle to end-stage dopamine neurons. As such, physicians and patients often delay starting levodopa to try to postpone these symptoms. However, there is no definitive evidence for this approach and the relationship between disease severity, levodopa treatment and dyskinesias remains unclear (Lees et al., 2009; Seppi et al., 2011; Vlaar et al., 2011). Patients may also develop dopamine dysregulation syndrome (see next paragraph).

Non-ergot dopamine agonists are also an effective treatment, some physicians preferring to use them first-line in younger patients. Side-effects include sleep attacks, ankle swelling and the development of addictive behavioural disorders such as impulse control disorders (ICDs), punding and other compulsive behaviours. Impulsive/compulsive behavioural phenomena have only recently described, first associated with taking large quantities of levodopa – dopamine dysregulation syndrome (DDS) (Giovannoni et al., 2000), and later associated with administration of dopamine agonists. The current rate of impulsive behaviours in UK and US PD clinics is 6% without and 17% with dopamine agonist therapy. Pathological behaviours can be highly significant and range from pathological gambling and punding to compulsive sexual behaviour, compulsive shopping and binge eating (Djamshidian et al., 2011).

Additional, second-line medications include selective type B monoamine oxidase inhibitors, amantadine and entacapone (Fox et al., 2011).

Non-motor symptoms have a wide range of medical management options although evidence exists for a limited few including Pramipexole and Venlafaxine for depression, Rivastigmine for dementia, clozapine for psychosis, melatonin for sleep disturbance, macrogol for constipation and botulinum toxin and glycopyrrolate for sialorrhea (Seppi et al., 2011).

1.2.8 Deep Brain Stimulation

Deep brain stimulation is a surgical therapy for PD. An electrode is stereotactically placed inside a basal ganglia target and chronically electrically stimulated via a pectorally placed

battery. The procedure derives from early lesioning of the basal ganglia structures which were noted to improve PD symptoms in the pre-levodopa era (Meyers, 1940; Cooper, 1953, 1964). These procedures were originally high-risk and a stereotactic surgical technique greatly improved operative outcomes (Spiegel et al., 1952). During lesioning operations, electrical stimulation was often applied to the brain as a way of functionally localising brain areas. However Hassler et al. documented improvements in PD symptoms during intra-operative electrical stimulation (Hassler et al., 1958). Following pioneers in movement disorder DBS surgery such as Mundinger (Mundinger, 1977) *chronic* electrical stimulation was applied to PD patients with tremor by Benabid in the 1980s (Benabid et al., 1987). A large European multi-centre study established the efficacy of thalamic DBS to improve tremor in 1999 (Limousin et al., 1999). In addition, results initially from primate, then human experiments suggested that stimulation of a new target, the subthalamic nucleus (STN), may help other symptoms in PD such as bradykinesia and rigidity (Limousin et al., 1998). Currently the commonest stimulation target is the STN although centres vary in their use of targeting techniques: some rely on entirely on pre-operative imaging (Foltynie et al., 2010), whilst others also rely on intra-operative electrophysiology (Gross et al., 2006).

The indications for DBS are tremor and dopamine-responsive motor fluctuations. Motor fluctuations respond to stimulation of the STN or Globus Pallidus interna (GPi), whereas tremor responds to STN or thalamic stimulation. A recent expert review suggested that inclusion criteria include (1) an excellent response to levodopa, (2) younger age, (3) no or few axial non–levodopa-responsive motor symptoms, (4) no or very mild cognitive impairment, and (5) absence of or well-controlled psychiatric disease (Bronstein et al., 2011). However, these are probably more stringent than what is practiced. More recently stimulation of a new target, the pedunculopontine nucleus (PPN), also shows promise as a therapy for gait freezing and postural instability.

Multiple randomised controlled trials have confirmed the utility of DBS in improving motor symptoms (Deuschl et al., 2006; Kleiner-Fisman et al., 2006; Weaver et al., 2009; Follett et al., 2010; Williams et al., 2010). A meta-analysis of *uncontrolled* cohorts calculated that on average, DBS reduced OFF medication UPDRS part III motor scores by 27.55 points, and reduced the oral levodopa intake by 55.9%. Dyskinesias were reduced by 69.1%, and time spent OFF reduced by 68.2%. Quality of life, assessed by the PDQ-39 was also increased by 34.5% (Kleiner-Fisman et al., 2006).

Controlled randomised trial data confirmed that STN stimulation improved motor UPDRS part III score in 71% of patients with a mean improvement of 19.6 points (Deuschl et al., 2006) at 6 months. A larger trial confirmed that these findings could be generalised to

patients over 75 years old, and also to either STN or GPi (Weaver et al., 2009). Here stimulation increased daily ON time by 4.6 hours (vs. control) and improved the motor UPDRS part III score in 71% of patients (v 31% of controls) at 6 months (Weaver et al., 2009). A UK based study compared any surgery (lesioning or DBS) with best medical treatment and found an increase in self-reported PDQ-39 of 5 points (0.3 points control) in the surgery group at 1 year (Williams et al., 2010).

Randomised trials comparing STN to GPi DBS have been inconsistent: one trial finding that GPi stimulation had a better cognitive side-effect profile than STN stimulation (Follett et al., 2010) and one lower powered trial finding that there was no difference (Okun et al., 2009). The current understanding is that STN stimulation results in improved motor outcomes when compared to GPI stimulation. This has been measured both directly in terms of rigidity (Okun et al., 2009) or indirectly inferred because GPi stimulation patients need more oral levodopa post-op to reach the same level of motor function (Follett et al., 2010).

The relationship between DBS and gait is more complex, with one uncontrolled study suggesting that STN, but not GPi, stimulation worsens gait after 2 years in spite of improvements in other parts of the UPDRS part III motor score (St George et al., 2010).

However, although it is clear that DBS improves quality of life and motor function, it is also clear that it has a significant adverse event profile. Surgical adverse event rates are highly variable and include intracranial haemorrhage (0%-10%), stroke (0%-2%), infection (0%-15%), lead erosion without infection (1%-2.5%), lead fracture (0%-15%), lead migration (0%-19%), and death (0%-4.4%) (Bronstein et al., 2011). Weaver reported that 49% of DBS patients experienced serious adverse events infection but the majority (83% of these) had resolved by 6 months (Weaver et al., 2009).

The commonest non-surgical adverse events include falls, dystonia and neurobehavioural disorders and overall they were worse following STN DBS as compared to GPi DBS (Hariz et al., 2008). Cognitive function has also been reported to worsen with STN or GPi DBS: scores being worse on tests of working memory, visuospatial memory and phonemic fluency, with no change in scores on the Mattis dementia or Beck depression scales (Weaver et al., 2009). There is also a small but important increase in the rate of completed (0.45%) and attempted (0.9%) suicide, when STN stimulation is compared with background rates (not control groups). This difference persists for at least 4 years post-operatively (Voon et al., 2008). There is also a risk of weight gain following DBS, which cannot be completely explained by the reduction in dyskinesia score (Montaurier et al., 2007). Finally speech intelligibility and loudness may worsen with STN stimulation, especially with high voltages in the left STN (Tripoliti et al., 2011).

Although traditionally, subjects with active psychiatric disease have been deemed unsuitable for DBS, it is unknown whether DBS helps or worsens patients with dopaminergic medication related addictive behaviours such as impulse control disorders, pathological gambling and dopamine dysregulation syndrome. Symptoms theoretically may improve because oral levodopa levels decrease significantly after successful DBS stimulation. On the other hand, the increased cognitive and psychiatric complications of DBS may worsen these behaviours. Studies have also been divided, with some showing worsening, and some showing improvement (Mallet et al., 2002; Ardouin et al., 2006; Smeding et al., 2007). However a recent larger (n=63) prospective study is more promising: it found dramatic improvements in DDS and ICD, without impairment of cognitive function in 63 PD patients following STN DBS (Lhommée et al., 2012). Current Practice regarding DBS in the UK is summarised in **Table 2**.

	Subthalamic nucleus	Globus pallidus interna
Indication and therapeutic effect	Motor fluctuations, tremor. Directly improves bradykinesia/rigidity/tremor – dyskinesias reduced as the result of medication reduction	Motor fluctuations. Directly abolishes dyskinesias – less effect of bradykinesia/rigidity/tremor
Motor benefit	Levodopa responsive motor deficits	
Potential motor adverse effects	On medication axial deficits can worsen, as can speech	On medication axial deficits can worsen, especially gait freezing
Non-motor effects	Greater risk of cognitive and psychiatric effects. Dopamine medication reductions may improve or worsen non-motor features (e.g. mood and impulse control disorders)	Less likely to cause cognitive/psychiatric effects
Typical candidate	Younger patient	Biologically 'older' patient and those with neuropsychological issues.

Table 2: Summary of current practice for STN vs. GPi DBS*. Neuropsychiatric effects are still debated. Adapted from* Thevathasan and Gregory (2010) *with permission from BMJ Publishing Group Ltd.*

1.3 The pathophysiological basis of Parkinsonian symptoms: function and dysfunction of the cortico-basal ganglia network

The heterogeneous nature of motor and non-motor symptoms in PD, and their differential response to treatments, suggests that different symptoms may have a different underlying pathophysiological basis. How can we reconcile the relatively specific neuronal degeneration associated with PD (loss of dopaminergic cells in the substantia nigra pars compacta) with the multiplicity of its symptoms? This may partially be explained by the multiple divergent projections of midbrain dopaminergic cells onto different cortico-basal ganglia circuits (Haber, 2003). Indeed pathophysiological models of PD primarily concern themselves with these circuits. In this section we will review the anatomical and physiological basis of these cortico- basal ganglia circuits before taking a look at the evidence of their dysfunction in PD.

1.3.1 The firing rate model of cortico-basal ganglia connectivity

The basal ganglia are an interconnected set of deep brain nuclei that were first thought to be linked to movement control by Ferrier in 1876 (Ferrier, 1876). This was further established by Wilson who characterised the predominantly motor impairment resulting from bilateral striatal copper deposition (Wilson, 1912). However, the first functional architecture of the basal ganglia was developed as late as the 1980s in a series of highly influential papers by Alexander and DeLong (Alexander et al., 1986; Albin et al., 1989; Alexander and Crutcher, 1990; DeLong, 1990). This model was mainly based on primate anatomical and electrophysiological data, and placed the basal ganglia in a partially closed circuit between the cortex and the thalamus. The overall function of the basal ganglia was proposed to be dependent on the balance of firing rate changes within different pathways through the basal ganglia, and therefore the model was also known as the firing rate model. Although, the more dorsal motor circuits remain the best characterised (Alexander et al., 1986; Bolam et al., 2000), recent research has also begun to focus on the more ventral, cognitive and emotional, functions of what Wilson termed, “the dark basement of the mind” (Wilson, 1925).

1.3.1.1 Parallel, partially segregated, partially closed circuits

Virtually the entire cerebral cortex projects into the main input zone of the basal ganglia, the striatum. However, the output zones of the basal ganglia, the globus pallidus internal (GPi) and substantia nigra pars reticulata (SNr), project to relatively specific parts of the cortex via

a thalamic relay (Kemp and Powell, 1971; Alexander et al., 1986; Bolam et al., 2000). Alexander et al. (1986) crystallized the anatomical basis underlying this imbalance in terms of two opposing processes: segregation and integration. Firstly, the input from topographically distinct cortical areas remains broadly segregated in the striatum. This segregation is kept both in the relay stations within the basal ganglia, the subthalamic nucleus (STN) and globus pallidus externa (GPe), and the GPi/SNr output complex. This output remains segregated in the thalamus from where it projects back to limited and discrete areas of the cerebral cortex. Based on the passage through the basal ganglia and the cortical output areas, Alexander et al. (1986) identified at least five such circuits (see

Figure 1, but also see section 1.4.5). The best characterised was the motor circuit, which received inputs from the primary motor, supplementary motor, arcuate premotor and somatosensory cortices. These inputs were then channelled through the posterior, dorsal aspect of the striatum (the putamen in primates) to the ventrolateral GPi and caudolateral SNr. Motor output then projected to the ventralis lateralis pars medialis and pars oralis nuclei in the thalamus before returning to the supplementary motor area (Kunzle, 1975, 1978; Alexander et al., 1986). In a similar fashion, segregated circuits were identified which projected to the frontal eye fields (the occulomotor circuit), the dorsolateral prefrontal cortex, the lateral orbitofrontal cortex and the anterior cingulate cortex. These circuits were only *partially* closed in that they had widespread cortical inputs, but projected back to only a subset of these areas. This implied that *within* each cortico-basal ganglia circuit there must be an integration or 'funnelling' of information. Crucially, integration was felt not to exist between different circuits leading to the description of parallel, partially segregated, partially closed circuits (Alexander et al., 1986). A more detailed description of the processing within each circuit was developed by the same group and others and requires a closer examination of the synaptic organisation of the basal ganglia.

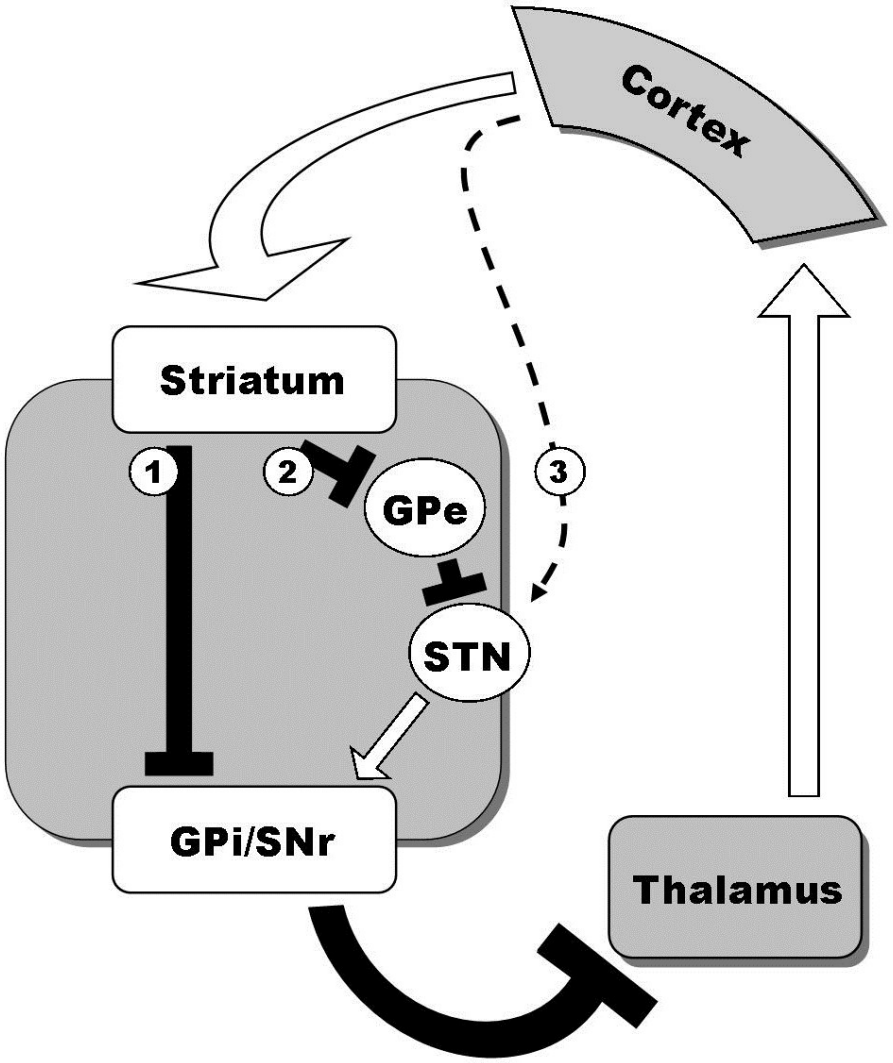

Figure 1: Simplified diagram of the basal ganglia circuit. *Multiple such circuits involve different cortical regions and remain partially segregated throughout the basal ganglia. Pathway 1 is the direct pathway, pathway 2 is the indirect pathway and pathway 3 is the hyperdirect pathway. GPI: Globus Pallidus interna, SNr: Substantia Nigra pars reticulate, STN: subthalamic nucleus, GPe: Globus Pallidus externa. Adapted from Jha and Brown (2010) with permission from Cambridge University Press.*

1.3.1.2 The striatum and the origin of the direct and indirect pathways

The striatum can be divided into dorsal and ventral regions. In primates, the dorsal striatum can be divided further into the dorsal and lateral caudate and putamen. The ventral striatum is composed of the nucleus accumbens, the medial and ventral edges of the caudate and putamen and the striatal cells of the olfactory tubercle and anterior perforated substance (Bar-Gad et al., 2003).

In addition to excitatory glutamatergic inputs from the cortex, the striatum receives inputs from the intralaminar thalamic nuclei, amygdala, hippocampus and dorsal raphe (Alexander et al., 1986; Bolam et al., 2000) making it ideally placed to integrate information from such different areas. Most cells in the striatum (>90%) project to other structures and are termed medium size densely spiny neurons (MSNs) because their spherically distributed dendritic branches are covered in spines (DiFiglia et al., 1976; Bolam et al., 2000). The resting membrane potential of MSNs is characteristically low (a 'down' state) and increases during periods of cortical excitation ('up' states) (Wilson and Groves, 1981; Stern et al., 1998; Bolam et al., 2000; Murer et al., 2002). At rest the MSNs do not fire, and therefore cortical input is thought to facilitate MSN firing during up states.

MSNs can be further classified into two groups. The first group express receptors for γ-aminobutyric acid (GABA), substance P, dynorphin and D1 dopamine receptors and preferentially projects directly to the GPi/SNr. This has been termed the 'direct' pathway. The second group express GABA, enkephalin and D2 dopamine receptors, projects to the GPI/SNr via the GPe and STN, and is known as the indirect pathway (Albin et al., 1989; Bolam et al., 2000; Bar-Gad et al., 2003). In addition to downstream projections, MSNs also project symmetrically to neighbouring MSNs (Bolam et al., 2000). All MSNs have inhibitory GABAergic output such that the net effect of cortical excitation of the striatum is inhibition of both downstream projection targets (GPi and GPe) and surrounding striatum. This property suggests that the striatum focuses or selects a range of cortical inputs.

1.3.1.3 The rate model explains movement and movement disorders

Based on the connections of the rate model, Albin et al. suggested a potential role for the basal ganglia in movement and movement disorders (Albin et al., 1989). Although substantial parts of this theory remain experimentally untested, it still forms the basis on which many current ideas about basal ganglia function are built.

The thalamus, which has excitatory output to the cortex, is under tonic inhibitory control from the GPi/SNr. During a movement, motor cortical activity is passed via the direct pathway

through the basal ganglia. This inhibits the GPi/SNr, therefore suspending the tonic inhibition of the thalamus and allowing excitation of the cortex and movement. At the same time, cortical activity from undesired movements is topographically separated in the striatum and sent through the indirect pathway. This causes the opposite effect on the GPi/SNr, increasing tonic inhibition on the thalamus and suppressing undesired movements (Alexander et al., 1986; Albin et al., 1989; Alexander and Crutcher, 1990; DeLong, 1990).

The imbalance between movement facilitating (direct) and inhibiting (indirect) pathways was also proposed to explain symptoms of movement disorders such as hemiballism, chorea and akinesia (Albin et al., 1989). In PD, for example, dopaminergic input from the substantia nigra pars compacta (SNc) to the striatum is reduced. This increases activity of D2 expressing MSNs (the indirect pathway) whilst decreasing the activity of D1 expressing MSNs (the direct pathway). The net result is an overactive STN, increased tonic inhibition of the thalamus and reduced motor cortical activity (Alexander et al., 1986; Albin et al., 1989; Alexander and Crutcher, 1990; DeLong, 1990). This proposed a mechanism for akinesia, but didn't explain symptoms and signs such as tremor or rigidity.

1.3.2 Revisions to and limitations of the rate model

1.3.2.1 The topography and organisation of cortical connections to the basal ganglia

Alexander et al. (1986) suggested that there were at least five partially segregated circuits projecting to the supplementary motor area, frontal eye fields, dorsolateral prefrontal cortex, lateral orbitofrontal cortex and anterior cingulate cortex (Alexander et al., 1986). Since then these findings have been extended in animals using retrograde transneuronal tracers, and some of them have also been confirmed in humans using diffusion tensor imaging (DTI).

Prefrontal connections are more extensive than previously thought, accounting for 27% of GPi and 45% of SNr output (Middleton and Strick, 2002). Areas specifically tested by this study on non-human primates included the superior medial prefrontal area (equivalent to Brodmann area 9), the dorsolateral prefrontal area (equivalent to Brodmann area 46) and the lateral orbitofrontal area (equivalent to Brodmann area 12). Additionally, nearby prefrontal cortical areas remain segregated from each other, and also other e.g. motor loops, as they pass through the nuclei of the basal ganglia. Closer examination of the supplementary motor complex, again reveals separate segregated loops. The GPi output to

the anterior pre-SMA is located in the rostral 'associative' part whilst the output to the SMA is located in the ventral 'sensorimotor' part (Akkal et al., 2007). Both pre-SMA and SMA also have segregated inputs into the striatum and the STN [(Inase et al., 1999), see also section 1.3.2.2].

The basal ganglia also project to some areas outside of the frontal cortex. A non-human primate study established the closed loop architecture of basal ganglia connections with the inferior temporal area, which is thought to be involved in the recognition of visual objects (Middleton and Strick, 1996). Additional connections with the cerebellum and brainstem have now been characterised (see section1.4.4).

Recent methodological advances in neuroimaging have allowed visualisation of segregated cortico-basal ganglia circuits in humans (Lehericy et al., 2004; Lehéricy et al., 2004; Draganski et al., 2008). Diffusion tensor imaging (DTI) allows non-invasive, three dimensional, tracking of axons in humans, although it does not have the ability to characterise directionality. DTI analysis of healthy volunteers revealed that striatal connections with the motor, associative and limbic parts of the cortex were also segregated at the striatal level (Lehéricy et al., 2004). However, compared with animal data, there was a paucity of parietal and cingulate connectivity with the striatum. Draganski et al. (2008) reproduced these findings in another cohort, and extended them to include thalamic circuits (Draganski et al., 2008). They used pre-specified cortical regions to parcellate the striatum, GPe and thalamus into characteristic but partially overlapping regions which were in keeping with prior data from animals.

Based on anatomical connectivity, cortico-basal ganglia circuits are now seen as a continuum of somatotopically organised circuits broadly organised, by their cortical output, into limbic, associative and motor circuits. The topography of these different circuits, and the sub-circuits within them, is kept at all stages of basal ganglia processing (Haber, 2003).

1.3.2.2 The subthalamic nucleus and the hyperdirect pathway

Recent work has focused on the importance of the subthalamic nucleus (STN) identifying it as a second major input into basal ganglia circuitry in addition to the striatum. It is an almond-shaped ~175mm^3 structure (Levesque and Parent, 2005) that lies between the zona incerta dorsally and the cerebral peduncle ventrally (Parent and Hazrati, 1995). Apart from medially merging into the lateral hypothalamus, it is separated from other grey matter structures by myelinated fibre tracts. It was originally thought to be a homogeneous structure with densely packed excitatory glutamatergic projection neurons (Parent and Hazrati, 1995;

Bar-Gad et al., 2003) but a recent post-mortem study of human STNs has revealed that at least 7.5% of cells stain positively for, glutamic acid decarboxylase (GAD), the GABA synthesizing enzyme (Levesque and Parent, 2005).

Afferent projections to the STN are mainly from the cerebral cortex and GPe but also the centeromedian-parafascicular complex of the thalamus (Feger et al., 1994), the substantia nigra, the dorsal raphe nucleus and the pedunculopontine tegmental nucleus (Parent and Hazrati, 1995; Mena-Segovia et al., 2004; Coizet et al., 2009). The direct cortical-subthalamic connections are sometimes referred to as the 'hyperdirect pathway.' Direct cortical afferents to the STN in the rodent include the primary motor and somatosensory cortex, prefrontal cortex, anterior and medial cingulate cortex and the insular cortex (Monakow et al., 1978; Nambu et al., 2002). Cortical afferents in the primate show similar afferents concentrated in the primary motor cortex (somatotopically to the dorsolateral STN) and the premotor cortex (Brodmann areas 6, 8 and 9) which terminates in the ventromedial STN (area 6 most ventral) (Parent and Hazrati, 1995; Nambu et al., 1996, 1997).

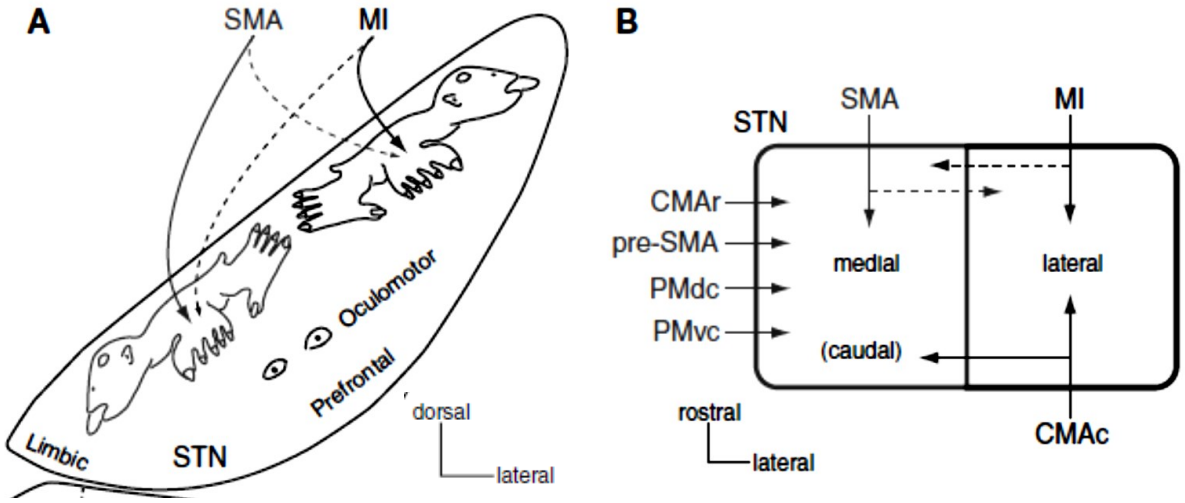

Figure 2: Distribution of afferents into the STN. *Reprinted from* Nambu, (2011) *in accordance with Frontiers Media SA.The vertical axis is in panel A is dorsal (top) to ventral (bottom), whilst the vertical axis in panel B is rostral (top) to caudal (bottom). Both panels have a horizontal axis which is lateral (left) to medial (right). Panel A shows that the SMA and M1 areas project to different but neighbouring regions of the STN. From a different viewpoint, panel B confirms this and also shows that other neighbouring motor regions project onto neighbouring regions of the STN. SMA supplementary motor area; pre-SMA pre-supplementary motor area; M1 primary motor cortex; CMAr rostral cingulate motor area, PMdc dorsal premotor area; PMvc; ventral premotor area; CMAc caudal cingulate motor area.*

Based on the distribution of cortical afferents to the STN, it has been divided into a dorsolateral sensorimotor region, a ventromedial associative territory and a medial limbic territory (Parent and Hazrati, 1995; Haber, 2003; Levesque and Parent, 2005). Further sub-parcellation can be made of the dorsolateral sensorimotor region, from the distinctive distribution of afferent projections from different parts of the motor system (see **Figure 2**). In addition, there has been recent evidence for histological inhomogeneities within the STN such as the relatively increased concentration of, likely GABAergic, interneurons in the limbic/associative segments of the STN (Levesque and Parent, 2005).

STN projection cells have sparsely spined dendrites arborizing along the main axis of the nucleus (Sato et al., 2000). Their predominant projection targets are the SNr, GPi and GPe (Sato et al., 2000), although projections to the striatum, the cerebral cortex, the substantia innominata, the pedunculopontine tegmental nucleus, and the mesencephalic and pontine reticular formation have been described (Parent and Hazrati, 1995). A recent systematic review of direct STN connections in mammals identified 130 papers and summarized them in an ideogram, although equal prominence was given to anatomical tracing and human diffusion tract imaging data (Lambert et al., 2011).

The role of the STN and the hyperdirect pathway remains uncertain, but its importance does not. It conveys cortical signals to the GPi/SNr faster than the direct and indirect pathways (Nambu et al., 2002; Nambu, 2008) and it has been implicated in inhibiting and changing motor plans (Aron et al., 2007a; Isoda and Hikosaka, 2008) and impulsive behaviour (Frank et al., 2007) and is the current most popular target for deep brain stimulation (DBS) in PD (Limousin et al., 1995; Rezai et al., 2008; Thevathasan and Gregory, 2010).

1.3.2.3 Complex connectivity between the striatum, GPe and GPi/SNr

Are the direct and indirect pathways clearly distinct? Recent studies in transgenic mice have confirmed that MSNs projecting to the SNr (the direct pathway) express only D1 receptors (Matamales et al., 2009; Bertran-Gonzalez et al., 2010), and are electrophysiologically different (Bertran-Gonzalez et al., 2010). On the other hand, anatomical tracing studies have shown that the vast majority of MSNs projecting to the GPi/SNr also send collaterals to the GPe (Wu et al., 2000). The most parsimonious explanation is that MSNs expressing D2 receptors project to the GPe only (the old indirect pathway) whereas MSNs expressing D1 receptors send collateral projections to a combination of GPi/SNr and GPe. However this hypothesis requires confirmation by a combined transgenic neurochemical and anatomical tracing study (Bertran-Gonzalez et al., 2010).

More extensive study of the GPe connections reveals that, in addition to the STN, it projects directly to the GPi/SNr and the dopaminergic cells of the SNc (Smith et al., 1998; Bolam et al., 2000), and also sends reciprocal projections back to the striatum and to itself (Bevan et al., 1998; Kita, 2001; Miwa et al., 2001; Nambu, 2008). Its connections suggest that the GPe plays a central role in basal ganglia processing and possibly in basal ganglia pathology (Magill et al., 2001).

1.3.2.4 The pedunculopontine nucleus

Preliminary work has identified a set of sub-cortical structures that input into the striatum via the midline intralaminar complex of the thalamus. These include the superior and inferior colliculi, the pedunculopontine nucleus (PPN), cuneiform area, periaquaductal grey parabrachial complex and other medullary and pontine reticular nuclei (McHaffie et al., 2005). Perhaps the best characterised of these are the interactions between the superior colliculus and basal ganglia – framed as a partially closed circuit, similar to cortico-basal ganglia circuits, between the colliculus, thalamus, striatum and GPi (McHaffie et al., 2005). However, we will focus on the cortical and basal ganglia connections to the PPN as this may be more clinically relevant for PD.

The PPN, located at the junction between the midbrain and pons, is bounded laterally by the medial leminiscus and medially by the superior cerebellar decussation. The caudal pole of the PPN lies adjacent to the locus coeruleus, the cuneiform and subcuneiform nuclei, whilst rostrally it is adjacent to the substantia nigra and retrorubral field (Pahapill, 2000). It is part of the reticular activating system and comprises cholinergic, glutamatergic and GABAergic cells (Wang and Morales, 2009). As a reticular nucleus, it has relatively indistinct boundaries and debate exists as to whether the extent of the nucleus should be defined histologically or immunochemically. It was first described histologically by Olszewski and Baxter (Olszewski and Baxter, 1982), who divided the nuclei into two regions based on cholinergic cell density: the dorsolateral caudal *pars compacta*, and the rostral *pars dissipata*. However Mesulam et al. recognized that cholinergic neurons within the PPN were part of a larger group of cholinergic neurons termed the Ch5 complex. The Ch5 complex also neighbours the cholinergic Ch6 complex, and so it is difficult to be certain of the boundaries of the PPN if one relies on cholinergic cells alone (Mesulam et al., 1989). However, a broad rostro-caudal distinction of the nucleus can be made based on the distribution of all cell types, and also provides a basis on which to categorise the heterogeneous anatomical connectivity of the nucleus (Martinez-Gonzalez et al., 2011).

The basal ganglia interact prominently with the PPN. The GABAergic output neurons from the substantia nigra pars reticulata and GPi (Semba and Fibiger, 1992; Parent et al., 2001) input into the predominantly GABAergic *rostral* PPN. Efferents from this region lead back to the substantia nigra pars compacta and reticulata, to the GPi and also to the hypothalamus, suggesting that this region may have a prominent role modulating basal ganglia processes (Martinez-Gonzalez et al., 2011). The *caudal* PPN receives afferents from the cortex and dorsal raphe onto its predominantly cholinergic and glutamatergic neurons. The efferents are to the thalamus (Lavoie and Parent, 1994), STN (Hammond et al., 1983; Lavoie and Parent, 1994; Parent and Hazrati, 1995), VTA and superior and inferior colliculi. This suggests that the caudal PPN is involved in regulating arousal via thalamocortical networks and importantly that the same network is responsible for descending projections to brainstem and spinal locomotion centres, and also to the STN (Martinez-Gonzalez et al., 2011). Cortical regions projecting to the caudal PPN include the auditory cortex (Schofield and Motts, 2009)(Schofield et al., 2010), the medial prefrontal cortex (Sesack et al., 1989), motor and premotor areas, the amygdala and the hypothalamus (Semba and Fibiger, 1992; Matsumura et al., 2000). The entire axis of the PPN receives afferents from the cerebellum (Hazrati and Parent, 1992).

Evidence of a similar functional distinction is minimal in humans. Low frequency stimulation of the PPN region alters resting cortical glucose metabolism and cerebral blood flow in a large network of areas that include the orbitofrontal cortex, cingulate, prefrontal areas, temporal lobe, thalamus and cerebellum (Ballanger et al., 2009; Ceravolo et al., 2011). However, functional magnetic resonance imaging (fMRI) and positron emission tomography (PET) have insufficient spatial resolution to reliably discern different areas of the PPN region (Ballanger et al., 2009; Snijders et al., 2011). Direct recordings of local field potentials (LFPs) from intracranial electrodes afford excellent spatial and temporal resolution: Thevathasan et al. recently demonstrated that oscillatory synchrony is topographically organized in the PPN region (Thevathasan et al., 2011).

1.3.3 Developing concepts of basal ganglia function

Many theories have been put forward regarding the computational processing performed by the basal ganglia (Alexander et al., 1986; Mink, 1996; Redgrave et al., 1999, 2010; Bar-Gad et al., 2003; Haber, 2003; Nambu, 2008), however, all remain largely speculative. A common theme is information selection by the striatum, and rather appealingly, the repeating modular nature of the basal ganglia suggests that similar computational processing in

different cortico-basal ganglia circuits (e.g. motor versus associative) may be similar (Alexander et al., 1986; Redgrave et al., 2010).

The somatotropic and interneuronal organisation of the striatum ensure that cortical signals associated with movement cause localised activation of MSNs within the striatum (Bolam et al., 2000; Nambu, 2008). Activated MSNs then inhibit surrounding MSNs via lateral projections or via inhibitory interneurons. The largest striatal interneurons are called tonically active neurons (TANs) due to their spontaneous 3-10Hz firing activity which is mainly due to their membrane properties. TANs require only a small cortical input to influence their firing pattern (Bolam et al., 2000; Bar-Gad et al., 2003). The striatum also contains GABAergic fast-spiking interneurons that stain positive for the calcium-binding protein parvalbumin. Although only representing 3-5% of the striatal neuronal population, these cells are coupled together via gap junctions and have a greater spatial spread than lateral MSN projections and, therefore potentially have a strong inhibitory effect on surrounding MSNs (Parthasarathy and Graybiel, 1997; Bolam et al., 2000; Bar-Gad et al., 2003).

The spatial focusing of competing motor programs is passed onto the thalamus via the direct pathway, ensuring that the tonic inhibition of the thalamus is only interrupted for desired motor programs whilst unwanted motor programs are suppressed (Mink, 1996; Nambu, 2008). A further refinement to this idea is that motor programs are also focused in time. This is achieved by prior, spatially broad excitation of the GPi/SNr via the faster STN hyperdirect pathway, and subsequent similar excitation by the slower indirect pathway (Mink, 1996; Nambu, 2008). More complex theories of the selection mechanism have been put forward including the suggestion that the cortical information is re-coded by the striatum and that this can be modelled as a dimensionality reduction similar to principal component analysis (Bar-Gad et al., 2003). However, most current theories agree that the each cortico-basal ganglia circuit outputs a selected subset of the data it receives.

But how do we combine data from different circuits, such as motivational and associative, to select an action? Recently, in addition to the integration *within* each circuit, theories have tried to understand the integration of information *between* separate cortico- basal ganglia circuits (Redgrave et al., 1999, 2010; Haber, 2003). Haber summarised two mechanisms by which such integration could take place based on non-human primate data (Haber, 2003). Spiral striato-nigral-striatal and thalamo-cortical-thalamic connections feed information from limbic circuits forward into associative and motor circuits. Thereby motor circuit activity, i.e. actions, could be influenced by motivational and cognitive circuitry (Haber, 2003).

1.3.4 The pattern model of movement disorders

1.3.4.1 Limitations of the rate model and emergence of the pattern model

While the rate model is seminal in our understanding of the basal ganglia, it fails to explain why functional neurosurgery is a successful treatment for PD (Marsden and Obeso, 1994; Brown and Eusebio, 2008). For example, destruction of the thalamus (thalamotomy) or GPi (pallidotomy) improved PD symptoms, but why does this not make movements worse (Marsden and Obeso, 1994)? The model suggests that these two lesions should obliterate basal ganglia output to the cortex completely. Alternatively, how does a pallidotomy, improve opposing symptoms such as akinesia and dyskinesias? Finally, the model suggests that lesioning the STN, should also improve symptoms of PD. However, although therapeutic high frequency DBS of the STN is very effective for PD, we are still unclear whether in fact its effect would be best modelled as a 'virtual lesion' or stimulation. These and other paradoxes were first summarized by Marsden & Obeso in 1994 (Marsden and Obeso, 1994). One of their postulates was that, in addition to firing rate, firing pattern may also be important in basal ganglia function. Abnormal patterns could act as a 'noisy' signal and disrupt basal ganglia function. The appeal of this idea was that it allowed multiple functional or dysfunctional networks, characterised by their firing pattern, to occupy the same anatomical circuit. Different patterns could be potentially associated with different symptoms.

In the same year, a landmark paper by Bergman et al. established the abnormal patterning of neuronal firing in the STN and pallidum in the 1-methy-4-phenyl-1,2,3,6-tetrahydropyridine (MPTP) treated primate model of PD (Bergman et al., 1994; Brown and Eusebio, 2008). Since then building evidence from human and animal studies suggests that abnormal patterning is a characteristic feature of Parkinsonian symptoms. Abnormal patterning can be revealed by either recording neuronal firing simultaneously at different sites or by measuring the synchronised local extracellular activity within a region. This later activity is thought to represent summed local dendritic currents due to excitatory and inhibitory post-synaptic potentials. This activity, called a local field potential (LFP), characteristically oscillates and can be characterised in terms of the frequency of oscillation (Buzsaki and Draguhn, 2004). The latter are especially convenient to record in humans as they are accessible temporarily via implanted DBS electrodes immediately post-operatively.

1.3.4.2 Beta oscillations and their relation to movement, dopamine and DBS

The clearest link between neuronal synchronisation and PD lies in the 10-30Hz range, often termed the beta range for convenience (Brown, 2007). Post-operative recordings in humans with PD have consistently shown that beta oscillations in LFPs are locally generated in multiple basal ganglia structures including the STN and GPi (Brown et al., 2001; Brown and Williams, 2005; Gatev et al., 2006; Hammond et al., 2007). Local spiking neuronal activity also oscillates in the beta frequency range (Levy et al., 2000) and, in the STN, seems to be tightly linked to LFPs recorded from the same region (Kuhn et al., 2005; Weinberger et al., 2006) but may underestimate the extent of synchrony at the population level (Schneidman et al., 2006). Animal data also show synchrony but at a lower frequency in primate models of PD (Hammond et al., 2007), and at similar frequencies in rat models (Sharott et al., 2005b).

Further evidence, linking beta synchronisation to movement dynamics and dopaminergic levels, is suggestive that beta synchronisation may be an anti-kinetic signal (Hammond et al., 2007; Brown and Eusebio, 2008). Dopamine suppresses beta synchronisation in the STN (Priori et al., 2004) and the degree of suppression correlates with improvement in akinesia (Silberstein et al., 2005; Kuhn et al., 2006b). In addition, beta synchronisation, in the STN and GPi, decreases just before and during movement (Amirnovin et al., 2004; Brown, 2007). Such oscillatory phenomena are known as event related desynchronisations (ERDs) and the timing of the beta ERD correlates with reaction time (Kuhn et al., 2004; Williams et al., 2005). Because the beta ERD occurs before movement, it presumably reflects motor preparation, rather than mere sensory re-afference. This is also consistent with retained beta desynchronisation, but not re-synchronisation (ERS), when subjects are asked to imagine a movement but not execute it (Kuhn et al., 2006a). As well as affecting resting levels of beta, dopamine also modulates the beta ERD with movement, and this modulation is inversely correlated to motor impairment (Doyle et al., 2005).

Deep brain stimulation of the STN inhibits local beta oscillations (Wingeier et al., 2006; Eusebio et al., 2010) but not necessarily in everyone, and the effect may be separate from that of dopamine (Giannicola et al., 2010). Additionally, stimulation of the STN reduces beta synchronisation in the downstream GPi (Brown et al., 2004), consistent with the idea that beta activity may be pathological in PD.

Finally, one may expect different territories within the STN to have different levels of beta synchronisation given that this signal seems to best correlate with motor impairment. Indeed most beta synchronisation occurs in the dorsolateral or ‘motor’ part of the STN (Kuhn et al.,

2005; Alonso-Frech et al., 2006; Weinberger et al., 2006) and the spatial spread of this synchronisation correlates with akinesia (Pogosyan et al., 2010; Zaidel et al., 2010).

Although there is ample correlative evidence for the role of beta synchronisation, causal evidence remains incomplete. Standard square-wave pulse stimulation of the STN at 10-20 Hz does worsen bradykinesia (Timmermann et al., 2004; Chen et al., 2007; Eusebio et al., 2008) but only by 5 – 10%. Brown and colleagues suggested reasons why this effect was so limited, including aspects of the stimulation parameters (clinical single pulse stimulation failing to mimic the endogenous bursting pattern of beta) and presumed ceiling effects on the endogenous presumably saturated beta synchronisation (Brown, 2007; Brown and Eusebio, 2008). A further study by the same group, using cortical *alternating* current stimulation at 20Hz (more similar to the natural oscillations occurring in the brain) found a consistent but similarly small effect on movement in healthy controls (Pogosyan et al., 2009). However, similar alternating current interference during a go/ no-go task reduced peak force and peak rate of force development by a dramatic 35% specifically during partially responded no-go trials (Joundi et al., 2012). Similar changes were not apparent with gamma stimulation, providing strong evidence for the role of beta oscillations in the inhibition of motor responses.

1.3.4.3 Theta-alpha oscillations and their relation to dystonia and dyskinesias

Several studies have also suggested that there is excessive synchronisation at less than 10Hz, in the alpha-theta range, in the pallidal LFP of patients with dystonia (Liu et al., 2002; Silberstein et al., 2003). Activity in this range in the basal ganglia has been implicated in the integration of sensory and motor signals (Bland and Oddie, 2001; Gengler et al., 2005) in keeping with the proposed abnormal mechanism behind dystonia.

One quirk of dystonia is that patients often have a ‘sensory trick’. The act of touching a specific part of the body (usually near the dystonic muscle) somehow temporarily suppresses dystonic movements. As predicted, the theta signal transiently abates during a sensory trick (Tang et al., 2007). It also seems that the specific frequency characteristics of this signal are linked to activity in the dystonic muscle itself (Chen et al., 2006a), and that activity appears in the pallidum before the dystonic muscle, suggesting a driving role for the theta activity (Foncke et al., 2007).

A similar correlation between levodopa-induced dyskinesias and theta activity in the local field potential has also been noted, suggesting that this abnormality may be common to conditions associated with excessive movements (Silberstein et al., 2003; Alonso-Frech et

al., 2006). After receiving dopaminergic medication, beta activity in the basal ganglia is suppressed in patients with Parkinson's disease, but as patients' dyskinesias supervene, activity in the theta range increases, as does that at frequencies of 60 to 95 Hz, a range called high gamma (Silberstein et al., 2003; Alonso-Frech et al., 2006). However, so far there is little evidence that stimulation of components of the basal ganglia at these frequencies causes dystonia or dyskinesias.

1.3.5 Characterising cortico- basal ganglia circuit activity in humans with PD

Although neuronal activity in individual regions of the basal ganglia circuit can be linked to symptoms in PD, it may be more informative to compare symptoms to the simultaneous activity in multiple regions. In this way, individual variation in symptoms can be accounted for not only by the degree of pathology in one region, but also by the compensatory activity of other parts of the network. Put another way, PD symptoms and treatment effects may be more accurately explained by emergent properties of cortico - basal ganglia connectivity. However, characterisation of these networks requires the simultaneous acquisition of temporally precise data from multiple points in the brain. This is difficult and so far human research has relied upon indirect measures, such as blood oxygenation, or measured distant neuronal activity at the cost of poor spatial resolution (i.e. electroencephalography). Additionally, computational models based on this data have focused on modelling single cortico - basal ganglia networks, and have not considered the role of separate limbic, associative and motor circuits and their presumably different roles in symptom generation (Bar-Gad et al., 2003; Humphries et al., 2006).

1.3.5.2 Functionally distinct circuits are spatially segregated

A large body of evidence has built up linking the function of segregated basal ganglia circuits to their anatomical underpinnings. Regions within the ventral circuits are involved in reward-based, addictive and re-inforcement behaviours (Schultz, 1997; Everitt et al., 2001; McClure et al., 2003; Knutson and Cooper, 2005; Delgado, 2007). Central regions have been implicated in set-shifting, response inhibition and working memory (Postle and D'Esposito, 2003; Crottaz-Herbette et al., 2004; Garavan et al., 2006; Monchi et al., 2006), whilst dorsolateral regions have been implicated in movement (Kuhn et al., 2005; Alonso-Frech et al., 2006). In fact a meta-analysis of 126 functional magnetic resonance imaging (fMRI) studies in which task subtractions revealed peak activations in the basal ganglia was in

keeping with this anatomically suggested structure (Postuma and Dagher, 2006). In addition, parietal cortex and insula seemed to be activated more often than predicted by anatomical models, and orbitofrontal cortex and anterior cingulate cortex less, but this could be due to task - specific bias.

However, these studies focused on regional activation during task and medication conditions and did not explicitly characterise *network* activity in different circuits. The latter can be characterised by calculating functional connectivity, which is the degree of correlation between spatially distant neuronal activity (Friston et al., 1993). A greater degree of correlation implies 'shared information' between the two regions i.e. a functional connection. Di Martino et al. examined functional connectivity between the striatum and cortex in healthy controls at rest using fMRI (Di Martino et al., 2008). The results were consistent with preceding anatomical data on the striatum in that, approximately, ventromedial striatum connected to the orbitofrontal area, the 'central' striatum with the dorsolateral prefrontal cortex and the dorsolateral striatum with motor areas. However, functional correlation suggested that there was much greater overlap and therefore integration between these circuits than previously thought. Dopamine strengthened connections from the putamen to the cerebellum and brainstem, and from the ventral striatum to the cingulate in healthy controls, but weakened connectivity between the caudate and a more widely distributed cortical network (Kelly et al., 2009). In keeping with and extending these findings, patients with PD had reduced posterior putamenal connectivity to the cingulate cortex, postcentral gyrus, parietal operculum, prefrontal cortex and temporal area (Helmich et al., 2010). Interestingly, cortical connectivity to the anterior putamen actually increased (Helmich et al., 2010).

In summary, as well as confirming previous anatomical data regarding fronto-striatal connections, functional studies in humans also point to the importance of other areas such as the brainstem, temporal and parietal lobes. Although, these spatially defined functional circuits may provide a substrate for different features of motor and cognitive processes, they rely on indirect measures of neural activity, have poor temporal resolution, and struggle to characterise connectivity from small, but important, structures such as the STN.

1.3.5.3 Cortico - basal ganglia circuits are frequency specific and dopamine sensitive

An alternative approach is to characterise the functional connections underlying basal ganglia-cortical circuits in terms of the degree of neuronal synchronisation between spatially

distributed neuronal populations (Fries, 2005). The oscillatory LFP activity of two brain regions can be correlated by the degree to which they share a consistent phase relationship (Buzsaki and Draguhn, 2004; Fries, 2005). This measure, called coherence, assumes that the two regions are synchronised at a specific frequency (Fries, 2005). Recordings from PD patients undergoing surgery for DBS demonstrate prominent coherence between different components of the cortico - basal ganglia circuit (Brown et al., 2001; Williams et al., 2002; Fogelson et al., 2006; Lalo et al., 2008). These studies have shown that PD patients have coherence between STN and GPi in the beta band, and that this is reduced with dopamine (Brown et al., 2001). Coherence between cortical EEG and STN or GPi is present in different frequency bands, is differentially distributed over the cortex depending on frequency, and has different responses to dopamine. Alpha-theta (2-10Hz) and beta (10-30Hz) band coherence are strongest and beta frequencies are predominantly midline (Williams et al., 2002; Fogelson et al., 2006). The role of dopamine is less clear at these frequencies although there is some suggestion that it may increase gamma (70-85Hz) coherence (Williams et al., 2002; Lalo et al., 2008). Whether this coherence is pathological, remains unclear, although animal data suggests there may be abnormally increased coherence in PD (Sharott et al., 2005b; Mallet et al., 2008). Electrical stimulation of the STN has suggested that cortico –basal ganglia loops may have resonant frequencies (Eusebio et al., 2009) leading to the intriguing hypothesis that the abnormally synchronised beta activity may be due to the failure of normal dopaminergic activity to suppress the system's resonant properties. However, significant coherence at different frequencies may not necessarily occur only through this mechanism. Recently it has been shown that theta-alpha coherence occurs between cortical EEG and the STN, and that this coherence correlates with the presence of dyskinesias and impulse control disorders associated with PD (Rodriguez-Oroz et al., 2011). Interestingly, this paper suggested that coherence in spatially different motor and associative-limbic circuits was related to dyskinetic and impulse control symptoms respectively.

In summary the spectral range, and cortical and subcortical distributions, of synchronised neuronal activity may be promising criteria by which distinct cortico-basal ganglia circuits may be disambiguated: the hope being that distinct circuits would correspond to distinct symptoms in PD. However, a clear relationship between the spectral range and cortical distribution of basal ganglia-cortical connections has proven difficult to establish in the EEG studies made to date. This is because scalp recording sites are necessarily very limited in peri-operative patients and the scalp topography of the EEG is deranged by the presence of burr-holes (Benar and Gotman, 2002; Oostenveld and Oostendorp, 2002). We use

simultaneous subcortical LFP and high-density MEG recordings to overcome this limitation (see section 2).

1.4 Quantifying cognitive functions: a psychological perspective

To identify the moment-to-moment cortico-basal ganglia activity underlying symptoms we must have an appropriate *dynamic* measure of the symptoms. This is easier for motor symptoms such as tremor (where we can use tremor amplitude and frequency) and even bradykinesia (where we can use reaction time as a surrogate), but more difficult for cognitive symptoms in PD such as slowness of thought processes (bradyphrenia) and changes to the way patients make decisions. In addition, day-to-day behavioural symptoms that patients complain of (such as difficulty preparing meals) require many mental processes in parallel, and as a consequence, a similar behavioural symptom may be caused by different patterns of neuronal dysfunction. However, psychologists and motor control theorists have, over the last century, attempted to fractionate day-to-day behaviours into a hierarchical structure of simpler 'cognitive' and motor sub-components.

From the time of Sherrington, evidence existed that actions (in this case spinal reflexes) were modulated by descending projections in the nervous system (Sherrington, 1925). This lead to the development of the idea that more complex actions could also be explained in terms of a system of hierarchical modulations, in order to achieve goals (e.g.(Craik, 1947)). 'Higher levels' in such a system would represent the *cognitive* processes that would 'control' lower level motor actions. The theoretical structure of such a system was formalised by Logan and Cowan in 1984 (Logan and Cowan, 1984). It consisted of an *executive* system that formed the behavioural, goal-directed intention and issued commands, and a *subordinate* system, that interpreted and carried out the commands. Postulated acts of executive control could include remembering things, predicting future events and redirecting attention. However Logan and Cowan focused on dynamically measuring the ability to *inhibit* actions. They formalised this measure using the stop-signal experimental paradigm, which crucially does provide trial-to-trial variation in behaviour that can be used to interrogate the function of neuronal networks (Logan and Cowan, 1984). Therefore in order to understand the neuronal network dysfunction responsible for the cognitive symptoms of PD, we need to rely on intermediary psychological models of behaviour, rather than focus on the symptoms themselves.

1.4.1 Response interference and inhibition

The terms 'inhibition', 'interference' and 'suppression' have been used by many psychological theorists and cover a broad range of behaviours (Harnishfeger, 1995). Mentioned by prominent psychologists such as James and Luria (James, 1890; Luria, 1961),

the term inhibition has been used to refer to the inhibition of motor behaviours, the inhibition or suppression of urges and the inhibition of other thoughts.

In this thesis, we restrict the term 'inhibition' to mean the last-minute prevention of a prepared motor act, or the replacement of such an act with something else. Early behavioural evidence suggested that inhibition and interference were a dissociable component of cognitive control during experimental paradigms such as the psychological refractory period (PRP) or dual-task paradigm (Welford, 1952). In this paradigm, subjects are asked to perform two separate responses to two closely presented stimuli. The reaction time for the second stimulus is consistently increased compared to the first (called interference), and this increase is greater if the stimuli are close together. However, if subjects were asked to *replace* the response to the first stimulus with a response to the second, the reaction time of the second response was relatively reduced. Therefore, inhibition of the first response allowed performance of the second to be quicker. Pioneering studies experimented with response inhibition by using a stop-signal (Vince, 1948; Lappin and Eriksen, 1966), but these stop-signal tasks was eventually mathematically formalised by Logan and Cowan in 1984 as a horse-race model (Logan and Cowan, 1984).

1.4.1.1 The stop –signal paradigm

Logan and Cowan aimed to design an experimental system where one could measure the length of time it took to inhibit an action or thought (Logan and Cowan, 1984). By comparing such times between subjects and experiment types, one could also infer the relative difficulty of inhibiting different behaviours – tasks that were more difficult to control, would require a longer period of time to inhibit. However, such a measurement is not trivial because successful inhibition necessarily has no behavioural marker, and therefore a straightforward measurement of the 'inhibition reaction time' is not possible. However, given certain assumptions, it is possible to infer this measurement in the following way using the stop-signal paradigm.

In the classic stop-signal task, subjects are asked to respond to an intermittent visual cue by pressing a button with their right hand, as quickly and accurately as possible. This part of the experiment is termed the primary task. During a randomly selected minority of trials (usually 25 - 30%), an audible tone is heard at a specified delay after the initial primary task cue. This tone, called the stop-signal, instructs the subjects to abort the primary task (i.e. withhold pressing the button) if possible. It follows that the ability to successfully inhibit the primary task depends on two crucial factors. Firstly, it depends on the reaction time of the primary

task, and secondly it depends on the delay between the primary task cue and the stop-signal (called the stop signal delay (SSD) or the stimulus onset asynchrony (SOA) – we shall use the later term). By repeating the task many times at a fixed SOA, the experimenter could empirically determine the percentage (and therefore probability) of stop-signal trials where the primary task was executed (i.e. inhibition failed). Then, by varying the SOA systematically, the probability of inhibition failure (equal to 1-probability of inhibition success) could be determined as a function of SOA. This function is sigmoidal and termed the inhibition function (see **Figure 3**).

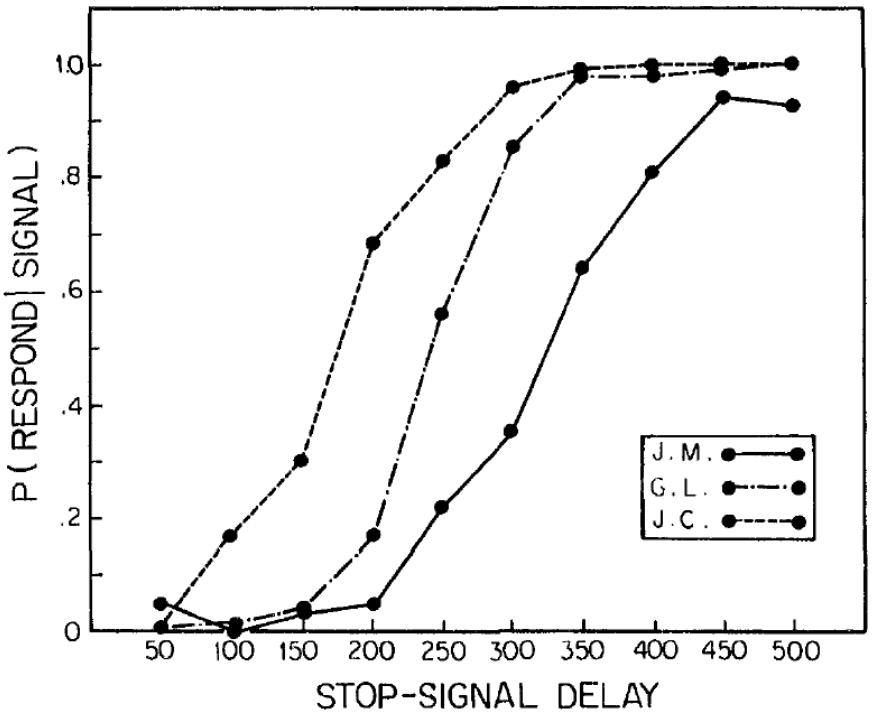

Figure 3: The inhibition function. *The empirically determined probability of response (i.e. inhibition failure) on stop-signal trials as a function of SOA (termed stop-signal delay here) in ms is displayed for 3 subjects. For all subjects, as the SOA increases (and therefore the time between the stop-signal and response decreases), the probability of failure increases in a sigmoid. This sigmoid function is the basic, non-normalised 'inhibition function'. Reprinted from Logan and Cowan (1984) with permission from the American Psychological Association.*

Additionally, by examining the reaction times of stop-signal trials with a response (failed inhibition trials), they were able to determine that such trials terminated quicker than the average primary task reaction time, and that such trials lengthened if the SOA lengthened. To explain these findings, Logan and Cowan proposed the horse-race model of inhibition,

and under the assumptions of such a model, more substantial inferences could be made from the same data (Logan and Cowan, 1984).

1.4.1.2 The horse-race model

This models reaction time data from the stop-signal experiment as resulting from two competing behavioural processes. The primary task (in this case pressing a button in response to the visual cue) and the stopping process race against each other. The outcome is determined by the winner of the horse-race i.e. whichever process is the first to finish. This idea is consistent with the behavioural findings – e.g. a short SOA, would mean that the primary task had had less time to progress and was therefore more likely to be inhibited.

Under the assumptions of the horse-race model, we need only two parameters (the primary task reaction time distribution, and the probability of inhibiting a response at a certain SOA) to estimate a third parameter – the stop-signal reaction time (SSRT). The stop-signal reaction time is a measure of the time it takes to successfully inhibit the primary task. Tasks with longer SSRTs are more difficult to control, hence SSRT was originally designed to be able to determine how difficult a task is to control.

The horse-race model, and therefore the estimate of SSRT, depends on a number of key assumptions hinging on the fact that the stop and go processes are independent.

The first assumption is that the primary task reaction time distribution is contextually independent of the stop-signal. In other words, the primary task reaction time distribution would be the same during a stop-signal trial, and during a trial without a stop-signal.

A second assumption, in some forms of analysis, is that the SSRT is a fixed value without a distribution. This is merely for convenience. A fuller model, where SSRT is modelled as a Gaussian distribution, is approximated reasonably well with this simplification (Logan and Cowan, 1984).

Thirdly it is assumed that the SSRT does not vary with varying SOA. In practice this assumption is threatened by the idea that go and stop processes may share limited neural resources (so interfere with each other). However the implications of this idea are that when the stop-signal occurs, it would divert resources away from primary task, and so stop signal-respond reaction times should be longer than no-signal reaction times, which is not the case. Additionally the longer the stop-signal delay, the longer the interference of the primary task, and therefore longer the predicted RT of signal-respond trials. Again this is not the case as stop signal-respond reaction time estimates increase with SOA.

Finally, in some methods of analysis, it is assumed that subjects do not guess. When guessing, the subjects decide to respond or not at the start of the trial. In this case, the probability of stopping on no-signal trials should be around ~50% which is not the case. A more subtle version of this is if they guess only on a certain proportion of the trials. In this case, the proportion of guesses is the same for no-signal and signal trials and so the primary task and stop-signal respond reaction time distributions will be noisier. One can see if this is the case as the lower bound of the inhibition function (see later) will not be zero, even if the stop signal is sufficiently early. A proportion of zero SOA trials will be guessed and therefore will have a response.

1.4.1.4 Different methods to estimate SSRT

The stop-signal task was initially performed with the SOA varying by a fixed interval between blocks. However, this allows the subject to predict the presence of a stop-signal. More recent experiments vary the SOA on a trial-by-trial basis to reduce the predictability of the timing and presence of a stop-signal. In addition, the SOA is varied according to a tracking staircase which aims to keep the probability of responding correctly at around 50%. This has several advantages: it efficiently samples an equal number of stop-fail and stop-success trials, it automatically adjusts for differences in SSRT between subjects, and it increases the difficulty of the task in subjects that strategically wait for the stop-signal. Different methods of mathematically determining the SSRT have been proposed and tested against each other (Logan and Cowan, 1984; Band et al., 2003; Boehler et al., 2012; Congdon et al., 2012). Although relatively robust as a measure, certain methods may poorly estimate the SSRT in certain conditions.

The principles underlying the relationship between the primary task reaction time distribution, the SOA and the SSRT are shown in **Figure 4**.

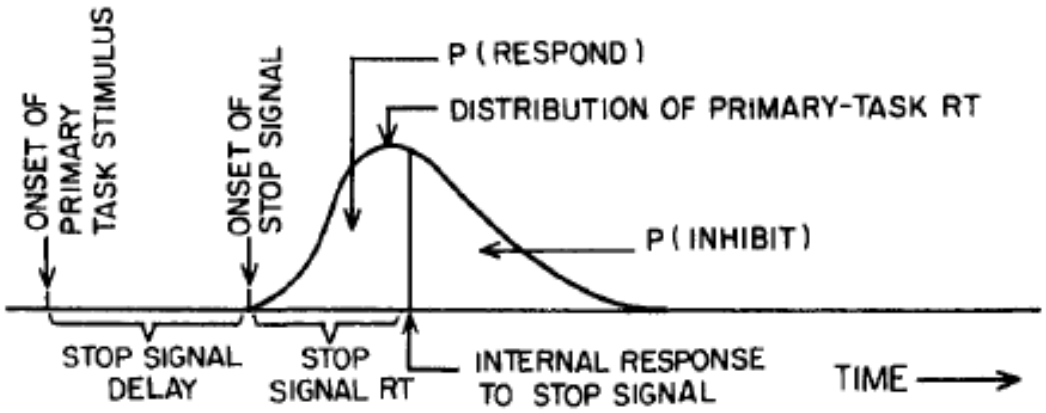

Figure 4: The horse-race model. *The probability of response (y axis) is plotted against time (x axis). The response distribution of the primary task can be seen as a skewed distribution. Overlaid onto this are the events during stop-signal trials with a fixed SOA (termed SSD here). Given a fixed primary task reaction time distribution, a fixed SSD and a fixed SSRT, the likelihood of successfully stopping can be calculated. In practice, the first and second parameters are empirically measured so the third can be calculated. Reprinted from Logan and Cowan (1984) with permission from the American Psychological Association.*

The mathematical formalisation of the above model is shown in **Equation 1.**

$$P_r\,(t_d) = \int_{-\infty}^{t_s+t_d} f(t)dt.$$

Equation 1: Mathematical Formalisation of the horse-race model. *Where* ***T****=the mean primary task reaction time;* ***f(t)*** *= the distribution of primary task reaction time;* $\boldsymbol{P_r}$ *= the probability of response;* $\boldsymbol{P_r\,(t_d)}$ *is the probability of response at given SSD* $\boldsymbol{(t_d)}$*;* $\boldsymbol{t_s}$ *= stop signal reaction time (internal stopping process and ballistic phase of response). In this case a response is a failure to stop.*

For a given stop-signal delay, and primary task reaction time distribution, the probability of a response (i.e. failure to stop) is the integral of the primary task distribution with respect to time, from –infinity to the time point when stop process finishes. Therefore $\boldsymbol{t_s + t_d}$ is the time point at which the cumulative integral of the primary task reaction time distribution is equal to

$P_r(t_d)$. Because we empirically know $P_r(t_d)$ for a range of t_d, then this provides a range of SSRTs (t_s) as a function of stop-signal delay. Alternatively, the SSRT is equivalent to the rank ordered primary task reaction time that corresponds to $P_r(t_d)$. For example if $P_r(t_d)$ =0.3, $t_s + t_d$ is equivalent to the 30th percentile quickest trial.

The integral method (or quintile method) of SSRT calculation uses the probability of inhibition and primary task RT to calculate an SSRT value at each SOA. These values can be used to determine the relationship between SOA and SSRT, or more commonly averaged to obtain a single SSRT estimate. This method assumes no variance in SSRT and needs lots of data at each SOA to estimate this (Band et al., 2003).

Alternatively, the average method assumes that the SOA is sampled around its mean (e.g. from a tracking algorithm, or because skews in the data have been corrected by discarding a proportion of trials). Therefore the SSRT is simply the average SOA subtracted from the primary task RT. Recent trends have acknowledged the non-gaussianity of reaction time data and have used the median rather than the mean. This method requires less data to estimate the SSRT but provides only one parameter per inhibition function (Band et al., 2003).

Band et al. suggested that 30-50 trials were needed to reliably estimate SSRT using tracking, and 50-100 without using tracking (Band et al., 2003). A more recent study has suggested that the quintile method is more accurate still, because it does not assume central sampling and is able to use more of the data (Congdon et al., 2012).

1.4.2 Factors modulating the stop-signal reaction time

1.4.2.1 The effect of stimulus characteristics

Converging evidence suggests that the overall the SSRT is relatively resistant to variations in stimulus characteristics (Verbruggen and Logan, 2009a). Conflicting data suggest that either visual cues produce faster primary task reaction times and faster SSRTs (by over 100ms) than auditory cues (Cabel et al., 2000) or that they produce SSRTs close to that associated with auditory stop signals (Colonius and Arndt, 2001; Ozyurt et al., 2003). However, this may be because of stimulus *intensity* rather than stimulus modality. Morein-Zamir and Kingstone found that mean saccadic SSRT was faster in trials with high intensity (SSRT=87ms) as opposed to low intensity (SSRT=110ms) visual stop-signals and additionally saccadic SSRT was faster in high intensity (SSRT=121ms) as opposed to low

intensity (SSRT=154ms) auditory stop-signals (Morein-Zamir and Kingstone, 2006). Hence apparent differences between auditory and visual stop signals may be due to confounding mismatch between the auditory and visual stimuli used. This is consistent with another recent study in which the SSRT was faster with an auditory rather than a visual stop-signal, but even faster for a louder stimulus (Van der Schoot et al., 2005). Primary task latencies are also faster to more intense stimuli (Reuter-Lorenz et al., 1991; Kingstone and Klein, 1993).

Placement of the stop-signal in the visual field has also been investigated. Armstrong and Munoz found shorter SSRTs if the stimulus was presented to the fovea, rather than in the peripheral visual field, but Asrress and Carpenter found no difference between these conditions (Asrress and Carpenter, 2001). One study found that SSRTs were quicker if the stop-signal was presented in the right, rather than left, visual field (Van der Schoot et al., 2003) but this has not been repeated.

The visual context, and the presence of distracters may have a non-specific lengthening effect on the primary task reaction time and also sometimes the SSRT. Morein-Zamir and Kingstone found that providing a gap between the presentation of the fixation cue and the presentation of the go cue (visual or auditory) resulted in ~10ms increase in saccade latency but not SSRT (Morein-Zamir and Kingstone, 2006). Co-presenting incongruent distractor information at the time of the go signal increased in primary task reaction time and also SSRT (Kramer et al., 1994; Ridderinkhof et al., 1999) . Some authors conceptualised this as focal inhibition (distractor processing) and global inhibition (stop-signal processing) (Ridderinkhof et al., 1999). Verbruggen et al. did find a dissociation between the effects of flankers on primary task reaction time and on SSRT: flankers non-specifically caused slowing down of primary task whereas SSRT lengthened only after neutral or incongruous flankers, suggesting that the interference occurs early during processing of the flanker signal (Verbruggen et al., 2004, 2006).

1.4.2.2 The effect of response characteristics

Stop signal reaction time estimates are remarkably similar (mean ~200ms) for different tasks such as typewriting and button pressing (Logan and Cowan, 1984) and reaching arm movements (Mirabella et al., 2006), although they are notably lower for saccadic countermanding (Hanes and Carpenter, 1999; Cabel et al., 2000). Saccades have shorter

SSRTs, possibly because the a visual stop-stimulus directly activates fixation neurons in the superior colliculus (Munoz and Wurtz, 1993). In addition, hand movements have a larger ballistic component (the time after which, if the response is initiated, it cannot be stopped) and there is greater ambiguity of hand responses (eyes just have to maintain fixation). However the idea of a ballistic phase has recently been challenged because EMG of arm movements have detected partial responses, not just instantaneous stops (McGarry and Franks, 1997). However both saccadic and hand response inhibition can be modelled by a horse-race (Logan and Irwin, 2000).

SSRTs estimates from stop-signal experiments are also roughly similar to SSRTs estimated from tasks requiring the stopping of on-going activity, such as continuous target pursuit (Morein-Zamir et al., 2004) speech with nonsense words (150-200ms) and saying single letters (Xue et al., 2008). Response side also does not affect SSRT: the SSRT to a centrally presented cue, is the same for left and right hand movements, regardless of faster right hand reaction time (Mirabella et al., 2006). However consistently crossing the side of visual stop and go signals with the required arm response results in an increased primary task reaction time and also increased SSRT (Mirabella et al., 2006).

1.4.2.3 The effect of subject characteristics

The primary task reaction time and SSRT is the same in men and women, although one study suggested that, in spite of this, the underlying neural correlates are different (Li et al., 2006). Initial studies failed to reveal differences in performance between children and adults (e.g. (Band et al., 2000)), however, studies using larger sample sizes and tracking algorithms have found a statistically significant elevated SSRT in younger children (e.g. (Williams et al., 1999; van den Wildenberg and van der Molen, 2004), even when accounting for the faster primary task reaction times (Ridderinkhof et al., 1999; Williams et al., 1999). The mean SSRT has been reported to be 305 ms in 6-8yr olds and 188 ms in adults in the same study, although the differences in SSRT are correlated with global reaction time changes (Ridderinkhof et al., 1999). There is weaker evidence that SSRT lengthens in older age (Williams et al., 1999) as compared to other psychological tasks (Kramer et al., 1994).

The stop-signal task has also been studied in people with impulsive personality traits (Logan, 1997; Stahl and Gibbons, 2007) and patients with obsessive-compulsive disorder (Chamberlain, 2006; Penades et al., 2007). Most consistently, SSRT is lengthened in children with attention deficit/hyperactivity disorder (ADHD) compared to control groups (Lijffijt and Kenemans, 2005). Adults with ADHD also show longer SSRTs compared to

control groups (e.g., (Aron and Dowson, 2003; Ossmann and Mulligan, 2003). The effects of Parkinson's Disease on SSRT will be discussed in section 1.5.4.

1.4.3 Modifications to the stop-signal task

1.4.3.1 The stop-change task

The stop-change task (also called the change-of-plan task) is very similar to the stop-signal task except that in response to the stop-signal (now called the change signal), the subject is required to make an alternate response. For example, on a trial where the primary instruction is to press a button with the left hand, if a change signal occurs on the trial, the subject is required to withhold the left button press *and then* press a button with the right hand.

Here, it will be helpful to make a distinction between the task-switching paradigm, the Psychological Refractory Period PRP paradigm, and the stop-change paradigm. The first important difference is temporal overlap: task-switching tasks (Jersild, 1927) present one stimulus on each trial and require switching tasks *between* trials. The PRP paradigm, (Telford, 1931; Welford, 1952), the stop-signal paradigm (Vince, 1948; Lappin and Eriksen, 1966; Logan and Cowan, 1984), and the stop-change paradigm (Logan and Burkell, 1986; Brown and Braver, 2005; Nachev et al., 2007), require response switching *within* a trial, as instructed by closely placed go and stop/change stimuli. Furthermore, there is a crucial difference between the PRP paradigm and the stop-signal paradigm: when the first and second stimuli (go1 and go2 in the PRP paradigm, go and stop in the stop-signal paradigm) are closer together, the go2 reaction time is longer in the PRP task, whereas the SSRT is shorter. This is consistent with the idea that in the PRP paradigm, because both responses are needed, the processing of the first response interferes with processing of the second response. Therefore if the stimuli for response one and response two are close together, there is greater temporal overlap, greater interference and a longer reaction time for response two. This is in contrast to the stop-signal paradigm, where the stop-signal *inhibits* the first response. If the go and stop signals are close together, the primary task response is less prepared, easier to cancel and therefore the SSRT is shorter. Therefore the stop-signal task can be modelled as a horse-race between two independent (as opposed to interfering) processes.

Logan and Burkell studied the stop-change task, and found that behaviour on this task was concordant with the stop-signal task (i.e. a horse-race) rather than the PRP task (Logan and Burkell, 1986). This raises a couple of questions: firstly whether changing a response is a unitary act of control (rather than separate acts for stopping and switching) and secondly, if separate, do the stop and switch processes occur in parallel or in series. Verbruggen et al. used a stop-signal followed by a change signal with two varying SOAs (go signal to stop signal and stop signal to change signal) to attempt to dissect out whether the changing is a unitary act, or put another way whether the primary task is simply stopped by preparation of the secondary task (Verbruggen et al., 2008b). They found that their data were the most consistent with a model that required a three part go-stop-change process with essentially a serial (or a weighted parallel model, with most of the weight of processing occupied by the stopping process) order of processing. However, in order to do this, they *a priori* assumed that the subjects strategically deferred stopping until after they had seen the change signal – therefore they biased the conclusions of their paper towards favouring models with three separate go-stop-change functions (Verbruggen and Logan, 2008, 2009b; Verbruggen et al., 2008a). In addition, they found that the SSRTs estimated with the stop-signal task were slightly shorter (206ms) than those estimated by the stop-change task (250ms), although SSRT was collapsed across SOAs and tracking was not used to ensure the data were centrally sampled. Similarly another study found that the SSRT was longer during the stop-change task, although changing required the use of a different effector (the foot) to going (De Jong et al., 1995). Therefore any differences between SSRT from stop-change and stop-signal trials remain equivocal. This lead to the idea that the response to the stop-signal was privileged: it was relatively fast, automatic and it did not need to share neural processing resources with 'go' processes (i.e. did not suffer from dual task interference) (Verbruggen and Logan, 2009b).

If both stop-change and stop-signal tasks share a similar underlying inhibition process, then why is the stop-change task needed? Indeed very little recent research has been undertaken with the stop-change task. However there is always a measurable response in the stop-change task. This has potential benefit in patient populations who may struggle with the task or who may have significant lapses of concentration. A lapse of concentration may inappropriately translate into successful response inhibition in the stop-signal task, whereas these trials could be excluded if the subject were to perform a stop-change task.

1.4.3.2 The LATER model

Attempts to relate behaviour and neuronal activity lead to fuller models of response inhibition. Aside from debates about the differences between the stop-change and stop-signal task, it was clear that both could be modelled as two (or possibly three in the stop-change task) competing processes in a horse-race. This race model was implemented more fully as the linear rise to threshold (LATER) model (Hanes and Carpenter, 1999). The original horse-race model was restricted to modelling the *finishing* times of the primary task and the inhibition process i.e. their latencies, and not the processes themselves. It had no memory of what happened on the previous trial and could not explain trial-to-trial variation in the probability of responding. The LATER model explicitly models the go and stop processes as linear functions. Crucially, the rate of rise, and the starting point of these functions varies between trials in a stochastic manner and can be used to explain the effects of prior beliefs (such as an increase in the frequency of the stop-signal would result in an increased starting point). Additional models which have been used include variants of stochastic accumulator models which have been developed by signal detection theorists. These models have three parameters that define competing go and stop processes: the *onset* of accumulation, the *rate* of accumulation, and the *threshold* of accumulation (Ratcliff and Smith, 2004). Control signals such as errors, response conflict, and stop-signal expectancy vary these parameters and alter primary task reaction time. For example delaying the onset increases primary task reaction time without affecting accuracy whilst reducing the rate increases reaction time whilst reducing accuracy.

1.4.4 Strategic adjustments in reaction time

In addition to the time taken to stop or cancel a response (the SSRT) recent research has also investigated how subjects strategically vary their behaviour on the primary task, during the stop-signal paradigm. Intuitively subjects have to balance against speed (going) and caution (stopping). Reaction time variation of the primary task has been categorised into strategic change (a change prescribed before the stop-signal is presented) and reactive change (the change in the primary task reaction time after a stop-signal has been presented). Strategic changes are thought to be partly due to expectation of the stop-signal. Therefore subjects tend to slow on the first few trials of the paradigm, even if they are all go only trials (Verbruggen and Logan, 2009b) and also if stop signals occur more frequently (Logan and Burkell, 1986; Emeric et al., 2007).

The characterisation of reactive changes has been more variable. Studies have reported greater post stop-signal slowing after successfully inhibited trials (Emeric et al., 2007), after failed inhibition trials (Schachar et al., 2004), or after both (Rieger and Gauggel, 1999). This variation is partially explained by Nelson et al, who found that slow fluctuation in primary task reaction time contaminated estimates of post stop-signal changes in reaction time (Nelson et al., 2010). Depending on the reaction time changes, different hypotheses have been put forward to explain them including conflict detection, error detection, surprise detection etc.

Bisset et al evaluated five different theories for strategic changes in primary task reaction time during variants of the stop-signal task (Bissett and Logan, 2011). They corrected slow fluctuations in the reaction time data by subtracting the reaction time of the previous go only trial from the post stop-signal trial. They found stop-signal slowing after both successful and unsuccessful stop trials and were thus able to reject theories based on error detection (slowing only after stop-fail trials) and response conflict (slowing greater on successful trials, as by definition, successfully stopped trials must have the highest conflict). Additionally, they confirmed that post-stop-signal slowing is greater if the frequency of stop-signal trials is increased, arguing against the surprise theory (the rarer the event, the greater the change in reaction time). Their results were compatible with two hypotheses which were not mutually exclusive. Firstly that after seeing any stop-signal, the subject is more cautious – the goal priority hypothesis. Here the goal priority varies between going and stopping after each trial. Secondly they found post stop-slowing after a repeated go cue only, and more so if the subject had successfully stopped. This suggested that the previous go stimulus – stop stimulus mapping was still partially active and interfered with the next trial, a hypothesis they called the memory hypothesis. Finally a separate experiment suggested that the difficulty of the task as measured by the probability of failure also increased post stop-signal slowing. However, this study also had limitations, in that the hypotheses tested were not mutually exclusive and were not tested in combination. For example although the data could not have been explained by either conflict or error detection alone, it can be explained by both theories used in combination together (Bissett and Logan, 2011; Yamaguchi et al., 2011).

However consistently across studies, changing goals, or switching stimulus-response mappings have been implicated in explaining primary task reaction time behaviour in the stop-signal task (Verbruggen and Logan, 2008; Leotti and Wager, 2010).

1.5 The neural correlates of response inhibition

The stop-signal task is able to isolate a measure, the SSRT that corresponds to the time it takes to stop an action. If SSRT is relatively constant across tasks, then this raises a question: are different actions inhibited by a similar brain network? Many studies have tried to address this issue, but there are significant methodological limitations to most: correlating brain activity with behaviour is not straightforward.

1.5.1 Lesion studies

First we will review some of the most convincing data, which is from human lesion studies. Early reports suggested that the damage to the frontal lobes may result in apathy or impulsive behaviour (Damasio et al., 1994). However, using the stop-signal paradigm in patients with frontal lesions, Aron et al. found that lengthening of the SSRT correlated most strongly with damage to the pars opercularis region (roughly BA 44), also termed the right inferior frontal gyrus (Aron et al., 2003). Rieger et al similarly found that, relative to orthopaedic controls, patients with right frontal and bilateral frontal lesions showed inhibitory deficits (Rieger et al., 2003). Interestingly, patients with cerebrovascular lesions in the basal ganglia were also significantly slower in inhibiting their responses. However, the study also highlights some of the difficulties in making inferences from lesion studies. Firstly the primary task reaction time was globally increased in subjects with any lesion, suggesting that to perform the stop-signal paradigm a subject recruits a large network of brain regions. If one of these regions is damaged, activity of 'healthy' regions may become abnormal to compensate, and therefore behaviour may best be explained as activity across a network of areas. However, lesion studies do provide data that a brain region is *necessary* to perform a particular function.

Similarly, Nachev et al. used a change-of-plan task to detect an increase in SSRT in a single subject with a unilateral pre-SMA lesion. They then performed fMRI to show that the non-damaged pre-SMA was active during the change-of-plan task (Nachev et al., 2007). Additionally studies in rats have shown that lesions to the orbitofrontal cortex, the dorsomedial striatum and the STN all lengthen SSRT (Eagle et al., 2008; Eagle and Baunez, 2010).

Human lesion studies are opportunistic by their nature, and effects of lesion size and subsequent neuronal plasticity make the data difficult to generalise to healthy populations. However temporary 'virtual lesions' of cortical areas can be induced in healthy control subjects by the application of repeated transient magnetic fields, i.e. with trans-cranial magnetic stimulation (TMS). In fact TMS over the right inferior frontal cortex, but not over the medial frontal cortex, or parietal cortex, increased SSRT and error rate (Chambers et al., 2006; Verbruggen et al., 2010) whereas TMS over the pre-SMA has been less consistent. Cai et al found an increased SSRT with TMS (Cai et al., 2012), whereas Verbruggen and colleagues did not (Verbruggen et al., 2010).

1.5.2 Single-cell activity

Further evidence has been obtained from single cell recordings in non-human primates performing the stop-signal task. Hanes et al. used a saccadic stop-signal paradigm to identify cells in the frontal eye field that generated signals sufficient to control gaze (Hanes et al., 1998). Similar signals were also later seen in the superior colliculus (Paré and Hanes, 2003). However, neurons in the supplementary eye field (Ito et al., 2003; Emeric et al., 2008) and anterior cingulate cortex (Ito et al., 2003), that fire specifically during stopping, fire *too late* to be causal, and have been postulated to monitor performance or to reflect error signals.

In contrast, Isoda et al used a change-of-plan paradigm to detect switch-specific signals in the pre-SMA that were early enough to be causal to changing plan (see **Figure 5**). Furthermore, stimulation of the pre-SMA replaced fast incorrect responses with correct slower responses (Isoda and Hikosaka, 2007). The same authors found a similar relationship between switching actions and activity in the subthalamic nucleus (Isoda and Hikosaka, 2008), and postulate a medial frontal – basal ganglia – superior colliculus network mediating stopping (Hikosaka and Isoda, 2010).

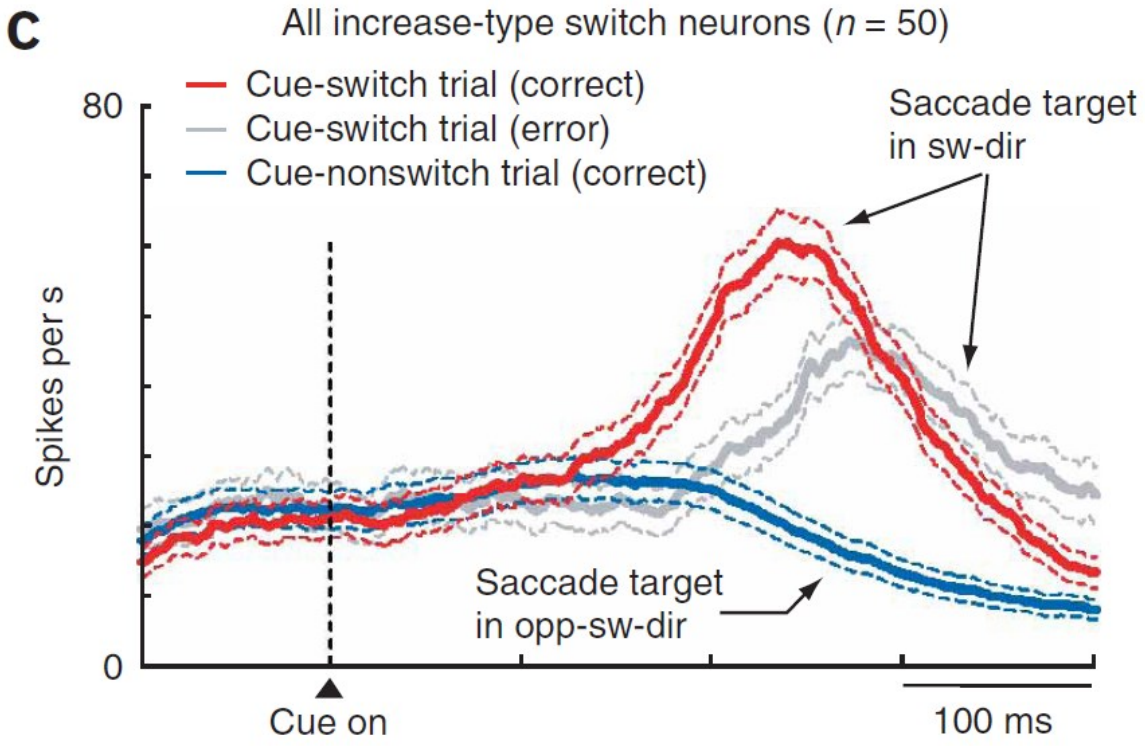

Figure 5: Spiking neurons in the pre-supplementary motor area (pre-SMA) of a rhesus monkey during switching. *Reprinted from* Isoda and Hikosaka, (2007) *with permission from Nature Publishing Group. The vertical axis is spiking density, whilst the horizontal axis is time. This figure shows the average response of 'switch sensitive' neurons in the pre-SMA during three trial types in a switch task. The responses are aligned to the initial cue which may or may not be associated with a valid switch cue. In 'go' trials where no switch is required (blue, labelled cue-nonswitch trial) no spiking response is seen. However, if the monkey successfully switches to a switch signal (red line) there is an increase in spiking. A similar delayed response is seen if the monkey is instructed to switch but fails (grey line).*

1.5.3 Human neurophysiology

Aron and colleagues have used fMRI in humans to consistently reveal a relationship between increased right inferior frontal activity and shorter SSRT (Aron and Poldrack, 2006; Aron et al., 2007a) although not with SSRT and pre-SMA activity.

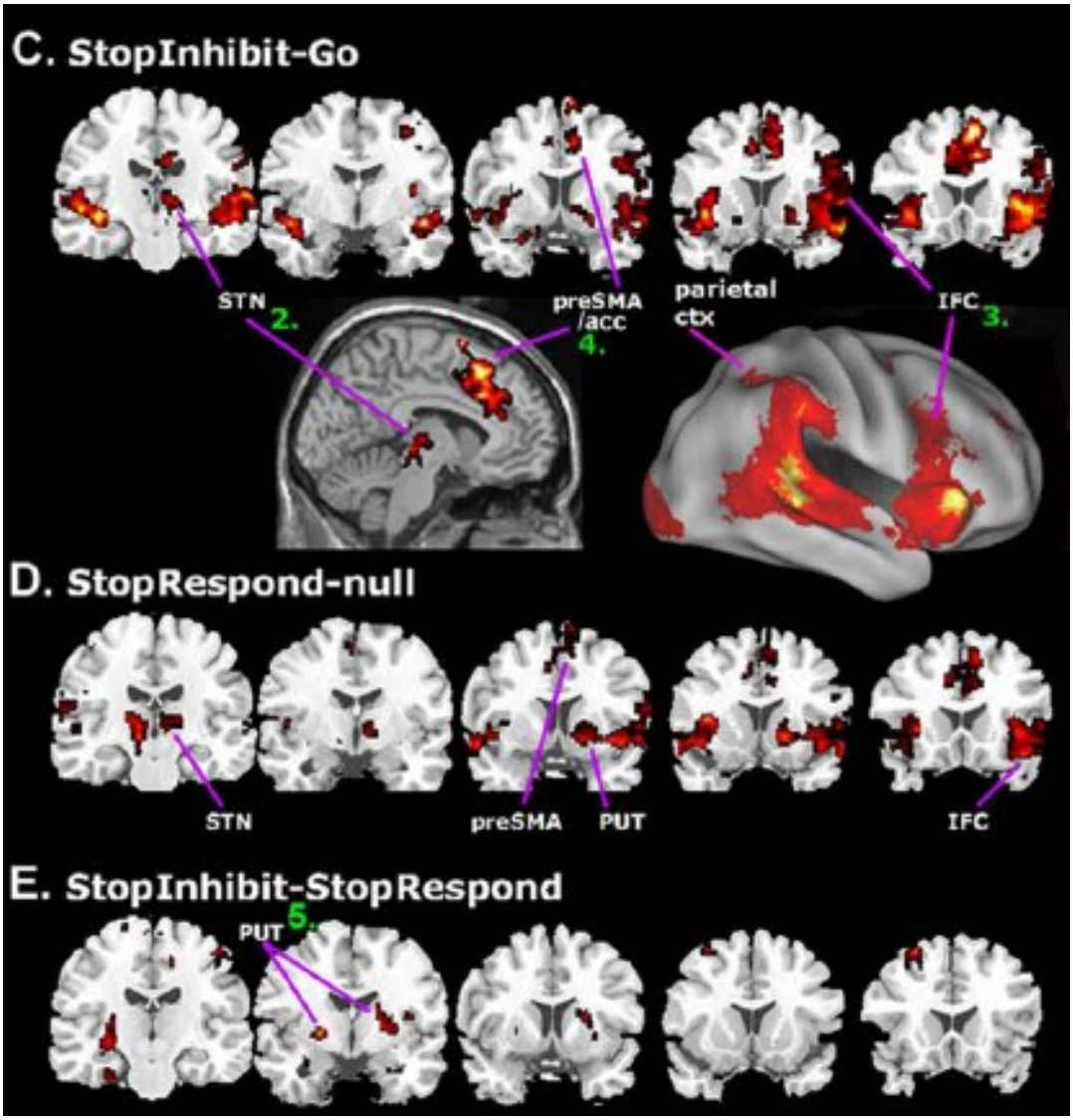

Figure 6: Brain networks activated during the stop-signal task. *Reprinted from* Aron and Poldrack, (2006) *with permission from the Society of Neuroscience. Activations are highlighted in red-yellow (according to their t score – colourbar not shown) and overlayed on a template image of the brain.* ***C:*** *The StopInhibit-Go contrast shows the effect of the stop-signal on brain activation, even though in this case, the stop-signal was not followed. Activated areas include the pre-SMA, anterior cingulate (acc), right inferior frontal cortex (IFC), parietal cortex and a diencephalic region the authors claim is the STN. It is clear that the spatial resolution is too poor to be sure that this is actually the STN, rather than a neighbouring nucleus. Furthermore, the most interesting contrast is* ***E:*** *Stopinhibit-StopRespond. However this contrast shows less convincing activation than other contrasts and is confounded by a movement present in the StopRespond condition which is not present in the StopInhibit condition. Contrast* ***D:*** *StopRespond-null shows all brain areas activated during movement preparation and successful stopping, so inference about the role of any particular brain region is limited. PUT, putamen; ctx, cortex.*

In 2006, Aron et al reported such a study (Aron and Poldrack, 2006). They used an auditory stop-signal that activated a wide cortical and subcortical network (see **Figure 6**). Cortical areas activated included bilateral auditory cortex, pre-SMA, anterior cingulate, parietal cortex, and bilateral orbital/insular cortex extending into the right inferior frontal gyrus. Subcortical structures included the thalamus, putamen, pallidum and STN - although it must be acknowledged that the resolution of fMRI is too poor to definitively demonstrate activity in the STN, and such activity may be related to a nearby structure such as the red nucleus or substantia nigra. The critical contrast of interest here is between successful and failed stop trials – the neural correlate of stopping. However this contrast is difficult because of two reasons. Firstly because failed trials are thought to have slower motor preparation than successful ones (reaction time confound) and because failed trials contain a motor response (movement confound). After accounting for these confounds the authors found no significant areas modulating successful and unsuccessful trials. As a secondary measure, the authors proceeded to compare successful stopping with go trials (to discount the effects of motor preparation). They found that activity in the right IFG, pre-SMA, GP and STN distinguished between these two conditions. In addition, activity of STN correlated only with the rIFG only, and rIFG activity negatively correlated with SSRT (Aron and Poldrack, 2006). Activity in the right IFG and pre-SMA also was consistently activated during the inhibition of nonsense words, single letters and right-handed key presses (Xue et al., 2008) although this study similarly suffered from confounds relating to reaction time and movement. Separate studies have supported the notion that the right (rather than left) IFG modulates stopping behaviour regardless of the hand that was used (Konishi et al., 1999).

Further fMRI studies have used the change task with high and low error rate conditions and found evidence of error monitoring in the anterior cingulate, pre-SMA , right dorso-lateral prefrontal cortex, parietal lobule and cerebellum, however it is unclear if the authors appropriately corrected for reaction time (Brown and Braver, 2005).

Studies with scalp EEG have consistently shown that stop signals are associated with a negative positive (N2P3) potential roughly 200ms – 300ms after the stop signal (Kok et al., 2004; Schmajuk et al., 2006; Dimoska and Johnstone, 2008). The positive component is delayed in unsuccessful trials and starts around ~250 ms after the stop-signal, just around the time of the stop stimulus – so it is unclear if this causally contributes to successful stopping, or is the consequence of it (Kok et al., 2004). On the other hand, Schmajuk et al found a larger right frontal N2 component in successful, as compared to unsuccessful, trials at around 200ms (Schmajuk et al., 2006). However, scalp EEG has relatively little localising power at the sensor-level. Swann et al looked at a unique cohort of 4 subjects with epilepsy who also had subdural electrocorticograph electrodes in place for the investigation of

seizures (Swann et al., 2009). Such electrodes provide high spatial and temporal fidelity of signals, although they are also not immune to the effects of volume conduction etc. They used a conditional stop-signal, where the subject ignores the stop-signal in a proportion of trials to improve the control condition of their recordings. They found an increase of beta activity in successful trials in electrodes over the right IFG around 100 – 250ms after the stop signal. A follow-up study in a subject with both right IFG and pre-SMA electrodes revealed that the pre-SMA was active at a higher frequency and (in the gamma region), and earlier in the task *prior* to stopping than the right IFG (Swann et al., 2012). Although interesting both studies suffer from a number of confounds. Firstly, both studies are on a small cohort of epilepsy subjects in whom brain activity may not represent that of healthy controls and also the authors used standard electrophysiological techniques which are incapable of handing the reaction time and movement confounds highlighted earlier.

1.5.4 Pathophysiology in Parkinson's Disease

Although the neural mechanisms underlying response inhibition are still unclear, converging evidence suggests that cortico-basal ganglia interactions play a key role. In particular connections between the pre-SMA and the STN or the right-IFG and STN may be particularly important. Parkinson's Disease offers a human model where the effects of a dopaminergic lesion on these cortico-basal ganglia interactions can be studied.

Patients with Parkinson's Disease have longer reaction times on simple and more complex tasks (Cooper et al., 1994).The SSRT is reported to be longer in treated PD than orthopaedic controls, even if the slowing of the primary task reaction time is taken into account (Gauggel et al., 2004). Obeso et al used a conditional stop-signal task, where some stop-signals are ignored (but still interfere with the primary task), as well as standard bedside frontal executive tests in order to study behaviour in PD (Obeso et al., 2011a). PD patients had a longer SSRT, compared to age-matched controls, even after controlling for depression, primary task reaction time and global cognitive impairment. In addition PD subjects found it more difficult to ignore stop-signals if instructed – suggested to be a defect of conflict resolution in the PD group. Surprisingly, there were no effects of dopamine on SSRT measurement (Obeso et al., 2011b). However, all studies of the stop-signal task use standard methodology to determine the SSRT. This may not be appropriate in Parkinson's patients because of the relatively high lapse rate and guessing rate of this cohort. For example, lapses in concentration, where the subject does not make a response, would be categorised as successfully inhibited trials unless due care is taken with the analysis.

Patients with PD undergoing DBS also offer an opportunity to study the role of the STN in stopping. Van den Wildenberg et al established that STN-DBS improved both primary task reaction time and SSRT in patients with PD, although both effects were independent of each other (Van den Wildenberg et al., 2006). The relationship between dopamine and STN stimulation is less clear. Treated PD patients undergoing unilateral STN-DBS with 'normal' initial SSRTs found that their SSRTs increased with stimulation – but only if the left STN was stimulated (Ray et al., 2009). However, another study in OFF patients found no side-specificity – only if *both* STN-DBS electrodes were stimulated, was there a reduction in SSRT. They additionally found no difference between dorsal and ventral stimulation and no change to primary task reaction times with stimulation. Finally PD patients OFF medications did not tend to wait and showed less post-stop reaction time slowing (Mirabella et al., 2011).

In addition, STN-DBS shows inconsistent effects across other measures of inhibition. STN stimulation improved random number generation, but caused more errors in a Stroop task. No change was detected with dual-task performance (Witt et al., 2004). Using a go-no-go task, Hershey et al reported more errors with ventral rather than dorsal stimulation of the STN (Hershey et al., 2010). This suggests that response inhibition in different tasks may not be mediated by the same neural structures, and that STN-stimulation may have different effects on these structures.

So what is the STN doing in the stop-signal task? Ray et al studied PD performing the stop-signal task in patients ON meds whilst recording STN activity from intracranial electrodes. They found that variability in primary task reaction time corresponded to variability of beta ERD onset and timing of the gamma peak. They also found a post stop-signal increase in beta, the onset of which correlated with SSRT between subjects (Ray et al., 2011). This is consistent with a similar increase in STN beta activity found after no-go trials in a go-no-go task (Kuhn et al., 2004).

Attempts to assess functional connectivity of cortical structures with the STN during the stop-signal paradigm are sparse. Swann et al stimulated bilateral STN whilst recording EEG (ON meds) whilst doing stop-signal task. They found that stimulation shortened SSRT without significantly affecting primary task reaction time. Stimulation also increased right frontal theta around the time of the stop-signal and started to increase right/midline frontal and parietal beta at 200ms after the stop-signal task (Swann et al., 2012).

1.6 Summary and thesis objectives

Parkinson's Disease is a common neurodegenerative condition characterised by basal ganglia dysfunction due to progressive dopamine depletion (Lees et al., 2009). Although typically presenting with movement impairment, more recent attention has also focused on the non-motor symptoms of PD (Evans and Lees, 2004; Chaudhuri et al., 2006). Treatment strategies include dopamine replacement therapy, and more recently deep brain stimulation.

There is considerable variation in symptoms and treatment response between PD patients and treatment side-effects can be dramatic and difficult to predict (Evans and Lees, 2004; Voon et al., 2008). Individualising treatment in such a patient group requires a better understanding of the pathophysiology of basal ganglia circuits and an ability to characterise these circuits in humans. Recent anatomical and functional studies have suggested that distinct, spatially segregated, basal ganglia circuits have distinct functions (Alexander et al., 1986; Haber, 2003; Postuma and Dagher, 2006). An intuitive extension of this hypothesis is that distinct symptoms in PD may be due to dysfunction of distinct basal-ganglia circuits (Alexander et al., 1986; Haber, 2003; Redgrave et al., 2010). Such circuit activity has proven difficult to characterise in humans and so far studies have had to rely on indirect measures of neuronal activity, such as blood oxygenation, or have been limited by poor spatial resolution. This thesis aims to take advantage of recent research about the frequency-specific nature of abnormal neuronal activity in PD (Brown, 2007), and recent methodological advances (Litvak et al., 2010) to characterise the function and dysfunction of cortico-basal ganglia circuits in humans with PD. We will focus on PD patients who are undergoing DBS as they often have the greatest need for individualised treatment, and also because they offer the opportunity to record neuronal activity directly from targets within the basal ganglia such as the subthalamic nucleus (STN). Cortical activity will be measured by simultaneous magnetoencephalography (MEG) allowing cortico-basal ganglia network activity to be characterised in terms of coherence - an electrophysiological measure of the correlation between two signals (Fries, 2005). We will characterise these networks initially at rest to determine if they can be spectrally and spatially disambiguated. Then we will interrogate how activity in these networks relates to a cognitive process – response inhibition, abnormalities in which may contribute to cognitive symptoms in PD.

The objectives of this thesis are:

1) To develop a study model and methodology to measure cortico-basal ganglia connectivity, based on simultaneous magnetoencephalographic and basal - ganglia recordings in Parkinsonian patients.

2) To determine if the cortical and subcortical spatial distribution of cortical-basal ganglia connectivity is frequency and dopamine dependent at rest.

3) To characterise the role and spectral signature of different cortical areas during the stop-signal task.

4) To characterise how activity in cortico-basal ganglia circuits changes during the performance of the stop-signal paradigm, and how these changes relate to behaviour in PD patients.

2. Methods

2.1 Subjects and Operative Procedure

2.1.1 Subject baseline clinical and psychological data

We studied healthy adults as well as patients with PD. The healthy control study was approved by the Imperial College Ethics committee, whilst all patient experiments were approved by the joint ethics committee of the National Hospital of Neurology and Neurosurgery and the University College London Institute of Neurology. All subjects gave their written informed consent. In addition to experimental data, age, gender and handedness were also recorded for healthy control subjects.

All patients studied were diagnosed with PD according the Queen Square Brain bank criteria (Gibb and Lees, 1988). They had recently undergone surgical implantation of intracranial electrodes prior to DBS therapy for PD. After the initial implantation procedure, these patients have their electrodes externalised for a period of about a week, during which recordings can be made from the implanted DBS electrode. We studied patients who had DBS targeted to either the STN or the PPNR. In both cases we studied subjects with unilateral and bilateral implants. We recorded the age, clinical symptoms, medications, handedness and length of disease of all patients.

Prior to surgery, the motor impairments of all patients were evaluated using part III of the Unified Parkinson's Disease Rating Scale (UPDRS) (Goetz et al., 2008) after omitting all dopaminergic medication overnight and then following administration of 200mg of levodopa. This motor score includes 14 items which assess axial function, gait, balance, rest tremor, bradykinesia, rigidity and postural tremor. The UPDRS scale is validated and correlates with disability (Goetz et al., 2008). Overnight omission of medication is regarded as a "practically defined OFF" state - although the prolonged half-life of some medications, especially dopaminergic agonists, means that a longer medication-free period would be required to provide a complete OFF. However such periods of time are too uncomfortable for the majority of patients.

Further clinical and psychological data were collected in various subsets of patients (see relevant chapters) and included the following.

The Gait and Falls Questionnaire (GFQ, score/64) which assesses Parkinsonian gait disturbance including gait freezing, festination and falls. The Freezing of Gait Questionnaire

(FOGQ, score/24) and Falls Question (FallsQ, score/4) are components of GFQ (Giladi et al., 2000, 2009).

Global cognitive and mental state were assessed at the bedside with the Addenbrookes Cognitive Examination-Revised (including mini-mental state examination, verbal and category fluency), Beck's depression inventory (Beck et al., 1988) and forward and backward digit span.

2.1.2 Surgical procedure

The indications for STN surgery were PD with motor fluctuations and/or tremors that were inadequately controlled with medical therapies (see section 1.2.8 and also (Foltynie et al., 2010)). The indications for PPNR surgery were PD with predominant levodopa-unresponsive gait impairment and/or falls due to either freezing or postural instability. Gait freezing and postural instability are common features of PD, especially as the disease progresses (Giladi et al., 2001; Bloem et al., 2004). However, medication-resistant gait freezing may also be due to atypical pathologies (Factor, 2008; Jankovic, 2008). In the absence of a definitive test in life, we stress that the diagnosis of PD in the PPNR implanted cohort is presumptive.

Subjects with STN and PPNR implants were studied in London and Oxford. The DBS electrode used was always model 3389 (Medtronic, Minneapolis, MN) with four platinum-iridium cylindrical surfaces of diameter 1.27mm, length 1.5mm, and centre-to-centre separation 2mm. The contacts were numbered 0 (lowermost) to 3 (uppermost). In the STN the inferior contact would usually lie just below or in the inferior portion of the STN whilst the superior contact would lie usually in the superior portion or just above the STN in the zona incerta. Electrode locations in the PPNR were more variable (see section 4).

Surgical targeting of the DBS electrode was based on preoperative stereotactic imaging (stereotactic proton density weighted magnetic resonance imaging (MRI) in London, and stereotactic computerised tomography (CT) fused with T2 weighted MRI in Oxford).

The STN, especially its medial border was targeted by examining it on the axial image containing the largest diameter of the ipsilateral red nucleus (Hariz et al., 2003). The centre of the STN was identified in a plane zero to one millimetre behind the anterior border of the ipsilateral red nucleus (Bejjani et al., 2000). Calculations of Cartesian coordinates of the target point were performed on Framelink software (Medtronic, Minneapolis, MN). A double oblique trajectory was planned on reconstructed three-dimensional images to avoid entry into sulci and ventricles (Zrinzo et al., 2009). The PPNR was targeted medial to the

lemniscal system and lateral to the superior cerebellar peduncle and its decussation (Pereira et al., 2008; Zrinzo et al., 2008; Foltynie and Hariz, 2010).

After implantation, electrodes were connected to an accessory kit, typically both connectors being tunnelled to the left temporoparietal area and externalised through the frontal region. No microelectrode recordings were made. The locations of the electrodes were confirmed with immediate post-operative stereotactic imaging. In London fast spin-echo T2 weighted 2mm thick contiguous axial slices were acquired with the Leksell frame still *in situ*. One patient was unable to tolerate a post-operative MRI and underwent stereotactic CT scanning instead. In Oxford postoperative stereotactic CT was routinely used.

2.2 Electrophysiological Data Acquisition

2.2.1 Magnetoencephalography

MEG aims to record the magnetic field generated by neuronal activity. In an MEG system, the subject's head is placed inside a helmet-shaped dewar, in which a number of magnetic sensors, called superconducting quantum interference devices (SQUIDS) are set. MEG recordings were performed in London with the 275 channel CTF (VSM MedTech Ltd., Vancouver, Canada) or in Oxford with the 306 channel Neuromag (Elekta Neuromag Oy, Helsinki, Finland) systems. The London CTF system is shown in **Figure 7**. Magnetic activity recorded from the brain is orders of magnitude lower than background activity due to the Earth's magnetic field, the movement of nearby metal objects (e.g. cars) and other forms of electrical activity (e.g. muscle activity and the heart beat). However, sources of noise are also much further away and therefore the *differential* between two neighbouring sensors provides a better estimate of brain activity: noise from far away sources will be the same on both channels and is therefore subtracted out, whereas for closer sources (including the brain), small differences in sensor position result in different estimates of brain activity by both sensors, and a larger differential signal. The two MEG systems differ in their arrangement of the squids. The CTF has axial gradiometers, where each SQUID is referenced to another directly above it. The Neuromag system has both unreferenced sensors (magnetometers) and SQUIDS arranged tangentially to the surface of the scalp – planar gradiometers. Therefore theoretically the same cortical source will have different predicted activity on the sensors of the two MEG systems: an important consideration during analyses combining data from both systems. However these differences can be addressed

by individualised head models (see source localisation) and with appropriate statistical modelling.

Figure 7: The CTF MEG system in London. *The subject sits in the chair and places their head inside the helmet-shaped dewar.*

Unlike electroencephalography (EEG), the subject's head is free to move a small amount with respect to the electrodes. Therefore the head location is tracked using three or four head coils, which are placed with reference to easily defined locations on the head, the fiducial markers. The fiducials are usually at the bridge of the nose (nasion) and 1cm anterior to the superior fold of the tragus of both ears (pre-auricular).

2.2.2 Intracranial electrode recordings

In PD patients, STN or PPNR electrode local field potentials (LFPs), both right and left first dorsal interosseus (FDI) electromyographic (EMG) signals and MEG data were acquired simultaneously. All non-MEG signals were referenced to the right or left mastoid and, due to safety and technical limitations, were acquired using different amplifiers. Over different experiments we used a Digitimer D360 amplifier (Digitimer Ltd, Hertfordshire, UK), a BrainAmp MR (Brain Products GmbH, Gilching, Germany), and the integrated EEG system available at both sites.

2.3 Pre-processing

The data were analysed using SPM8 (http://www.fil.ion.ucl.ac.uk/spm/) and Fieldtrip (http://www.ru.nl/neuroimaging/fieldtrip/), (Litvak et al., 2011b; Oostenveld et al., 2011). Raw data contains both signals of interest (i.e. neural signals) and signals in which we have no interest (e.g. muscle activity, head movement). Transformation of the raw data in order to emphasise data features of interest, and supress other features is known as pre-processing and is a crucial step before statistical analysis can be meaningfully performed. Different research questions require different pre-processing pipelines, however here we will review some of the basic elements, the order and specifics of which are detailed within the results chapters.

2.3.1 Sampling rate

Data were usually acquired at high sampling rates (600 – 2400Hz). Higher sampling rates allow examination of higher frequencies of neuronal activity, up to the nyquist limit (nyquist frequency limit = sampling rate / 2). However, they also increase data storage requirements and computation demands. The CTF MEG system we used automatically filters the raw acquisition at the sampling rate/4. Because we were primarily interested in frequencies up to

100Hz, we later further downsampled the data to 300Hz, which is still well above the nyquist limit for that frequency of interest.

2.3.1 Filtering

The acquired data were hardware filtered during acquisition but also filtered during the pre-processing pipeline. Filtering the data essentially removes frequency components that we are not interested in. During acquisition, high frequency components are removed from the data with a low-pass filter (cut off e.g. 600Hz). This is essential as signal activity above the nyquist limit can cause artefacts at lower frequencies, unless they are removed. At the same time, a high-pass filter (cut off e.g. 1Hz) removes low frequency fluctuations in the signal due to gradual build-up of electrical charge [Direct Current (DC) offset] which may saturate the recording equipment. During processing, filters are also used to remove unwanted noise from mains interference (notch-filters) and to pre-process data acquired with different acquisition parameters into a standard format. For this step a Butterworth filter is often used, which is designed to give a maximally flat frequency profile of the retained frequencies.

2.3.2 Artefact rejection

The acquired raw LFP and MEG data are usually contaminated with artefacts. These include spikes (brief large magnitude deflections which revert to baseline), jumps (brief large magnitude deflections which do not revert to baseline), interference from ferromagnetic components, and muscle activity artefact. Different pre-processing techniques have been used to remove different types of artefact – for example beamformers were used to remove ferromagnetic artefact. However, simple techniques such as thresholding can remove important artefacts. Here the time domain data are visualised and data larger than a certain value are marked as bad. After marking, depending on the type of subsequent analysis to be performed, either just the bad segment can be removed from the data, the whole trial containing the bad segment, or even a whole channel if it contains many bad segments. A crucial step is determining the threshold at which to reject bad trials. Although this is usually done visually, this process can also be partially automated by standardising the signal (subtracting the mean of the signal and dividing by the standard deviation), and setting the threshold as a number of standard deviations – for example eight standard deviations. Artefacts can also be handled at a group level by using robust averaging. Robust averaging is a special case of the robust general linear model (Holland and Welsch, 1977; Wager et al., 2005; Litvak et al., 2012a) . In this framework, outliers are down-weighted when computing

the average, making it possible to suppress artefacts restricted to narrow time and frequency ranges without rejecting whole trials.

2.3.3 Frequency transformation

Interesting data patterns can be recognised by simply examining variation of the magnetic field with respect to time. When such analysis is locked to an event (such as a visual stimulus) and averaged over a number of trials, the resulting waveform is referred to as an evoked response or event-related field (ERF). An alternative method of analysis can be performed in the frequency- (rather than time-) domain and is termed an induced response. The latter is sensitive to variations in underlying neuronal oscillations that are not phase-locked to the stimulus. In order to perform such analysis, the data must first be transformed into the frequency-domain. This is done by the Fourier Transformation (FT), which results in a complex number representing the phase and amplitude of the oscillatory component of the signal at each given frequency.

$$S(f) = \int_{-\infty}^{\infty} s(t).\, e^{-i2\pi ft} dt.$$

Equation 2: Continuous Fourier Transform. *The signal over time, s(t), is transformed into a complex number representation of its frequency component S(f) at a certain frequency f. In signal processing the discrete version of this transform is used.*

The FT can be evaluated over multiple frequencies, and each resulting complex output squared (i.e. the complex conjugate calculated) to result in a single value per frequency. This value, termed power essentially discards the phase information of the initial signal. The distribution of power over different frequencies is a standard way to visualise the spectral properties of a signal and is termed the autospectrum, or simply the power spectrum. However, the FT assumes that the signal is stationary. In practice, neural signals are rarely stationary over periods of more than a few seconds, and therefore the FT is usually done on short segments of data. The advantage here is that phase and amplitude estimates can be calculated as a function of time – so called time-frequency analysis. FT over shorter segments provides a greater sensitivity to variations in neuronal responses, but at the cost of

a more noisy estimation of the Fourier coefficients and a loss of frequency resolution. Multiple techniques have been developed to provide optimal time and frequency resolution, including the use of overlapping temporal windows and convolutions of the time-domain signal with canonical shapes (e.g. Hanning windows, wavelets, multitapers). We have tended to use multitapers, which allow for greater flexibility in terms of frequency and time resolution (Thomson, 1982).

2.4 Connectivity Metrics

In addition to studying the activity of a single brain region, we can also examine how distant brain regions are coupled together. Indeed some behaviours may be better modelled as an emergent property of the functional relations between brain regions, rather than by the specialised activity in one region (Friston, 2002). There are many techniques available that quantify the connectivity between two regions, but it is customary to divide them into three groups: *anatomical* connectivity, based on retrograde tracing studies in animals or diffusion tractography in humans, aims to understand the static synaptic organisation of brain circuits; *functional* connectivity, based on human EEG/MEG or fMRI measurements, aims to determine how similar two brain regions are in terms of their activity over time – the statistical dependence of two signals; and finally *effective* connectivity aims to determine the influence of one brain region over another over time (Friston et al., 2012). In this thesis we are concerned with the various forms of functional connectivity.

2.4.1 Coherence

Coupling between different regions is probably both a linear and nonlinear process, and many different measures of *functional* connectivity have been put forward – each focusing on particular similarities between different signals. However as a first step, we focus on a linear measure of coupling called coherence (Thatcher et al., 1986; Rappelsberger and Petsche, 1988; Shen et al., 1999; Buzsaki and Draguhn, 2004; Magill et al., 2006a).

$$C_{xy} = \frac{\left|G_{xy}\right|^2}{G_{xx}G_{xy}}$$

Equation 3: Coherence. *At a given frequency, the coherence, C_{xy}, between two signals x and y is calculated by dividing the square of the modulus of the cross spectrum of the two signals, G_{xy}, by the product of the autospectra of each signal (G_{xx} and G_{yy}).*

Coherence is a value bounded between 0 and 1 and quantifies any linear relationship between two time-invariant signals at a specific frequency. It is the frequency-domain counterpart of a cross-correlation and statistically similar to a correlation coefficient. The coherence value can also be thought of as the fraction of one signal that contributes to the other (although it does not suggest causation). As such it is theoretically normalised to isolated variations of power. This metric also forms the basis for the communication-through-coherence (CTC) hypothesis (Fries, 2005). In this hypothesis, coherent oscillations play a role in communication between different brain regions and neurons can be differentially sensitive to inputs arriving at different phases of the local oscillation.

2.4.2 Granger causality

After establishing that two signals are linearly coupled, i.e. are coherent, the question then arises as to which signal temporally precedes the other– the so called *directed* functional connectivity (Friston et al., 2012). Again, different techniques have been proposed to assess directed functional connectivity between different brain regions. In this thesis, we focus on Granger based techniques. Granger causality determines whether activity in signal A is a better predictor for later activity in signal B, than just signal B itself - i.e. how much the information in one signal temporally precedes another (Granger, 1969). Originally developed for relationships in the time domain, this technique has been extended to the frequency domain (Geweke, 1982) and also the time and frequency domains (Geweke, 1984; Chen, 2006). The most parsimonious explanation for such a relationship between two coherent population activities is that the temporally leading population drives the lagging population. However, this may not be the only explanation. Driving may be direct or indirect, via one or more unrecorded structures, or activity in both recorded structures may be driven by a third unrecorded structure (Sharott et al., 2005a). Given this, we use the term ‘effective direction of coupling’ to describe a pattern of temporal relationships rather than a measure of direct coupling. Crucially this is distinct from *effective connectivity,* which relies on generative neuronal models and differential equations (Friston et al., 2012). Different mathematical formulations of Granger causality exist, including the Directed Transfer Function (Kaminski and Blinowska, 1991; Korzeniewska et al., 2003) and the Partial Directed Coherence

(Baccala and Sameshima, 2001), which are designed to account for activity from multiple recorded sources, and which have differential sensitivity to pre-processing manipulations such as filtering (Florin et al., 2010).

2.5 Source localisation

Traditionally EEG and MEG data are analysed with regard to the distribution of the recording sensors at the scalp. This 'sensor-space' analysis, however has limited localising power, and at best, can be used to say something like 'electrodes placed over the temporal lobe show an evoked response at 150ms'. As a result, EEG analysis has traditionally focused on temporal differences of evoked responses, or magnitude differences at particular sensors. However, more recent computational algorithms have been developed to use *all* the channel data simultaneously, to localise the origin of the source. To understand the principles behind such approaches, it is useful to review the basis of the electromagnetic signal generated by the brain.

2.5.1 The basis of the electromagnetic signal recorded by EEG and MEG

Similar to direct recording of local field potentials (LFPs), MEG and EEG activity represents the summed activity of dendritic potentials. Considering a typical cortical pyramidal cell as an example, cells are aligned such that their dendrites extend radially outward. Thousands of other neurons synapse onto each pyramidal cell's dendritic tree and the resulting excitatory and inhibitory post-synaptic potentials (EPSPs and IPSPs) cause a gradient and therefore flow of current along the dendrites towards the cell body. This flow of current inside the cell (primary current) causes compensatory currents to flow in the opposite direction outside the cell (secondary currents). The activity of a single cell is too small to be detected by distant MEG/EEG sensors, but if many cells and dendrites are aligned, in the way that cortical pyramidal cells are, these currents can summate over space and time to be detectable by sensors that do not have the spatial resolution to pick up cellular processes. Such summed activity is called a local field potential, or, on a still larger scale the EEG, and can be modelled as an equivalent current dipole (ECD) - a single point source with a location, an orientation (which probably corresponds to the predominant direction of the dendrites), and a magnitude.

2.5.2 The inverse problem and its solutions

Understanding the pattern of activity one would expect to detect on the EEG/ MEG sensors, given a particular ECD, is called the forward problem. This can be relatively easily predicted using Maxwell's equations. The accuracy of this process is less for EEG, because the pattern of electrical activity is determined to a large extent by the not precisely known conductivity profiles of neuronal tissue, bone, CSF and skin, whereas this is not the case for MEG. In spite of this, given a realistic head model, with different tissue compartments modelled accurately, an adequate forward model can be generated for both EEG and MEG. However, the reverse is more difficult. Predicting the source, given the data at the MEG or EEG sensors, is called the inverse problem and is ill-posed, because it does not have a unique solution (i.e. multiple source combinations can result in a similar pattern of activity at the EEG/MEG sensors).

Different methods have been developed to address this, each relying on different assumptions about the nature of the data. The simplest of these, called a 'dipole fit' simply minimises the difference between the predicted and observed sensor data by optimising the dipole parameters: location and orientation. However, it assumes that the number of sources is known *a priori* and that there are only a few sources in total. An alternative to this are distributed solutions (e.g. 'minimum norm') – here, a cortical mantle of sources and orientations are pre-specified, leaving only the activity (energy) at each source to be fit to the data. Since the number of cortical sources exceeds by far the number of sensors, additional constraints are necessary to determine the most plausible solution. Different constraints result in different method variants. Distributed solutions require a high signal-to-noise ratio (e.g. an evoked response), otherwise can lead to broad activation patterns and can be very sensitive to artefacts. Given our dataset has high noise levels, due to ferromagnetic artefact from DBS leads, and an unknown number of sources, we used another technique – beamforming (Litvak et al., 2010).

2.5.3 Beamformers

Unlike dipole fitting and minimum norm methods, beamforming does not set out to explain all the data at all the sensors. Rather it aims to find the combination of sensors that best explain activity from a given source location and orientation, whilst suppressing interference from other sources in the data. Crucially, other sources are separated out, based on the fact that they have a differential variance over time. Hence beamformers assume that activity at different sources is not highly correlated. Mathematically, the beamforming method is based on a linear projection of sensor data using a spatial filter computed from the lead field of the

source of interest and either the data covariance (time domain)) (Van Veen et al., 1997) or cross-spectral density matrix (frequency domain) (Gross et al., 2001). The beamformer equation is below.

$$w(r) = [H^T(r)Cov^{-1}(x)H(r)]^{-1}H^T(r)Cov^{-1}(x)$$

Equation 4: The beamforming spatial filter. *The beamformer weights [w] for a given brain location [r], are a function of the lead field of that location [H(r)] and the covariance matrix of [Cov] the sensor activity [x]. In addition, two constraints ensure that the activity on the source of interest is amplified with a gain of 1 [w(r)H(r) =1], and that other sources are blocked – i.e. we minimise the variance of the filter output (min[var(s)]). S=activity at region r estimated with beamforming.*

2.6 Statistical analysis

2.6.1 General Linear Model as applied to images

Statistical analysis was performed by using a general linear model (GLM) approach with Statistical Parametric Mapping (SPM) software (Litvak et al., 2011b). SPM is a specialised Matlab toolbox that was originally designed to make inferences about regionally specific effects in the brain. However, the underlying principles can also be extended to make inferences about regionally specific effects in any 2 or 3 dimensional space, for example time-frequency images (Kilner and Friston, 2010).

SPM employs a mass univariate approach to the statistical analysis of images: statistical questions are posed in terms of differences between sets of images (for example images from group A are different to those from group B) and then each voxel undergoes a separate standard statistical test (such as a *t*- or F- test) using the relevant voxel values from all images (Friston et al., 1994). The resulting image is a statistical parametric map – an image of values distributed under the *t*- or F distributions. These values are thresholded to provide appropriate false positive rates (usually p=0.05). Those voxels lying above the threshold can be inferred to lie in regions showing a significant effect. Depending on the question of

interest, different design variants such as ANOVAs, regression analysis and *t*-tests may be specified, but all designs are simply instances of the GLM outlined below.

$$Y = \beta X + e$$

Equation 5: *The General Linear Model. See text for discussion.*

The data [Y], are modelled by predictor variables X. The predictor variables are optimally fit to the data by choosing scaling variables [β] that minimise in a least squares fashion, the error [e]. Alternatively, β estimates can also be obtained from more a robust maximum likelihood estimating algorithm. The predictor variables can be used to code factors (i.e. grouping variables) or continuous regressors (parametric modulators) or both. The key assumption is that the error term [e] is identically and independently distributed. However, this latter assumption is usually untrue in repeated measures designs, or if the data are temporally correlated. Therefore, methods to handle this non-sphericity of error have been established and include using a whitening matrix, to account for such correlations in the model (Worsley and Friston, 1995).

The simplicity of this approach and much of its appeal lies in the fact that it is based on standard well-understood univariate tests. If a statistical test is performed at every voxel, then a large multiple comparisons problem ensues. Given that the activity at individual voxels is correlated, the voxels more closely resemble a continuous random field of values, rather than truly independent measurements. This spatial correlation can be measured by the smoothness of the data, and given a specified smoothness, the number of expected topological features such as peaks and clusters can be estimated using the *Euler characteristic* (Worsley and Evans, 1992). Hence if the expected or 'null' distribution of peaks is known, then this can be used to threshold the statistical parametric map.

2.6.2 Event-related convolution analysis

In chapters 5 and 6 we develop and use a convolution model for analysing event-related MEG data. We explain the approach fully in the methods sections of those chapters as the motivation is intrinsically linked to the aims of the data analysis. Briefly, MEG data are

presented as a continuous vector (*Y*) over time. Individual experimental events are modelled as a brief (about 2s) window of activity triggered to their time of onset (*X)* and regressed against the data. In chapters 5 and 6, this approach is used in the frequency domain and the output provides an estimation of the induced response to each experimental event.

2.7 Summary of Limitations

In this section, we will briefly recapitulate the major methodological obstacles, which we will attempt to overcome in the following experimental chapters.

2.7.1 Phenotypic variation and lesion effects

Although in some senses PD is well-characterised neurodegenerative disorder, there remains considerable variation in the clinical presentation of PD. Some subjects have predominant tremor, some have predominant gait difficulty, and some rapidly progress to dementia. In addition, treatment response is variable to both medical therapies as well as DBS. Finally, for a brief period after the DBS operation, peri-electrode oedema causes a temporary pathological lesion of the target nucleus, which clinically improves the patient's Parkinsonian symptoms. This so called 'stun effect' is variable (Lalo et al., 2008).

In summary, many factors conspire to introduce additional functional variation in our subjects. Therefore when performing *functional* imaging analyses, as we do, we must take care to ensure that our inferences reflect the symptoms and treatment responses of the cohort of subjects that we have studied. Indeed, it may be optimal to explicitly model some of this clinical symptomatic variation in our imaging analyses.

2.7.2 Variation in surgical practice and MEG systems

We have recorded data from subjects in both London and Oxford. In some situations, we have included data from both centres in the same analysis. When doing so it will be important to account for different subject selection, surgical targeting techniques, and MEG systems. The later may especially result in artefactual differences between subjects and must be carefully evaluated, ideally by comparing data from different centres to ensure consistency.

2.7.3 Artefacts in the MEG signal

Performing MEG of subjects with intracranial ferromagnetic extension wires results in prominent electrode artefact at the sensor level. This artefact is worsened by involuntary movements such as the tremor and dyskinesias associated with PD. Together, these artefacts are extremely challenging to overcome, and may lead to greatly reduced sensitivity in our analysis, unless handled appropriately. However, as we demonstrate, the analyses can be adequately performed in the presence of artefacts.

3: Resting cortico-subthalamic nucleus connectivity in Parkinson's Disease

3.1 Introduction

In this chapter, we sought to investigate the functional connections underlying cortico-subthalamic circuits in terms of the degree of electrophysiological synchronisation between spatially distributed neuronal populations. This chapter has been adapted from a published article (Litvak, Jha et al., 2011a) with permission from Oxford University Press.

Recordings from PD patients undergoing surgery for DBS demonstrate prominent oscillatory synchronisation between different levels of basal ganglia-cortical loops (Brown et al., 2001; Marsden et al., 2001; Williams et al., 2002; Fogelson et al., 2006; Kuhn et al., 2006b; Lalo et al., 2008) and suggest that the preferred frequencies of such activity may vary between different loops (Fogelson et al., 2006). This synchronisation, or coherence, between levels appears to be exaggerated in PD (Sharott et al., 2005b; Mallet et al., 2008) and may have significance for our understanding of brain function. Moreover, the different resonance characteristics of distinct loops might be useful in characterising these circuits (Eusebio et al., 2009), and may ultimately prove useful in predicting the clinical response to particular DBS parameters.

However, a clear relationship between the spectral range and cortical distribution of basal ganglia-cortical connections has proven difficult to establish in the electroencephalographic (EEG) studies made to date. This is because scalp recording sites are necessarily very limited in peri-operative patients and the scalp topography of the EEG is deranged by the presence of burr-holes (Benar and Gotman, 2002; Oostenveld and Oostendorp, 2002). On the other hand, analysing simultaneously recorded magnetoencephalographic (MEG) signals and intracranial local field potentials (LFPs) in patients following DBS surgery is hampered by the presence of high-amplitude artefacts in the MEG due to the presence of percutaneous extension wires made of stainless steel close to the MEG sensors. Previously, Litvak et al described these artefacts and showed that despite their presence, topographical mapping of coherence between bipolar LFP channels and the MEG sensors can disclose physiological patterns (Litvak et al., 2010). Furthermore, they demonstrated that beamforming effectively suppresses artefacts and thereby enables both localization of cortical sources coherent with the STN and the extraction of artefact-free virtual electrode data from these sources. Here, by building on these methodological advances, we establish the detailed cortical topography of subthalamic-cortical loops in PD patients at rest, characterised by different frequencies of

oscillatory coupling and different effects of dopaminergic medication. The results support the notion of spatio-temporal segregation in these circuits.

3.2 Methods

3.2.1 Participants and surgery

We studied 13 patients who had undergone STN DBS electrode implantation prior to DBS therapy for PD. All but one patient were implanted bilaterally. Four additional patients were entered into the study but were unable to complete the experimental protocol of paired on and off-drug recordings and were excluded from analysis. Clinical details are given in table 1. All patients were diagnosed with PD according the Queen Square Brain bank criteria (Gibb and Lees, 1988). The indications, operative procedure, targeting and beneficial clinical effects of STN stimulation have been described previously [see chapters 1.2.8, 2.1.2 and (Foltynie et al., 2010)]. Prior to surgery the motor impairments of all patients were evaluated using part III of the Unified Parkinson's Disease Rating Scale (UPDRS) after omitting all dopaminergic medication overnight, and following administration of 200mg of levodopa.

Although electrodes were considered to lie within or abutting STN, we cannot assume that all contacts on each electrode shared this localisation; indeed, this would seem highly unlikely given the size and orientation of the nucleus in relation to electrode trajectory. Given this, and to avoid any selection bias, we analysed the coherence between cortex and all three bipolar electrode pairs, and considered these to lie in the STN region.

Case	Age (years)/ Sex	Disease duration (years)	Predominant symptoms (in addition to akinesia)	UPDRS ON/OFF medication	Pre-operative medication (total daily dose)
1	40/M	10	Gait impairment, tremor	9/30	Stalevo 600mg Co-careldopa 687.5mg Pramipexole 5mg
2	55/M	15	Tremor, gait freezing	5/19	Co-beneldopa 1000mg Ropinirole16mg Selegiline10mg Amantadine100mg
3	45/F	8	Tremor	50/50	Ropinirole 27mg
4	58/F	14	Gait freezing, pain, dyskinesias	18/71	Pramipexole 4mg Stalevo 250mg
5	51/M	9	Gait impairment, tremor	21/49	Co-beneldopa modified release 375mg Co-beneldopa 562.5mg Rasagiline 1mg
6	60/M	15	Dyskinesias, gait freezing	10/56	Co-careldopa 1125mg Co-beneldopa 250mg Ropinirole 18mg Selegiline 10mg Amantadine 200mg
7	54/M	8	Gait impairment, dyskinesias	9/38	Cabergoline 4mg Entacapone 800mg Co-careldopa 1200mg Amantadine 300mg
8	48/M	11	Gait freezing, tremor	16/72	Rasagiline 1mg Co-careldopa 1250mg Entacapone 500mg
9	61/M	9	Gait freezing, tremor	5/28	Co-careldopa 1875mg Pramipexole 500micrograms
10	58/F	10	Dystonia,	16/55	Pramipexole 3mg

			dyskinesias		Stalevo 400mg Rasagiline 2mg Co-beneldopa 62.5mg as required
11	52/M	12	Dystonia	10/35	Rotigotine 4mg Stalevo 950mg Rasagiline 1mg
12	58/M	13	Gait freezing	25/43	Co-careldopa 1000mg Co-careldopa modified release 125mg Amantadine 400mg Co-beneldopa 125mg Entacapone 600mg Rasagiline 1mg
13	57/M	17	Gait impairment, pain, dyskinesias	14/54	Co-careldopa 1125mg Co-careldopa modified release 250mg Co-beneldopa 200mg Entacapone 1600mg Selegiline 10mg Amantadine 200mg

Table 3: Clinical features of patient cohort. *All patients received bilateral STN DBS electrodes except for case 3. Stalevo is a proprietary combination of levodopa, carbidopa and entacapone for which the dose of levodopa is given. The dose of pramipexole is given as a salt.*

3.2.2 Simultaneous STN-LFP and MEG recordings

Patients underwent simultaneous STN electrode LFP and 275 channel MEG (CTF/VSM MedTech, Vancouver, Canada) recording between 2-6 days post-operatively. The data were sampled at 2400 Hz and stored to disk. For subsequent off-line analysis the data were low-pass filtered at 100 Hz and down-sampled to 300 Hz. Simultaneous to the MEG signal, the LFP, electro-oculographic (EOG) and electromyographic (EMG) signals were recorded using the integrated EEG system and high-pass filtered in hardware above 1 Hz to avoid saturation of the amplifiers due to DC offsets. Four intracranial LFP channels were recorded on each side, referenced to a cephalic reference (forehead for the first two patients, right mastoid for the rest). LFP recordings were converted off-line to a bipolar montage between adjacent contacts (3 bipolar channels per side) to limit the effects of volume conduction from distant sources. EMG was recorded from right and left first dorsal interosseous (FDI) muscles with a reference at the muscle tendon.

Recordings were done twice. Once after omitting all dopaminergic medication overnight and once during the patient's usual medication regime, in an order counterbalanced across patients. Each recording involved rest blocks and task blocks in a randomised order. In this chapter, we will focus on data collected during the resting blocks which lasted 3 minutes each and were cued visually using Matlab (The Mathworks, Inc, Natick, MA) and a custom script based on the Cogent toolbox (http://www.vislab.ucl.ac.uk/cogent.php). During the rest block, the patient was asked to keep still, relax with their eyes open and focus on a fixation point. A neurologist was present in the magnetically shielded room during the experiment to monitor the patient's well-being and performance of the task.

3.2.3 Data pre-processing and beamformer approach to localisation of coherent sources

The data were analysed using custom Matlab scripts based on SPM8 (http://www.fil.ion.ucl.ac.uk/spm/) and Fieldtrip (http://www.ru.nl/neuroimaging/fieldtrip/) toolboxes. The continuous resting recording was divided into arbitrary epochs with duration of 3.41 sec (1024 samples). In all but the first subject head position was recorded continuously during the rest recording. After the data were epoched, trials with greater than 1cm head displacement (compared to the mean) were rejected. All subjects had at least 48/52 acceptable trials apart from one (31/52 trials). In the first subject, trial-rejection based on head location was omitted but this subject was relatively young and was able to keep quite still. The data were high-pass filtered above 1 Hz and the line noise artefacts at 50 Hz

and 100 Hz were removed using notch filters (5th order zero-phase Butterworth filters). Trials with artefacts in the LFP recording were rejected by thresholding the peak-to-peak LFP amplitude at 100 μV.

Coherence was the principal measure of functional connectivity used in this study. It provides a frequency-domain measure of the linear phase and amplitude relationships between signals (Thatcher et al., 1986; Rappelsberger and Petsche, 1988; Shen et al., 1999; Buzsaki and Draguhn, 2004; Magill et al., 2006a). Cortical sources coherent with STN-LFP activity were located using the Dynamic Imaging of Coherent Sources (DICS) beamforming method (Gross et al., 2001). To begin with, all MEG and bipolar STN-LFP channel trial data were converted to the frequency domain (range 5 to 45 Hz with frequency resolution of 2.5 Hz) using the multitaper method (Thomson, 1982). Coherence can then be calculated at the sensor level between each STN-LFP channel and each MEG channel or, using beamforming, coherence can be calculated between each STN-LFP channel and a 3 dimensional grid of points representing potential sources within the brain (Gross et al., 2001). We used the former approach to define frequency bands of significant coherence within each patient (see below) and the latter to locate coherent cortical sources spatially.

The beamforming method is based on the linear projection of sensor data using a spatial filter computed from the lead field of the source of interest and either the data covariance (time domain) (Van Veen et al., 1997) or cross-spectral density matrix (frequency domain) (Gross et al., 2001). Lead fields were computed using a single-shell head model (Nolte et al., 2004) based on an inner skull mesh derived by inverse-normalizing a canonical mesh to the subject's individual pre-operative MRI image (Mattout et al., 2007). Co-registration between the MRI and MEG coordinate systems used 3 fiducial points: nasion, left and right pre-auricular. The coherence values were computed on a 3 dimensional grid in MNI space with spacing of 5 mm bounded by the inner skull surface. Values at the grid points were then linearly interpolated to produce volumetric images with 2 mm resolution. These images were further smoothed with an 8 mm isotropic Gaussian kernel.

3.2.4 Characterisation of coherent sources within a single patient

Single-subject analyses were designed to ensure that cortical–STN coherence was spectrally and spatially restricted within each patient, before group analysis. Coherence was computed at the sensor level between each bipolar STN-LFP and all MEG channels between 5-45 Hz (low frequency) with 2.5 Hz resolution and between 60-90 Hz (high frequency) with 7.5 Hz resolution. Scalp maps of coherence for each frequency bin were

linearly interpolated to produce a 2D image (64 x 64 pixels). The resulting images were stacked to produce a 3D image with two spatial and one frequency dimension (Kilner & Friston 2010). This resulted in separate images for high and low frequency. To determine significant regions within this image it was compared with null (surrogate) data in which any coherence was destroyed. Ten surrogate coherence images were generated from the same MEG data but with the order of STN-LFP trials shuffled. The original and surrogate images were smoothed with a Gaussian kernel (a 10 mm x 10mm x 2.5 Hz for the lower frequencies, 10 mm x 10mm x 7.5 Hz for the higher frequencies to ensure conformance to the assumptions of Random Field Theory) and subjected to a two-sample t-test, using standard Statistical Parametric Mapping (SPM) procedures. The SPMs were thresholded at $p<0.01$ (family-wise error corrected) to identify significant regions in sensor space and frequency. For each STN-LFP, this provided frequency ranges where there was significant sensor level coherence over channels. These frequency ranges were entered into a DICS beamformer and the global maximum of the resulting DICS image was defined as the location of the cortical source coherent with the STN. Crucially, the significance of this source is established by the SPM analysis. This is because the significant (frequency-specific) coherence, seen in the sensors, has to be caused by sources. The orientation of the cortical source was defined as the normalized imaginary part of the cross-spectral density vector between STN-LFP and the three orientations of MEG source, located at the grid point closest to the optimal location. Typically orientation is defined by the direction of maximum power (Gross et al., 2001). We chose the imaginary part (i.e. non-zero lag) to specifically focus on physiological signals transmitted with delay between the STN and the cortex (Nolte et al., 2004) assuring additional immunity from the artefact.

A DICS beamformer image always has a global maximum even in cases of meaningless or erroneous localization. Therefore, we performed supplementary analyses to verify the internal consistency of the implicit source localisation. The idea was to generate a simulated coherence pattern that would be expected from the localized source and compare it with the original coherence pattern. The observed coherence pattern is determined by the location and orientation of the generating source as well as by the signal-to-noise ratios at different MEG channels or, in other words, by other cortical sources and artefacts. In our case, large metal artefacts might distort the observed coherence patterns, relative to what would be expected on the basis of source lead field alone. We therefore combined the simulated data with the original data to make the simulation as realistic as possible. STN-LFP data and the corresponding extracted source data were shifted by one trial with respect to the original data. The source data were then projected through the source lead field and added to the

original (non-shifted data) to create simulated MEG data. We then computed the coherence between the shifted STN-LFP and the simulated MEG. Shifting eliminated the coherence between STN-LFP and the original MEG. Thus the coherence between shifted STN-LFP and simulated MEG was solely due to the simulated component of the MEG. However, the artefacts and non-coherent brain sources were the same as in the original data. The simulated and original coherence topographies for all sources were inspected. In the case of any discrepancy (on visual inspection), sources were excluded from further analysis.

3.2.5 Characterisation of effect of dopaminergic medication and frequency on coherence topography across patients

The aim of this analysis was to determine if the topography of cortico-subthalamic coherence was frequency and medication dependent. To allow group comparison of data, DICS images were generated at fixed frequency bands in the alpha (7-13 Hz) and beta (15-35 Hz) ranges in all patients using each of the bipolar STN-LFP channels as a reference. Unthresholded Individual images were normalised by dividing the coherence value at each beamformer grid point by the mean value of that image. This potentially removes confounds related to nuisance variations in signal-to-noise ratio such as variable head distance from MEG coils. However, it also constrains the analysis to distinguish changes in topography (not absolute values). Images were smoothed as described previously. To account for the predominantly asymmetric nature of the disease and to increase our sample size, each STN was treated as a separate subject. Half of the resulting images (all left STN) were reflected across the median sagittal plane to allow comparison of ipsilateral and contralateral sources to the STN regardless of original STN side. These images were then subjected to a fixed-effect 2x2 factorial ANOVA, with frequency and medication as factors in SPM. The main effects of frequency and medication were estimated with an F-contrast whilst post-hoc one-tailed t-contrasts were used to determine the direction of significant effects and to generate frequency-specific search volumes, within which to search for a simple main effect of medication at a particular frequency. All analyses were corrected for multiple comparisons within the search volume (using random field theory) and thresholded at $p<0.01$.

Peak voxels resulting from group-level SPMs underwent further exploratory analysis for directionality, local power and correlation with clinical features. First, we performed extraction of the time-series (virtual electrode) data using a linearly constrained minimum variance (LCMV) beamformer (Van Veen et al., 1997) and 0.01% regularization. The covariance matrices for beamforming were computed based on the epoched data and the

position and orientation of the source was as defined above. Source and STN-LFP power estimates are presented as the mean across all STN bipolar contacts and patients.

Directionality: Coherence *per se* gives no information about the direction of coupling between synchronized populations of neurons, i.e. which population activity leads in time. The most parsimonious explanation for such a relationship between two coherent population activities is that the leading population drives the lagging population. However, this may not be the only explanation for such a relationship, and driving may be direct or indirect, via one or more unrecorded structures, or activity in both recorded structures may be driven by a third unrecorded structure (Sharott et al., 2005a). Finally, most connections in the brain are bidirectional (reciprocal), which means the concept of a driving population is a category error. Given this, we use the term 'effective direction of coupling' (distinct from effective connectivity (Friston et al., 2012)) to describe a pattern of temporal relationships rather than a measure of coupling. We characterised this using partial directed coherence or PDC (Baccala and Sameshima, 2001). Previous studies (Cassidy et al., 2002; Sharott et al., 2005b; Lalo et al., 2008) have used directed transfer function or DTF (Kaminski and Blinowska, 1991) which is another measure based (as with PDC) on the notion of Granger causality (Granger, 1969). Granger-based estimates have the advantage that, unlike phase estimates, there is no ambiguity in systems with bidirectional coupling, such as basal ganglia-cortical loops (Cassidy and Brown, 2003). We used PDC in the present study as this measure has been recently shown to be more robust to distortions resulting from filtering and downsampling of the data (Florin et al., 2010). Where the PDC of coherent activity at two sites is asymmetrical, the 'effective direction of coupling' is said to predominate in one direction and coherent activity or activities in one population of neurons tend to lead in time (Sharott et al., 2005a). Within each hemisphere and frequency band, we considered the STN-LFP with the largest coherence to give the best estimate of source activity and used this contact to calculate the PDC. We computed the PDC with the multivariate autoregressive modelling toolbox in SPM8. This relies on a Bayesian estimation algorithm described by Penny and Roberts (Penny and Roberts, 2002). PDC was computed for each trial in the original data and in surrogate data generated by shifting the STN-LFP by one trial with respect to the virtual electrode data above. Two-sample t-tests were then performed between the original and surrogate PDC estimates averaged over the frequency range of interest for each direction. If both t-tests were significant ($p<0.05$) the connection was categorised as, "bidirectional". Chi-squared tests were used to determine significant variation in the proportional distribution of directionality estimates in different frequency bands and medication states.

Correlation with clinical features: To explore whether motor function correlated with activity in any of the circuits identified, we correlated three pre-operatively determined clinical scores with cortico-subthalamic coherence and log cortical power. The clinical scores were the total Unified Parkinson's Disease Rating Score (UPDRS) part III score, a hemi-body akinesia and rigidity (Hammond et al., 2007) score (sum of items 22-26 of the UPDRS part III) and a hemi-body tremor score (sum of items 20-21 of the UPDRS part III). Correlations with symptom severity were assessed with data collected when patients were withdrawn from their medication overnight. The motor UPRDS was tested in this practically defined off state (so that patients had their last antiparkinsonian medication 9 -12 hours prior to testing). The effect of dopamine was assessed by correlating the change in clinical variables after dopamine with the change in electrophysiological variables. Spearman's rho was used for all correlations and correction for multiple comparisons was performed by a Bonferroni correction, set to an alpha of 0.05. It should be noted that patients studied post-operatively often have a temporary amelioration of their Parkinsonism due to a 'stun' or 'microlesional effect. This was not quantified in the present study.

To ensure that significant medication effects on coherence were not merely due to confounding local changes in cortical power we also correlated change in cortico-subthalamic coherence after dopaminergic medication with change in local cortical power, for each source.

3.3 Results

3.3.1 Clinical features

Clinical details are presented in **Table 3**. The mean age of this cohort was 53.6yrs, with a male: female sex ratio of 3.3:1. All patients responded to levodopa (mean UPDRS score off medication = 46, on medication = 16), except case 3 who was unable to tolerate the medication. Although no subjects had active psychiatric symptoms during the time of the operation, patients 7 and 11 had previously reported symptoms of medication-induced hypersexuality and patient 5 had previously developed dopamine dysregulation syndrome.

3.3.2 Contact location

Out of 25 STNs, the most superior contact was located rostral to the STN in 6 hemispheres, rostral but near the superior border of the STN in 4 hemispheres, rostral and touching the

superior border of the STN in 6 hemispheres, medial to the superior STN in 7 hemispheres (five touching), touching the medial aspect of the middle anteromedial region in one hemisphere and inside the superior region in one hemisphere.

The most inferior contact was usually located inside (8 hemispheres) or outside, but near (10 hemispheres), the inferior STN. Two cases were medial and touching and one case lateral and touching the inferior STN. Two cases were touching the medial aspect of the middle posterolateral region and one case was inside this region. The final case was outside but medial to the centre of the STN. No contact was lateral to the STN.

3.3.3 Individual patients display spectrally and spatially restricted sensor-level patterns of cortico-subthalamic coherence

Sensor level coherence analysis identified significant areas of cortico-subthalamic coherence over neighbouring channels and frequency bins. An example of coherence in the beta frequency range is given in **Figure 8**. The frequency band over which coherence was significant was used to create a DICS image. The global maximum of the DICS image was registered onto the patient's pre-operative MRI. **Figure 8** demonstrates that in this individual, an ipsilateral cortical source was coherent with the left STN in the beta frequency range. Further analysis of this source with an LCMV beamformer identified the frequency at which there was maximal coherence and confirmed that maximal coherence was within the significant frequency range identified by the sensor-level SPM analysis.

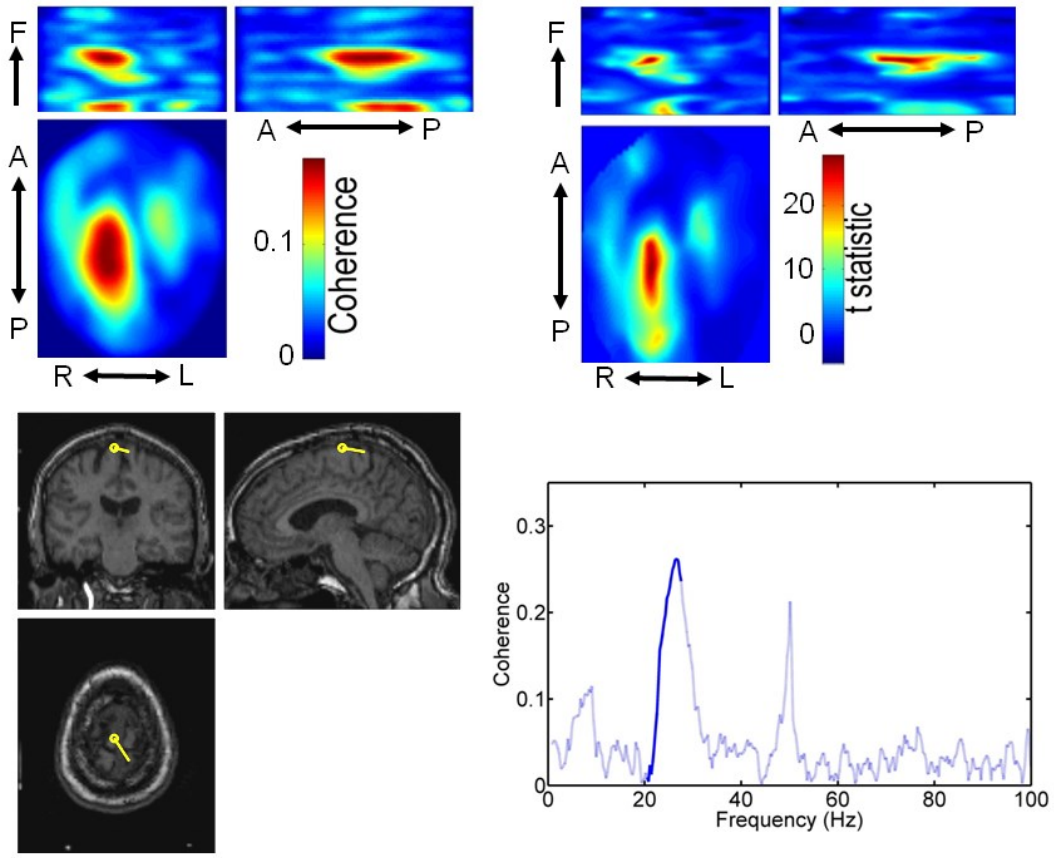

Figure 8: Example analysis representing beta frequency coherence referenced to a bipolar left STN DBSE channel in one patient. *Scalp maps of coherence at each frequency bin were interpolated to a 2D grid (64x64 points) and stacked to produce an image with two spatial and one frequency dimension (top left images). Frequency bands with significant coherence were identified by shuffling STN-LFP data and performing t-tests with SPM (top right image). The significant frequency range (in this case 20.5-27.5 Hz) was used to create a DICS image, and the global maximum was plotted on the patient's MRI (bottom left image, yellow circle is DICS maximum, and line represents orientation). An LCMV beamformer was used to extract the source activity at this location and the coherence between this and the STN bipolar channels was calculated across the entire frequency range (bottom right image: the significant range is represented by a solid blue line (other frequencies by a semi-transparent blue line). Anterior (A), posterior (P), left (L), right (R), frequency (F). Warmer colours correspond to increased cortico-subthalamic coherence.*

3.3.4 Spatial location of cortical sources coherent with STN is consistent across patients

In total, cortico-subthalamic coherence was estimated for 25 subthalamic nuclei from 13 patients (one with a unilateral electrode). Each of the three STN bipolar channels (apart from one STN where only one bipolar channel was available due to an artefact in the other channels) was used as a reference to calculate the location and frequency range over which significant cortical coherence existed. Although the frequency ranges spanned 5 – 90 Hz, none of the sources above 45 Hz had a scalp pattern typical of a focal cortical source. These high-frequency sources were therefore excluded from further analysis (see section 3.2 and **Figure 9**). It was also apparent that two DICS images from separate bipolar contacts within one STN could generate two spatially and spectrally similar cortical sources which were in fact slightly different estimations of the same cortical source. To counter this redundancy, we only included the maximally coherent source from each STN, if sources were within 15 mm and 3 Hz of each other. This resulted in a total of 68 cortically coherent sources in the alpha and beta ranges whilst patients were off their medication, and 67 sources whilst patients were on their medication (mean of 5.2 cortical sources per STN in each medication condition). In the off medication condition, nine patients had at least one alpha source, and 11 patients had at least one beta source. In the on medication condition, 10 patients had alpha sources and 12 patients had beta sources. The peak frequency and spatial location of coherent cortico-subthalamic sources are displayed in **Figure 10** and **Figure 11**. In the frequency range below 45 Hz, sources fell into two broad bands, which we will term the alpha band at 7-13 Hz and the beta band at 15-35 Hz. These ranges formed the basis of the fixed frequency bands used for group analysis. Sources in the beta range clustered around medial motor/premotor areas ipsilateral to the STN, whilst alpha range sources clustered in bilateral temporoparietal regions, but with ipsilateral predominance. The peak coherences in the two bands were not (inversely) correlated within hemispheres (**Figure 12**), so that it is unlikely that the different spectral activities were mutually exclusive.

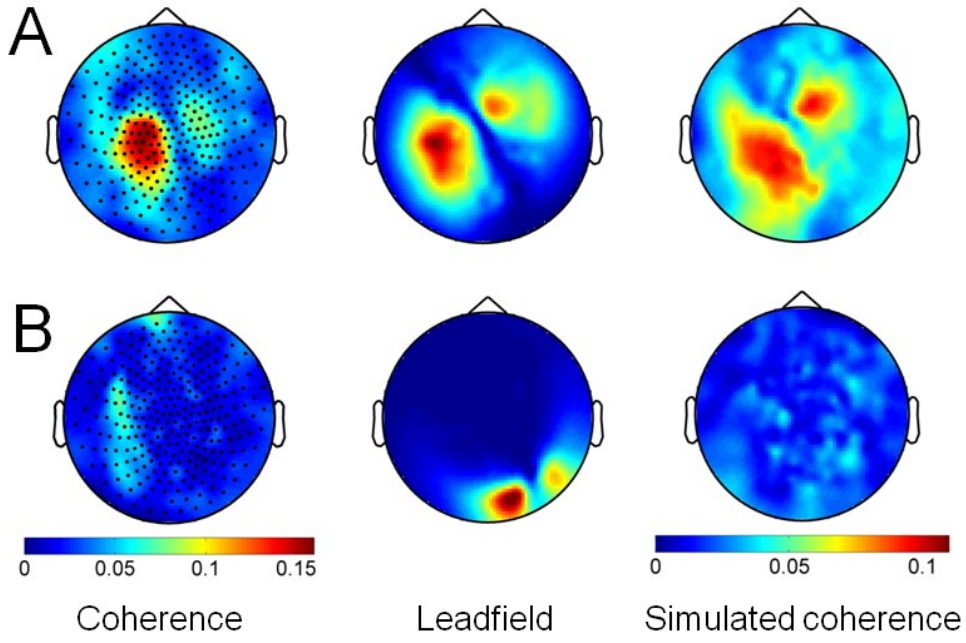

Figure 9: Topographical maps of coherence. *Maps from a significant beta source (top row, A) and a significant gamma source (bottom row, B). The first image in each row is the original coherence scalp map (the black dots correspond to channel location), the second is the map of absolute values of the putative source lead field and the third is the simulated coherence plot (after adding in noise). The beta source shows a convincing relationship between the images whereas the gamma source shows no such characteristic pattern, and has a much smaller maximum coherence.*

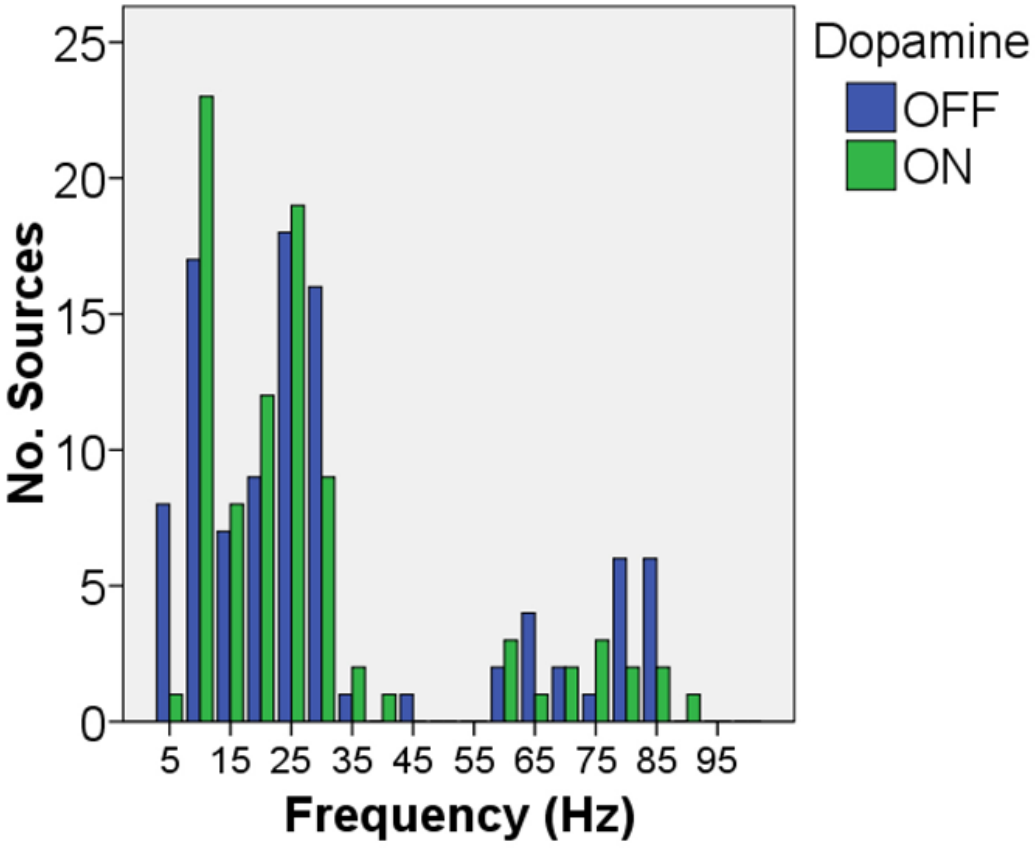

Figure 10: Frequency distribution of potential cortical sources. *Thirteen patients (25 STNs) recorded twice in PD patients with (ON) and without (OFF) dopaminergic medication (n=135). We searched for coherent sources between 5-45 Hz and 60-90 Hz, although after subsequent visual lead field inspection we excluded sources above 45 Hz (see methods). Note that notch filters were used to remove line noise at 50 and 100 Hz.*

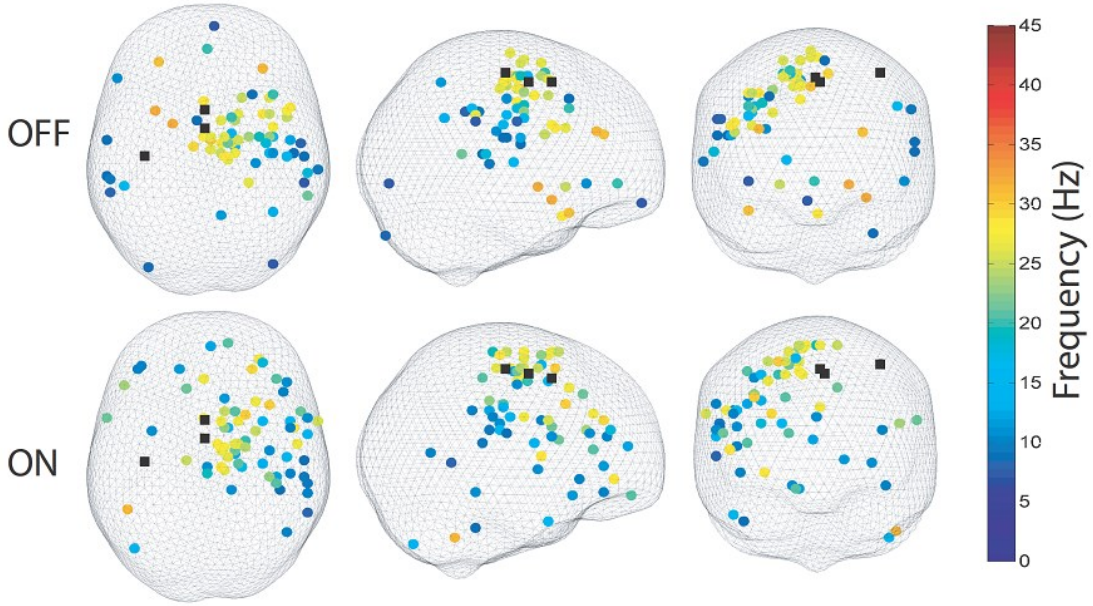

Figure 11: The variation in location and peak frequency of significant cortical sources coherent in the 5-45 Hz frequency range. *Results from 25 STNs. The images are 'glass brains' (inner boundary of skull marked with grey mesh) viewed from the above, right and front. All left STN sources are reflected across the middle sagittal plane to allow comparison of ipsilateral (right) and contralateral (left) sources. Results are separately displayed for the ON (bottom row) and OFF (top row) medication conditions. The peak frequency of the coherence is represented by a colour scale where warmer colours reflect higher frequencies. Black squares have been used to represent the middle of the motor cortex (most posterior, lateral), supplementary motor area (SMA, medial), and pre-SMA (most anterior, medial). The distribution of sources remained remarkably similar in both drug conditions, in spite of the fact that these recordings were acquired on different days and undoubtedly with different confounding parameters (e.g. distance of head from the MEG sensors).*

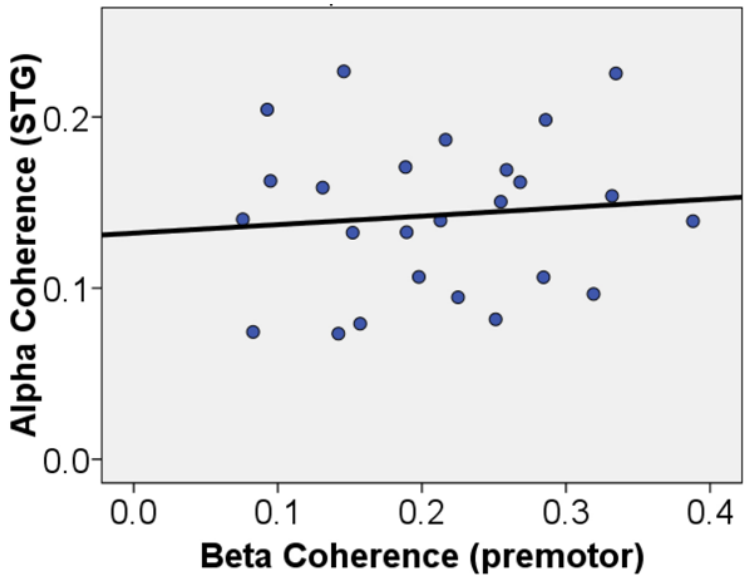

Figure 12: Independence of peak alpha and beta coherence within individual hemispheres. *To ensure that the group analysis did not mask an individual tendency to have either ipsilateral alpha or ipsilateral beta coherence, but not both, we compared the peak beta coherence (premotor location) with peak alpha coherence (superior temporal gyrus, STG, location) within hemispheres. There was no significant correlation in either the OFF medication condition (Pearson's r=0.09, p=0.66, see graph), or the ON medication condition (Pearson's r= -0.08, p=0.70, not shown).*

3.3.5 Topography of cortical activity coherent with STN activity is frequency dependent across patients

We tested for the effect of frequency and dopaminergic medication on coherence by performing a group analysis. We computed DICS images with the standardised frequency bands (alpha 7-13 Hz and beta 15-35 Hz). All three bipolar images per STN were entered into a fixed-effect ANOVA with frequency and medication as factors. To address confounding issues, and allow a meaningful comparison between different frequencies (see methods) DICS images were normalised by dividing by the mean value over voxels. Consequently, we were comparing differences in the topography of cortico-subthalamic coherence. The mean of all the normalised DICS images revealed a temporoparietal and brainstem preponderance for alpha coherence and a supplementary motor area (SMA)/premotor preponderance for beta coherence (**Figure 13**). The main effect of frequency was highly significant across multiple brain regions (**Figure 14**). Regional coherence was greater in the beta band than the alpha band in a predominantly ipsilateral fronto-medial distribution. Conversely, regional coherence was greater in the alpha band in bilateral temporoparietal regions, with an ipsilateral predominance, and in the brainstem (SPM thresholded at $t(1,264)=5.45$, $p=0.01$ for display purposes). In addition, the mean absolute (non-normalised) coherence spectra were computed for virtual electrode data extracted for the peak voxel within each cluster using an LCMV beamformer. These coherence spectra (**Figure 14**, right) confirmed the group (normalised) analysis findings that beta coherence was higher in the premotor and prefrontal regions and alpha coherence higher in the temporoparietal regions and brainstem.

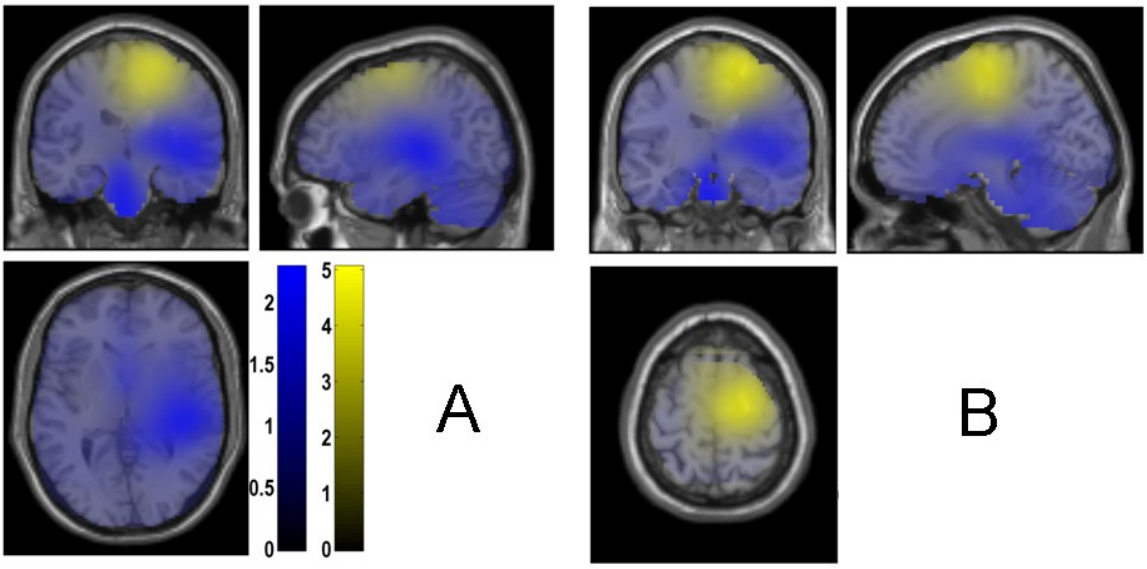

Figure 13: Mean of the normalised DICS images. *Unthresholded alpha (blue) and beta (yellow) coherence superimposed is onto a T1 weighted canonical MRI. Coronal, sagittal and axial sections through the image are displayed, oriented to the image local maxima in the temporoparietal region (A, alpha, centred at global alpha peak) and the premotor/SMA region (B, beta, centred at global beta peak). The colour scale is coherence normalised to individual image global values (arbitrary units). A value greater than 1 unit means that the activity in that voxel is consistently greater than the mean across the image.*

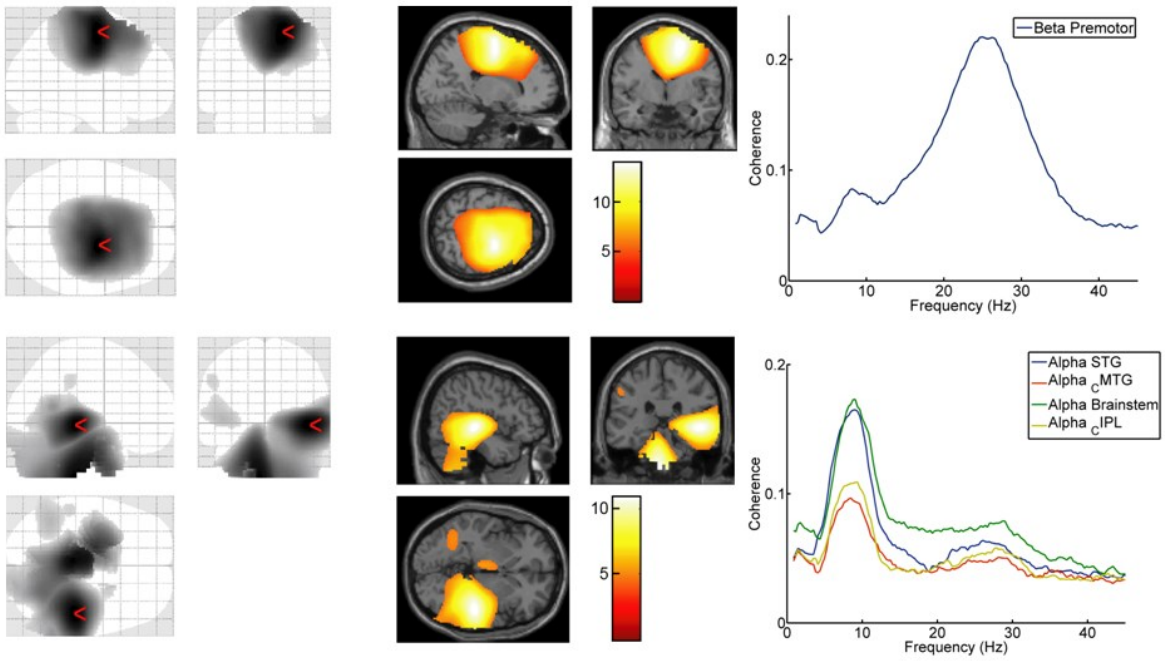

Figure 14: SPMs showing differences in the relative topography of alpha and beta band coherence between cortex and subthalamic region. *[Top Row] Voxels where beta is significantly greater than alpha coherence normalised with respect to image mean. A local maxima was identified in the supplementary motor/premotor area (18 -6 58, F(1,264) = 192, p<0.001, red arrowhead). The mean absolute coherence spectrum for this voxel (labelled Beta Premotor) is shown on the right. [Bottom row] Voxels where alpha was significantly greater than beta coherence normalised with respect to image mean. Local maxima were identified in the ipsilateral superior temporal gyrus (STG, 46 -30 -2, F(1,264)=119, p<0.001, red arrowhead), and brainstem (20 8 -44, F(1,264)=29, p=0.001) and also in the contralateral medial temporal gyrus (CMTG, -44 -54 4, F(1,264)=32, p<0.001) and inferior parietal lobule (CIPL, -54 -34 40, F(1,264)=25, p=0.004). The mean absolute coherence spectrum for these voxels is shown on the right. Colour bar indicates t statistic.*

3.3.6 Dopaminergic medication has an effect on topography of cortico-subthalamic coherence in the beta frequency band

There was no significant main effect of dopaminergic medication. However, there was a significant simple main effect of dopaminergic medication on coherence in the beta frequency band in two ipsilateral prefrontal regions (SPM thresholded at t(1,264)=4.10, p=0.01, small volume corrected for a search volume specified by the main effect of beta frequency; **Figure 15**). This was not due to confounding local changes in power (**Figure 16**). There were no medication effects detected in the alpha band.

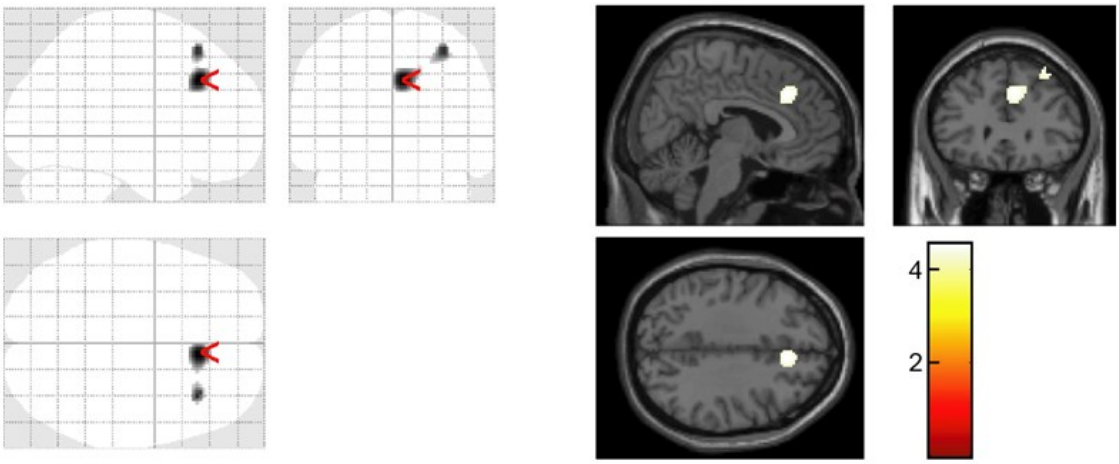

Figure 15: SPMs testing for the effect of dopaminergic medication on coherence. *Beta coherence relative to image mean, increased with dopaminergic medication in two prefrontal clusters medially (PFCM, 6 30 36, t(1,264)=4.52, p=0.002, red arrowhead) and laterally (PFCL, 34 28 54, t(1,264)=4.42,p=0.003, small volume corrected). Colour bar indicates t-statistic.*

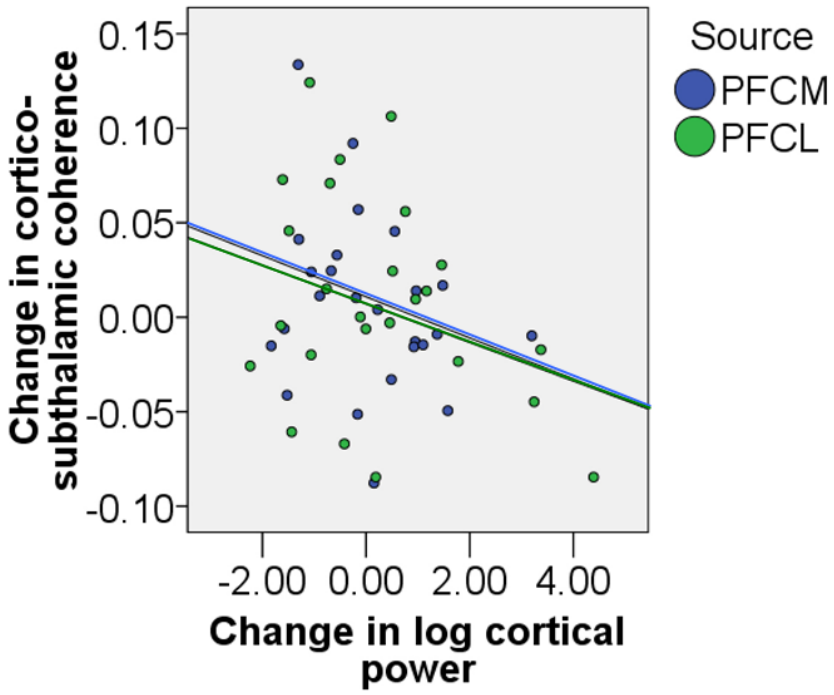

Figure 16: Simple effect of dopaminergic medication on beta frequency coherence was not due to local changes in cortical power. *To determine this we performed a Pearson's correlation between log source peak beta frequency power and beta frequency coherence across STNs. There was no significant relationship in either the medial (PFCM, r=-0.19, p=0.37) or lateral (PFCL, r=-0.15, p=0.47) prefrontal sources.*

3.3.7 Relationship between cortical activity, STN activity and coherence

For each STN, cortical source activity (non-normalised) was extracted at each of the (seven) peak voxels from the group SPMs above. The mean cortical source activity in each medication condition is shown in **Figure 17** together with mean STN-LFP power (across all three bipolar contacts) and mean coherence. Dopamine subtly increased beta coherence in the PFC regions, but the relatively small effect suggests the group effect of dopamine on these regions could also have been partially explained by a reduction in mean beta coherence across other brain regions with medication; so that beta coherence became more focal with dopamine. Beta activity in the STN was divided into a lower frequency component (15-20 Hz), which was more prominent in the OFF condition and highly responsive to dopamine, and a higher frequency component (25-35 Hz), which was most evident in the ON condition; although also suppressed by treatment, and was at the same frequency as cortico-subthalamic beta coherence. Cortical activity was concentrated below 15 Hz in all sources, even in those displaying maximal coherence at higher beta frequencies.

3.3.8 Effective direction of cortico-subthalamic connectivity

Extracted, non-normalised, cortical source and STN activity (see above) was also used to investigate functional connectivity. The partial directed coherence was used to ascribe an effective direction of connectivity between each cortically coherent source and each STN bipolar contact. The connectivity was categorised as STN leading, cortex leading or bidirectional. Connectivity was predominantly cortex leading (chi-squared (d.f. =2) =239, $p<0.001$;**Figure 18**) and was not affected by dopaminergic medication (Pearson chi-squared (d.f. =2) =2.0, $p=0.32$). However, cortical source location (**Figure 19**; Pearson chi-squared (d.f. =12) = 37, $p<0.001$) and frequency of coherence (**Figure 18**; Pearson chi-squared (d.f. =2) = 54, $p<0.001$) with the STN did modify the effective direction of connectivity.

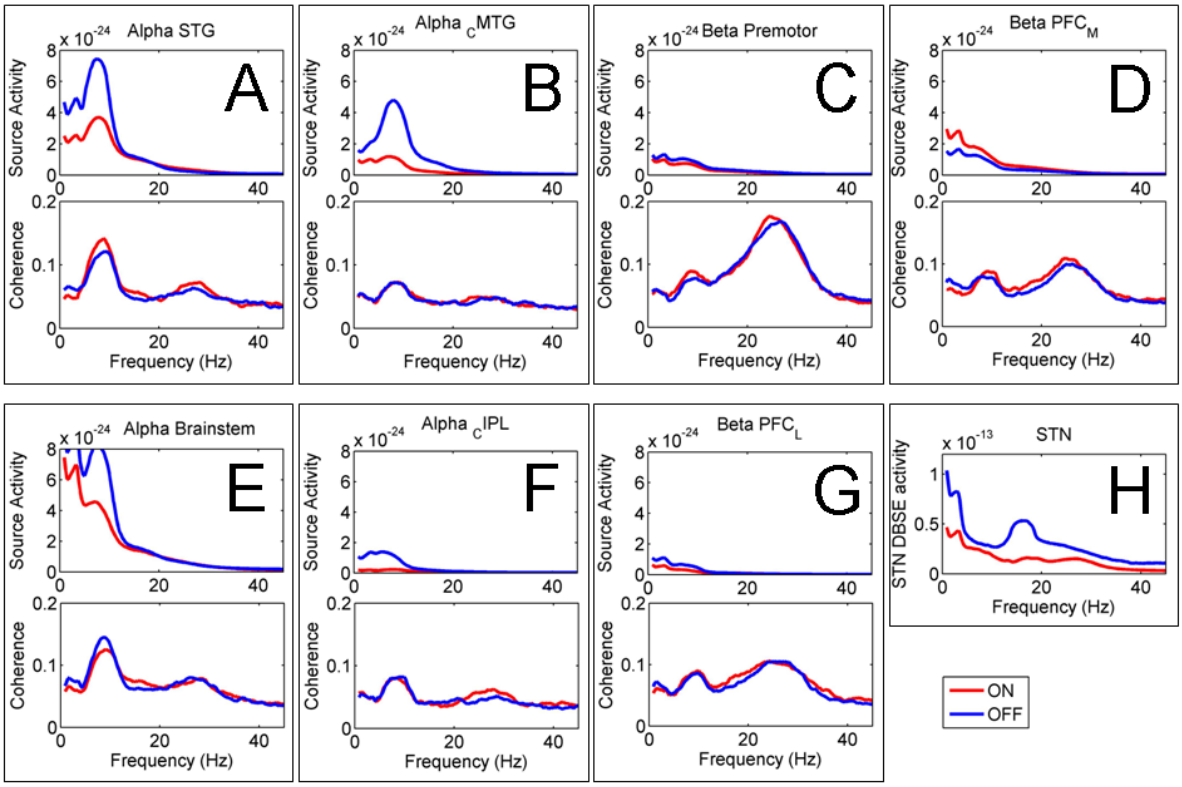

Figure 17: Relationship between cortical activity and cortico-subthalamic coherence. *The cortical power spectrum and cortico-subthalamic coherence spectrum is shown for the seven peak voxels (panels A-G) derived from the group comparison. Each graph displays the mean non-normalised activity ON (red line) and OFF medication. Panel H shows the mean STN activity for comparison. Note that alpha sources (panels A,B,E,F) show larger alpha coherence, whilst beta sources (panels C,D,G) show larger beta coherence. Most cortical power is below 15Hz. Note also that peak beta power in the STN region is at a much lower frequency than peak beta coherence for the beta sources. Panels are labelled A, alpha superior temporal gyrus (STG); B, alpha contralateral medial temporal gyrus (CMTG); C, beta premotor; D, beta medial prefrontal cortex (PFCM); E, alpha brainstem; F alpha contralateral inferior parietal lobule (CIPL); G beta prefrontal cortex (PFCL); H subthalamic nucleus (STN) region.*

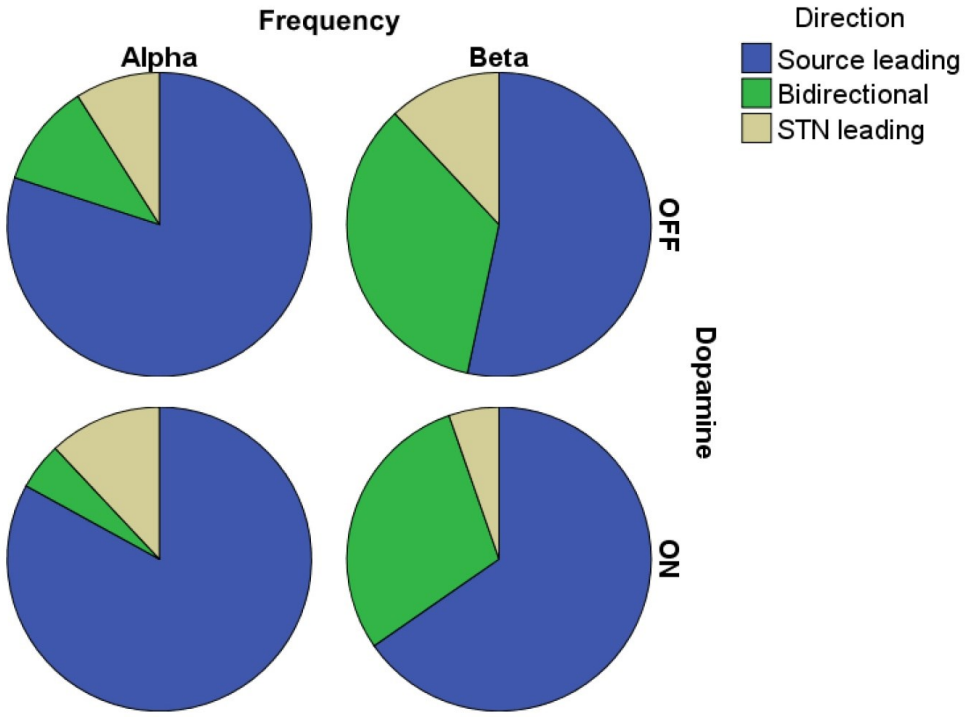

Figure 18: Effective direction of coupling between cortex and subthalamic region. *Frequency does, but dopaminergic state does not, have an effect on the effective direction of cortico-subthalamic connectivity. Cortical sources led in both medication conditions.*

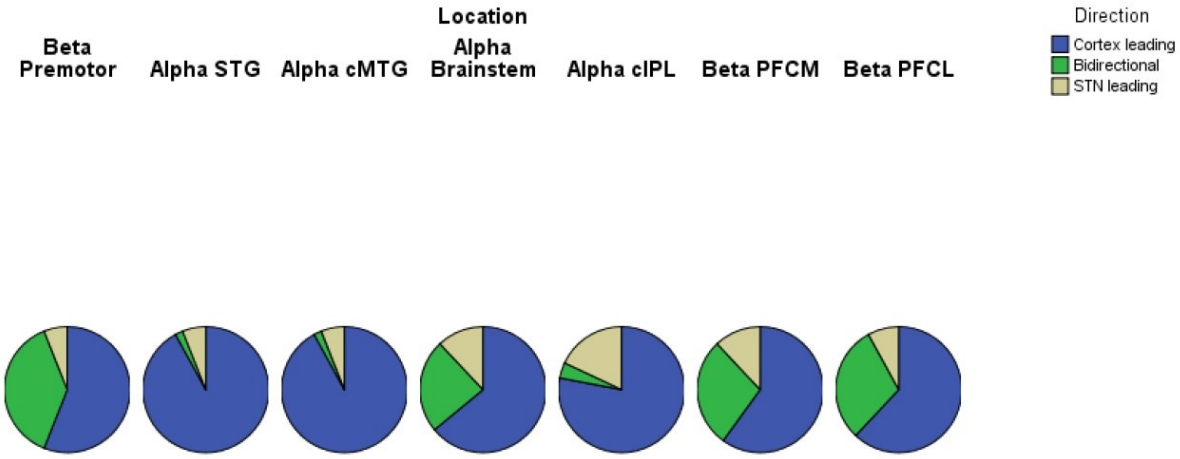

Figure 19: Variation in the effective direction of coupling between cortex and subthalamic region according to cortical location. *Sources are in the premotor area/SMA (Beta Premotor), superior temporal gyrus (Alpha STG), contralateral medial temporal gyrus (Alpha CMTG), the brainstem (Alpha Brainstem), the contralateral inferior*

parietal lobule (Alpha CIPL), the medial prefrontal cortex (PFCM) and the lateral prefrontal cortex (PFCL).

3.3.9 Correlation between effect of dopaminergic medication on source activity and clinical variables

We investigated whether clinical symptom severity (as assessed by the total UPDRS score, hemi-body tremor score and hemi-body akinesia-rigidity score recorded preoperatively OFF dopaminergic medication) correlated with cortical coherence or log cortical power at each of the source locations from the group analysis. To investigate the effect of dopaminergic medication on these correlations, we also compared change in these clinical scores with dopamine (ON – OFF medication) with change in the same electrophysiological parameters. No comparisons survived the Bonferroni correction for 84 multiple comparisons (equivalent to uncorrected $p < 0.0006$).

3.4 Discussion

We have demonstrated two major spatio-temporally organised and stereotyped patterns of coupling between the cerebral cortex and STN region in patients with PD. The first was manifest in the alpha frequency band and involved coherence between the subthalamic area and bilateral temporoparietal cortex and the brainstem. It was distinct from the previously described alpha network coherent with Parkinsonian rest tremor (Timmermann et al., 2003; Pollok et al., 2009). Changes in alpha activity in the subthalamic region have also been reported in response to emotional stimuli (Brucke et al., 2007). However, the areas of cortical involvement and the fact that subjects were at rest, suggest that the network involving the subthalamic area, bilateral temporo-parietal cortices and the brainstem might influence attentional levels, particularly as the processes controlling the latter often involve oscillations at about 10 Hz (Palva and Palva, 2007). Similarly, alpha band oscillations with a putative role in attention have been recorded in the brainstem pedunculopontine region, which is directly connected with the STN (Androulidakis et al., 2007). The ability of MEG to pick up signals from the brainstem is not well-established in the literature. However, Parkkonen et al reported recording of brainstem early auditory evoked responses with MEG(Parkkonen et al., 2009) and Schnitzler et al showed, using DICS beamformer, that the brainstem is involved in the network associated with essential tremor (Schnitzler et al., 2009). Therefore, our finding of brainstem involvement in the alpha network is not implausible. Additionally we should note that the spatial resolution of beamforming is poor in

this area (due to the correlation between lead fields) and therefore we have been conservative in our interpretation of statistically significant activity near the brainstem (e.g. in the cerebellum). Further studies are needed to identify whether this activity truly represents other sources separate from the brainstem.

The second pattern of coupling was evident in the beta frequency band and predominantly involved coherence between the subthalamic area and the ipsilateral anterior parietal and frontal cortices. The areas of cortical involvement suggest that this network, recorded at rest, might be engaged in setting the level of preparedness for executive functions. This would be compatible with the emerging view that beta activity may promote the status quo at the expense of action (Hammond et al., 2007; Engel and Fries, 2010). Overall, there were clear topographical differences between the activities in the alpha and beta frequency bands, despite normalisation to the mean power in each band. The results support the general hypothesis described by Fogelson et al. (Fogelson et al., 2006) that "frequency of synchronisation may be exploited as a means of marking and segregating processing in the different functional subloops, over and above any anatomical segregation of processing streams."

Importantly our findings are broadly consistent with a parallel study performed in a similar group of subjects with non-ferromagnetic wires (Hirschmann et al., 2011). The use of such wires, reduces sensor-level ferromagnetic artefact – a major challenge for MEG recordings. Hirschmann et al used similar beamforming techniques to localise beta cortico-subthalamic coherence in motor areas and alpha coherence in temporal areas supporting our findings of two separate networks at rest.

3.4.1 Supremacy of the cortical drive to the STN area

One marked finding was the predominance of the PDC from cortex to the STN region. Similar apparent driving of LFP activity in the STN region in the beta band by cortex in PD patients has been noted using linear regression of phase (Brown et al., 2001; Williams et al., 2002; Fogelson et al., 2006) and the DTF (Lalo et al., 2008). This has been further replicated in animal models of PD (Sharott et al., 2005a; Lalo et al., 2008; Mallet et al., 2008). These observations are compatible with the recent demonstration in a rodent model of PD that it is

sufficient to stimulate the afferents to the subthalamic nucleus at high frequency, rather than the local neurons themselves, to overcome Parkinsonism (Gradinaru et al., 2009).

The asymmetry of the PDC is also important in suggesting that coherence represented physiological coupling with delays, rather than volume conduction. Volume conduction between high amplitude cortical sources and low amplitude subthalamic LFPs is a real concern given the similarity between subcortical and cortical activities and their coupling. Many arguments have been put forward to refute an influence of volume conduction under these circumstances (reviewed in (Brown and Williams, 2005)), but the most convincing is the demonstration that the discharge of neurons in the STN tends to be locked to the beta activity in the LFP (Levy et al., 2002; Kuhn et al., 2005). In the current study, we limited the effects of volume conduction by estimating coherence between cortex and the subthalamic region using only bipolar derivations of DBS electrode contacts.

3.4.2 Frequency of subthalamo-cortical coherence

Another interesting feature of the subthalamo-cortical coherence is that it was focussed in the upper beta frequency band. LFP power in the STN region, on the other hand, was greater in the lower beta frequency range, in patients withdrawn from medication. The implications are twofold. First, the difference in frequencies between peak subthalamic power and peak subthalamo-cortical coherence reinforces the notion that subcortico-cortical coherence is not a simple passive phenomenon, but that its pattern is dictated by the transfer characteristics of the pathways involved. Second, the difference in frequencies adds weight to the argument that subthalamic activities in the lower and upper ranges of the beta frequency band may have somewhat different functional significance (Williams et al., 2002; Priori et al., 2004; Fogelson et al., 2006). Activity in the upper beta band seems to be more strongly coupled with cortical activity, and relatively less modulated by dopaminergic therapy.

3.4.3 Is subthalamo-cortical coherence at rest due to default brain networks?

Why should there be such a spatio-temporally organised and stereotyped pattern of coupling between the cerebral cortex and STN region at rest? Current thinking is that when one is awake and at rest, brain activity, as reflected in blood oxygenation-level-dependent and

electroencephalographic signals, switches to default processes (Laufs et al., 2003). The present findings could be interpreted as extending this notion of default networks to include basal ganglia-cortical coupling. The characterisation of these networks as default, as opposed to resting, would also seem preferable, as it allows for ongoing postural activity, rigidity and rest tremor in our patients. However, it should be acknowledged that we have not directly shown that these basal ganglia-cortical networks are suppressed when subjects are engaged with novel stimuli or new tasks. On the other hand, previous studies have demonstrated that beta band coupling between cerebral cortex and the STN region drops before and during movement (Cassidy et al., 2002; Lalo et al., 2008), during imagination of movement (Kuhn et al., 2006a) and during action observation (Alegre et al., 2010). The functional networks described here are also entirely consistent with anatomical evidence from humans and non-human primates, which have shown that the basal ganglia project to the frontal and prefrontal cortex (Alexander et al., 1986; Middleton and Strick, 2002; Lehéricy et al., 2004; Akkal et al., 2007; Draganski et al., 2008), temporoparietal regions (Alexander et al., 1986; Middleton and Strick, 1996; Lehéricy et al., 2004) and the brainstem (Lehéricy et al., 2004; McHaffie et al., 2005).

So are the two networks primarily pathological or physiological, given that they were recorded in patients with PD? Without the opportunity to record from the subthalamic area in healthy subjects, or at least non-Parkinsonian patients, we cannot answer this question directly. A common approach under these circumstances is to determine whether dopaminergic therapy alters the pattern of activity noted in the untreated state. The approach is based on the premise that the core deficit in PD is partially reversed by exogenous dopaminergic input, although the homology between brain states in treated PD and the healthy subject is only likely to be approximate at best. Surprisingly, then, treatment with levodopa made relatively little difference to the default functional connectivity between STN and cortex, other than to increase coupling in the beta band in the region of the prefrontal cortex. Similarly, Lalo et al. (2008) found little effect of medication with levodopa on the STN-cortex DTF below 35 Hz, although there was an increase in the gamma band. Williams et al. (2002) did find a suppression of beta band STN-cortex coherence at rest following medication, but this was in a much smaller sample of patients. It may be that some of the negative findings relate to stun effects in the immediate post-operative period (Lalo et al., 2008). However, the limited changes in the networks following dopaminergic therapy might also suggest that they may be at least partly physiological phenomena in patients. Further support for this is provided by recent studies of cortico – basal ganglia functional connectivity based on functional magnetic resonance imaging and positron emission tomography. Both healthy subjects (Postuma and Dagher, 2006) and PD patients (Helmich et al., 2010;

Hirschmann et al., 2011) show resting connectivity between the basal ganglia and the supplementary motor area, the temporoparietal area and parts of the prefrontal cortex. Additionally, one study found connectivity between the brainstem and putamen in some healthy subjects (Kelly et al., 2009).

The limited changes following dopaminergic therapy are themselves surprising, given that such therapy leads to a marked improvement in motor behaviour. However, other studies comparing PD patients with controls (Helmich et al., 2010) and healthy subjects before and after receiving levodopa (Kelly et al., 2009) have also been unable to detect a change in motor or premotor cortex connectivity with the basal ganglia. This raises the possibility that the major effect of dopaminergic medication on coherence is not to modify the nature of basal ganglia-cortical connectivity at rest, but to increase its reactivity to stimuli and task demands. Indeed recent studies have found a link between *movement-related* cortico-subthalamic gamma coherence and effect of levodopa on bradykinesia (Litvak et al., 2012a). Furthermore, reduction in rigidity associated with stimulation of the STN correlates with low alpha (6-10Hz) and low beta (12-20Hz) frequency activity over central motor regions(Airaksinen et al., 2012). Therefore although we have identified two resting networks at alpha and beta frequencies, different frequencies and/or a multivariate frequency spectrum may correspond better with behaviour during task performance.

In summary, the findings support the general hypothesis that basal ganglia-cortical loops are characterised by both their topography and also by the pass band of their activities. More specifically, the results suggest the existence of two networks involving the subthalamic area and particular cortical regions synchronised at different frequencies. It remains to be seen whether these networks identified at rest are functionally involved in disengaging attention and action.

4: Resting cortico-pedunculopontine nucleus region connectivity in Parkinson's Disease

4.1 Introduction

The pedunculopontine nucleus (PPN), located at the junction between the midbrain and pons, is comprised of cholinergic, glutamatergic and GABAergic cells (Wang and Morales, 2009) and has been implicated in locomotion (Garcia-Rill et al., 1987; Skinner et al., 1990), sleep (Boeve et al., 2007; Lim et al., 2007, 2009; Arnulf et al., 2010), reward (Chen et al., 2006b; Norton et al., 2011), and arousal (Moruzzi and Magoun, 1949; Garcia-Rill and Garciarill, 1991). Recently, its role as part of the functionally defined mesencephalic locomotor region (an area that generates walking behaviour when stimulated in decerebrate animals) has become paramount because of its emergence as a stimulation target in patients with Parkinson's Disease (PD) and gait problems (Pahapill, 2000; Mazzone et al., 2005; Plaha and Gill, 2005; Stefani et al., 2007b; Ferraye et al., 2010; Moro et al., 2010; Alam et al., 2011). However, the efficacy of PPN deep brain stimulation (DBS) is variable (Stefani et al., 2007a; Ferraye et al., 2010), and the optimal target location is unclear. One possibility underlying variability in outcome is that different areas in the PPN region (PPNR) are functionally coupled with and modulate different brain circuits, only some of which are dysfunctional in gait disorders. Indeed whether the PPN itself or a neighbouring region is empirically the optimal surgical target region remains unclear. The importance of functional specialization in this region, particularly along the long axis of the PPN, is becoming increasingly apparent in animal studies (Martinez-Gonzalez et al., 2011).

In humans, functional magnetic resonance imaging (fMRI) and positron emission tomography (PET) have insufficient spatial resolution to reliably discern different areas of the PPNR (Ballanger et al., 2009; Snijders et al., 2011). However, direct recordings of local field potentials (LFPs) from intracranial electrodes afford excellent spatial and temporal resolution: we recently demonstrated that the nature of spontaneous oscillatory synchrony picked up in the LFP is topographically organized in the PPNR (Thevathasan et al., 2011, 2012). In particular, we showed that local activity in the alpha frequency band is maximal in a region that lies 2 mm to 6 mm below the pontomesencephalic junction. This area may correspond to the caudal PPN, and specifically to the caudal 'pars dissipata' – a diffusely bordered region containing a greater number (but lower concentration) of cholinergic neurons than the central PPN 'pars compacta' (Manaye et al., 1999). Importantly, alpha activity in this area correlated with gait performance, and DBS improved gait more when

delivered to this area, as opposed to more rostral and caudal regions of the PPNR(Thevathasan et al., 2012). Studies that have recorded EEG simultaneously with PPNR LFP have been encouraging in so far as functional coupling can be demonstrated between the PPNR and cerebral cortex, but these studies could not associate this coupling with particular cortical regions, due to the necessarily limited scalp recording sites in peri-operative patients and the presence of burr holes, which together preclude any spatial mapping (Gaynor et al., 2008; Classen and Schnitzler, 2010; Tsang et al., 2010; Thevathasan et al., 2012). Neither have these studies addressed the issue of how any coupling with cortical areas varies within the PPNR.

Here, we characterise how different brain areas may be differentially coupled at rest within the PPNR, taking advantage of recent methodological developments to simultaneously record LFP data from intracranial electrodes and magnetoencephalography (MEG) in a cohort of five Parkinsonian patients undergoing surgery for PPN DBS. MEG allows dense sampling of cortical activity even in post-surgical patients and is resistant to distortion by skull defects, so that cortical localisation can be performed in spite of prominent artefact due to the ferromagnetic electrode extension wires (Litvak et al., 2010, 2011a). Accordingly, we test whether PPNR coupling with different distant brain areas is frequency specific, modulated by dopamine and depends upon the position of the electrode within the PPNR. The results are important in understanding the diverse nature of the distributed brain networks involving the PPNR and how these may be organized through spatio-temporal patterning in this region.

4.2 Methods

4.2.1 Participants and surgery

We studied 5 (4 from Oxford, 1 from London) patients who had undergone PPN DBS electrode implantation prior to DBS therapy for PD. Four subjects had bilateral implants; although we were not able to record from one electrode in a subject due to a damaged electrode extension wire. One patient had a unilateral implant. These patients also took part in other experiments, some of which involved electrophysiological recordings and all of which have been reported elsewhere (Thevathasan et al., 2012). Clinical details (adapted from Thevathasan et al., 2012) are given in **Table 4**. Note that EMG recordings performed at the time of MEG demonstrated tremor in subject 4, who was known to have tremor, and in

subject 2, who was not known to have clinically significant tremor. However, in both cases, tremor was detectable for less than approximately a third of the time.

Patient	Age (years)	PD Duration (years)	UPDRS III off/on meds	IT27-30 off/on meds	Preoperative/ postoperative GFQ	FOGQ	FallsQ	L-dopa dose equivalent (mg/day)	Supportive for UK Brain Bank criteria*
1	55	14	35/24	7/6	55/38	22	4	1600	A,P
2	55	25	33/22	6/5	36/15	15	3	300	D,A,P
3	68	9	40/26	11/8	49/42	24	2	1650	A,P
4	70	20	35/22	6/5	36/28	13	3	900	D,A,T,P
5	71	20	37/19	10/5	na	na	2	1450	D,A,T,P

Table 4: Clinical details of the study participants *(adapted from* (Thevathasan et al., 2012)*). All patients were operated in Oxford except patient five (London). All patients were male. All subjects had bilateral PPNR implants except subject 5, who had a unilateral right PPNR implant. We were only able to record from the right PPNR in subject 1 due to a damaged electrode extension wire. Rostro-caudal stimulation location and clinical outcome data for all these subjects has been reported previously, with cases 1-5 corresponding to cases 1 and 3-6 in Thevathasan et al., (2011). Outcome was assessed by a drop in GFQ postoperatively. Outcome in patient 5 was assessed with UPDRS II items scoring freezing, falls and gait with the combined score being 5/16 preoperatively and 4/16 postoperatively (on medication).UPDRS III = part III (motor) of the Unified Parkinson's disease rating scale (score/108). IT27-30 = items 27-30 UPDRS III assessing gait, posture and balance (score/16). GFQ = Gait and Falls Questionnaire (score/64). FOGQ = Freezing of Gait Questionnaire (score/24). Falls Q = Falls Questionnaire (score/4). NA = not assessed. For all motor scales, higher scores indicate worse function. Key to UK Brain bank criteria; D=dyskinesias, A = asymmetry persistent, T=tremor at rest, P=progressive disease course. *Additional to disease duration and levodopa response as documented elsewhere in the table.*

The indications for surgery were PD with predominant levodopa-unresponsive gait impairment and/or falls due to either freezing or postural instability.

Prior to surgery, the motor impairments of all patients were evaluated using part III of the Unified Parkinson's Disease Rating Scale (UPDRS) after omitting all dopaminergic medication overnight and then following administration of 200mg of levodopa. Patients treated in Oxford also prospectively completed the Gait and Falls Questionnaire (GFQ, score/64) which assesses Parkinsonian gait disturbance including gait freezing, festination and falls. The Freezing of Gait Questionnaire (FOGQ, score/24) and Falls Question (FallsQ, score/4) are components of GFQ (Giladi et al., 2000, 2009). The London patient was assessed with UPDRS (part II) items assessing gait, freezing and falls (combined score/16). For all motor scales, higher scores indicate worse function.

Techniques to target and implant DBS electrodes in the PPN have been described previously (Pereira et al., 2008; Zrinzo et al., 2008; Foltynie and Hariz, 2010). In this study, preoperative stereotactic imaging (stereotactic proton density weighted magnetic resonance imaging (MRI) in London, and stereotactic computerised tomography (CT) fused with T2 weighted MRI in Oxford) were used to target the PPN medial to the lemniscal system and lateral to the superior cerebellar peduncle and its decussation. The DBS electrode used was model 3389 (Medtronic, Minneapolis, MN) with four platinum-iridium cylindrical contacts of diameter 1.27mm, length 1.5mm, and centre-to-centre separation 2mm. After implantation, electrodes were connected to an accessory kit, typically both connectors being tunnelled to the left temporoparietal area and externalised through the frontal region. No microelectrode recordings were made. To confirm correct placement, electrodes were visualised on immediate post-operative imaging with the surgical frame *in situ* (proton density weighted MRI in London and CT (1mm slice thickness) fused with pre-operative T2 weighted MRI in Oxford). To facilitate comparison across subjects, the postoperative images were linearly transformed into Montreal Neurological Institute (MNI) space using the fMRIB Software Library (Smith et al., 2004). The coordinates of each contact were determined (in millimetres) relative to the midline (X, laterality), ventrodorsal distance from floor of the fourth ventricle (d, anteroposterior location) and rostro-caudal distance from a pontomesencephalic (PM) line connecting the pontomesencephalic junction to the caudal end of the inferior colliculi (h, height), as described previously (Ferraye et al., 2010). Lead locations are summarised in **Figure 20**.

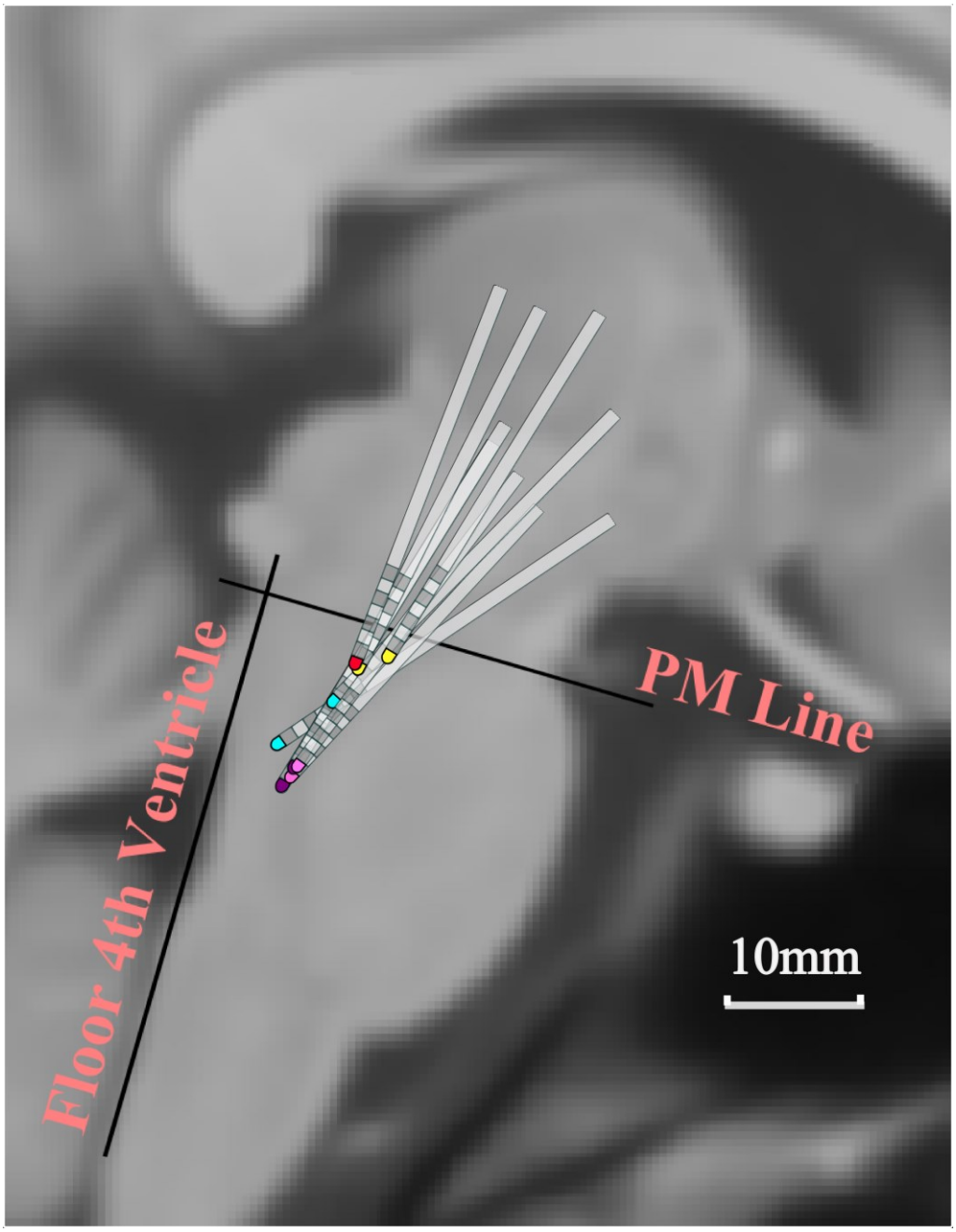

Figure 20: Localisation of contact locations within the brainstem, represented in Montreal Neurological Institute (MNI) space (sagittal view). *PM = Pontomesencephalic line connecting the pontomesencephalic junction to the caudal end of the inferior colliculi. Electrodes from different subjects have different coloured tips. Not all contacts are within the PPN, affording us the opportunity to divide the sampled brainstem region according to height with respect to the PM line. Note that this Figure is adapted from* (Thevathasan et al., 2012) *to show only those five subjects that were recorded concurrently with MEG. We were unable to record from one of the 9 electrodes shown, because of a damaged electrode extension wire. Flair MRI of case 2 showing axial slices at different depths is illustrated in supplementary material to* (Thevathasan et al., 2012).

4.2.2 Simultaneous PPNR-LFP and MEG recordings

MEG recordings were performed in London with the 275 channel CTF (VSM MedTech Ltd., Vancouver, Canada) or in Oxford with the 306 channel Neuromag (Elekta Neuromag Oy, Helsinki, Finland) systems. Simultaneous to the MEG recording, both right and left first dorsal interosseus (FDI) electromyographic (EMG) signals, and four intracranial LFP channels were recorded per electrode. All EMG recordings, and London LFP recordings, were referenced to the right mastoid and acquired using the integrated EEG system In Oxford, LFP signals in the PPNR were acquired in a bipolar configuration via a Digitimer D360 amplifier (Digitimer Ltd, Hertfordshire, UK), and high-pass filtered at 0.5 Hz. All data were sampled at 2400 Hz and stored to disk for subsequent off-line analysis. MEG, LFP and EMG data were hardware high-pass filtered at 0.03Hz (Oxford MEG and EMG) or 1Hz (London EMG and LFP; Oxford LFP only) and low-pass filtered at 600Hz (all signals). London LFP recordings were converted off-line to a bipolar montage between adjacent contacts (3 bipolar channels per side) to limit the effects of volume conduction from distant sources (Oxford LFP recordings were already recorded in this format).

Recordings were performed between 2-6 days post-operatively, after omitting all dopaminergic medication overnight (OFF condition). The recording was then repeated approximately 30-60mins after administration of the patient's usual dopaminergic medication dose (minimum given was 200mg levodopa, ON condition). One subject (from London) only completed the OFF recording. Each recording comprised rest blocks followed by task blocks. In this report, we focus only on the resting data, which was collected in two blocks lasting 3 minutes each (except the subject from London who only completed one 3 minute block). During the rest block, the patients were asked to keep still, relax with their eyes open and focus on a fixation cross. A neurologist was present in the magnetically shielded room during the experiment to monitor the patient's well-being. It is worth noting that due to the often frail nature of these patients, we performed only one recording session, and were therefore unable to counterbalance the ON and OFF conditions.

4.2.3 Data pre-processing, artefact rejection, and head localisation

The data were analysed using SPM8 (http://www.fil.ion.ucl.ac.uk/spm/) and Fieldtrip (http://www.ru.nl/neuroimaging/fieldtrip/), (Litvak et al., 2011b; Oostenveld et al., 2011). The continuous resting recording was down-sampled to 300 Hz, high-pass filtered above 1 Hz and the line noise artefacts at 50 Hz and 100 Hz were removed using notch filters (5th order zero-phase Butterworth filters). It was then divided into arbitrary 1 second trials. EMG data were divided into arbitrary 1 second blocks, rectified and then converted to the frequency

domain (range 5 to 45 Hz with frequency resolution of 2.5 Hz, and 2.5Hz spectral smoothing) using the multitaper method (Thomson, 1982). The presence of resting tremor was determined visually.

Head position was recorded continuously within the MEG, and in London was recomputed to correspond to the mean of the trials used for the analysis. Similar head movement compensation could not be made for Oxford subjects as the proprietary software had difficulty extracting the head location signal in the presence of metallic artefact from DBS extension leads. We therefore used the starting head location in these cases. Unlike the CTF system, the Neuromag MEG system contains magnetometers (a type of sensor) which, due to their greater sensitivity to distant sources and environmental noise, are more contaminated by metal artefacts. We, therefore, only based our analysis on planar gradiometers similarly to Hirschmann et al. who also used the Neuromag system(Hirschmann et al., 2011). Oxford subjects had 360 trials (from 6 min of data), whilst the London subject had 180 trials (from 3 min of data) per condition.

4.2.4 The beamformer approach to coherent source localisation

Coherence was the principal measure of functional connectivity used in this study. It provides a frequency-domain measure of the linear phase and amplitude relationships between signals (Thatcher et al., 1986; Rappelsberger and Petsche, 1988; Shen et al., 1999; Buzsaki and Draguhn, 2004; Magill et al., 2006b). Cortical sources coherent with PPNR-LFP activity were located using the Dynamic Imaging of Coherent Sources (DICS) beamforming method (Gross et al., 2001). To begin with, all MEG and bipolar PPNR-LFP channel trial data were converted to the frequency domain (range 5 to 45 Hz with frequency resolution of 2.5 Hz, and 2.5Hz spectral smoothing) using the multitaper method (Thomson, 1982). Using beamforming, coherence can be calculated between each PPNR-LFP channel and a 3 dimensional grid of points representing potential sources within the brain (Gross et al., 2001). The beamforming method is based on the linear projection of sensor data using a spatial filter computed from the lead field of the source of interest and either the data covariance (time domain) (Van Veen et al., 1997) or cross-spectral density matrix (frequency domain) (Gross et al., 2001). Lead fields were computed using a single-shell head model (Nolte et al., 2004) based on an inner skull mesh derived by inverse-normalizing a canonical mesh to the subject's individual pre-operative MRI image (Mattout et al., 2007). Co-registration between the MRI and MEG coordinate systems used 3 fiducial points: nasion, left and right pre-auricular; see (Litvak et al., 2010) for further details. The coherence values were computed on a 3 dimensional grid in MNI space with spacing of 5 mm bounded by the

inner skull surface. Values at the grid points were then linearly interpolated to produce volumetric images with 2 mm resolution. These images were further smoothed with an 8 mm isotropic Gaussian kernel. Although we do not perform sensor-level analyses in this paper, we acknowledge that if sensor-level coherence data are severely affected, this may produce noisy source-level results. We, therefore, checked the plausibility of our source-level results by comparing the actual coherence topography with that expected from the sources we found with and without artefacts. The procedure for this comparison is described in detail in Litvak et al. (Litvak et al., 2010, 2011a). Briefly, virtual electrode data from the peak source coherent with PPNR-LFP were projected back to the sensors, via the source's putative lead field and added to the original MEG data shifted by one trial. This shifting destroys the original coherence between PPNR-LFP and MEG so that the coherence pattern observed in the synthetic data can be used to disambiguate between true coherence and the effects of artefacts on coherence estimates. We also compared the original and synthetic coherence patterns with the topographical map of absolute values of the lead field coefficients, which resembles the expected coherence pattern of a single focal source coherent with PPNR in the absence of artefacts and additional brain sources.

4.2.5 Characterisation of effects of dopaminergic medication, frequency and electrode height on coherence topography across patients

The aim of this analysis was to determine if the topography of cortico-pedunculopontine region coherence was frequency and medication dependent, and also if these effects depended on the position of the electrode along the rostro-caudal axis of the PPNR (termed 'height' from now). To allow group comparison of data, DICS images were generated at fixed frequency bands in the alpha (7-13 Hz) and beta (15-35 Hz) ranges in all patients using each of the three bipolar PPNR-LFP channels as a reference. Unthresholded individual coherence images were normalised by dividing the coherence value at each beamformer grid point by the mean value of that image. This potentially removes confounds related to nuisance variations in signal-to-noise ratio such as variable head distance from MEG coils and the use of different MEG systems. However, it also constrains the analysis to distinguish changes in the relative topography of coherence, rather than absolute values. Images were smoothed as described above. Half of the resulting images (all left PPNR) were reflected across the median sagittal plane to allow comparison of ipsilateral and contralateral sources to the PPNR regardless of original PPNR side. These images were then analysed using standard procedures to produce statistical parametric maps (SPMs) testing for regionally specific effects of interest.

The coherence data at each voxel were subjected to a fixed-effects ANCOVA with frequency and dopamine as factors of interest, the interactions of those factors with electrode height position as covariates of interest, and subject and side as nuisance factors. In our cohort, the height of electrode placement (taken as the mean height of all 4 contacts per electrode), varied between PPNRs from -9.4mm to +2.1mm relative to the PM line. Previous PPNR-LFP recordings suggest that centrally placed contacts between -2mm and -6mm relative to the PM line exhibit greater local alpha power, and that activity in this region correlates with gait speed (Thevathasan et al., 2012). Given this variation, in addition to testing for effects on coherence with the PPNR as a whole, we also endeavoured to model differential effects across subregions of the PPNR. This was done by modelling the effect of electrode (taken as a mean of the height of all 4 contacts per electrode) as a quadratic function of electrode height. This allowed for a maximum effect between -2mm and -6mm, thereby mirroring the variation in local alpha power previously reported (Thevathasan et al., 2012). Modelling interactions between electrode height and other factors allowed us to test for differential effects of dopamine and frequency across subregions of the PPNR. All main effects, interactions and covariates were estimated with F contrasts; while post hoc one-tailed *t* contrasts were used to visualise the direction of significant effects. The form of significant covariate interactions was examined by plotting the predicted effect (based on the significant parameter estimates of our model) and residuals, adjusted for confounding factors. All analyses were corrected for multiple comparisons (using random field theory) and thresholded at $p<0.05$, with a minimum cluster volume of 5 voxels. The anatomical locations of the peak voxels showing significant effects were labelled using AAL software (Tzourio-Mazoyer et al., 2002).

4.2.6 Directionality

A variant of Granger causality was used to explore the direction of coupling between synchronized populations of neurons, i.e. which population activity leads in time. The most parsimonious explanation for such a relationship between two coherent population activities is that the leading population drives the lagging population. However, this may not be the only explanation. Driving may be direct or indirect, via one or more unrecorded structures, or activity in both recorded structures may be driven by a third unrecorded structure (Sharott et al., 2005a). Given this, we use the term ‘effective direction of coupling’ to describe a pattern of temporal relationships rather than a measure of direct coupling. Finally, volume conduction artefact may manifest as ‘bidirectional’ coupling in such an analysis. However

this is unlikely in the current study because we use bipolar montages of the electrode recordings and orient the beamformer sources to the direction of maximal imaginary coherence with the PPNR (see below).

Significant peak voxels resulting from the SPMs underwent further quantitative analysis of the effective direction of coupling and local power. First, we extracted time-series (virtual electrode) data at significant SPM maxima, using a linearly constrained minimum variance (LCMV) beamformer (Van Veen et al., 1997), 0.01% regularization and orientation in the direction of maximum imaginary coherence (Litvak et al. 2010). Coherence was then calculated between each peak voxel ('the source') and each PPNR-LFP contact in each subject. The effective direction of coupling was tested between each bipolar contact and the source using a non-parametric variant of Granger causality (Brovelli et al., 2004). Both measures were computed based on multitaper spectral analysis with spectral resolution and smoothing of 2.5 Hz. The significance of Granger causality was tested by repeating the computation 100 times for data with the PPNR signal reshuffled across trials. The significance level used was $p<0.01$ (corrected), i.e. frequencies were declared significant where the spectra exceeded the 99^{th} percentile (across all frequencies) of the Granger causality values computed from reshuffled data for the same pair of channels and direction. To be more conservative we also applied an extent threshold and excluded the cases when only a single frequency bin was significant and the adjacent ones were not. Subsequently the effective direction of coupling in each frequency bin was categorised as either 'source-to-PPNR' , 'PPNR-to-source', 'bidirectional' or 'none' depending on whether it showed significant Granger causality for one of the directions, both or none, respectively. Note that effective directions were characterised separately for different conditions.

4.3 Results

4.3.1 Intracranial electrode recordings correspond to activity of the PPN and neighbouring regions.

Electrode positions are summarised in **Figure 20**.The mean ± SD distance from the PM line was -3.9 ± 4.9 mm, the mean anteroposterior distance was 7.4 ± 1.8mm and the mean laterality was -6.7 ± 1.7mm on the left side and 9.0 ± 3.0mm on the right side. There greatest anatomical variation in contact location was therefore along the rostrocaudal axis. This variability along the rostrocaudal axis meant that many electrode contacts lay out with the assumed boundaries of the PPN, affording us the opportunity to examine the distribution

of subcortico-cortical coherence with respect to this broad PPN region (PPNR). We thus divided this region covered by electrode contacts into three subregions and considered the nature of subcortico-cortical coherence with respect to these. The three subregions were the (1) upper PPNR (e.g. structures near to and including the rostral PPN); (2) middle PPNR (e.g. structures near to and including the caudal PPN) and (3) lower PPNR (e.g. structures caudal to the PPN).

Still the above detail would only be useful if LFPs were focal, allowing discrimination between subregions. Both alpha and beta band power were relatively focal. Alpha power dropped to 44.4 ± 7.2 (SEM) % from the contact with peak alpha power to the mean of the remaining contacts on each electrode. Beta power similarly dropped to 49.8 ± 7.2 %. The mean frequency of the maximum power in the alpha and beta bands was 8.3 ± 0.1 and 16.9 ± 0.3 Hz respectively.

4.3.3 Networks involving the PPNR are frequency specific

The mean images of alpha and beta coherence shown in **Figure 21** highlight both a large central overlap region (including the brainstem, thalamus and anterior basal ganglia) and regions that show a differential effect of frequency. Although the central activity may represent genuine coherence with the PPNR - across both alpha and beta frequency bands - we should note that beamformers also tend to project noise centrally. However, we can make less ambiguous inferences by comparing conditions in an ANCOVA framework. In accord with this, the main effect of frequency was significant in the ipsilateral cerebellum and a broad medial frontal region centred at the cingulate, but including the SMA and the premotor regions (**Table 5**, **Figure 21** and **Figure 22**). Post hoc tests indicated that regional beta coherence was greater in the medial frontal areas, whilst alpha coherence was greater in the cerebellum. Note that although the main effect of frequency was detected at two cerebellar sources, to avoid bias from this region, only the most significant one was included in the subsequent LCMV and directionality analyses (i.e. **Figure 25** and **Figure 26**). The mean frequency of the peak voxel coherence in the alpha and beta bands was 9.6 ± 0.1 and 24.8 ± 0.7 Hz respectively.

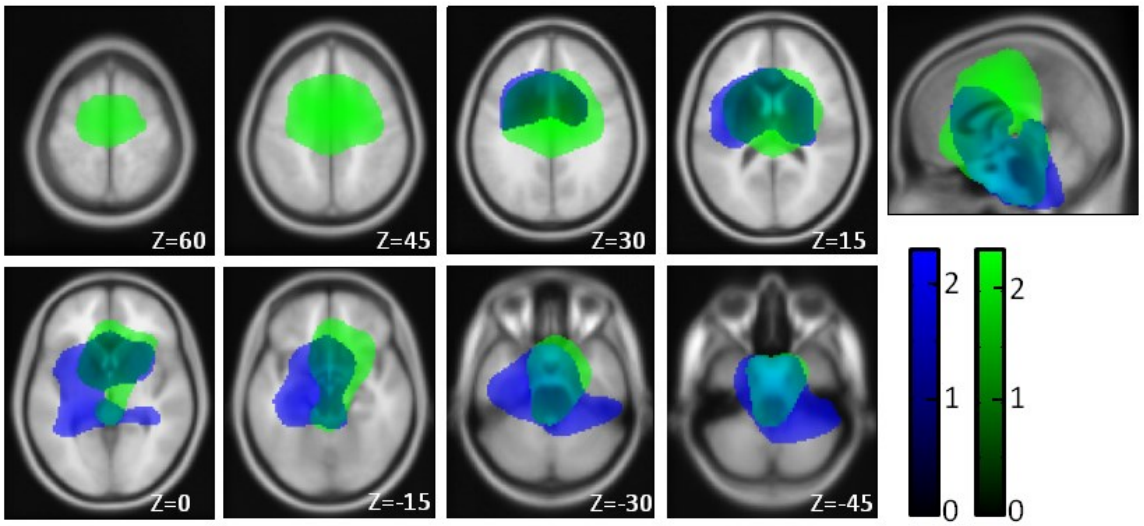

Figure 21: Mean beamformer images of coherence with PPNR activity. *Mean alpha (blue) and beta (green) range coherence images are shown thresholded to 2 standard deviations. Images are a series of axials separated by 15mm intervals along the z axis and overlayed onto corresponding sections through an averaged T1 weighted MRI in MNI space. Overlap regions are cyan and may represent either genuine coherence at both frequencies, or projected noise. Coherence is in arbitrary units.*

Contrast	Location	Peak co-ordinates	Statistic	p value
Frequency	Cingulate	-2 -6 46	F(1,76)=40.73	<0.001
	Ipsilateral cerebellum	34 -52 -46	F(1,76)=24.71	0.010
	Ipsilateral cerebellum*	56 -74 -36	F(1,76)=20.34	0.043
Dopamine x Frequency	Ipsilateral inferior temporal	58 -74 -6	F(1,76)=22.52	0.020
	Ipsilateral superior temporal	66 -42 20	F(1,76)=20.39	0.042
Depth x Frequency	Contralateral orbitofrontal	-46 34 -10	F(1,76)=21.56	0.028
Depth x Dopamine	Contralateral precuneus	-8 -52 56	F(1,76)=24.39	0.011

Table 5: Brain regions where a significant condition effect or an interaction between condition effects was detected. *The statistics shown correspond to the peak voxel in each cluster. *This cluster is slightly posterolateral to the other ipsilateral cerebellar cluster showing a main effect of frequency.*

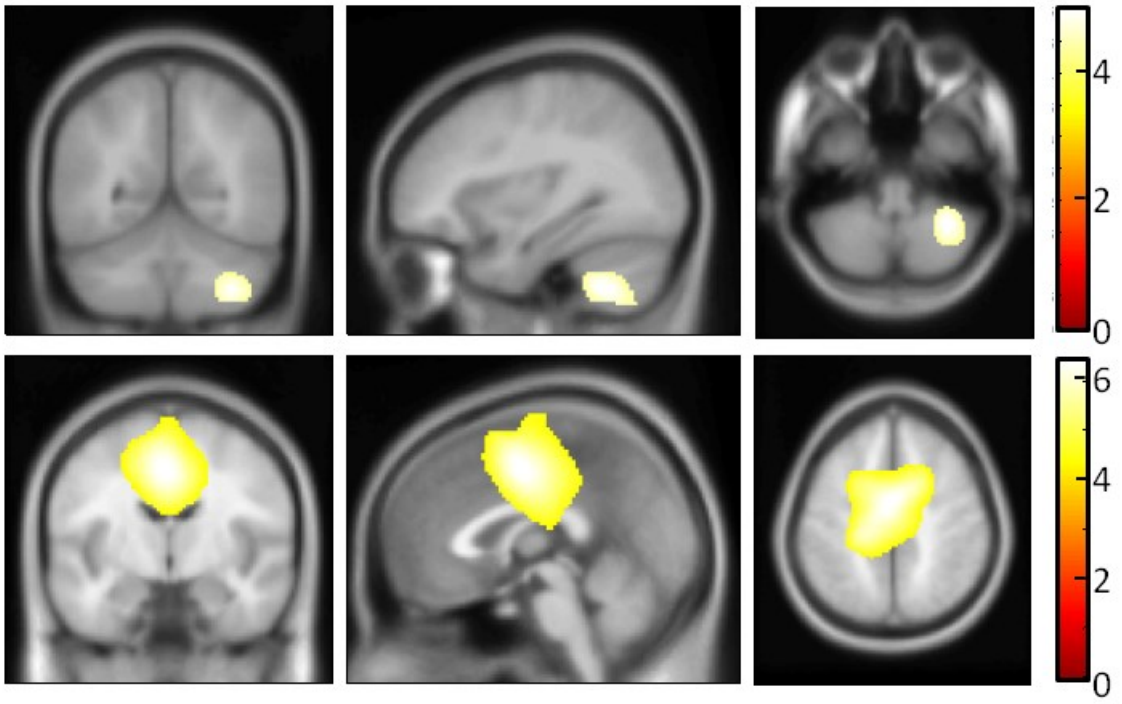

Figure 22: SPMs testing for the main effect of frequency on coherence with the pedunculopontine region. *Images are overlayed onto corresponding orthogonal sections through an averaged T1 weighted MRI in MNI space. Top: Voxels where regional alpha is greater than beta coherence. Bottom: Voxels where regional beta is greater than alpha coherence. The colour bar represents the post hoc t statistic (see* ***Table 5*** *for F statistics). Images are thresholded to p<0.05 (corrected).*

4.3.4 Networks involving the PPNR are modulated by dopamine in a frequency-specific manner

The main effect of dopamine was not significant. However, the interaction between dopamine and frequency was significant in the ipsilateral inferior and superior temporal lobe (**Table 5** and **Figure 23**). Post hoc tests suggested that dopamine decreased regional alpha coherence, whilst increasing regional beta coherence at both locations. To confirm that the dopaminergic effects on coherence at these peak voxels were not due to spurious non-linear effects of power, we correlated the dopamine induced change in log source power with the dopamine induced change in source-PPNR coherence. There were no significant correlations in the alpha (r=0.11, p=0.64) and beta (r=0.14, p=0.55) frequency bands in the inferior temporal lobe, and the alpha (r=0.03, p=0.88) and beta (r=0.03, p=0.9) bands in the superior temporal lobe. Therefore these effects cannot be accounted for by potentially confounding changes in local power.

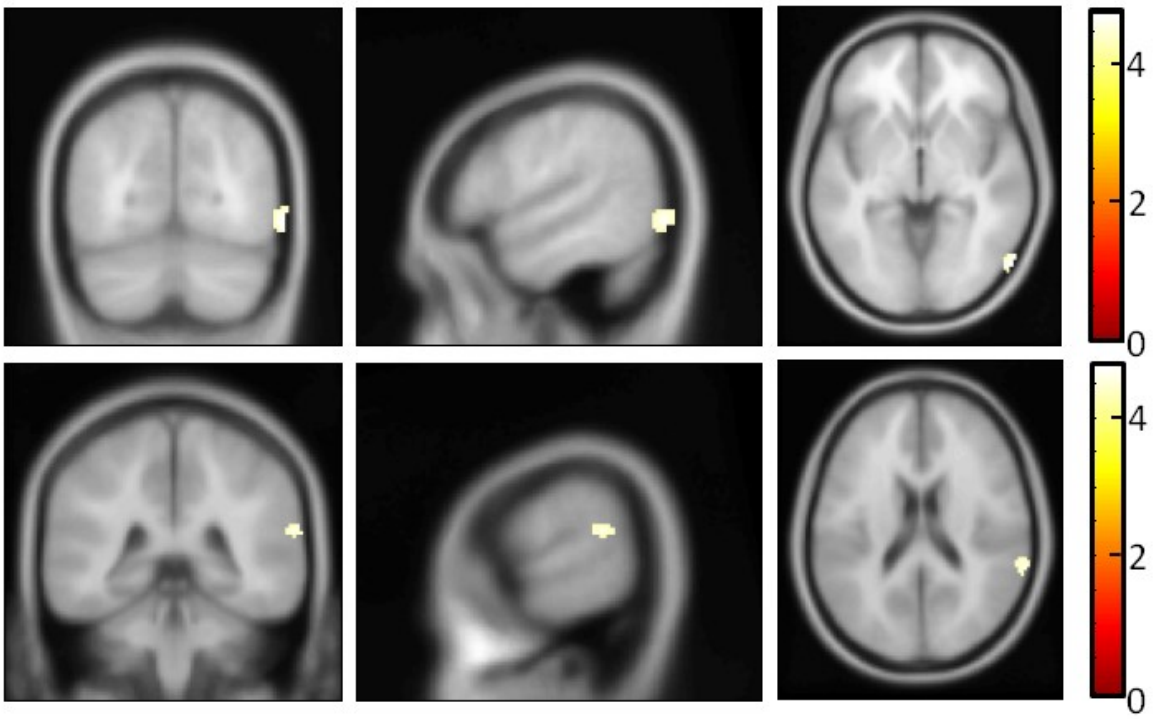

Figure 23: SPMs testing for an interaction between the effects of dopamine and frequency on coherence with the pedunculopontine region. *Images are overlayed onto corresponding orthogonal sections through an averaged T1 weighted MRI in MNI space. Both rows of images show voxels where dopaminergic medication reduces alpha coherence whilst increasing beta coherence. The colour bar represents the post hoc t statistic (see* ***Table 5*** *for F statistics). Images are thresholded to p<0.05 (corrected). We note that some voxels in the top panel appear out with the standard averaged template MRI used for presentation and may therefore represent edge artefact. However, the underlying t image, when thresholded to p<0.001 uncorrected shows that this region is the outer tip of a larger intracranial activation, suggesting that it is not a mere extracranial artefact.*

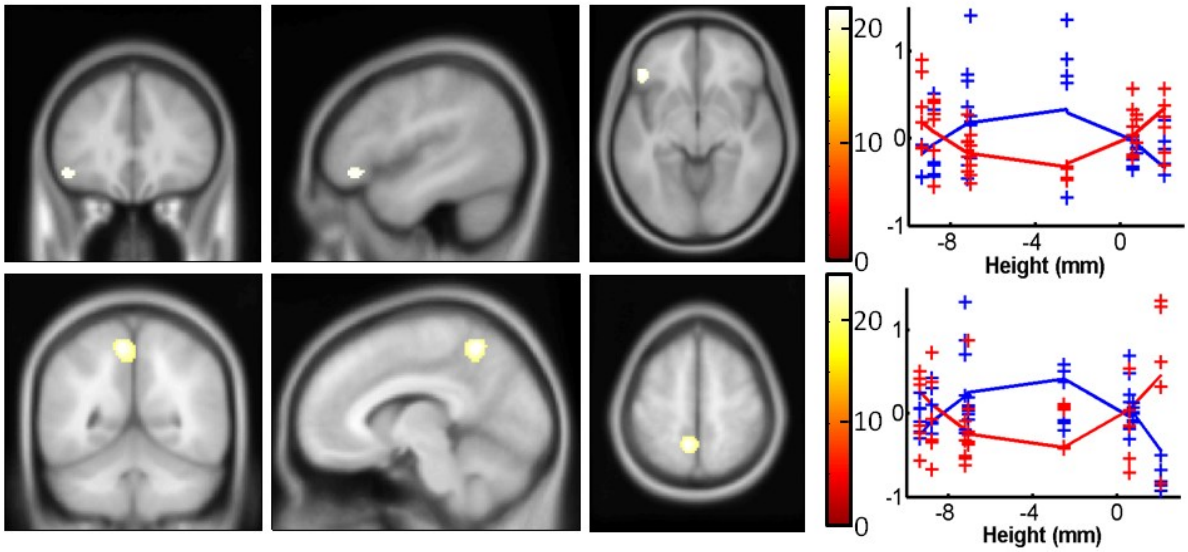

Figure 24: SPMs testing for an interaction between the effect of height (of electrode relative to PM line) and other effects of interest. *Images are overlayed onto corresponding orthogonal sections through an averaged T1 weighted MRI in MNI space. Top row: Voxels where frequency interacts with a quadratic function of height. Top right: The modelled effect of height (line), and the model plus residual error (crosses) are plotted separately for alpha (blue) and beta (red) coherence at the corresponding peak voxel. Relative to beta coherence, alpha coherence with the contralateral orbitofrontal cortex is increased centrally within the pedunculopontine region (which may correspond to the caudal PPN). Bottom row: Voxels where dopamine interacts with a quadratic function of height. Bottom right: The modelled effect of height (line), and the model plus residual error (crosses) is plotted separately for OFF (blue) and ON (red) medication conditions at the corresponding peak voxel. Coherence with the contralateral precuneus is greater OFF dopaminergic medication centrally within the pedunculopontine region (which may correspond to the caudal PPN). Effects are in arbitrary units and are adjusted for confounding factors. The colour bar represents the F-statistic. Images are thresholded to p<0.05 (corrected).*

4.3.5 Coherence is topographically modulated within the PPNR in a frequency and dopamine dependent manner

Alpha power in the PPNR LFP has been reported as maximal around 6 to 2 mm below the PM line which may correspond to the caudal PPN (Thevathasan et al., 2012); given that the present cases represent a subset of this earlier report, we evaluated the effect of electrode height on coherence by modelling it with a quadratic function (centred at -4mm with respect to the PM line, in the middle of the region of maximal alpha power noted by Thevathasan et al). Note that here the main effect of electrode height was not estimable, as all between-PPNR variation was already modelled by nuisance regressors. The interaction between the effect of frequency and electrode height was significant in the contralateral inferior frontal area (**Table 5** and **Figure 24**). Plots of the adjusted effects suggested that alpha coherence with the inferior frontal region was predominantly within the middle PPNR (defined here as -2 to -6 mm with respect to the PM line). In addition, the interaction between the effects of dopamine and electrode height was significant in the precuneus (**Table 5** and **Figure 24**). Plots of the adjusted effects suggested that dopamine decreased coherence with the precuneus mainly within the middle PPNR. There was no three-way interaction. To support our findings and their relationship to previous work (Thevathasan et al., 2012), we confirmed a similar distribution of alpha coherence within the PPNR, as that previously reported for power. **Figure 25** illustrates the distribution of raw unnormalised coherence between all significant cortical sources and the PPNR at different distances from the PM line. Spatial resolution is effectively determined by the binning of electrode height relative to the PM line and is sparse. Nevertheless, alpha band coherence with distant sites tends to be maximal in the middle PPNR, which includes the caudal PPN. Coherence in the beta band was lower and more diffusely spread. To detect any differences between data collected from the two MEG systems, we also present the mean power spectra and coherence spectra at peak voxels from the SPM analysis in **Figure 26**. Data from Oxford and London show broadly similar features in spite of different surgical targeting, MEG sensor types and LFP amplification. However, not all effects highlighted by the SPM analysis are apparent in the raw coherence data averaged across subjects, presumably because they are masked by variation with depth or between subjects.

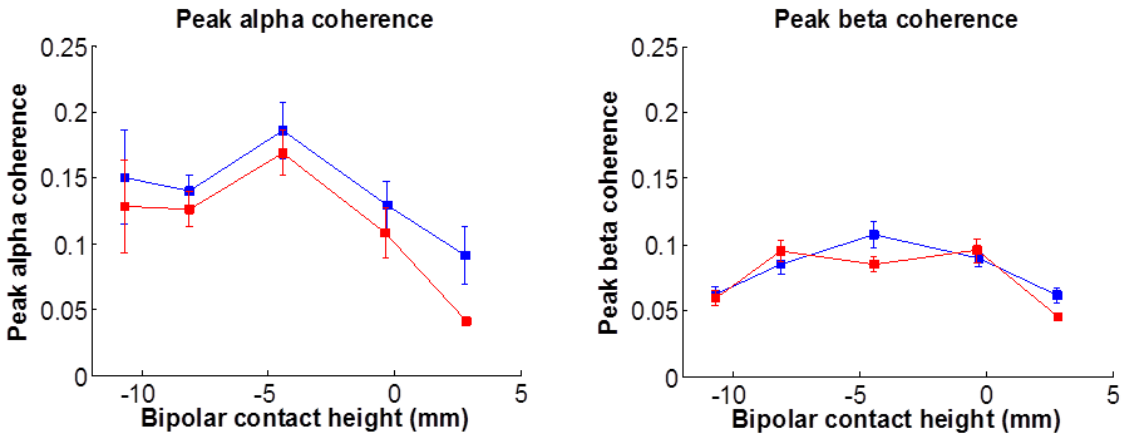

Figure 25: Mean unnormalised coherence between the PPNR and significant peak voxels from the SPM analysis, plotted as a function of electrode height (mm). *Values are plotted separately for alpha (left) and beta (right) coherence. Means were calculated ON (red) and OFF (blue) dopaminergic medication. Error bars represent SEM.*

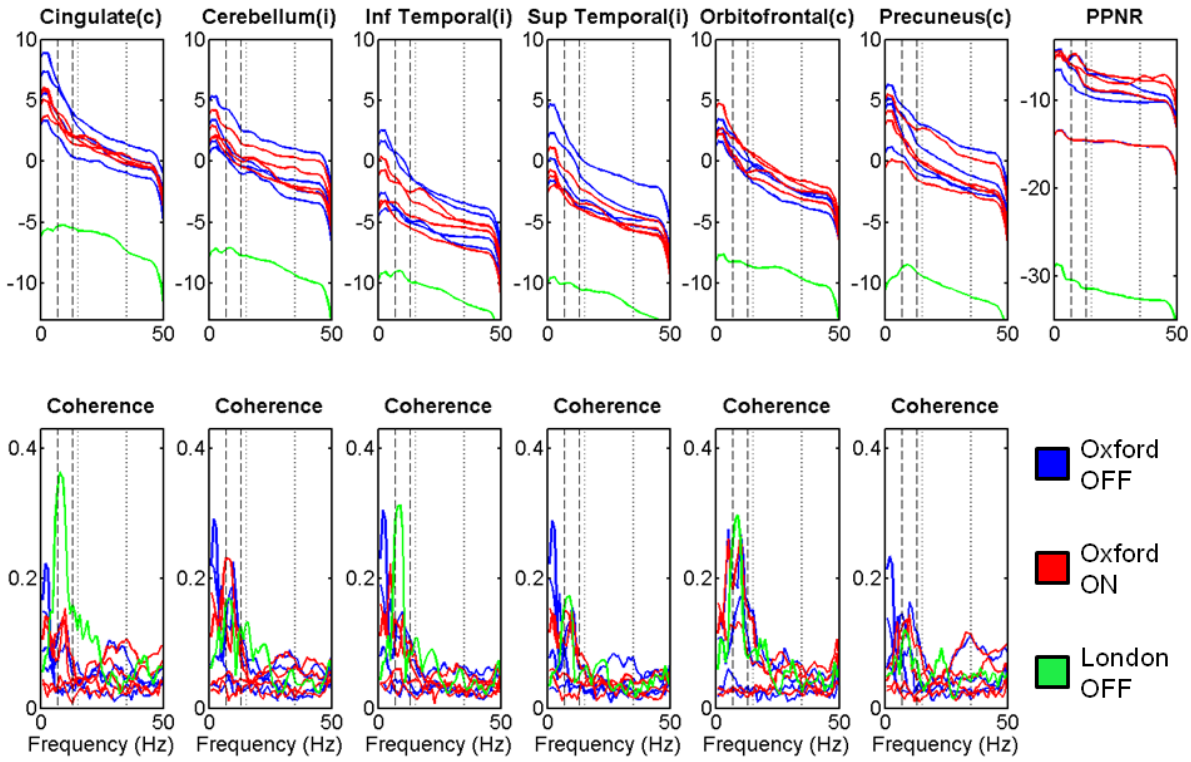

Figure 26: Individual subject mean log source power (top row) and source-PPNR coherence (bottom row) data for the 4 Oxford subjects (red and blue lines) and the London subject (green lines). *Each column represents spectra for one source from the SPM group analysis or the PPNR electrode. The alpha range (7-13Hz) is shown bounded by dashed lines and the beta range (15-35Hz) is shown bounded by dotted lines. Spectra are plotted separately for OFF medication (blue) and ON medication (red) conditions for the Oxford patients. Note the London subject was only recorded OFF medication. Although magnitude of source and PPNR LFP power are very different between the Oxford MEG system and the London MEG system, their general features and the source-PPNR coherence data are similar as expected. Both London and Oxford subjects show a predominance of alpha power in all cortical locations and the PPNR, and a predominance of alpha coherence between cortical sources and the PPNR. Beta power peaks can also be seen in some individual PPNRs and to a lesser degree in some cortical sources. Individual beta coherence peaks are visible, mainly in the cingulate, but also in other cortico-PPNR coherence spectra. There is relatively greater ratio of beta, to alpha coherence in the cingulate when compared with the cerebellum in the Oxford subjects, but interestingly the opposite is seen in the London subject. Given the similar source and PPNR power spectra, this is unlikely due to a difference in recording equipment, but rather represents a biological difference possibly due to the relatively rostral location of the contacts in the London subject*

(mean height +0.8mm) relative to the mean of the cohort (-3.9mm). The effect of dopamine on PPN coherence with the temporal lobe cannot be seen underlining the importance of modelling subject and depth effects to increase sensitivity in this small cohort of subjects. Inf (inferior), Sup (Superior), c (contralateral), i (ipsilateral), PPNR (pedunculopontine region). Note that a 50Hz notch filter has been applied to all power spectra.

4.3.6 Variation in the effective direction of coupling with height of electrode

We examined the effective direction of coupling at the peak voxels from the SPM analysis using a non-parametric Granger technique (**Figure 27**). This is presented as the fraction of electrodes (i.e. the number of electrode contacts per directional category divided by the total number of electrode contacts) showing significant directionality per frequency bin. Graphs are presented separately for dopaminergic state and bipolar contact height (categorized into 3 bins). Inspection of these distributions suggests that coupling is maximal below -2mm, and especially in the middle PPNR (which includes the caudal PPN), between -2mm and -6mm relative to the PM line, and that, at least in the alpha band such coupling is mainly bidirectional. There is a tendency for treatment with levodopa to increase PPNR-to-source coupling particularly in the beta band and in the middle PPNR, where bidirectional coupling is reduced to almost undetectable levels after levodopa.

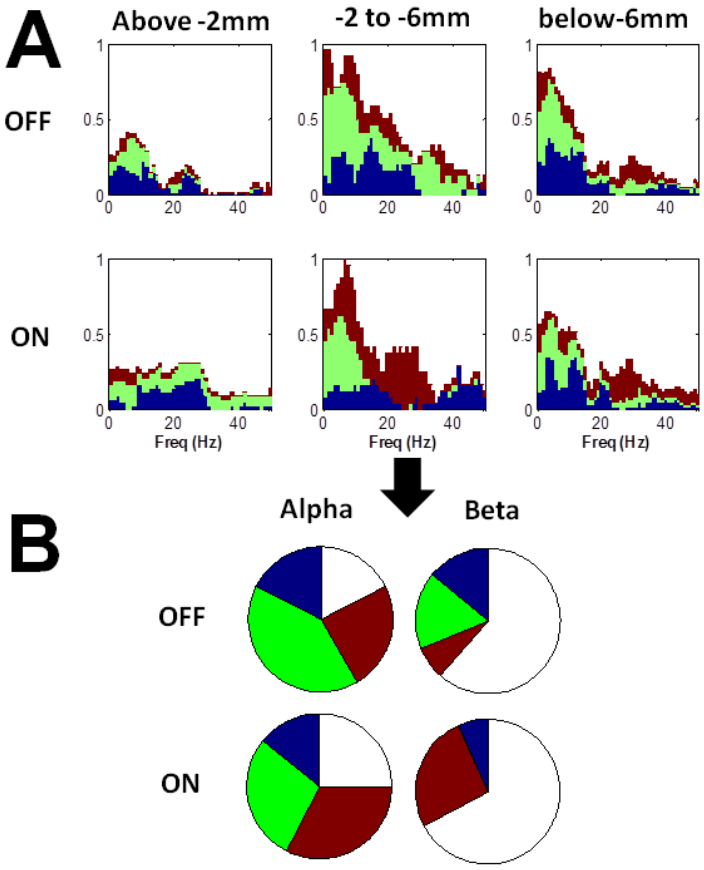

Figure 27: The effective direction of coupling. A*: Coupling OFF and ON dopaminergic medication (top and bottom respectively) grouped for electrodes at different heights within the PPNR (left, above -2mm termed the upper PPNR (including the rostral PPN); middle, -2 to -6mm termed the middle PPNR (including the caudal PPN); and right, below -6mm termed the lower PPNR (including the region below the caudal PPN). Each chart shows the fraction of PPNRs in different directionality categories stacked on top of each other (sum is always 1). B: Pie chart showing coupling in the -2mm to -6mm region only, averaging across alpha (left) and beta (right) frequency ranges in the OFF (top) and ON (bottom) dopamine conditions. Blue represents 'source-to-PPNR', green 'bidirectional' and red 'PPNR-to-source' directionality. Clear space means that there was no definite effective direction.*

4.3.7 Assessment of the impact of ferromagnetic electrode artefact and the use of different MEG systems on sensor and source level coherence.

Beamforming has previously been shown to extract source-level coherence from MEG recordings contaminated by DBS electrode metal artefact (Litvak et al., 2010, 2011a), and reassuringly these results are similar to data acquired using non-ferromagnetic wires (Hirschmann et al., 2011). However, to confirm the validity of sensor-level coherence estimates in this cohort, we considered the effect of simulated noise on the sensor-level coherence patterns of peak beamformer sources in different conditions, subjects and MEG systems (**Figure 28**). By comparing original coherence patterns (a combination of genuine source-PPNR coherence possibly from multiple sources, and contributions of artefacts from ferromagnetic electrodes and non-coherent brain activity), with absolute values of the source lead field (representing only genuine source-PPNR coherence) and simulated coherence (a combination of genuine single source-PPNR and artefacts), we were able to determine the effect of the artefact on sensor-level coherence. We present four cases that all show distinguishable sensor-level coherence patterns but that also contain variable amounts of noise. In some cases, artefactual effects on coherence dominate at the sensor-level. To determine whether the beamformer was able to suppress artefactual noise adequately, and to compare recordings from different MEG systems we present individual subject coherence and power spectra in **Figure 26**. These figures show a large variation in power between the different MEG and intracranial electrode amplification systems used in London and Oxford. However, in spite of this, the profile of power spectra in both groups was similar and crucially coherence estimates were relatively comparable between MEG systems, even before normalisation. Individual alpha and beta coherence peaks can be seen in a range of sources and subjects.

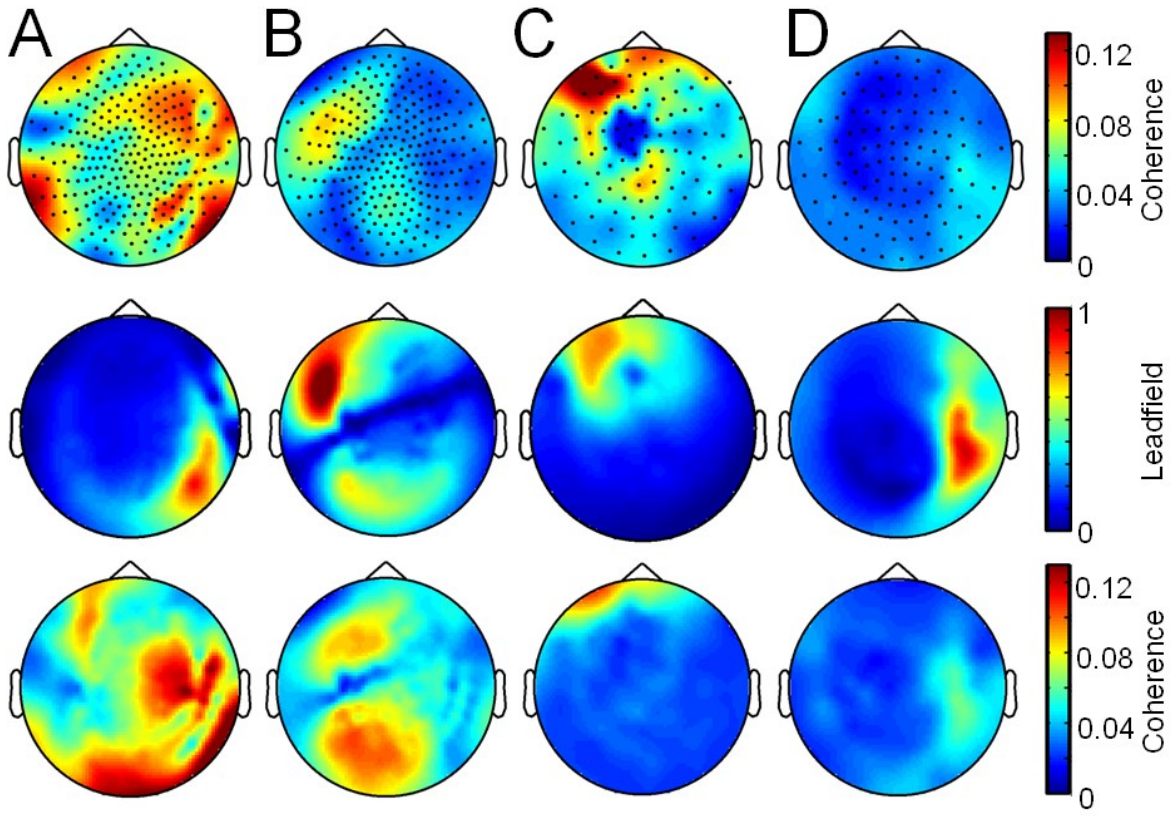

Figure 28: Sensor level analysis. *Coherence patterns (top row), absolute values of lead fields (middle row) and simulated coherence (bottom row) for four MEG-PPNR electrode pairings. Absolute values of lead fields have been differentially multiplied by 1x1012 (columns B and D), 2x1012 (column C) and 4x1012 (column A) for visualisation purposes. Column A is an example of alpha coherence, off medications in the London subject and column B is beta coherence in the same subject. Column C represents beta coherence on medication, and column D represents alpha coherence on medication, in two separate Oxford subjects. In cases B and D, there is a clear consistency between the original coherence pattern, the lead field and simulated coherence at the same location with simulated noise. In cases A and C, although features resembling the lead field can be identified to a varying degree in the original and simulated coherence patterns, both sensor-level maps are contaminated with noise either from other brain sources or from ferromagnetic DBS electrode artefact.*

4.4 Discussion

We have shown that the PPNR in patients with PD is functionally coupled with diverse brain regions in two frequency bands at rest. Although possibly partially overlapping in a central area that includes the brainstem, thalamus and anterior basal ganglia, each resting state network (RSN) can be shown to dominate in different regions. The alpha band RSN dominates in the cerebellar cortex, whereas the beta band RSN dominates in frontal motor cortical areas. This broad distinction into two networks, reinforced by the selective effects of treatment with levodopa, highlights the functional position of the PPNR at the junction between motor cortical planning areas and the cerebellum. The extent of functional coupling with the PPNR was remarkable, given the evidence of partial loss of cholinergic neurons in the PPN pars compacta, in PD (Jellinger, 1999; Manaye et al., 1999).

Before discussing the implications of these findings, we should outline some of the important limitations of this study. Firstly, we studied a relatively small number of subjects. However, given the scarcity of human PPNR functional connectivity data, we believe these results are still valuable. Secondly, these data are susceptible to confounds related to the use of different MEG systems and to ferromagnetic artefact from DBS electrodes. However, by using techniques such as spatial filtering (beamforming) and spatial normalisation, we were able to obtain comparable coherence estimates between subjects and conditions – although this constrains the analysis to distinguish changes in the relative topography of coherence, rather than absolute values. Finally, some of the intracranial electrodes lie outside the presumed PPN, therefore we primarily report connectivity with the PPNR as a whole. However, as we had both electrode contacts within and outside of the PPN we were able to contrast activities across this area and define effects of dopamine and frequency that were highly specific to a central subregion within the PPNR, corresponding to the caudal PPN. Overall, we acknowledge that our analysis may have reduced sensitivity, and what we present is a conservative, but specific account of PPNR functional connectivity.

The extensive patterns of cortical coupling with the PPNR are in keeping with this region's rich direct and indirect, polysynaptic connectivity in humans and other animals (Sesack et al., 1989; Hazrati and Parent, 1992; Pahapill, 2000; Mena-Segovia et al., 2004; Aravamuthan et al., 2008; Schofield and Motts, 2009; Alam et al., 2011; Martinez-Gonzalez et al., 2011). More specifically, the cortical and subcortical topographies of the two RSNs characterised by activities in the alpha and beta bands share some similarity with those with

similar spectral organization demonstrated to be coupled with the subthalamic nucleus (STN) in PD patients (Hirschmann et al., 2011; Litvak et al., 2011a), underscoring the functional interdependency of the PPNR and STN. However, it is important to acknowledge that although the pattern of distributed connectivity may be broadly similar between these two subcortical hubs (although the STN was not coherent with the cerebellum), the directionality of effective coupling was rather different. Coupling from source to STN dominates (Litvak et al., 2011a), but this was certainly not the case for coupling from source to PPNR. This tendency to more bidirectional and efferent (PPNR-to-source) coupling, particularly in the treated Parkinsonian state, is in line with the PPNR's position closer to the outflow of the basal ganglia to the brainstem and thalamus.

Many of the areas of the brain coupled with the PPNR at rest have been shown to be modulated by gait or differ in activity between PD patients with and without FOG -the major symptom in our cohort (reviewed in (Bartels and Leenders, 2008)). For example, PD patients show altered gait-related perfusion in the precuneus (reviewed in (Nutt et al., 2011)) and temporal cortex (Hanakawa et al., 1999) compared to controls, while gait reduces dopamine transporter (DAT) availability in the orbitofrontal cortex of patients with PD but not in control subjects (Ouchi et al., 2001). The suggestion in these previous studies has been that these distinct areas are enlisted in an attempt to compensate for gait impairment. It is interesting to note that we have identified a corresponding set of functional connections between all these areas and a key locomotor region, the PPNR, suggesting that the PPNR may act as a hub through which these cortical effects are co-ordinated. Indeed, low frequency stimulation of the PPNR alters resting cortical glucose metabolism and cerebral blood flow in a large network of areas that include the orbitofrontal cortex, cingulate, prefrontal areas, temporal lobe, thalamus and cerebellum (Ballanger et al., 2009; Ceravolo et al., 2011).

What specialised functions might the two RSNs mediate? The alpha frequency band has often been associated with attention and the allocation of processing resources (Palva and Palva, 2007), and we have previously suggested that the somewhat similar alpha band RSN with the STN may subserve attentional functions in patients with Parkinson's Disease (Litvak et al., 2011a). The latter may be particularly critical in the present patient group which was preselected for the prominence of gait difficulties, particularly freezing. A relationship between attentional control and gait performance is increasingly recognised (Yarnall et al., 2011). Gait speed reduces in healthy subjects, elderly fallers and in Parkinson's disease

during the performance of a second, unrelated task ('dual tasking') (Hausdorff et al., 2003; Springer et al., 2006; Lamoth et al., 2011). Dual tasking and other processes that divert attention away from walking can all also precipitate gait freezing (Springer et al., 2006). In PD, attentional deficits are increased in patients that fall (Allcock et al., 2009) and freeze during gait (Amboni et al., 2008; Yogev-Seligmann et al., 2008).

The PPN is considered a component of the 'reticular activating system' and may modulate states of arousal and attention (Winn, 2006). In line with such a role, PPN stimulation in patients with Parkinson's disease (PD) may increase rapid eye movement sleep (Romigi et al., 2008; Lim et al., 2009) and diurnal vigilance (Ferraye et al., 2010), and there is PPNR-cortical coherence in the alpha band during wakefulness (Androulidakis et al., 2008). We suggest that the PPNR may be another subcortical relay in attentional networks characterised by oscillatory activity in the alpha frequency band (Litvak et al., 2011a; Thevathasan et al., 2012). That said, the precise homology between the alpha band RSNs coherent with the STN and PPNR can only be determined in the future through simultaneous recordings of MEG and subthalamic and PPNR LFPs in the *same* subjects. Given the functional and anatomical heterogeneity of the PPNR, and the spread of electrodes within it, one may have expected a large variation in coupling due to electrode position within the PPNR. Indeed single-subject raw coherence data do suggest considerable variation between subjects exists (**Figure 26**) presumably partially due to differences in electrode position. The middle PPNR (including the caudal PPN), between 2 to 6mm below the PM line, may be particularly important in supporting a possible role in gait control through attentional modulation. Local oscillatory synchrony in the alpha band was maximal here and has been shown to correlate with gait performance (Thevathasan et al., 2012). Consistent with the special importance of this middle section of the PPNR, this region showed the greatest average raw coherence with different cortical locations (**Figure 25**). It was preferentially coherent with the inferior frontal region in the alpha band and was coupled to the precuneus in a dopamine sensitive manner. We have previously argued that this middle section of the PPNR includes the caudal part of the 'pars dissipata' of the PPN (Thevathasan et al., 2012). The pars dissipata of the PPN, as defined by immunohistochemical labelling of choline-acetyltransferase in humans, extends both rostrally and caudally from the central pars compacta, (Mesulam et al., 1989; Manaye et al., 1999), and has been implicated in gait and its dysfunction (Karachi et al., 2010). It should, however, be acknowledged that the pars dissipata of the PPN has indistinct boundaries, and of note, just medial to its caudal boundary is the laterodorsal tegmental nucleus which is also rich in cholinergic neurons (Manaye et al., 1999).

Still, it must be stressed that the association of the PPNR alpha band RSN with attentional function remains speculative. Nor does it discount the possibility that the beta band RSN may also play a role in attention, possibly through its functional connectivity with the medial prefrontal cortex, including the cingulate. Thus it has been suggested that the medial prefrontal cortex is involved in compensation for low-arousal states where attention is still necessary, such as in monotonous vigilance tasks like walking (Portas et al., 1998; Coull et al., 2004; Gilbert et al., 2006; Fischer et al., 2008). This compensation has been linked to enhanced frontal power in the beta frequency band (Fischer et al., 2008) - precisely the frequency of dominant connectivity between midline frontal regions and the PPNR. Of course task-related modulation of activity in the beta RSN, with its extensive connectivity to motor areas, may also contribute to more explicitly motor aspects of gait. Consistent with this, both beta band LFP power in the PPNR, and beta coherence between the medial frontal cortex and the PPNR are reactive to movement in patients with PD (Tsang et al., 2010).

Our results may also afford insight into dysfunction in the PPNR and its functional connectivity in the Parkinsonian state. Basal ganglia pathophysiology in PD is classically modelled as a relative overactivity of the polysynaptic indirect pathway. This potentially upregulates two sets of competing inputs to the downstream PPN: inhibitory GABAergic influences from the GPi and SNr and excitatory glutamatergic influences from the STN. Although still debated, several lines of evidence suggest that the inhibitory inputs dominate, resulting in an overall pathological inhibition of the PPN in PD (but on the other hand, see (Teo et al., 1997, 1998)). Hence acetylcholine synthesis is suppressed in the PPN in the Parkinsonian state (Gomez-Gallego et al., 2007). Reducing PPN activity, as occurs with destructive lesions, leads to a Parkinsonian-like state (Aziz et al., 1998), and there is a relationship between the loss of cholinergic neurones in the PPN pars compacta and the severity of Parkinson's disease (Zweig et al., 1989). Furthermore, akinesia in MPTP treated monkeys may be reversed by the microinjection of the GABA antagonist, bicuculline, into the PPN (Nandi et al., 2002). Our directionality data were broadly in keeping with an exaggerated inhibition of the PPN in untreated PD, in so far as the dopamine prodrug levodopa released outflow from the PPNR, most clearly in the beta frequency band. This was evident as a shift in favour of effective coupling directed from PPNR, particularly the middle PPNR, to distal sources at the expense of source-PPNR and bidirectional coupling. Furthermore, the emphasis on a change in directionality in the beta band supports and

extends the hypothesis that dopamine-induced beta activity in the PPNR is ‘prokinetic’ in contrast to the posited ‘antikinetic’ nature of beta activity in the basal ganglia in PD (Classen and Schnitzler, 2010; Tsang et al., 2010).

Although we cannot discriminate the specific effect of dopamine on the coupling from pallidum to PPNR, our methodology does help define effects on the coupling between the cerebral cortex and PPNR. Treatment with levodopa led to a retuning of coherence between the PPNR and temporal cortex in favour of activities in the beta band, at the expense of those in the alpha band. In addition, dopamine reduced coherence in the alpha and beta band between the precuneus and middle PPNR (which includes the caudal PPN).

Our results support the notion of two principal RSNs involving the PPNR, which may be distinguished in terms of their spectral tuning and their wider connectivity. This represents an initial step in determining the different functional associations of these circuits which, although characterised here at rest, may still be important during gait. In particular, the results lead us to posit a contrasting beta-tuned predominantly motor planning RSN and alpha-tuned predominantly attentional RSN, and encourage future explorations of how these networks are modulated during walking or imagined gait. Eventually, it may be possible to differentially modulate these systems through stimulation, by harnessing their different resonance properties and any fine scale differences in their organisation within the PPNR.

5. Functional roles of the pre-SMA and right IFG during stopping in healthy controls

5.1 Introduction

So far we have demonstrated how the spatial and spectral properties of cortico- subthalamic and cortico-pedunculopontine connectivity can be used to distinguish different cortico- basal ganglia networks. But do these networks subserve different functions? As we have reviewed, the particular spatial and spectral properties of each of the resting networks can *suggest* that the basal ganglia are involved in motor, cognitive and attentional processes, but this has to be experimentally confirmed using dynamic tasks. In this chapter, we first pilot novel experimental and analytical methods to examine dynamic task-related electromagnetic activity in healthy controls. In doing so, we disambiguate the specialised function of two key cortical areas involved in the act of stopping. Directly following on from this work, we apply the same analysis procedure to understand the cortico- basal ganglia dynamics responsible for stopping in PD in the next chapter.

Stopping may imply an absence of movement, but it does not imply the absence of action. This is because an action is defined not only by the mechanics of its execution but also by the conditions that attend it. Indeed the importance of stopping usually lies in the context – stopping may be particularly important if one hears a car horn whilst walking across a road – rather than the execution itself. Therefore the neural correlate of stopping must invoke brain regions which are sensitive to the context, in addition to those responsible for executing the stop.

Stopping has been experimentally studied using the stop-signal paradigm (Logan and Cowan, 1984). Here, the subject is asked to press a left or right button in response to a directional go cue – the primary task. In a minority of trials, a second visual cue (the stop-signal) is presented quickly after the first, instructing the subject to inhibit the planned response. The *efficiency* of stopping can be estimated by varying the time in which the subject has to stop (the delay between the primary task and stop cues – termed the stimulus onset asynchrony (SOA)), and relating this to the success rate of stopping. This relationship, known as the inhibition function, has a midpoint that represents the average time taken to stop – the stop-signal reaction time (SSRT) (Logan and Cowan, 1984; Hanes and Carpenter, 1999; Band et al., 2003; Congdon et al., 2012).

Using this paradigm, two candidate regions have been identified as pre-eminent within the cortical network associated with stopping: the pre-supplementary motor area (pre-SMA) (Isoda and Hikosaka, 2007; Nachev et al., 2007) and the right inferior frontal gyrus (IFG) (Aron et al., 2003; Aron and Poldrack, 2006). Although lesions in both regions reduce stopping efficiency (Aron et al., 2003; Nachev et al., 2007), their individual roles remain controversial. Nachev et al. reviewed different experimental paradigms implicating the pre-SMA and hypothesised that activity in this region corresponded to the contextual complexity of a task: tasks which are more contextually complex, having a greater number of contextual factors (Nachev et al., 2008). In contrast, converging evidence directly relates right IFG function to the efficiency of stopping (i.e. its execution) *regardless* of the experimental context (Aron et al., 2003, 2007a; Aron and Poldrack, 2006; Xue et al., 2008). However, the role of these two regions has yet to be disambiguated, partly due to the inherent methodological limitations when associating human behaviour with neuronal activity.

Functional magnetic resonance imaging (fMRI) studies routinely use a convolution model in order to disambiguate the haemodynamic responses associated with different events during the stop-signal task. However most fMRI studies have not found convincing differences between successful and unsuccessful stopping (Aron and Poldrack, 2006; Aron et al., 2007b), and it can be difficult to meaningfully relate behaviour occurring over hundreds of milliseconds to a dispersed haemodynamic response occurring a few seconds later. Electroencephalographic studies generally afford greater temporal information (Kok et al., 2004; Schmajuk et al., 2006), but at the cost of spatial precision. Recent studies, though, have measured electrophysiological activity more focally in rarer patient populations with intracranial (Ray et al., 2011) or subdural electrodes (Swann et al., 2009, 2012) and have suggested that during the stop-signal task, early gamma frequency activity in the pre-SMA and later beta frequency activity in the right IFG and subthalamic nucleus may be important in stopping. However, unlike routine fMRI analysis, conventional electrophysiological averaging techniques cannot disambiguate the induced responses to closely temporally related events such as the go signal, stop-signal and the button press during the stop-signal paradigm. This is critical because if the neuronal responses to individual events cannot be disambiguated, successful-stop and failed-stop trials cannot be compared meaningfully without the confounding presence of a movement during failed-stop trials only.

In this study we overcame previous methodological limitations by applying a novel convolution model for electrophysiological analysis (Litvak et al., 2012b) to simultaneously acquire high temporal and spatial resolution magnetoencephalography (MEG) data. We hypothesised that the pre-SMA is preferentially sensitive to the *context* of stopping, whilst the right IFG is preferentially involved in the *efficiency* of its execution.

5.2 Methods

5.2.1 Subjects and paradigm

Nine healthy right-handed subjects were studied (mean age 31 years (range 21 – 38yrs); 5 females). To dissociate the effects of contextual complexity, we used four variants of the stop-signal paradigm that all had the same requirement for inhibition – the inhibition of the primary task – but with additional modulators of the contextual parameters of the action (see **Figure 29**). We modulated the contextual parameters in two ways. Firstly, we manipulated the complexity of the required response by using both the stop-signal task and the change-of-plan task. In the latter, visual cues remain the same as in the stop-signal paradigm, but the subject is required to inhibit the primary task and also press the opposite button in response to the stop-signal, - now called a change-signal in this context (Logan and Burkell, 1986; Brown and Braver, 2005; Nachev et al., 2007). However, a direct comparison of stop-signal and change-of-plan tasks would not only represent increased contextual complexity but would also be confounded by increased conflict between the tasks (Botvinick, 2007). Therefore, secondly, we manipulated the stop/change instruction, using either a vertical bar or a directional arrow always opposite to the primary task arrow. The interaction between both manipulations isolates the effect of conditional complexity, where more complex actions are conditional on a greater number of contextual factors (Nachev et al., 2007). An arrow is a contextually simpler change cue, because it explicitly specifies the direction of change whereas the direction of change to a vertical bar is additionally dependent on a second contextual parameter – the direction of the primary go cue. The reverse is true for stopping only. Now, a vertical bar stop cue always means stop. However, in the arrow condition, because the both the primary task cue and stop cue are directional arrows, the stop arrow only means stop if it is following another arrow i.e. it is dependent on an additional contextual cue. This reversal of effects isolates contextual complexity whilst removing idiosyncratic cue or response related confounds.

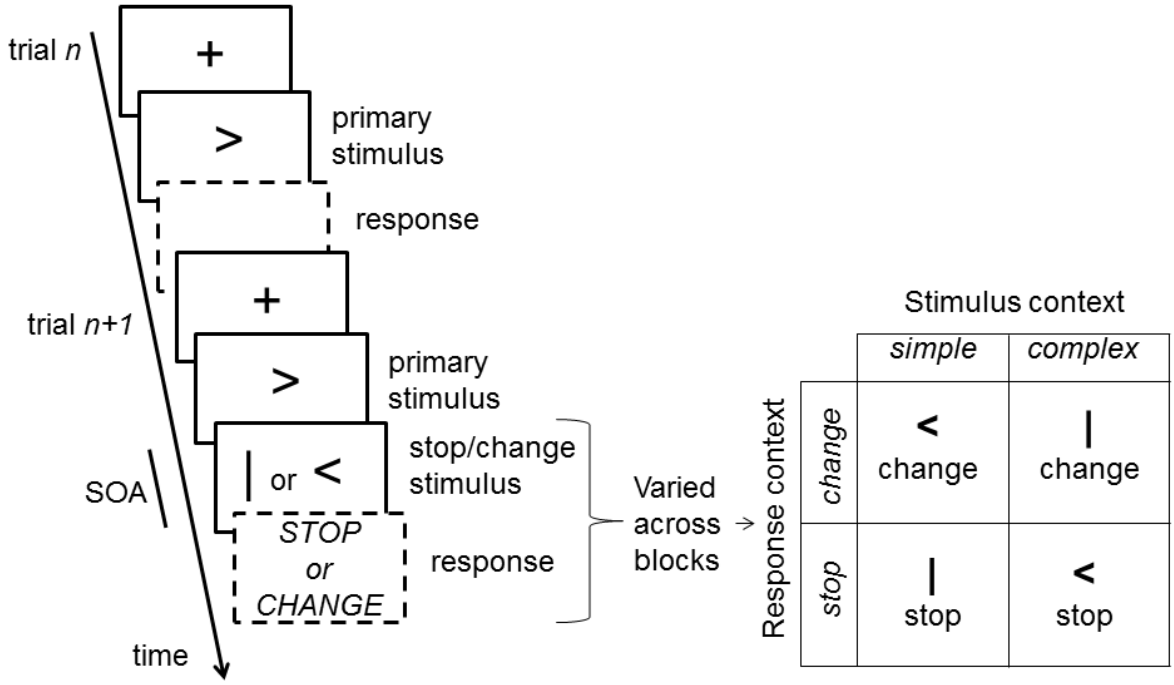

Figure 29: Paradigm details. *We used four variants of the stop-signal paradigm arranged within a 2x2 factorial design. Each trial consisted of a left- or right- pointing go arrow instructing the subject to press the corresponding button quickly (go trials, e.g. trial n in figure). In 50% of trials, after a variable delay (the SOA), a further visual stimulus was presented. Depending on the variant of the paradigm (a single variant was used per task block) the subject was asked to either inhibit the planned response (stop response context) or to inhibit the planned response and additionally press the opposite button (change response context), in response the second visual stimulus. In addition to response context, we manipulated the stop/change stimulus context by using either a vertical bar or a directional arrow (always opposite to the primary task arrow) as the instruction to change or stop. The interaction between both manipulations isolates the effect of contextual complexity A successful change in response to a vertical bar is conditional on the direction of the primary go cue (complex context), whereas the direction is explicitly specified if the change stimulus is an arrow (simple context). The reverse is true for stopping – stopping to a vertical bar requires no additional information as a bar always means stop (simple context), but one usually presses a button in response to an arrow, and only stops to an arrow in the context of an immediately preceding arrow (i.e. it is dependent on a second piece of information - complex context). The SOA was dynamically altered between trials to strive for a 50% correct response rate. RT is the trial reaction time.*

Each task block contained only one paradigm variant, and the order of task blocks was balanced across subjects. During each paradigm, the subject was presented with a fixation cross (lasting 1.3 – 1.5s, the duration was drawn from a uniform distribution) which, after a 200 ms pause with a blank screen, was followed by a green left- or right- pointing arrow (the primary task stimulus, or 'go signal'). The subject was asked to make a button-press with the thumb of the corresponding hand as quickly as possible. In a randomly selected 50% of trials, a further red visual signal was presented at a variable latency (called the stimulus onset asynchrony, SOA) after the primary task stimulus. In response to this second signal, the subject was asked to either inhibit the button press (stop-signal task) or change to pressing the opposite button (change-of-plan task) depending on the task variant. We used two different symbols as the stop/change cue in each task: a directional arrow (<) or a vertical bar (|). The SOA was dynamically altered on a trial-by-trial basis according to a staircase – a correctly switched/stopped response resulted in the SOA increasing by 50ms (making the task more difficult) whereas after a failure to change/stop, the SOA reduced by 50ms (allowing more time to stop/change the response, making the task easier) (Levitt, 1971). This staircase tracking procedure aims to fix the probability of successfully stopping/changing at ~0.5 so that successful-stop/change and failed-stop/change conditions were equally sampled. The SOA was randomly drawn from 2 independent staircases, so that both the presence and timing of the stop/change-signal remained difficult for the subject to predict.

5.2.2 Behavioural analysis

The aims of the behavioural analysis were threefold: to determine whether experimental modulations were evident in behaviour; to identify and exclude experimental runs where behaviour was anomalous; and to provide behavioural summary measures which could be used as predictor variables in the electrophysiological analysis. Stimuli and response timings were recorded and analysed offline using custom Matlab scripts, the Psignifit toolbox (Fründ, I, Haenel, NV, Wichmann, 2011) and SPSS software version 20.

Three key trial-types were considered: go only trials (where the stop/change-signal is not presented), successful-stop/change trials (where the stop/change signal is presented and subject successfully changes or stops) and failed-stop/change trials (where the stop/change signal is presented, but the subject fails to inhibit or change the response). Other trials, such as non-change signal trials where the left button was pressed in response to the right arrow were considered unclassified errors and discarded.

Subject	Condition	Presented trials	trials	Classified trials	Change fraction	Fail fraction	Go RT	Fail RT	Succ RT	Fail SOA	Succ SOA	SSRT
	3	155	10	145	0.49	0.31	0.64	0.59	0.94	0.50	0.45	161
1	4	154	14	140	0.48	0.34	0.54	0.48	0.84	0.35	0.30	217
	1	155	8	147	0.50	0.49	0.43	0.39		0.25	0.20	189
	2	153	10	143	0.50	0.42	0.44	0.42		0.30	0.25	154
	3	156	12	144	0.51	0.47	0.41	0.38	0.52	0.25	0.15	215
3	4	155	20	135	0.50	0.45	0.37	0.34	0.43	0.20	0.15	189
	1	155	8	147	0.50	0.35	0.71	0.66		0.55	0.45	212
	2	122	8	114	0.48	0.29	0.73	0.70		0.58	0.50	165
	3	155	14	141	0.49	0.33	0.71	0.60	1.01	0.48	0.45	212
4	4	155	12	143	0.47	0.33	0.63	0.54	0.94	0.47	0.40	179
	1	153	4	149	0.49	0.33	0.57	0.54		0.42	0.40	101
	2	155	4	151	0.50	0.20	0.72	0.71		0.60	0.55	55
	3	155	12	143	0.49	0.35	0.78	0.68	1.09	0.60	0.50	228
5	4	155	36	119	0.48	0.27	0.63	0.50	0.79	0.40	0.35	139
	1	154	6	148	0.51	0.40	0.53	0.48		0.35	0.30	208
	2	151	4	147	0.48	0.39	0.65	0.61		0.50	0.45	204
	3	151	18	133	0.50	0.23	0.86	0.71	1.10	0.70	0.60	134
6	4	155	12	143	0.52	0.37	0.76	0.69	0.95	0.60	0.50	200
	1	156	10	146	0.49	0.42	0.54	0.48		0.40	0.35	189
	2	154	6	148	0.49	0.40	0.50	0.47		0.35	0.30	149
7	3	155	16	139	0.49	0.43	0.55	0.50	0.72	0.35	0.30	208

	4	155	14	141	0.50	0.44	0.61	0.56	0.85	0.45	0.40	185
	1	155	7	148	0.48	0.42	0.43	0.42		0.25	0.25	169
	2	155	8	147	0.50	0.38	0.54	0.50		0.30	0.30	240
	3	154	31	123	0.48	0.24	0.74	0.56	0.86	0.50	0.45	96
8	4	156	38	118	0.48	0.24	0.58	0.48	0.75	0.32	0.33	110
	1	154	10	144	0.48	0.44	0.57	0.53		0.30	0.25	302
	2	154	8	146	0.50	0.36	0.56	0.47		0.35	0.30	172
	3	154	25	129	0.50	0.35	0.60	0.52	0.67	0.35	0.30	201
9	4	156	37	119	0.49	0.34	0.53	0.51	0.61	0.35	0.30	161
M		**153**	**12**	**141**	**0.49**	**0.39**	**0.57**	**0.52**	**0.80**	**0.39**	**0.34**	**194**

Table 6: Trial numbers and reaction time data for each subject and condition. *Note data from subject two, and conditions 1 and 2 from subject one were discarded due to drowsiness and a software error, respectively. Otherwise each subject performed four variants of the task defined by the stop/change stimuli (| or >) and the response required (stop or change). The conditions were: (1) stop |, (2) stop <, (3) change |, (4) change <. The total of presented trials per condition is shown with the number of classified trials taken onto further analysis. Unclassified trials include the first 5 trials of every condition and trials where the subject lapsed or made unclassified errors (e.g. pressed two buttons). The change fraction is the fraction of change trials/ total trials. The fail fraction is the fraction of unsuccessful trials/all change trials. The median reaction times of go only trials (Go RT), failed stop/change trials (Fail RT) and successful stop/change trials (Succ RT) are presented. Successful stop trials do not have a reaction time. Median SOA for failed and successful stop/change trials is presented. The stop-signal reaction time (SSRT) estimate (as the threshold of the psychometric function) is also given for each condition. Some subjects and conditions were rejected from further analysis due to low fail fractions (highlighted by red fail fractions) and poorly fitting psychometric functions (highlighted by red SSRTs). The mean (M) of the data, after having removed these trials, is given in the bottom row.*

We performed two analyses to check that the subject had engaged in the task appropriately. Firstly, we looked at basic reaction time measures: we calculated the median reaction times for each trial type in each condition, the median SOA in each condition and the proportion of unsuccessful stop/change trials (error fraction) per condition. One subject was excluded at this stage because of reported drowsiness during the experiment and reaction times greater than 1s (data not presented), and two conditions were discarded for another subject due to a software error. Trial numbers and these behavioural summary measures are presented per subject in **Table 6**.

Secondly, we modelled the inhibition function of each data run whilst trying to protect against non-stationarities in the data (e.g. reaction time drift) and behavioural confounds (guessing and lapses in concentration). The inhibition function models the proportion of correct responses, i.e. successful stops or changes, as a function of the SOA and is linear around central SOAs. To allow comparison between conditions with different primary reaction times it is often normalised - for example by subtracting the SOA from the median primary task reaction time (Logan and Cowan, 1984; Band et al., 2003). We began by visually inspecting reaction time trends and the SOA staircases to ensure that the both SOA staircases converged (see %% for an example). Whist performing the task, subjects tended to progressively delay responses to the primary task – to *wait* for the stop/change signal, presumably to increase their success-rate. However, this creates a non-stationary primary task reaction time which violates the underlying assumptions of the horse-race model. To adjust for this we fitted cubic splines to the SOA and the go only reaction time data. This provides a *predicted* go reaction time for stop/change trials – an estimate of how the subject would have responded on stop/change trials if they had been go only trials, based on the reaction times of neighbouring trials (Nachev P, unpublished, http://ukpmc.ac.uk/theses/ETH/445162). On stop/change trials we subtracted the SOA from the predicted go spline to estimate the *decision time* per trial - the post-stop/change signal latency required to make a correct or incorrect decision on that trial, correcting for reaction time drift in the data. The ratio of successful:total stop/change trials was calculated as a function of decision time in 100ms bins. We fitted an inhibition function to this data using a Bayesian Markov Chain Monte Carlo (MCMC) procedure, which is superior to other methods such as bootstrapping (Kuss et al., 2005; Fründ, I, Haenel, NV, Wichmann, 2011). The psychometric function fitted was a sigmoid defined by four parameters (with standard prior distributions): the upper limit of the function or 'lapse rate' (prior: gamma(2,400)), the 50% point of the function or 'threshold' (prior: beta(1.5,10)), the 'slope' at 50% of the function (prior: beta(1.5,10)), and the lower limit or 'guess rate' (prior: gamma(2,400)). Calculating the Bayesian posterior for such a model is *analytically* intractable, but it can be approximated by

the MCMC procedure, which generates many samples of the posterior according to a particular algorithm (Kuss et al., 2005). We generated 4000 samples, discarding the first 2000 samples, to estimate an approximation to the posterior of the inhibition function. In this scenario the threshold of the function, i.e. the decision time which reflects mid-point of the inhibition function, is equivalent to the SSRT of that subject during that condition. We assessed the goodness-of-fit of the model by calculating the deviance, which is a generalisation of the sum-of-squares metric that applies to binomial data (Fründ, I, Haenel, NV, Wichmann, 2011).

To look for behavioural evidence of complexity, median reaction time estimates were subjected to a mixed hierarchical model in SPSS with response (stop or change), cue type (| or >) and previous trial (previous successful stop/change, previous failed stop/change, previous go only trial) as fixed factors and subject as a random factor. SSRT and the slope of the inhibition function were subjected to similar models, omitting the previous trial factor. We confirmed that post-stop signal changes apparent when examining median reaction times were not merely due to different amounts of drift, by limiting the analysis to only post stop/change-signal trials and calculating a corrected post-stop signal reaction time (current trial go only reaction time - previous go only trial reaction time). To increase trial numbers, we included trials where a go only trial was preceded by several stop/change trials, as long as the outcome for all stop/change trials was the same (similarly to (Bissett and Logan, 2011)). The median of these corrected reaction times per condition were also subjected to a mixed hierarchical general linear model with stop/change stimulus (< or |), response (stop or change) and previous trial history (previous successful stop/change trial, previous unsuccessful stop/change trial) as fixed-factors and subject as a random factor.

5.2.3 Magnetoencephalographic data acquisition and pre-processing

MEG data were acquired at 600Hz with a 275 channel CTF system. The data were stored and analysed off line using SPM8 (Litvak et al., 2011b) and Fieldtrip (Oostenveld et al., 2011) toolboxes. They were down-sampled to 300Hz, high-pass filtered above 0.1 Hz, and the line noise artefacts at 50 Hz and 100 Hz were removed using notch filters (5th order zero-phase Butterworth filters). We then extracted time-series data from cortical regions of interest using a linearly constrained minimum variance beamformer (LCMV) beamformer (Van Veen et al., 1997). Although we were primarily interested in the right IFG and pre-SMA, we also looked at other cortical regions implicated within the stopping network, to support the regional specificity of the effects of interest (Aron et al., 2007a). The MNI co-ordinates (x,y,z) of locations of interest were taken from the literature and included the pre-SMA

(2,30,48 taken from (Nachev et al., 2007)), the right and left IFG (±42,26,14 from (Aron et al., 2007a)), the SMA (-2,-10,59 adapted from (Mayka et al., 2006)) and both the primary motor cortices (±37,-25,62 adapted (Mayka et al., 2006)). Locations obtained from Mayka et al. were converted from Talaraich to MNI space using a transform devised by Mathew Brett (http://imaging.mrc-cbu.cam.ac.uk/imaging/MniTalairach). The beamforming method involves linearly projecting the MEG sensor data using a spatial filter computed from the lead field of the source of interest and the data covariance (Van Veen et al., 1997). The spatial filter is designed to extract activity from the region of interest, whilst suppressing activity from other sources. Lead fields were computed using a single-shell head model (Nolte et al., 2004) based on an inner skull mesh derived from a canonical T1 MRI. We specified 0.01% regularization and defined the orientation of each source to be in the direction of maximum power. In order to determine if we had sufficient signal separation for the different sources of interest, we correlated the beamformer filter coefficients between each source of interest and all the other sources (Barnes et al., 2004).

Time-series data were then standardised by subtracting the mean and dividing by the standard deviation. To make standardization robust to possible artefacts, medians of the raw and squared signals were computed for non-overlapping 10 s segments and averaged yielding first and second moment estimates. Time-frequency representation of the data was generated using multitaper spectral analysis (Thomson, 1982). We computed continuous power over the whole data run in time windows of 0.4s shifted in steps of 0.05s over a frequency range of 2.5 to 90 Hz in steps of 2.5 Hz. The frequency resolution was set to the inverse of the time window (2.5 Hz) for up to 25 Hz, then 0.1 times the frequency for 25 to 50 Hz and then to a constant 5 Hz. Because power is a non-linear measure, the square root of power (i.e. root mean square (RMS) amplitude) was taken forward to the following linear convolution model.

MEG data were analysed hierarchically: summary measures of induced responses were obtained with a first-level convolution model, then transformed into time-frequency images and finally subjected to a standard general linear model at the second level.

5.2.4 The convolution model for magnetoencephalographic data

To characterise and disambiguate induced responses to the events of interest, regressors were generated for each event-type, and assembled as predictors of continuous amplitude in a general linear model (GLM) at each frequency. Each event was modelled as a delta function (a spike) and then convolved with a set of Fourier basis functions spanning -0.5 to

+1.5s relative to each event (the peri-stimulus time-window). GLM coefficients were estimated using ordinary least squares. The induced response for a particular event-type and frequency can be reconstructed by multiplying the basis functions with the parameter estimates corresponding to the event-type and frequency in question (Litvak et al., 2012b). When this is repeated for all frequencies – and the same event-type – the ensuing response functions of peri-stimulus time constitute a time-frequency image of the amplitude per event-type. In the simplest case, with non-overlapping events, this would be equivalent to averaging time-frequency images centred on an event of interest. However, our data contains multiple temporally overlapping responses. Therefore the convolution model was superior to event-locked routine averaging. This is because, at each frequency, multiple-event types are modelled *in the same* GLM, and therefore the variance that each regressor (corresponding to an event-type) explains is independent of every other regressor. As a result, closely overlapping responses can be disambiguated if they do not always occur together. For example, the induced response to a failed stop-signal can be disambiguated from the associated button press, allowing for a direct comparison of successful and failed stop-signal induced responses, having accounted for the confounding button press. Individual regressors were specified for the fixation cross, the primary task stimulus (separately for left and right arrows), and button press responses (separately for left and right responses) and the stop/change signal (separately for successful and failed change conditions). Separate models were used to estimate induced responses during different stop-signal task variants. The data and the design were filtered below 0.25 Hz.

Previous studies have shown that post stop-signal trials are longer than other trials (Verbruggen and Logan, 2009a; Bissett and Logan, 2011) and that the medial frontal cortex is sensitive to reaction time changes (Grinband et al., 2011; Yeung et al., 2011). Increasingly conditionally complex tasks increase reaction time, therefore we sought to model the neural responses associated with contextual complexity, having taken into account any changes in reaction time *not* due to contextual complexity. In order to do this, we included trial reaction time in our model by using the predicted go spline as a parametric modulator of the go signal event. *After* modelling the mean go event, and variation due to go-reaction time drift, we then estimated induced responses separately for all combinations of the current trial (left or right cue) and previous trial-type (go only trial, successful stop/change trial, failed stop/change trial). The resulting induced responses across different go events are independent of reaction time drift (e.g. due to attentional lapses, or strategic changes), independent of reaction time changes due to previous trial-type, and balanced across different conditions with potentially different percentage of stop/change errors. In addition, stop/change

successes have longer reaction times than stop-change failures. We modelled this variation by using the stationary measure of decision time (primary task go only reaction time – SOA spline) as a parametric modulator of the stop/change signal. Use of the spline, rather than actual reaction times allows estimates of decision time where no reaction time is available (e.g. successful stopping).

5.2.5 Analysis of time-frequency images

After eliminating reaction-time confounds, we generated time-frequency images for each event-type and entered these into within-subject ANOVAs for each cortical source. We studied responses to two event-types statistically: the stop/change signal - with success (successful or failed), stop/change stimulus (< or |) and response (stop or change) as factors, and the go signal – with the current trial (left or right cue) and previous trial-type (go only trial, successful stop/change trial, failed stop/change trial) as factors. Two tailed t-tests were performed for each main effect and interaction and were thresholded at p=0.05 FWE, taking non-sphericity of error into account using standard procedures (Litvak et al., 2011b).

5.3 Results

5.3.1 Subject task performance

Nine subjects performed all four conditions of the task in an order counterbalanced across subjects. One subject was drowsy during the experiment, with resulting primary task reaction times greater than 1s and was excluded from further analysis. A software error made data from two conditions from subject one uninterpretable, and so data from these experiments were discarded. Trial numbers and behavioural estimates from the remaining subjects and conditions are shown in **Table 6**. The lowest number of trials per condition was 118.

To determine whether subjects performed the tasks appropriately, we examined the following data features: SOA staircase convergence; the number of unsuccessful stop/change trials as a fraction of the total number of stop/change trials (fail fraction); and the fit of the psychometric inhibition function, based on the deviance estimated from the Bayesian MCMC procedure. An example of this process can be seen in **Figure 30**, and the psychometric fits for all the subjects and conditions can be seen in **Figure 31**.

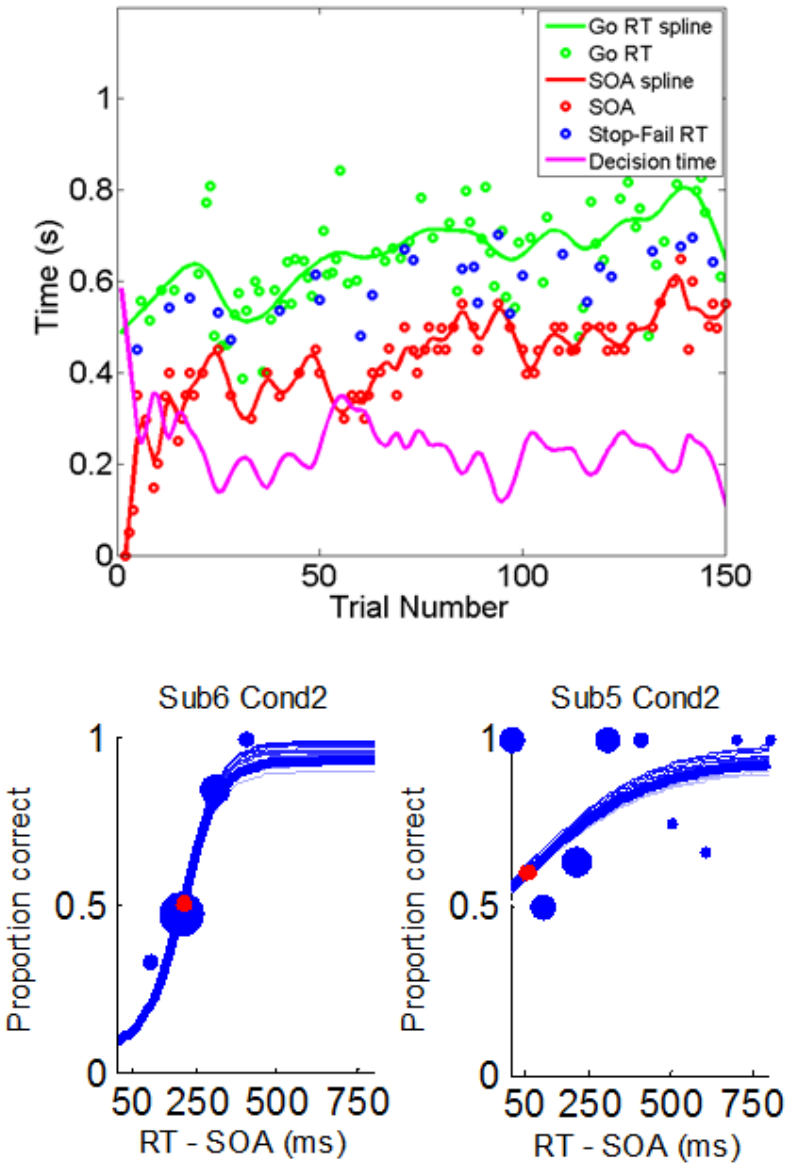

Figure 30: Behavioural data examples. *The top image shows the timing of various trial events during 150 sequential trials in one subject during a stop-signal task. Green circles represent the reaction time during go only trials. A green spline has been fitted through these trials to highlight reaction time drift. Half of the trials had a stop signal, after a delay (SOA) represented by a red circle. Again a spline has been fitted to the SOA to visualise drift. Note how the two SOA staircases converge during the first few trials. Finally blue circles represent reaction times during stop-fail trials. Although there is some drift to both go reaction time and SOA, the resulting stop/change decision time (Go only spline – SOA spline) is stationary. The first 5 trials of every block (shown here) have been excluded from behavioural and*

electrophysiological analysis, as the stop/change decision time is poorly estimated here. The plots beneath show the inhibition functions for the same dataset (left) and a separate run (right). The plot on the left shows the proportion of successful responses to the stop-signal as a function of predicted RT (the Go RT spline) – SOA. The data are represented by blue circles, with larger trials numbers resulting in larger circles. The fitted psychometric function is also displayed by a blue line, with 20 alternative samples from the distribution of the function presented in light blue. The 50% threshold of the function, equivalent to the SSRT, is highlighted with a red circle. The deviance (Dev) of the model represents the goodness-of-fit to the data. The condition on the left shows a good fit (Dev=2.4), whereas the condition on the right shows a poor fit (Dev=28.7) – the latter was rejected from further analysis.

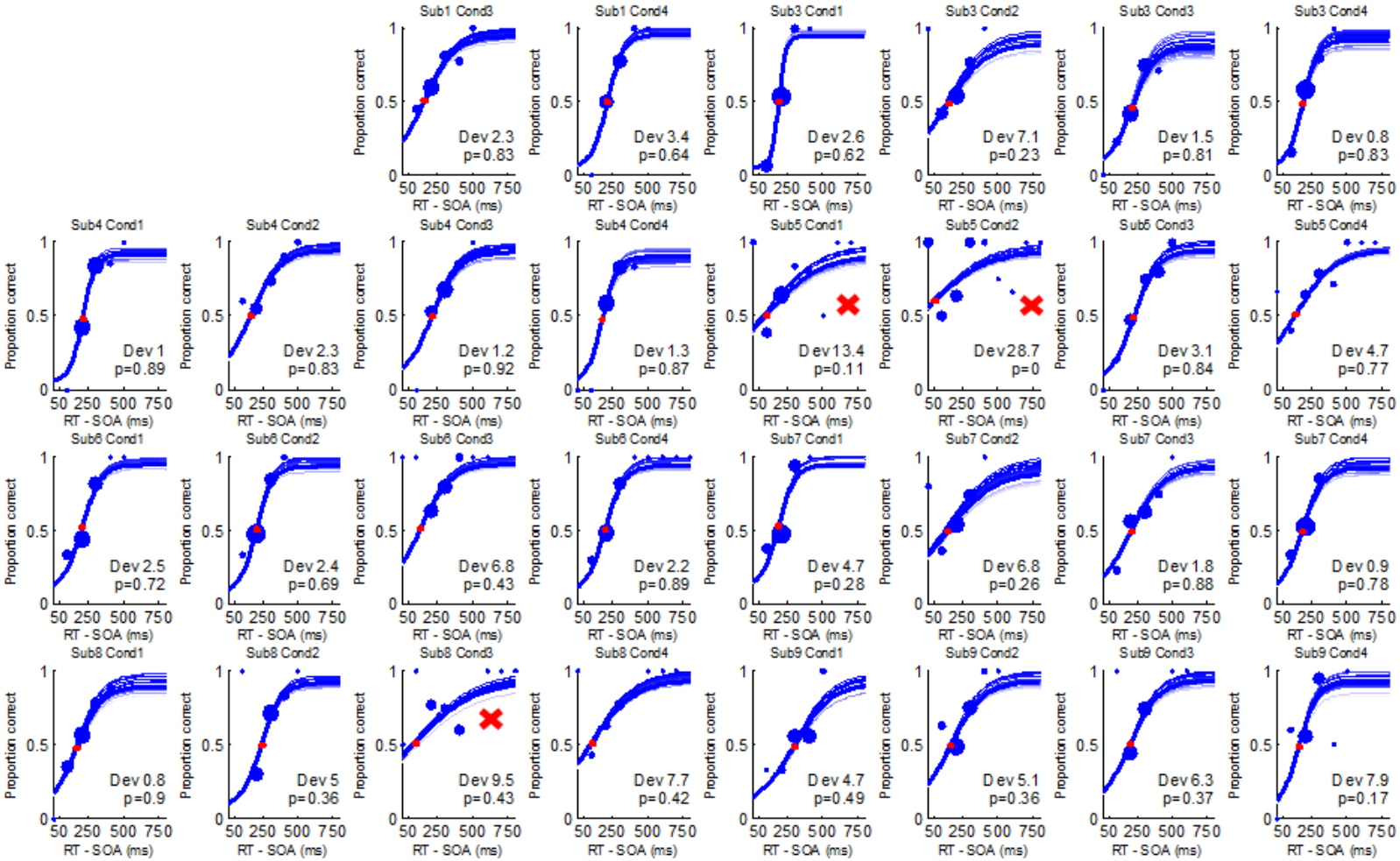

Figure 31: Inhibition functions for each subject and condition. *Each plot shows the proportion of correct stops or changes as a function of the SOA, normalised by subtracting the predicted go reaction time. The trial data is binned in 100ms bins and plotted as blue circles – a larger circle corresponding to more trials. The Bayesian MCMC fit is plotted in darker blue, and 20 samples from the posterior are plotted in lighter blue in order to aid visualisation of the posterior distribution. The threshold (equivalent to the SSRT) is highlighted by a red circle. The deviance (Dev) of the data is also shown - three data runs with deviance greater than 8 were excluded and are highlighted by a red cross. A p value, reflecting the Bayesian probability of the fit being part of the initial data distribution is also presented, but this value was redundant in calculations and not used further.*

Both SOA staircases converged in all conditions of all subjects. The fail fraction varied from 0.2 to 0.49. Although lower than other studies, the higher fraction of stop/change trials in this study affords a greater stop/change signal expectancy and therefore a higher stop/change success rate. However, very low error fractions may be indicative of waiting, where a subject delays the primary task reaction time as a strategy to increase success rate on stop/change trials. The resultant non-stationarity in the primary task reaction time can compromise the SSRT estimate. Visual inspection of the inhibition functions revealed that the majority of subjects performed as expected resulting in a sigmoidal psychometric function. However, some runs displayed poor data fit (high deviance), suggesting that during some conditions the subjects were not adhering to the task rules appropriately (e.g. by waiting, or guessing). In order to balance removal of outliers whilst conserving as much data as possible, we removed data runs with either an arbitrary error fraction less than 0.28 or a deviance greater than 8. Two data runs had both a high deviance and error rate, one run had only a high deviance and 3 further runs had only low error rates – therefore a total of 6 out of 30 runs were excluded from further analysis.

5.3.2 Primary task reaction time depends on task complexity and the previous trial

We examined primary task reaction times in order to confirm that modulations of conditional complexity were evident in behaviour as increased primary task reaction time. We additionally modelled the effects of previous trial type on current trial type (Bissett and Logan, 2011), to ensure that complexity was behaviourally evident, even after the effects of previous trial type had been accounted for.

In order to obtain a stable reaction time estimate for this analysis, we discarded the first and last 15 trials of each data run. With the remainder, we calculated the median reaction time of go only trials, and subjected it to a mixed hierarchical general linear model with stop-change stimulus (< or |), response (stop or change) and previous trial history (previous go only trial, previous successful stop/change trial, previous unsuccessful stop/change trial) as fixed-factors and subject as a random factor. A full factorial model was specified. Here, because the conditional complexity of the stop/change cue is *reversed* for stop versus change trials, the effect of complexity is seen as an interaction between the stop/change cue and response. The main effect of previous trial ($F(2,52.81)=12.50$, $p<0.001$) and the interaction between stop/change stimuli and response ($F(2,53.44)=4.27$, $p=0.044$) were significant,

whereas the interaction between response and previous trial ($F(2,52.81)=3.01$, $p=0.058$) almost reached significance (**Figure 32**). All other effects were not significant. These results confirm that primary task reaction time increases with task complexity, and that this cannot be explained by differences in accrual of post-stop signal changes. In addition, although all post stop/change trials appear to be slower than post go only trials, the plots suggest that go only reaction time may be relatively longer after stop-fail and change-success trials (although the equivalent statistical test, the interaction between response and previous trial, was just non-significant). However, post stop-signal reaction times calculated in this manner are confounded if reaction time drift is different in different conditions (Bissett and Logan, 2011). In order to address this we re-analysed *only* post stop/change go only trial reaction times. We subtracted the previous go only trial reaction time from the current go only trial reaction time to eliminate the effects of drift in the data. To increase trial numbers, we included trials where a go only trial was preceded by several stop/change trials, as long as the outcome for all stop/change trials was the same (similarly to (Bissett and Logan, 2011)). The median of these adjusted reaction times per condition were subjected to a mixed hierarchical general linear model with stop/change stimulus (< or |), response (stop or change) and previous trial history (previous successful stop/change trial, previous unsuccessful stop/change trial) as fixed-factors and subject as a random factor. A full factorial model was specified. The interaction between response and previous trial was now significant ($F(1,34.97)=17.10$, $p<0.001$) - all other effects were not significant (**Figure 33**). Therefore there is a genuine dissociation between greater post-stop slowing after a stop-fail trial but greater post-change slowing after a change-success trial, and this is not due to go reaction time drift.

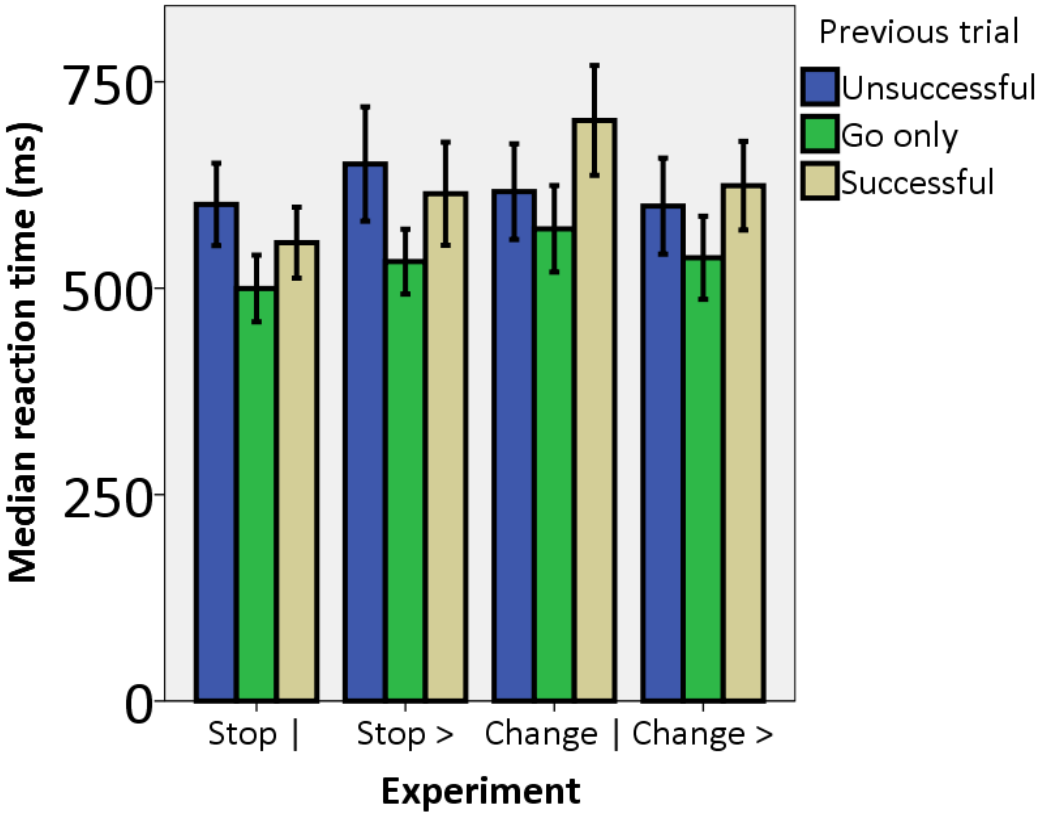

Figure 32: GO reaction time and trial history. *Go only reaction time is shown grouped according to previous trial type, response type (stop or change) and the stop/change signal stimuli (| or >). The median primary task reaction times for go only trials are shown as a function of the stop-signal task variant and previous trial. See text for discussion. Error bars represent ± standard error.*

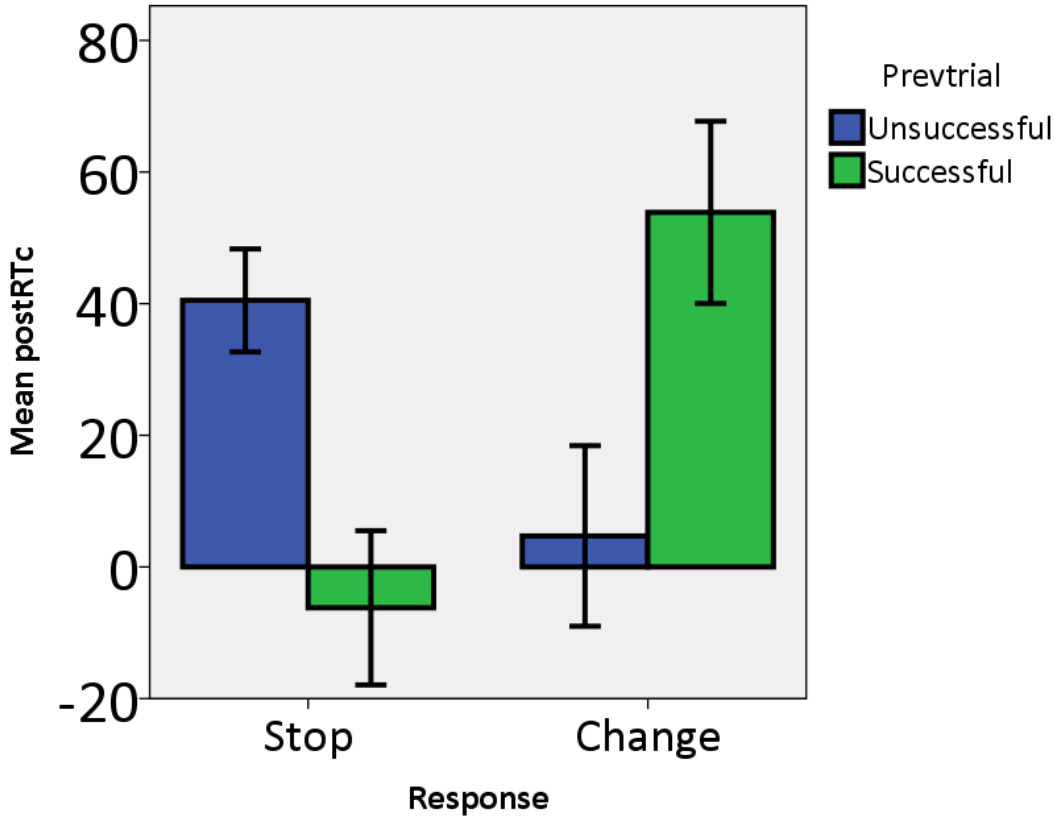

***Figure 33:* Post stop/change trial go only reaction times adjusted for the previous go only reaction time.** *Times therefore represent the adjustment to go reaction time made after a stop/change signal as a function of previous trial history and response. See text for discussion. Error bars represent ± standard error.*

5.3.3 Complexity affects the slope of the inhibition function but not the stop-signal reaction time

We looked for evidence for the effect of complexity on a measure of stopping efficiency, the SSRT, expecting to find that experimental modulations of conditional complexity do *not* affect stopping efficiency – consistent with the view that all stop-signal task variants require the *same* inhibition process. The SSRT was subjected to a mixed hierarchical general linear model with stop-change stimulus (< or |) and response (stop or change) as fixed-factors and subject as a random factor. Again the effect of complexity is the interaction between response and stimuli. The effect of signal ($F(1,20)=3.01$, $p=0.098$), response ($F(1,20)<0.01$, $p=0.985$) and their interaction ($F(1,20)=0.32$, $p=0.578$) were not significant. The slope parameter of the inhibition function was subjected to a similar analysis. The effect of response ($F(1,18.02)=0.693$, $p=0.416$) and signal ($F(1,15.761)=0.01$), $p=0.91$) on the slope were not significant, but there was a significant interaction between the two

(F(1,15.76)=10.28, p=0.006). Therefore complexity does affect the slope of the inhibition function. Although this suggests that contextual complexity affects the relationship between successful stopping and the time given to stop, it is difficult to be certain about the mechanism underlying this process. This is in part due to the fact that contextually complex tasks also have greater primary task reaction times which may confound estimates of inhibition function slope. At most we can say that complexity non-specifically affects sensitivity of the inhibition function to the SOA.

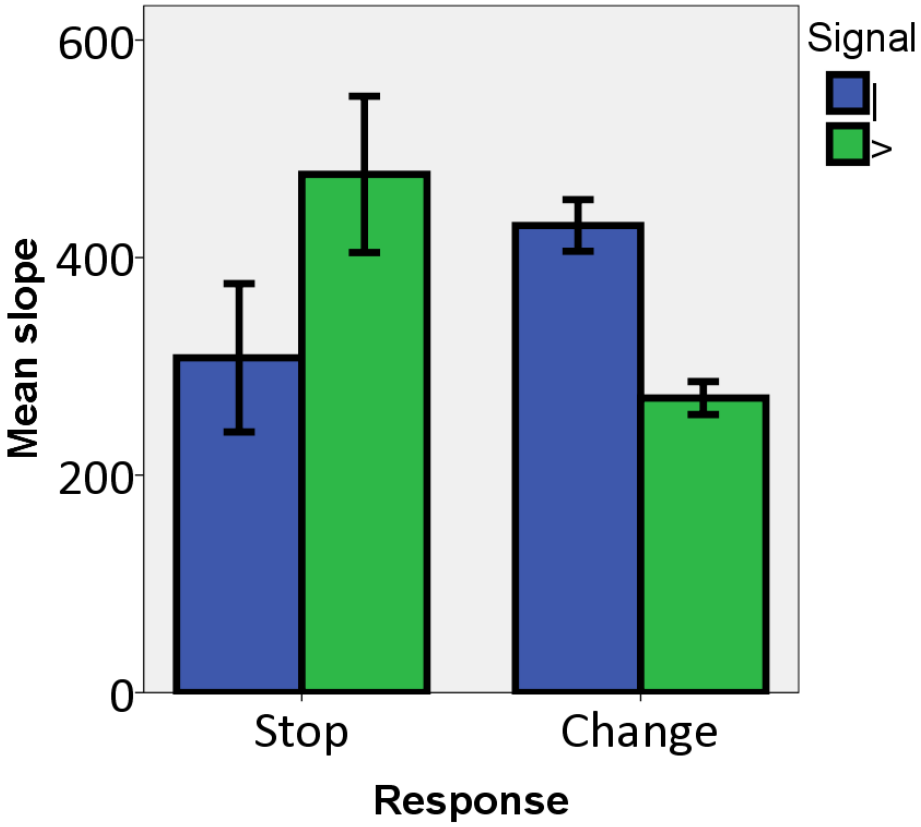

Figure 34: Effects of stimuli type (< or |) and response (stop or change) on the slope of the inhibition function. *There is a significant effect of complexity (interaction between signal and response). Error bars represent standard error.*

5.3.4 Beamforming adequately separates cortical sources involved in the stop/change process

Source activity was extracted from six *a priori* cortical locations: the pre-SMA, the SMA, and the left and right primary motor cortex and inferior frontal gyri. To determine whether data from these sources were adequately separated we correlated the beamformer filters (weights applied to the sensor data) of each source with all other sources per data run. These coefficients (Pearson's r^2) were then averaged across conditions and subjects. The maximal mean correlation was low at 0.05 (between the SMA and the pre-SMA, see **Figure 35**) confirming that cortical sources were adequately separated (i.e. on average only 5% of the variance shared between these two sources can be attributed to non-physiological factors). To illustrate these correlations, we correlated the source filter at the locations of interest with the filter of every other voxel in the image and then averaged these images over runs and subjects. This image shows the spatial specificity of the beamformer in terms of the region of interest from which our source data come from (see **Figure 35**).

A

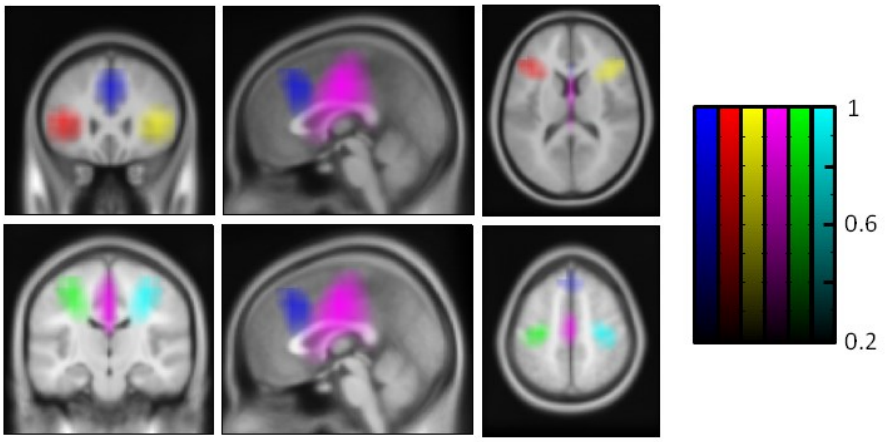

B

	M1L	M1R	SMA	pre-SMA	rIFG	lIFG
M1L	1.000	0.012	0.038	0.023	0.002	0.015
M1R		1.000	0.038	0.015	0.011	0.001
SMA			1.000	0.050	0.007	0.005
pre-SMA				1.000	0.010	0.008
rIFG					1.000	0.009
lIFG						1.000

Figure 35: Regions of interest. A*: Beamformer filters for each location of interest were correlated with filters for the rest of the brain. These correlation images were averaged across subjects and then thresholded at r^2=0.2. Each resulting image represents a maximal region of interest. Locations are the left (red) and right (yellow) inferior frontal gyrus, the pre-SMA (blue), the SMA (purple), and the left (green) and right (cyan) primary motor cortices. The colour scale represents r^2.* ***B:*** *Individual correlations of filters between point source locations are presented. Values represent r^2. Locations are left (M1l) and right (M1r) primary motor cortex, SMA, pre-SMA, right (rIFG) and left (lIFG) inferior frontal gyri.*

5.3.5 The convolution model extracts time-frequency data typical of basic responses

We used a novel convolution model to address reaction time confounds between contrasts of interest. Although we were primarily interested in cortical activity during the stopping/changing processes, given the novelty of our methods, we present the induced responses to the primary task go stimulus and the button press to demonstrate that they are similar to induced responses reported from standard analyses elsewhere (see **Figure 36**).

5.3.6 Stop/change signals are associated with a rapid, global theta/alpha synchonisation

Because all stop-signal task variants have the same requirement for stopping, we predicted that cortical areas involved in stopping would be similarly activated by the stop/change signal in all tasks. Stop/change induced responses were estimated by the convolution model and converted to time-frequency images in peri-stimulus time (from 0.5s before to 1.5s after the stop/change stimulus). We subjected these time-frequency images to a within-subject ANOVA with success (successful or failed), stop/change stimulus (< or |) and response (stop or change) as factors in a full factorial design. Two-tailed tests of main effects and interactions were thresholded at p=0.05 FWE. The results of significant tests are shown in **Figure 37** and **Figure 38**. The mean overall response to a stop/change signal is a global theta/alpha RMS amplitude increase that was significant in all areas except primary motor cortex. This activity peaks between 200 and 250ms post stop/change signal, and has an onset just before stop/change-fail trials terminate and a peak just before go only trials terminate, confirming that it is in a temporal window consistent with the neural correlate of the stop/change signal. Similar to the SSRT, task stimuli, response requirements and conditional complexity do not significantly affect the theta/alpha component of the induced response.

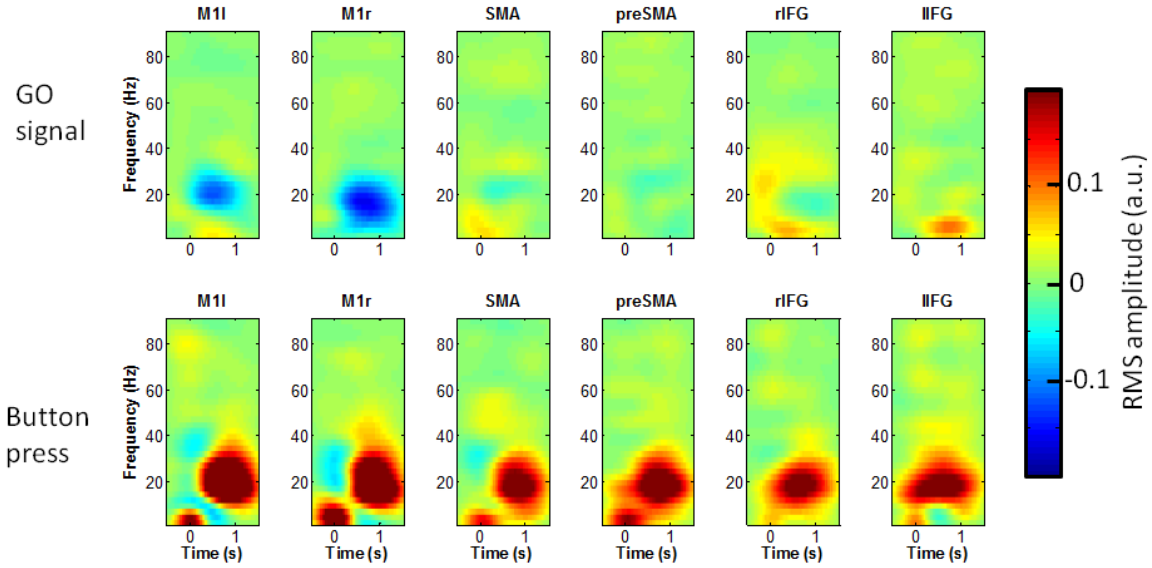

Figure 36: Estimated event-related activity from the convolution models of cortical activity. *Each image is the induced response to the go signal (top row, go event is at time=0), and to the button press (bottom row, button press is time=0) at different cortical locations. Locations are left (M1l) and right (M1r) primary motor cortex, SMA, pre-SMA, right (rIFG) and left (lIFG) inferior frontal gyri. Note that the button press causes a global induced response involving all areas tested. The colour scale represents the RMS amplitude in arbitrary units.*

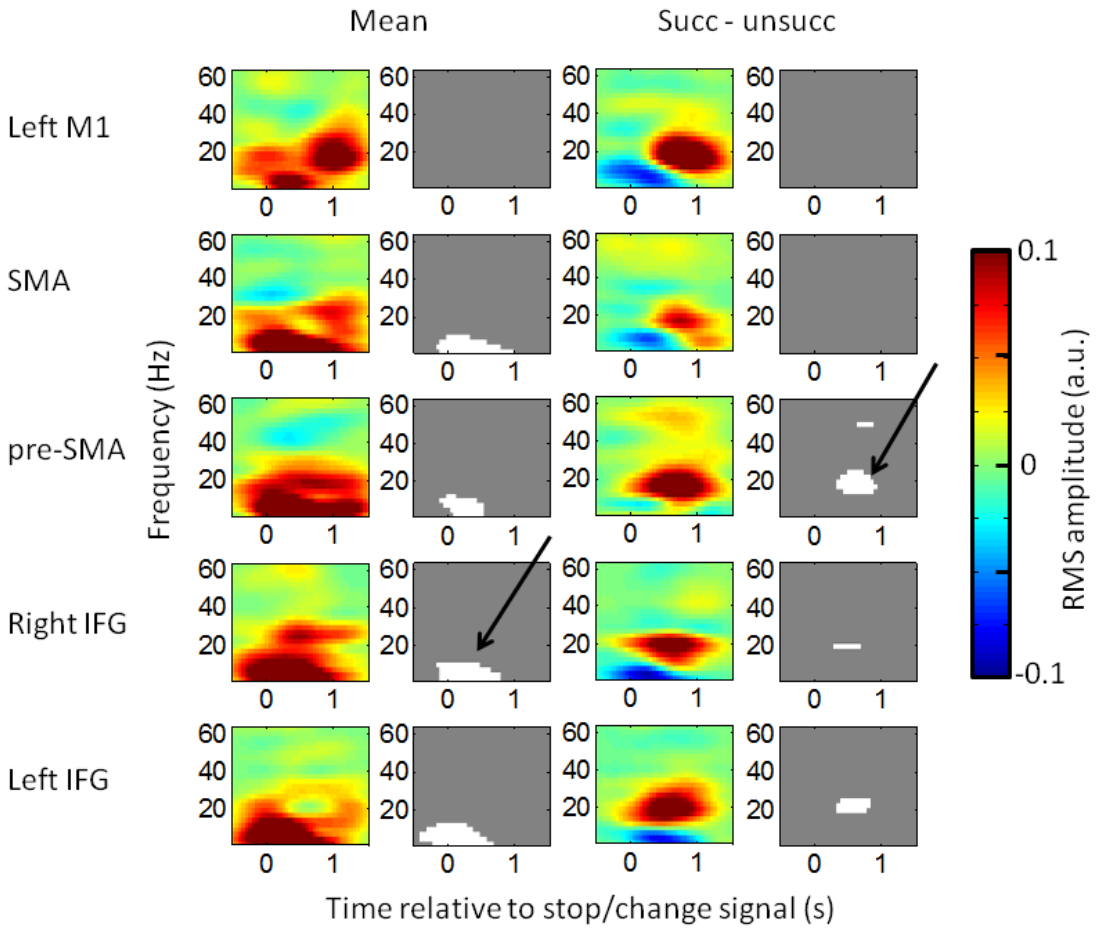

Figure 37: Time-frequency SPMs triggered to the stop/change signal. *Each subimage displays RMS amplitude changes associated with the stop/change signal as a function of frequency (y axis, Hz) and peri-stimulus time (x-axis, seconds, the stop change event occurs at t=0). Each row contains information from separate cortical areas. Images are in pairs: the colour image is the contrast image, whilst the greyscale image is a mask identifying significant increases (white) and decreases (black) in RMS amplitude triggered to the stop/change signal. The first column displays the mean induced response to the stop change signal across all conditions (labelled 'mean all'), with the associated statistical maps on the right. The third column displays the difference image between successful and unsuccessful stop/change trials (labelled 'succ – unsucc') and the associated statistical maps on the right. Two major frequency patterns are visible (black arrows): a global theta increase around the time of stop/change signal presentation, and a later beta increase in successful stop/change conditions restricted to more frontal regions. The colour scale represents the RMS amplitude in arbitrary units.*

The data suggest that a global theta/alpha response time-locked to the stop/change signal may be causal to inhibiting an action (**Figure 38**). If this is correct then theta/alpha activity should be more efficient during stop/change-fail trials which occur close to the stop-change signal, as opposed to trials which occur longer after the stop/change signal. We therefore divided subjects and conditions into those that had a shorter than average and those that had longer than average fail decision times (fail decision time = median fail trial RT – median SOA). We calculated the peak rate of rise of the theta/alpha activity in a -0.2 s to 0.5s window relative to the stop/change signal, in the right and left IFG and the pre-SMA and entered this into a mixed hierarchical linear model with source location (left IFG, right IFG and pre-SMA), and average fail decision time (long or short) as fixed factors and subject as a random factor (**Figure 39**). Short decision times had a greater rate of theta/alpha rise than long decision times (mean short=0.032, mean long=0.022, $F(1,44.71)=8.70$, $p=0.005$), and there was a significant source x decision time interaction ($F(2,62.10)=4.027$, $p=0.023$). Post hoc t-tests showed that the right IFG was affected by fail decision time ($t(1,16.03)=2.98$, $p=0.009$), but not the left IFG ($t(1,18.95)=-0.43$, $p=0.67$), or the pre-SMA ($t(1,22.95)=-0.98$, $p=0.34$). These results suggest that although the theta/alpha induced response is global, the right IFG is coupled most closely with the efficiency of the actual stopping process.

5.3.7 Stop signals are followed by changes in beta activity in frontal structures

The contrast between successful and unsuccessful stop/change trials reveals increased beta band activity in the successful condition in the pre-SMA, right and left IFG, regardless of trial complexity (see **Figure 37** and **Figure 38**). However, the interaction between success and response was also significant at the same time-frequency region (**Figure 40**). Inspection of the underlying beta amplitude dynamics in different conditions suggests that in the left IFG, right IFG and pre-SMA, stop-success is associated with a post-signal increase in beta, whilst stop-fail is associated with a post-signal decrease in beta amplitude. Switching does not have a significant effect on beta amplitude.

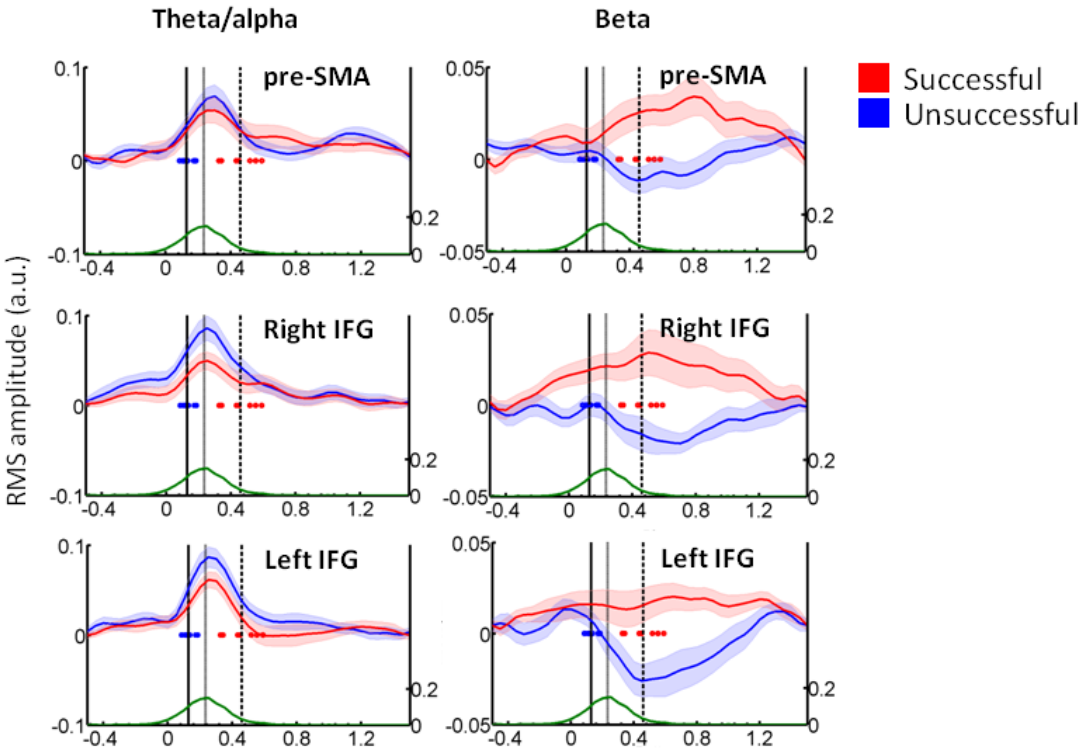

Figure 38: Timing of significant theta/alpha and beta RMS amplitude changes induced by the stop/change event. *The theta/alpha RMS amplitude (2-12 Hz, left) and beta RMS amplitude (15-25 Hz, right) changes (y axis) are plotted over time (x axis). Raw RMS amplitude estimates (from the convolution model) have been averaged over subjects and conditions and are represented as a mean (dark lines) and standard error (shaded area). Different rows display activity from different cortical sources during successful (red) and unsuccessful (blue) change trials. Behavioural data have been overlaid onto these plots: the median timings of the button press in stop/change-fail (blue) and change-success (red) trials of each subject are plotted as circles (calculated as the difference between the SOA and the reaction time of each condition). The overall median timing of button presses is presented for stop/change-fail trials (a solid black line), and change-success trials (dashed black line). The median predicted Go only reaction time during stop/change trials (derived from the Go only reaction time spline) is presented as a gray line, whilst the actual cumulative Go only reaction time distribution (after the mean SOA has been subtracted) is plotted as a green line with a separate y axis (right). In order for an oscillatory change to be potentially causal to switching/stopping, it must occur or have a substantial portion between 0s and the predicted go reaction time. This criteria is fulfilled by theta/alpha changes whereas beta changes predominantly occur after this behavioural marker. Units are arbitrary units of RMS amplitude.*

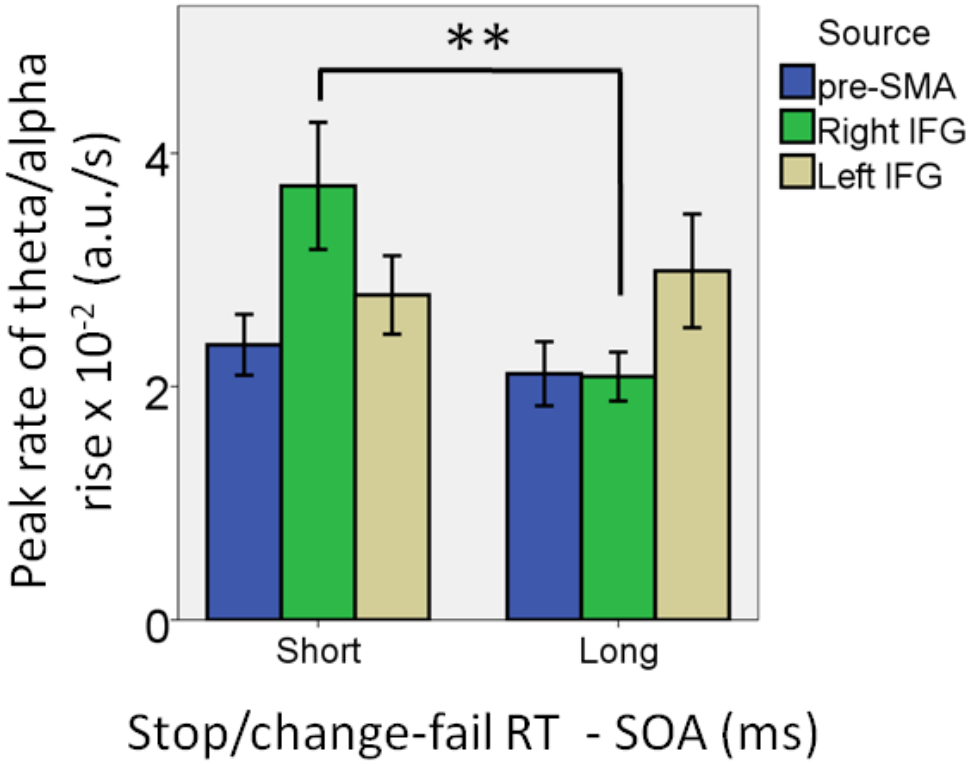

Figure 39: Peak rate of theta/alpha rise in different cortical locations. *The peak rate of rise of the theta/alpha response is steeper for efficient (short stop/change-fail RT- SOA) as compared to less efficient stopping/changing (short stop/change-fail RT- SOA) in the right IFG only. Peak rate of theta/alpha is presented as arbitrary units of RMS power per second.*

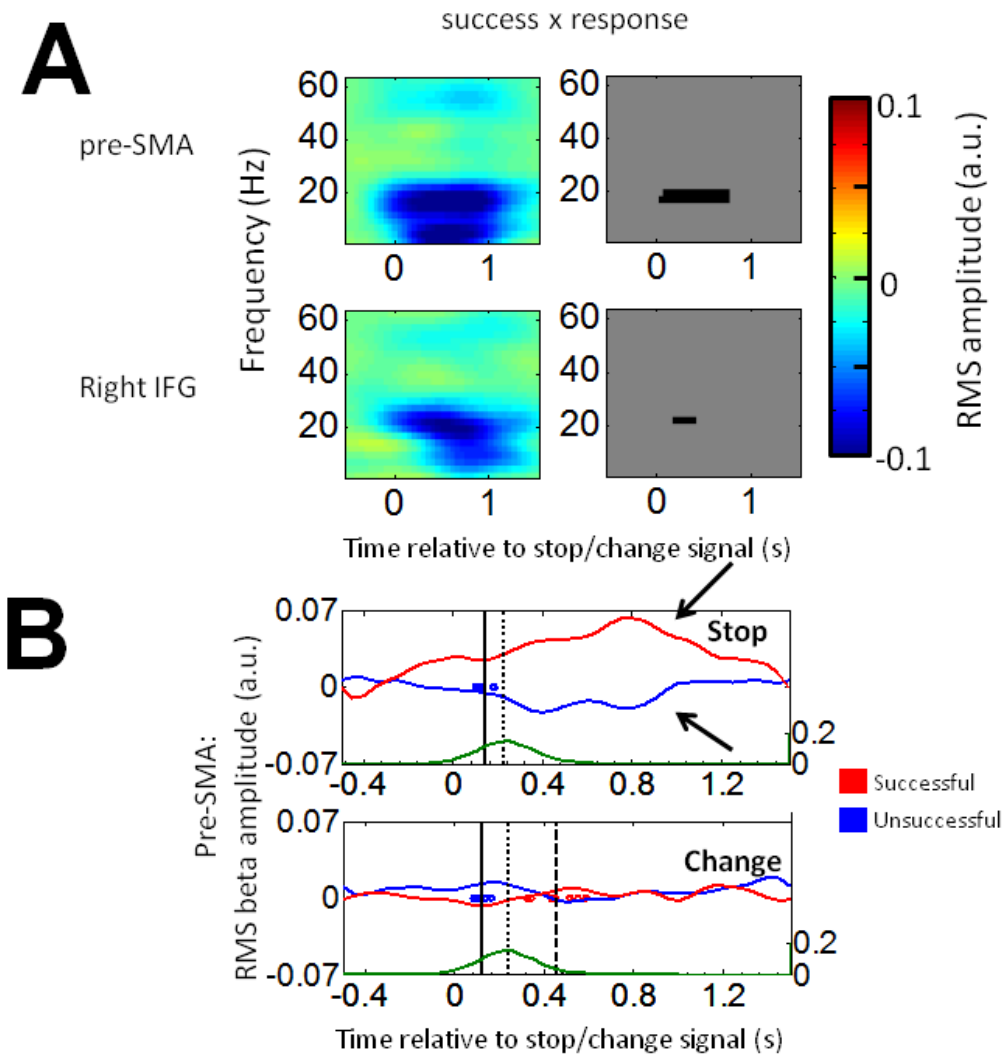

Figure 40: Time-frequency SPMs (A) and beta RMS amplitude plots (B) showing the interaction between the success and response in the pre-SMA and the right IFG. *Figure conventions and behavioural markers are the same as for* ***Figure 37*** *and* ***Figure 38****. A significant beta power decrease can be seen in both areas following the stop/change event. RMS amplitude in pre-SMA over time is shown separately for stop (top plot) and change (bottom plot) conditions and for successful (red) and unsuccessful (blue) trials, to highlight the success x response interaction, in panel B. Beta activity rises after successful stopping, drops after unsuccessful stopping (black arrows), but does not change during switch trials. Activity in the right IFG (not shown) shows a similar pattern. Units are arbitrary units of RMS amplitude.*

5.3.8 Task complexity modulates go signal related activity.

To look for the electrophysiological correlate of the effect of trial history and complexity on go reaction times, we modelled the effect of the stop/change stimulus (< or |), response (stop or change) and previous trial history (previous go only trial, previous successful stop/change trial, previous unsuccessful stop/change trial) on the induced response to the go signal event. Crucially, we excluded drifts in reaction time (modelled by the go only reaction time spline) by modelling it as a confounding covariate in the convolution model. Two-tailed tests of the main effects and interactions were thresholded at p=0.05 FWE. The results of significant contrasts are shown in **Figure 41**. There was a significant effect of trial complexity (the interaction between stop/change stimuli and response) on the gamma induced response in the pre-SMA before the average onset of the stop/change signal. There were no effects of trial history on the go induced response.

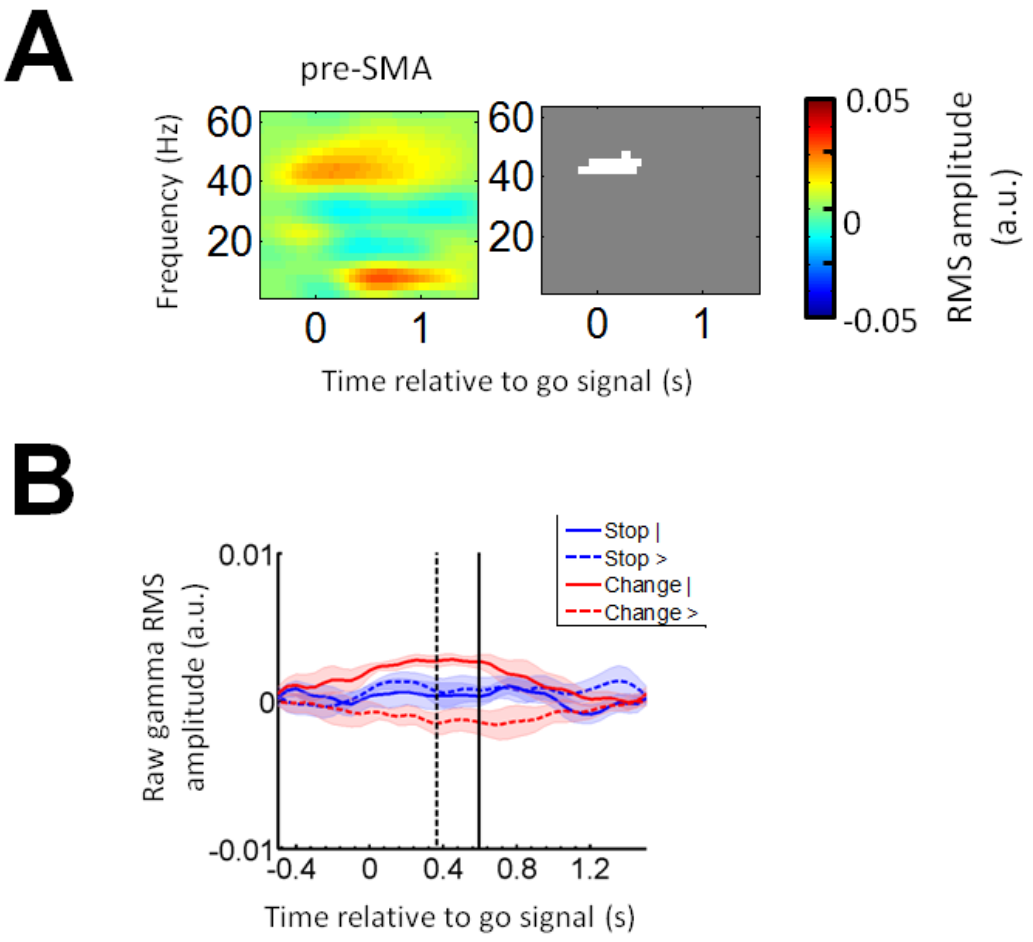

Figure 41: Time-frequency SPMs and RMS amplitude plots showing the effect of complexity on the induced response to the Go signal in the pre-SMA. *Panel A displays the effect of complexity on the mean induced response to the Go signal (see* ***Figure 34****) as a function of frequency (y axis, Hz) and peri-stimulus time (x-axis, seconds, the go signal*

*occurs at t=0). The neighbouring greyscale image is a mask identifying significant increases (white) and decreases (black) in RMS amplitude triggered to the go signal. The colour scale represents the RMS amplitude in arbitrary units. Panel **B** presents the significant effects as gamma amplitude changes over time in the pre-SMA. Behavioural markers showing timing of the median SOA (dashed black line) and the median button press to go only trials (solid black line) have been overlaid onto the plot. Increased complexity (and increased go only reaction time) is associated with increased gamma activity in the pre-SMA.*

5.4 Discussion:

In this study, we set out to dissociate the function of the pre-SMA and the right IFG whilst stopping a prepared movement. To this end, we designed four variants of the stop-signal paradigm that allowed us to modulate the context of the task, whilst keeping the inhibited response the same. We found that neural activity underlying stopping was dissociated spatially, temporally and spectrally into two components: the conditional complexity of the task was modulated most by an early persistent gamma response in the pre-SMA, whilst the efficiency of stopping was closely related to the post stop/change-signal theta/alpha induced response in the right IFG. We additionally found post-stop signal changes in beta activity in the left and right IFG and pre-SMA.

5.4.1 Pre-SMA gamma and modulation of context

We modulated the contextual complexity of stopping in two ways: firstly by changing the response required from a stop to a change (which includes stopping the primary task) and secondly by changing the stop/change instruction cue from a vertical bar to a directional arrow. Crucially, the complexity of the context effect is reversed for stopping versus changing: a vertical bar results in a more complex change, but a simpler stop. Therefore the interaction between response required and stop/change cue *isolates* the effect of conditional complexity whilst controlling for idiosyncratic confounds related to the stop/change cue and the type of response required, including possible increased conflict in the change task. Behavioural measures were in keeping with this because more contextually complex tasks had significantly longer reaction times (i.e. a significant response x signal interaction). This effect was true of reaction times even after taking into account, post stop/change-signal effects on reaction time, suggesting that the effect of complexity is a set effect that applies to all trial types. Complexity also interacted with the inhibition process in a non-specific way –

as shown by modulation of the inhibition function slope – without the altering the mean marker of stopping efficiency – the SSRT.

The neural correlate of contextual complexity was identified as an early and persistent gamma response found in the pre-SMA. This feature is particularly interesting as gamma responses generally represent local cortical processing (e.g. (Swettenham et al., 2009)) rather than network processing, and early gamma activity in the pre-SMA has been seen in a conditional variant of the stop-signal task in a single subject with subdural electrodes over the medial frontal wall (Swann et al., 2012). However, previous studies have conflicted as to whether neuronal firing in the pre-SMA differentiates successful and unsuccessful stop/change trials early enough to be potentially causal (Isoda and Hikosaka, 2007; Scangos and Stuphorn, 2010). Our findings are separate from this debate: we found contextual modulation of pre-SMA activity to be both early and a set effect. Therefore, pre-SMA gamma activity increases with increasing contextual complexity on *all* trials prior to the presentation of the first go signal and does not differentiate later success or failure at stopping. Finally, recent fMRI studies have suggested that medial frontal activity is most parsimoniously related to 'time on task' rather than experimental manipulations of conflict or error-rate ((Grinband et al., 2011) but see also (Yeung et al., 2011)). By using a convolution framework, we were able to estimate the effects of contextual complexity on pre-SMA activity *after* removing the effects of 'time on task' and corresponding reaction time drift – therefore our results are unlikely to be confounded by simple differences in reaction times.

5.4.2 Global theta/alpha responses in a spatially diffuse 'stopping network'

Across all stop-signal trial variants, the most consistent response to the stop/change signal was a brief theta/alpha induced response which peaked around the same time as the SSRT. This response was relatively widespread - found in the pre-SMA, left and right IFG and SMA (but was not significant in the primary motor cortex itself). It is unlikely that the spatially diffuse nature of this response is due to methodological confounds such as volume conduction or correlated lead fields, because the maximal mean squared correlation coefficient of the beamformer filters between sources was minimal. We therefore believe that the stop/change signal causes parallel activation of multiple hubs of a stopping network, and that different cortical regions within this network may have different functions. Although similar medial frontal theta has been shown to be a marker of cognitive interference (Nigbur et al., 2011) and to predict error-monitoring (Cavanagh et al., 2009), in our experiment, the theta response was unaffected by the presence of an error (stop-fail or change-fail trial)

irrespective of the stop/change stimulus cue. This is in keeping with our behavioural data which showed no changes in the SSRT with our experimental modulations. So how can a ubiquitous theta/alpha response be causal to stopping? Unlike fMRI studies where the haemodynamic responses are delayed, we have been able to look at this issue by relating behavioural data directly to the induced electromagnetic responses seen. We suggest that *all* attended stop/change cues elicit a theta/alpha response – and that stop/change failures are trials where the primary task terminates earlier than average. In keeping with this, the median stop/change-fail reaction time is around the time that the theta/alpha response is starting, the median go only reaction time is just before the theta/alpha peaks, and successful change reaction times occur well after the peak theta response. Explaining successful and unsuccessful stopping behaviour in terms of a *temporal* relationship to the induced response negates the requirement to find changes in response *amplitude* causal to stopping. This is in keeping with fMRI studies which have consistently found a global network activation in response to a stop-signal, but have found it difficult to find amplitude differences between successful and unsuccessful trials (Aron and Poldrack, 2006; Aron et al., 2007a).

5.4.3 Right IFG theta/alpha corresponds to stopping efficiency

Different spatial or spectral elements of such a global network may operate different functions required for stopping an ongoing process. To isolate the region most closely related to executing the stop itself, we looked for the region which was most sensitive to stopping efficiency. At each cortical region, we modelled variation in the slope of the induced theta/alpha response as a function of the average time available to stop/change. We hypothesised that, in subjects and conditions where a longer than average time was available for stopping/changing, the cortical theta alpha response would be less efficient (less steep). This relationship was only significant in the right IFG, suggesting that this part of the cortical stopping network is most closely related to the actual stopping process. This is consistent with human lesion (Aron et al., 2003) and fMRI data (Aron and Poldrack, 2006) which have correlated right IFG damage and blood oxygenation with another measure of stopping efficiency - SSRT. Our results have also highlighted that right, as opposed to left, IFG activity is most closely related to stopping. It remains unclear why, but this asymmetry exists regardless of the hand being used to stop (Konishi et al., 1999), and whether a hand movement or verbal response is being stopped (Xue et al., 2008), supporting the idea the right IFG operates a fundamental operation in stopping.

5.4.4 Beta changes selective to stopping only

We found a novel behavioural dissociation between the reaction time changes following stopping and changing – greater increases in primary task reaction time occurred after stop-failures (rather than successes) and change-successes (rather than failures). Primary task reaction time during the stop-signal task has been reported to be lengthened after successfully inhibited trials (Emeric et al., 2007), after failed inhibited trials (Schachar et al., 2004) and after both (Rieger and Gauggel, 1999; Bissett and Logan, 2011), suggesting that undefined variations in the task or subject group may lead to different behaviours. However the brain signals underlying these responses are not clear. We found significantly increased post-stop/change signal beta activity differentiated between successful and unsuccessful trials in the pre-SMA, and left and right IFG, but *after* the median go only reaction time. This response was significantly stronger for post-stop signal responses and almost absent in the change condition. This has two implications. Firstly, the relative absence of beta changes in successfully changed trials, suggest that it is not a *necessary* cortical response for stopping. Secondly, beta activity may play a specific role when the subject requires only a stop, and not a further response. So what role does cortical beta activity play in stopping? Stop-failures were associated with reduced beta and lengthened subsequent reaction times, suggesting that a drop in beta activity may be an error-monitoring signal or a signal to update the motor plan. If an error signal, there would be no change in beta after a successful stop - this is not the case, and therefore we favour the idea that after a successful stop, the current motor set is reinforced with a corresponding increase in beta. This is in keeping with the idea that increased beta activity maintains the current motor set (Engel and Fries, 2010; Jenkinson and Brown, 2011) after a correct response whilst reduced beta favours motor-reprogramming after a failed stop response. However, we did not find similar cortical responses to explain the behaviour in the change paradigm, suggesting that post-change responses may be modulated by a different mechanism (e.g. locked to the motor response rather than the change-signal).

5.5 Conclusion

In this study we modulated the conditional complexity of stopping using 4 variants of the stop-signal task. We found that the left and right IFG and pre-SMA were all sensitive to the presence of a stop-signal, and that a theta/alpha synchronisation in these areas was early enough to be temporally causal to stopping. Of these areas, the right IFG was most closely associated with stopping efficiency. Gamma activity in the pre-SMA was sensitive to modulations in contextual complexity, suggestive of local cortical processing. We additionally

found post-stop signal cortical responses that may explain primary task reaction time changes in the stop-signal task.

6. Dynamic cortico-basal ganglia connectivity during response inhibition in PD

6.1 Introduction

In chapters 3 and 4, we designed and tested an experimental model that allowed direct measurement of cortico-basal ganglia interactions in humans with PD. This approach relies on simultaneous MEG and depth electrode recordings and is able to segregate cortico-basal ganglia activity based on its spatial and spectral properties. But how does the activity of these *resting* networks relate to *dynamic* cognitive function and dysfunction in Parkinsonian patients? In chapter 5 we piloted novel experimental and analytical methods to examine *dynamic* network activity albeit restricted to cortical networks in healthy controls. In doing so, we disambiguated the specialised function of two key cortical areas involved in the act of stopping. Directly following on from this work, we now apply the same analysis procedures to understanding the cortico- basal ganglia dynamics associated with stopping in PD.

Converging evidence suggests that cortico-basal ganglia interactions play a key role in response inhibition (Aron and Poldrack, 2006; Aron et al., 2007a). PD offers a human model where the effects of a dopaminergic lesion on these cortico-basal ganglia interactions can be studied. Behavioural data in PD subjects suggest that stopping efficiency, as indexed by the SSRT during a stop-signal paradigm, is worsened (i.e. SSRT is lengthened) compared to controls, and that this does not improve after administration of levodopa (Gauggel et al., 2004; Obeso et al., 2011b). However, the classical stop-signal task and standard assessment of the SSRT may not be optimal in peri-operative PD subjects. This is because PD patients, due to unclear reasons, miss more trials and/or guess on more trials than control groups. This is especially important in the stop-signal task, where lapses in concentration where the subject does not make a response, would be categorised as successfully inhibited trials unless due care is taken with the analysis. Additionally, assumptions of SSRT stationarity may not hold in PD patients, or may be affected by the administration of dopaminergic medication (Mirabella et al., 2011).

Neural connections thought to be of particular importance during stopping include those between the pre-SMA and the STN and those between the right-IFG and STN (Aron and Poldrack, 2006; Aron et al., 2007a) and are postulated to be monosynaptic – the so called hyperdirect pathway (Nambu et al., 2002). Although dynamic connectivity *between* these regions has not been convincingly characterised, studies have demonstrated individual roles for the cortical structures (see chapter 5) and also for the STN during response inhibition

(Kuhn et al., 2004; Ray et al., 2011). An increase in beta frequency activity in the STN has been reported after a successful stop-signal (Ray et al., 2011) and also after a successful no-go response (Kuhn et al., 2004), although the classical event-related averaging analysis techniques from both studies make it unclear whether this increase is due to response inhibition, or reaction time confounds inherent in the study.

In this chapter, we address the limitations of previous studies by optimising three features. Firstly, we use an adapted version of the stop-signal paradigm - the change-of-plan paradigm (Logan and Burkell, 1986; Husain et al., 2003). This paradigm has the same visual cues as the stop-signal paradigm, but instead of inhibiting a button press in response to the stop-signal, the subject is required to additionally press the opposite button. This ensures that trials where there is a lapse in concentration can be excluded because they have no output. We combine this with previously demonstrated methodology to account for non-stationarity in SSRT measurement and to ensure that the task is performed correctly (see chapter 5). Secondly, we simultaneously record whole-head MEG data and STN LFP data during the performance of the paradigm. This allows us to, not only look at the activity of individual regions, but also to characterise the connectivity between them at a high temporal resolution. Finally, we use a novel method of analysing continuous electromagnetic data within a General Linear Model (GLM) framework, which allows us to disambiguate induced responses to closely overlapping events (also see chapter 5).

However, as we shall see, combing the electrophysiological, behavioural and statistical analysis techniques from previous chapters is difficult in this cohort and still needs future validation. Therefore, rather than providing a definitive account of biological findings, this chapter seeks to present a ‘proof-of-principle’ careful provisional analysis of the data highlighting its current limitations and suggesting some potential solutions.

6.2 Methods

6.2.1 Participants and surgery

We studied a total of 16 subjects (10 in London, 6 in Oxford) who had undergone bilateral STN DBS electrode implantation prior to DBS therapy for PD. All subjects were diagnosed with PD according the Queen Square Brain bank criteria (Gibb and Lees, 1988). Clinical details of the subjects are summarised in **Table 7** (also see section 6.2.2 for further details on UPDRS score calculation). The indications, operative procedure, targeting and beneficial clinical effects of STN stimulation have been described previously [see chapters 1.2.8, 2.1.2

and (Foltynie et al., 2010)]. However, the imaging modality used during the targeting procedure varied across sites as follows. In London preoperative stereotactic imaging was performed with stereotactic proton density weighted MRI, whilst stereotactic CT fused with T2 weighted MRI was used in Oxford. To confirm correct placement, electrodes were visualised on immediate post-operative imaging with the surgical frame *in situ* (proton density weighted MRI in London and CT (1mm slice thickness) fused with pre-operative T2 weighted MRI in Oxford). Although electrodes were considered to lie within or abutting STN, we cannot assume that all contacts on each electrode shared this localisation; indeed, this would seem highly unlikely given the size and orientation of the nucleus in relation to electrode trajectory. Given this, and to avoid any selection bias, we entered data from all three bipolar electrode pairs into our statistical analyses (except where explicitly mentioned), and considered these to lie in the STN region.

Case	Age (years)/ sex	Disease duration (years)	Predominant symptoms (in addition to bradykinesia)	UPDRS OFF/ON medication	Pre-operative medication (total daily dose)
LN01	53/F	12	Tremor, freezing, foot dystonias, restless legs.	19/14	Stalevo 750mg Amantadine 200mg Pramipexole 3.375mg Rescue apomorphine
LN02	60/F	32	Tremor, dyskinesias, leg dystonias.	34/14	Rasagiline 1mg Stalevo 300mg Co-careldopa 562.5mg Co-careldopa CR 200mg
LN03	53/M	17	Motor fluctuations, dyskinesias, freezing.	29/21	Co-careldopa 1350mg Trihexyphenidyl 6mg Pramipexole 375micrograms Rasagiline 1mg
OX01	54/M	6	Tremor, dyskinesias, freezing	28/28	Co-careldopa 1325mg Pramipexole 1.5mg Pramipexole XL 2.25mg
OX02	63/F	11	Tremor, freezing, dyskinesias.	57/40	Co-careldopa 1000mg Co-beneldopa 125mg Ropinirole XL 20mg Entacapone 1200mg
LN05	55/M	11	Tremor, dopamine dysregulation	*/40 (31/8)	Selegiline 10mg Tolcapone 300mg

			syndrome, motor fluctuations, depression, freezing, falls.		Co-careldopa 1125mg Co-careldopa CR 600mg
OX04	64/F	15	Dyskinesias, dystonia, freezing	25/16	Apomorphine 6mg Co-beneldopa 750mg Amantadine 200mg Rotigotine16mg Selegiline (as *Zelapar*) 1.25mg
OX06	53/M	13	Tremor, freezing, dyskinesia.	37/30	Co-careldopa 800mg Amantadine 200mg
LN06	57/F	3	Depression, falls, dyskinesia, tremor.	60/* (41/26)	Co-careldopa 187.5mg Previously on apomorphine (discontinued prior to DBS procedure)
OX09	64/M	13	Tremor, dyskinesia.	26/* (33/6)	Rasagiline 1mg Ropinirole 16mg Pergolide 3mg Co-careldopa 500mg
LN07	47/M	10	Tremor, motor fluctuations.	52/28	Rasagiline 1mg, Pramipexole XL 3mg Co-beneldopa 700mg Co-beneldopa CR 100mg Entacapone 800mg
LN08	56/M	9	Dystonia, motor fluctuations, freezing, depression, urinary urgency.	29/* (41/20)	Ropinirole 24mg Trihexyphenidyl 12m, Co-beneldopa 62.5mg Co-careldopa 375mg Co-careldopa CR 200mg
LN09	59/M	17	Tremor, dopamine dysregulation syndrome, hallucinations, REM sleep disorder, dyskinesias.	56/19	Co-beneldopa 600mg Co-beneldopa CR 650mg Stalevo 525mg Trihexyphenidyl 2mg
LN11	59/M	14	Tremor, dyskinesias, freezing, eyelid apraxia.	34/* (29/6)	Co-careldopa 1125mg Entacapone 800mg Co-careldopa CR 100mg

					Ropinirole XL 16mg
OX13	64/M	16	Dyskinesias, motor fluctuations	34/26	Co-beneldopa 187.5mg Stalevo 400mg Amantadine 100mg
LN13	58/M	11	Dyskinesias, motor fluctuations	*/11 (22/7)	Stalevo 750 Cabergoline 8mg Amantadine 300mg

Table 7: Clinical details of the study participants. *All subjects have been anonymised using a study code. *UPDRS scores reported are at the time of recording. Because not all subjects completed both ON and OFF medication conditions, not all subjects have both ON and OFF UPDRS scores. In these cases a pre-operative OFF/ON UPDRS score is also provided in brackets – although the scores are not directly comparable (due to e.g. 'stun effect', see section 6.2.2). Stalevo is a proprietary combination of levodopa, carbidopa and entacapone for which the dose of levodopa is given. Pramipexole doses are given as a salt. REM = rapid eye movement.*

6.2.2 Experimental Paradigm

Experiments were performed between 2-6 days post-operatively. Subjects were asked to perform up to 8 blocks (about 4 minutes each) of the task, interleaved by rest periods. Recording sessions did not last more than one hour and were performed whilst the patient was seated inside the MEG scanner. Visual stimuli were back-projected onto a screen in front of the subjects and were controlled using Presentation software (Neurobiological Systems). During each trial, the subject was presented with a fixation cross (lasting 1.3 – 1.5s, the duration was drawn from a uniform distribution) which, after a 200ms pause with a blank screen, was followed by a green left- or right- pointing arrow (the primary task stimulus, or 'go signal'). The subject was asked to make a button-press with the thumb of the corresponding hand as quickly as possible. In a randomly selected 50% of trials, a further red arrow, pointing in the opposite direction to the first arrow, was presented at a variable latency (SOA) after the primary task stimulus. In response to this second signal, the subject was asked to change to pressing the opposite button. The SOA was varied trial-by-trial – increasing by 50ms after a successful change but decreasing by 50ms after a failure to change (Levitt, 1971). This tracking procedure aims to fix the probability of successfully changing at ~0.5 so that successful- and unsuccessful-change conditions were equally sampled. The SOA was randomly drawn from 2 independent staircases.

As part of the experimental protocol, each subject was asked to repeat the experimental paradigm twice – once after omitting all dopaminergic medication overnight (OFF medication condition) and once following administration of 200mg of levodopa (ON medication condition), the order counterbalanced across subjects. To assess the severity of motor impairment in this cohort, all patients were evaluated using part III of the Unified Parkinson's Disease Rating Scale (UPDRS) *during* each experimental condition (ON and OFF), i.e. at the time of the electrophysiological recordings. However, of the 16 subjects, only 9 completed both ON and OFF sessions. In addition 5 were recorded OFF medication only and 2 were recorded ON medication only. In these cases, we also retrospectively recorded a pre-operative UPDRS score performed up to 6 months prior to surgery. Although the patients underwent a similar procedure to record OFF and ON UPDRS scores, there is expected variance between pre-operative and post-operative UPDRS scores because of many factors including post-op fatigue, variation in medications and the 'stun effect' (see chapter 7 for further discussion). A neurologist was present in the magnetically shielded room during the experiment to monitor the patient's well-being.

6.2.3 Behavioural analysis

Behavioural analysis was similar to that performed in chapter 5. The aims of the behavioural analysis were threefold: to determine whether experimental modulations were evident in behaviour; to identify and exclude experimental runs where behaviour was anomalous; and to provide behavioural summary measures which could be used as predictor variables in the electrophysiological analysis. Stimuli and response timings were recorded and analysed offline using custom Matlab scripts (The Mathworks, Inc, Natick, MA), the Psignifit toolbox(Fründ, I, Haenel, NV, Wichmann, 2011) and IBM SPSS version 20.

Three key trial-types were considered: go only trials (where the change-signal is not presented), successful-change trials and unsuccessful-change trials. Other trials, such as non-change signal trials where the left button was pressed in response to the right arrow were considered unclassified errors and discarded.

We performed two analyses to check that subjects had engaged in the task appropriately. Firstly, we calculated the proportion of unsuccessful change trials (error fraction) per condition. Secondly, we modelled the inhibition function of each data run whilst trying to protect against non-stationarities in the data (e.g. reaction time drift) and behavioural confounds (guessing and lapses in concentration). The inhibition function models the proportion of correct responses, i.e. successful changes, as a function of the SOA, or the

SOA corrected for reaction time (primary task RT – SOA)(Logan and Cowan, 1984; Band et al., 2003). Subjects tended to *wait* for the change-signal, presumably to increase their success-rate. To adjust for the resulting non-stationarity in primary task reaction time we fitted cubic splines to the SOA and the go only reaction time data. This provides a *predicted* go reaction time for stop/change trials – an estimate of how the subject would have responded on stop/change trials if they had been go only trials, based on the reaction times of neighbouring trials (Nachev P, unpublished, http://ukpmc.ac.uk/theses/ETH/445162). On change trials we subtracted the SOA from the predicted go spline to estimate the *decision time* per trial - the post-stop/change signal latency required to make a correct or incorrect decision on that trial, correcting for reaction time drift in the data. The ratio of successful:total stop/change trials was calculated as a function of decision time in 100ms bins. We fitted a sigmoid inhibition function to this data using a Bayesian MCMC procedure, which is superior to other methods such as bootstrapping (Kuss et al., 2005; Fründ, I, Haenel, NV, Wichmann, 2011). The function was defined by four parameters (with standard prior distributions): the upper limit of the function or 'lapse rate' (prior: gamma(2,400)), the 50% point of the function (prior: beta(1.5,10)), the 'slope' at 50% of the function (prior: beta(1.5,10)), and the lower limit or 'guess rate' (prior: gamma(2,400)). Calculating the Bayesian posterior for such a model is *analytically* intractable, but it can be approximated by the MCMC procedure, which generates many samples of the posterior according to a particular algorithm (Kuss et al., 2005). We generated 4000 samples, discarding the first 2000 samples, to estimate an approximation to the posterior of the inhibition function. In this scenario the decision time at the mid-point of the inhibition function is equivalent to the SSRT. We assessed the goodness-of-fit of the model by calculating the deviance, which is a generalisation of the sum-of-squares metric that applies to binomial data (Fründ, I, Haenel, NV, Wichmann, 2011). Trial numbers, behavioural summary measures and discarded data runs are shown in **Table 8**.

To look for behavioural evidence of experimental modulations, median reaction time was estimated per condition. We were able to fully remove the effects of reaction time drift when only analysing post change trials by calculating a corrected post-change signal reaction time (current trial go only reaction time - previous go only trial reaction time). To increase trial numbers, we included trials where a go only trial was preceded by several change trials, as long as the outcome for all stop/change trials was the same (similarly to Bissett and Logan (Bissett and Logan, 2011)). All behavioural measures including SSRT, slope, reaction time and adjusted reaction time data were subjected to mixed hierarchical general linear models with fixed-factors as previously described, and subject as a random factor.

6.2.4 Simultaneous STN-LFP and MEG recordings

MEG recordings were performed in London with the 275 channel CTF (VSM MedTech Ltd., Vancouver, Canada) or in Oxford with the 306 channel Neuromag (Elekta Neuromag Oy, Helsinki, Finland) systems. Simultaneous to the MEG recording, both right and left first dorsal interosseus (FDI) electromyographic (EMG) signals, and four intracranial LFP channels were recorded per electrode. All EMG recordings (across both sites), and LFP recordings from the first 4 London subjects were acquired using the integrated EEG systems. The London LFP acquisition system was then updated to a BrainAmp (Brain Products GmbH, Munich, Germany) monopolar recording system for the remainder of the subjects. All monopolar LFP and EMG recordings were referenced to the right mastoid. In Oxford, LFP signals in the STN were acquired in a bipolar configuration via a Digitimer D360 amplifier (Digitimer Ltd, Hertfordshire, UK), and high-pass filtered at 0.5 Hz. All data were sampled at 2400 Hz and stored to disk for subsequent off-line analysis. MEG, LFP and EMG data were hardware high-pass filtered at 0.03Hz (Oxford MEG and EMG) or 1Hz (London EMG and LFP; Oxford LFP only) and low-pass filtered at 600Hz (all signals). London LFP recordings were converted off-line to a bipolar montage between adjacent contacts (3 bipolar channels per side) to limit the effects of volume conduction from distant sources (Oxford LFP recordings were already recorded in this format).

6.2.5 Data pre-processing, artefact rejection, and head localisation

The data were analysed using SPM8 (http://www.fil.ion.ucl.ac.uk/spm/) and Fieldtrip (http://www.ru.nl/neuroimaging/fieldtrip/), (Litvak et al., 2011b; Oostenveld et al., 2011). The continuous recording was down-sampled to 300 Hz, high-pass filtered above 1 Hz and the line noise artefacts at 50 Hz and 100 Hz were removed using notch filters (5th order zero-phase Butterworth filters). Head position was recorded continuously within the MEG, and in London was recomputed to correspond to the mean of the trials used for the analysis. Similar head movement compensation could not be made for Oxford subjects as the proprietary software had difficulty extracting the head location signal in the presence of metallic artefact from DBS extension leads. We therefore used the starting head location in these cases. Unlike the CTF system, the Neuromag MEG system contains magnetometers (a type of sensor) which, due to their greater sensitivity to distant sources and environmental noise, are more contaminated by metal artefacts. We, therefore, only based our analysis on planar gradiometers similarly to Hirschmann et al. (2011) who also used the Neuromag system.

6.2.6 Beamformer source extraction

We extracted time-series data from cortical regions of interest using an LCMV beamformer (Van Veen et al., 1997). The MNI co-ordinates (x,y,z) of locations of interest were taken from the literature and included the pre-SMA (2,30,48 taken from (Nachev et al., 2007)), the right and left IFG (±42,26,14 from (Aron et al., 2007a)), the SMA (-2,-10,59 adapted from (Mayka et al., 2006)) and both the primary motor cortices (±37,-25,62 adapted (Mayka et al., 2006)). Locations obtained from Mayka et al. were converted from Talaraich to MNI space using a transform devised by Mathew Brett (http://imaging.mrc-bu.cam.ac.uk/imaging/MniTalairach). The beamforming method involves linearly projecting the MEG sensor data using a spatial filter computed from the lead field of the source of interest and the data covariance (Van Veen et al., 1997). The spatial filter is designed to extract activity from the region of interest, whilst suppressing activity from other sources. Lead fields were computed using a single-shell head model (Nolte et al., 2004) based on an inner skull mesh derived by inverse-normalizing a canonical mesh to the subject's individual pre-operative MRI image (Mattout et al., 2007). Co-registration between the MRI and MEG coordinate systems used 3 fiducial points: nasion, left and right pre-auricular; see (Litvak *et al.*, 2010) for further details. Data covariance matrices were computed using all the data from a recording block, for each block separately. We specified 0.01% regularization and defined the orientation of each source to be in a fixed direction. Medial frontal sources (the SMA and pre-SMA) were oriented horizontally, whilst all other more lateral cortical sources (primary motor cortex and IFG) were oriented vertically. To determine whether data from these sources were adequately separated we correlated the beamformer filters (weights applied to the sensor data) of each source with all other sources per data run. These correlation coefficients (equivalent to Pearson's r^2) values were then averaged across conditions and subjects.

Time-series data from the LCMV extracted cortical sources and each bipolar STN-LFP channel were then standardised by subtracting the mean and dividing by the standard deviation. To make standardization robust to possible artefacts, medians of the raw and squared signals were computed for non-overlapping 10 s segments and averaged yielding first and second moment estimates.

6.2.7 Time-frequency analysis and epoching

A time-frequency representation of the data was generated using multitaper spectral analysis (Thomson, 1982), in time windows of 0.4s shifted in steps of 0.05s over a frequency range of 2.5 to 90 Hz in steps of 2.5 Hz. The frequency resolution was set to the inverse of the time window (2.5 Hz) for up to 25 Hz, then 0.1 times the frequency for 25 to 50 Hz and

then to a constant 5 Hz. The resultant continuous power data were transformed with the square root transform to obtain RMS amplitude which better conforms to the linearity assumption of the convolution method (Litvak et al., 2012b). RMS amplitude data were then analysed using both standard epoching techniques and the novel convolution technique. The aim of the epoching analysis was to ensure that individual data in our cohort (contaminated by the presence of ferromagnetic wires) looked comparable to previously published data at the individual level, and that there were no gross differences between electromagnetic activity recorded by both CTF and Elekta systems. The aim of the convolution analysis was to provide a basis on which meaningful group level statistical tests could be performed.

For the epoching analysis, RMS amplitude data were epoched into 5s trials centred around all go signals and all button presses. The resulting time–frequency images were then averaged using robust averaging (Holland and Welsch, 1977; Wager et al., 2005; Litvak et al., 2012a) , and percentage change time–frequency responses were obtained relative to the baseline (1.8 to 1 s) before the trigger. Robust averaging is a special case of the robust general linear model (Holland and Welsch, 1977; Wager et al., 2005; Litvak et al., 2012a) . In this framework, outliers are down-weighted when computing the average, making it possible to suppress artefacts restricted to narrow time and frequency ranges without rejecting whole trials.

Cortico-subthalamic coherence was also computed over a 5 second epoch using a robust averaging technique as follows. The complex cross-spectral density (CSD) between the two sources of interest (e.g. the motor cortex and the STN) was calculated for each trial. The complex CSDs were then weighted according to the absolute value of CSDs, before being averaged to obtain coherence. Percentage changes in cross-spectral responses were computed as above (Oswal et al., 2012).

6.2.8 The convolution model for magnetoencephalographic data

In the convolution framework, RMS amplitude data were analysed hierarchically: summary measures of induced responses were obtained with a first-level convolution model, then transformed into time-frequency images and finally subjected to a standard general linear model at the second level. To characterise and disambiguate induced responses to the events of interest, regressors were generated for each event-type, and assembled as predictors of continuous frequency-specific amplitude in a general linear model (GLM). Each event was modelled as a delta function (an impulse) and then convolved with a set of Fourier

basis functions spanning -0.5 to +1.5s relative to each event (the peri-stimulus time-window). GLM coefficients were estimated using ordinary least squares treating the different frequencies separately in mass-univariate fashion. The induced response for a particular event-type was reconstructed by multiplying the basis functions with a matrix of parameter estimates corresponding to the event-type in question (Litvak et al., 2012b). In the simplest case, with non-overlapping events, this would be equivalent to averaging time-frequency images centred on an event of interest. However, because our data contains multiple temporally overlapping responses, the convolution model was superior to event-locked routine averaging. Because, multiple predictors (different events) are included *in the same* GLM, the induced responses to different event-types can be disambiguated from each other, if they do not always occur together. Individual regressors were specified for the fixation cross, the primary task stimulus, the button press responses (separately for left and right responses) and the change signal (separately for successful and failed change conditions). Previous studies have suggest that the medial frontal cortex is sensitive to reaction time changes (Grinband et al., 2011; Yeung et al., 2011), therefore we sought to include this confound in our model by using the predicted go spline as a parametric modulator of the go signal induced response. *After* modelling the mean go event, and variation due to go-reaction time drift, we then estimated induced responses separately for all combinations of the current trial (left or right cue) and previous trial-type (go only trial, successful-change trial, failed-change trial). The resulting induced responses are independent of reaction time drift. In addition, we modelled variation of the stationary measure of decision time (primary task go only reaction time – SOA spline) as a confounding parametric modulator of the change signal. The data and the design were filtered below 0.25 Hz.

After eliminating reaction-time confounds, we generated time-frequency images for each event-type and entered these into within-subject ANOVAs for each cortical source. We studied responses to two event-types statistically: the change signal - with success (successful or failed), and dopamine (OFF or ON) as factors, and the go signal – with the current trial (left or right cue) and dopamine (OFF or ON) as factors. Two tailed t-tests were performed for each main effect and interaction and were thresholded at p=0.05 FWE (peak-level), taking error non-sphericity into account using standard procedures (Litvak et al., 2011b). Currently, coherence cannot be analysed using the convolution model because it is computed across trials.

6.3 Results

6.3.1 Subject behavioural data

It was apparent that, as predicted, not all subjects optimally engaged in the task. Therefore we excluded sessions in which the subject's behaviour did not conform to the assumptions of the task. Sessions were discarded if the error fraction (the number of failed change trials divided by the number of successful change trials) was less than 0.1 of if the deviance of the inhibition function was greater than 13. Using these arbitrary criteria, seven sessions were discarded, leaving a total of 43 sessions (subjects x dopamine x side; see **Table 8** and **Figure 42**).

		Number of Trials		Change Fraction		Error Fraction		Go RT		Fail RT		Succ RT		Fail SOA		Succ SOA	
Subject	**Dopamine**	**L**	**R**	**L**	**R**	**L**	**R**	**L**	**R**	**L**	**R**	**L**	**R**	**L**	**R**	**L**	**R**
'LN01'	1	133	135	0.47	0.39	0.27	0.38	0.742	0.672	0.687	0.802	0.947	0.997	0.353	0.348	0.273	0.300
	2	111	118	0.46	0.46	0.25	0.56	0.550	0.518	0.527	0.480	0.868	0.925	0.250	0.225	0.200	0.150
'LN02'	1	96	98	0.47	0.53	0.07	0.27	1.040	1.112	0.813	0.995	1.615	1.487	0.747	0.800	0.723	0.650
	2	101	110	0.49	0.53	0.14	0.31	0.755	0.740	0.817	0.538	1.225	1.128	0.500	0.398	0.398	0.398
'LN03'	1	51	61	0.61	0.46	0.32	0.50	0.662	0.430	0.397	0.462	0.437	0.437	0.200	0.275	0.100	0.125
	2	78	76	0.59	0.62	0.39	0.36	0.785	0.713	0.767	0.537	0.907	0.743	0.300	0.300	0.200	0.150
'OX01'	1	142	137	0.50	0.49	0.30	0.33	0.861	0.875	0.779	0.744	1.207	1.197	0.550	0.600	0.499	0.449
	2	143	145	0.52	0.50	0.38	0.26	0.836	0.822	0.762	0.734	1.049	1.033	0.599	0.551	0.476	0.500
'OX02'	1	39	45	0.51	0.47	0.15	0.52	0.775	0.740	0.694	0.992	1.138	1.000	0.350	0.249	0.200	0.152
'OX04'	1	141	138	0.48	0.49	0.19	0.21	0.962	1.027	0.887	0.966	1.090	1.110	0.750	0.750	0.550	0.550

	2	49	55	0.49	0.47	0.25	0.23	1.007	0.892	0.767	0.824	0.977	1.024	0.675	0.650	0.550	0.575
'LN05'	2	64	60	0.45	0.45	0.10	0.07	1.018	1.023	1.343	1.010	1.029	0.977	0.948	0.701	0.725	0.599
'OX06'	1	133	141	0.53	0.50	0.30	0.31	0.705	0.725	0.601	0.611	0.835	0.749	0.450	0.400	0.350	0.300
	2	122	135	0.53	0.54	0.31	0.36	0.770	0.706	0.664	0.616	0.845	0.839	0.425	0.449	0.350	0.400
'LN06'	1	66	56	0.52	0.50	0.26	0.36	0.699	0.508	0.561	0.517	1.129	1.240	0.300	0.349	0.300	0.326
'OX09'	1	118	131	0.47	0.50	0.21	0.42	0.608	0.614	0.546	0.508	0.730	0.706	0.350	0.350	0.251	0.224
'LN07'	1	102	105	0.57	0.54	0.28	0.30	0.773	0.726	0.771	0.682	0.873	0.882	0.600	0.499	0.449	0.499
	2	108	100	0.56	0.47	0.23	0.32	0.672	0.678	0.633	0.562	0.813	0.882	0.474	0.450	0.399	0.376
'LN08'	1	115	128	0.57	0.48	0.28	0.49	0.626	0.525	0.611	0.550	0.791	0.930	0.275	0.251	0.199	0.151
'LN09'	1	111	123	0.55	0.50	0.10	0.15	1.563	1.546	1.410	1.411	1.469	1.562	0.974	0.951	0.701	0.700
	2	119	132	0.56	0.49	0.13	0.09	1.343	1.215	0.996	1.296	1.396	1.491	0.849	0.974	0.700	0.699
'LN11'	1	69	65	0.57	0.49	0.36	0.50	0.520	0.473	0.463	0.483	0.698	0.715	0.275	0.299	0.249	0.200
'OX13'	1	141	145	0.49	0.48	0.09	0.19	1.164	1.086	0.909	0.974	1.445	1.296	0.850	0.899	0.798	0.600
	2	71	67	0.54	0.55	0.32	0.49	0.777	0.726	0.757	0.703	0.980	1.084	0.450	0.451	0.400	0.400

'LN13'	2	150	144	0.48	0.48	0.32	0.58	0.541	0.485	0.481	0.493	0.768	0.818	0.249	0.252	0.151	0.200
MEAN		**103**	**106**	**0.52**	**0.50**	**0.24**	**0.34**	**0.830**	**0.783**	**0.746**	**0.740**	**1.010**	**1.010**	**0.510**	**0.497**	**0.408**	**0.387**

Table 8: Descriptive statistics of change-of-plan task in patients. *Each row represents data from one subject (coded with an anonymous study code e.g. LN01) whilst on (dopamine=2) or off (dopamine=1) dopaminergic medication. Note that not all subjects were recorded in both conditions. Data is separated into left (L) and right (R) sides for each value. As well as the total number of trials used, the change fraction (the number of change trials divided by the total number of trials) and the error fraction (the number of error change trials divided by the total number of change trials) is shown. Median reaction times for the go trials (Go RT), failed change trials (Fail RT) and successfully changed trials (Succ RT) are presented with their corresponding median stimulus onset asynchrony values (SOAs). All values are in seconds. Conditions with an arbitrary error fraction of less than 0.1 are highlighted in red and were excluded from further analysis. Mean group values (excluding all excluded runs) are presented on the bottom row.*

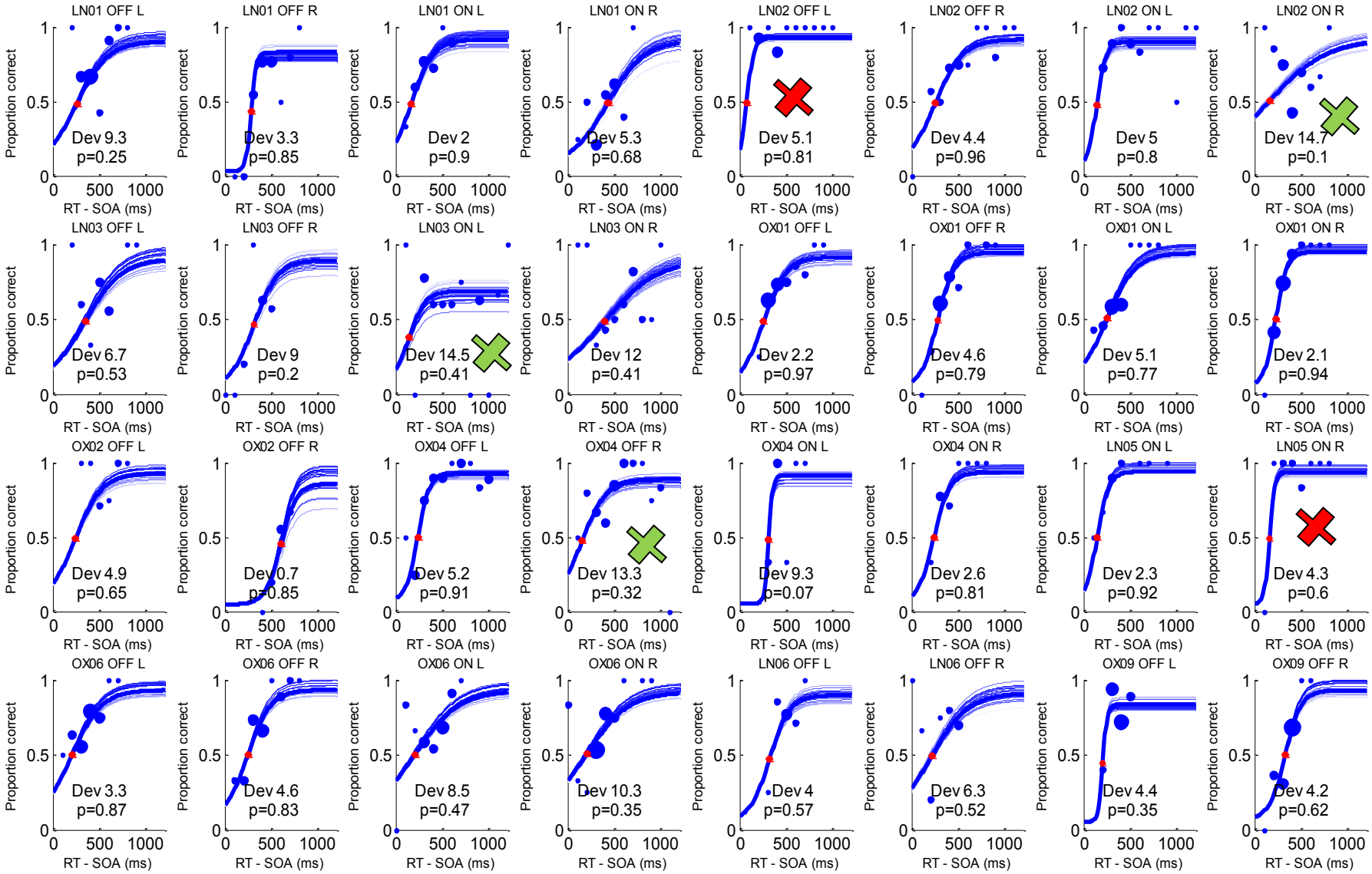
LN01 OFF L
Dev 9.3
p=0.25
LN01 OFF R
Dev 3.3
p=0.85
LN01 ON L
Dev 2
p=0.9
LN01 ON R
Dev 5.3
p=0.68
LN02 OFF L
Dev 5.1
p=0.81
LN02 OFF R
Dev 4.4
p=0.96
LN02 ON L
Dev 5
p=0.8
LN02 ON R
Dev 14.7
p=0.1
LN03 OFF L
Dev 6.7
p=0.53
LN03 OFF R
Dev 9
p=0.2
LN03 ON L
Dev 14.5
p=0.41
LN03 ON R
Dev 12
p=0.41
OX01 OFF L
Dev 2.2
p=0.97
OX01 OFF R
Dev 4.6
p=0.79
OX01 ON L
Dev 5.1
p=0.77
OX01 ON R
Dev 2.1
p=0.94
OX02 OFF L
Dev 4.9
p=0.65
OX02 OFF R
Dev 0.7
p=0.85
OX04 OFF L
Dev 5.2
p=0.91
OX04 OFF R
Dev 13.3
p=0.32
OX04 ON L
Dev 9.3
p=0.07
OX04 ON R
Dev 2.6
p=0.81
LN05 ON L
Dev 2.3
p=0.92
LN05 ON R
Dev 4.3
p=0.6
OX06 OFF L
Dev 3.3
p=0.87
OX06 OFF R
Dev 4.6
p=0.83
OX06 ON L
Dev 8.5
p=0.47
OX06 ON R
Dev 10.3
p=0.35
LN06 OFF L
Dev 4
p=0.57
LN06 OFF R
Dev 6.3
p=0.52
OX09 OFF L
Dev 4.4
p=0.35
OX09 OFF R
Dev 4.2
p=0.62
Proportion correct
RT - SOA (ms)
0
0.5
1
500
1000

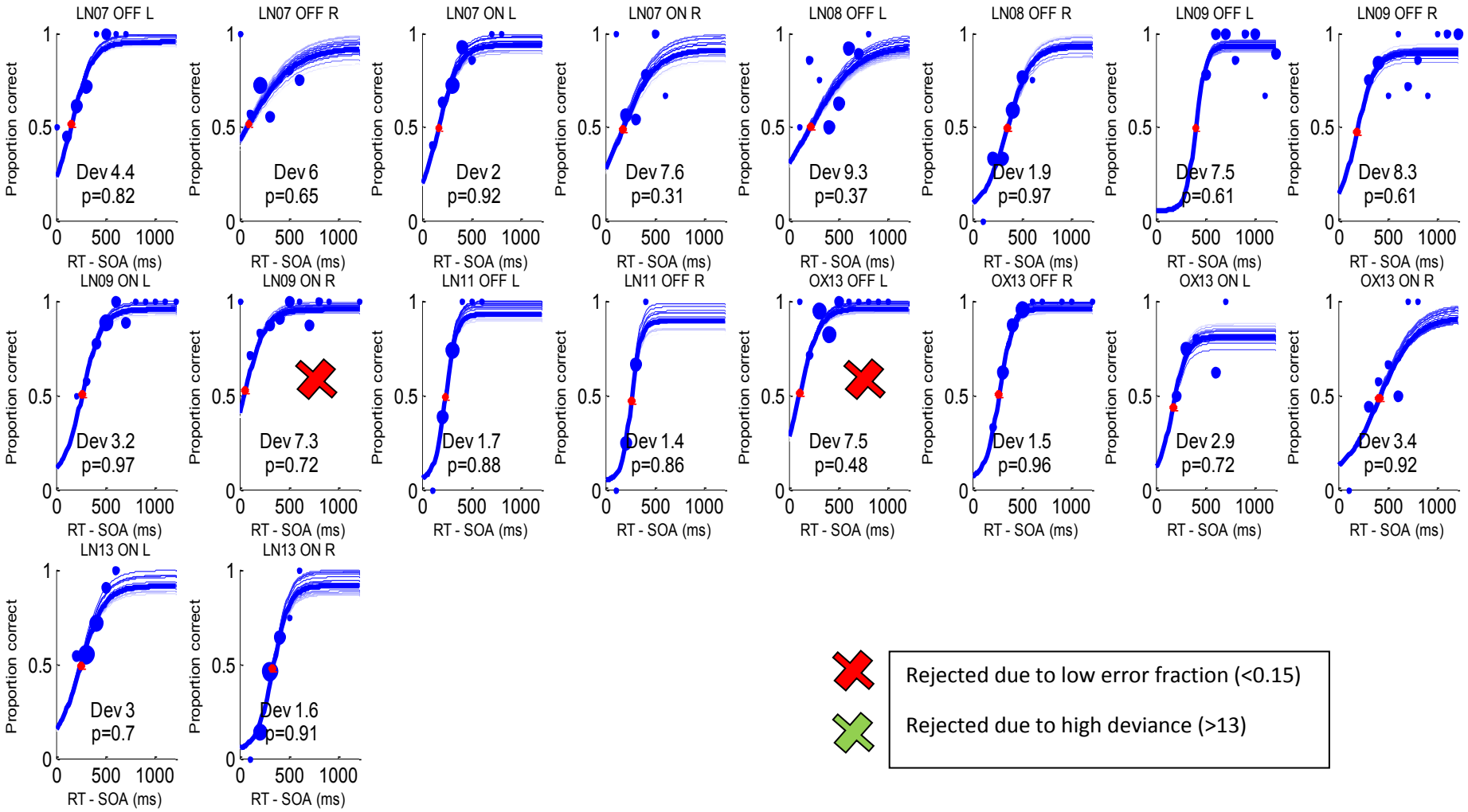

Figure 42: Inhibition functions for each subject and condition. *Each plot shows the proportion of correct changes as a function of the SOA, normalised by subtracting the predicted go reaction time. The trial data is binned in 100ms bins and plotted as blue circles – a larger circle*

corresponding to more trials. The Bayesian MCMC fit is plotted in darker blue, and 20 samples from the posterior are plotted in lighter blue in order to aid visualisation of the posterior distribution. The threshold (equivalent to the SSRT) is highlighted by a red circle. The deviance (Dev) of the data is also shown - data runs with deviance greater than 13 were excluded and are highlighted by a red cross. Data runs with an error fraction lower than 0.1 were also excluded and are highlighted by a green cross. A p value, reflecting the Bayesian probability of the fit being part of the initial data distribution is also presented, but this value was redundant in calculations and not used further.

6.3.2 Beamforming adequately separates cortical sources involved in the change process

Similarly to our healthy control data (chapter 5), source activity was extracted from six *a priori* cortical locations: the pre-SMA, the SMA, and the left and right primary motor cortex and inferior frontal gyri. Because of the increased artefact in the MEG data from these subjects – due to both increased head movement and the presence of ferromagnetic wires – the beamformer may potentially not be able to adequately separate the cortical sources of interest. To determine whether data from these sources were adequately separated we correlated the beamformer filters (weights applied to the sensor data) of each source with all other sources per data run. This was done separately for ON and OFF medication conditions (see **Figure 43** and **Figure 44**). These coefficients (Pearson's r^2) were then averaged across conditions and subjects. The maximal mean correlation was low at 0.15 (between left M1 and the pre-SMA) confirming that cortical sources were adequately separated (i.e. on average only 15% of the variance shared between these two sources can be attributed to non-physiological factors). To illustrate these correlations, we correlated the source filter at the locations of interest with the filter of every other voxel in the image and then averaged these images over runs and subjects. This image shows the spatial specificity of the beamformer in terms of the region of interest from which our source data come from (see **Figure 43** and **Figure 44**).

A OFF meds

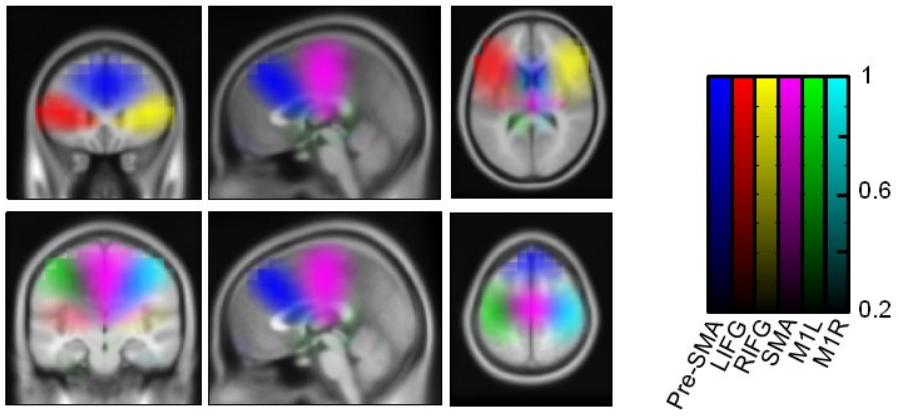

B

	M1L	M1R	SMA	pre-SMA	rIFG	lIFG
M1L	1.000	0.034	0.053	0.081	0.048	0.073
M1R		1.000	0.014	0.039	0.029	0.026
SMA			1.000	0.098	0.117	0.098
pre-SMA				1.000	0.026	0.031
rIFG					1.000	0.087
lIFG						1.000

Figure 43: Regions of interest in the OFF medication condition. A*: Beamformer filters for each location of interest were correlated with filters for the rest of the brain. These correlation images were averaged across subjects and then thresholded at r^2=0.2. Each resulting image represents a maximal region of interest. Locations are the left (red) and right (yellow) inferior frontal gyrus, the pre-SMA (blue), the SMA (purple), and the left (green) and right (cyan) primary motor cortices. The colour scale represents r^2.* ***B:*** *Individual correlations of filters between point source locations are presented. Values represent r^2. Locations are left (M1l) and right (M1r) primary motor cortex, SMA, pre-SMA, right (rIFG) and left (lIFG) inferior frontal gyri.*

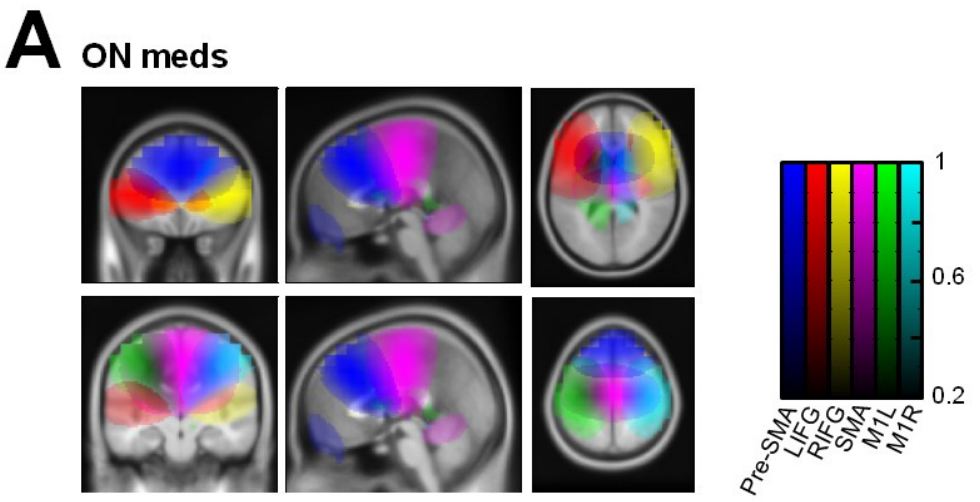

B

	M1L	M1R	SMA	pre-SMA	rIFG	lIFG
M1L	1.000	0.051	0.082	0.151	0.041	0.047
M1R		1.000	0.024	0.066	0.027	0.020
SMA			1.000	0.085	0.091	0.073
pre-SMA				1.000	0.051	0.038
rIFG					1.000	0.113
lIFG						1.000

Figure 44: Regions of interest in the ON medication condition. *The figure details are identical to* ***Figure 43****.*

6.3.3 Epoched data shows that event-related oscillatory responses can be visualised individually in the majority of subjects

Prior to performing group analysis, we examined single subject data to ensure that reasonable and comparable event-related signals could be extracted from the MEG and LFP data, in spite of prominent artefact and the use of varied recording systems. In this section we use classically analysed robustly averaged data of left M1 (**Figure 45** and **Figure 46**) and left STN (**Figure 47** and **Figure 48**) activity during the presentation of a right go signal and right button press. We found that there was a consistent beta RMS amplitude decrease and subsequent rebound that occurred after the go signal and during the button press in both M1 and the STN. During the button press further gamma activity was demonstrated most clearly in the STN but also in primary motor cortex. There were no significant differences in the pattern of activity between subjects recorded in Oxford and London. Therefore the data we have collected is reassuring in that classical averaging of the raw signal reveals event-related modulations that can be visualised at the individual subject level

in different frequency bands. However the same analysis highlights the problem if we were to use this as a basis for group analysis. Namely that it remains ambiguous whether the beta depression, for example, is locked to the go signal or to the button press. As previously shown (see chapter 5), if individual event-related responses cannot be disambiguated, then it is difficult to make a meaningful inference from the data. Therefore further analysis of the amplitude is performed using the continuous GLM (see section 6.3.4).

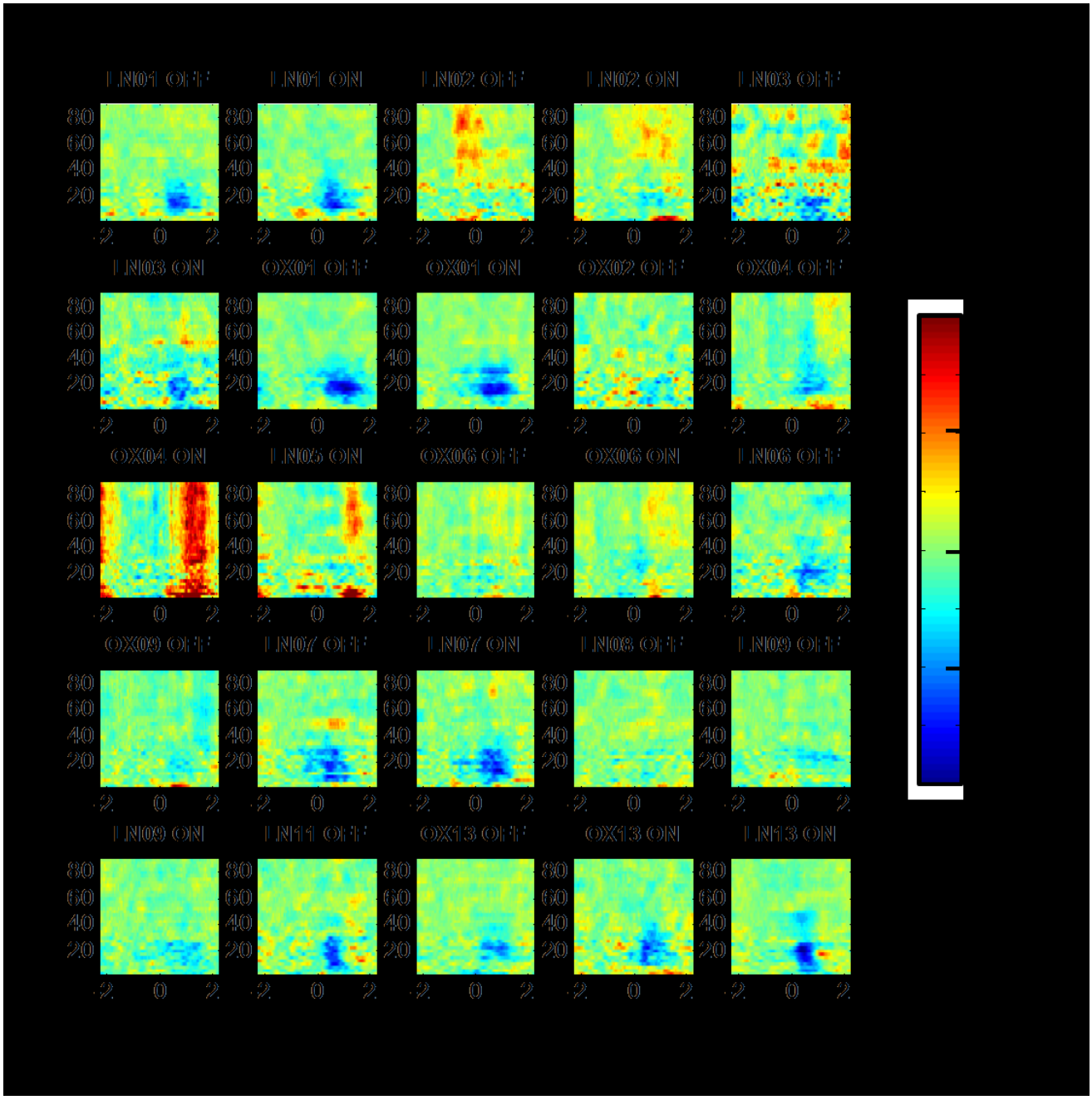

Figure 45: Individual time-frequency images of left M1 activity during a right go signal. *Each subimage displays frequency (y axis, Hz) against peri-stimulus time (x axis, s). The go signal is presented at t=0. Neural activity is presented as a percentage change in RMS*

amplitude relative to the baseline (-1.8s to 1s). The title of each image identifies the subject (e.g. LN07) and the medication condition. These images demonstrate a clear decrease in beta activity in the motor cortex after presentation of a go signal. There is no clear difference in pattern between subjects recorded in Oxford ('OX') and London ('LN'). Subject OX04 may have spike artefact during the button press – seen as a broad band increase in amplitude around the time of the button press.

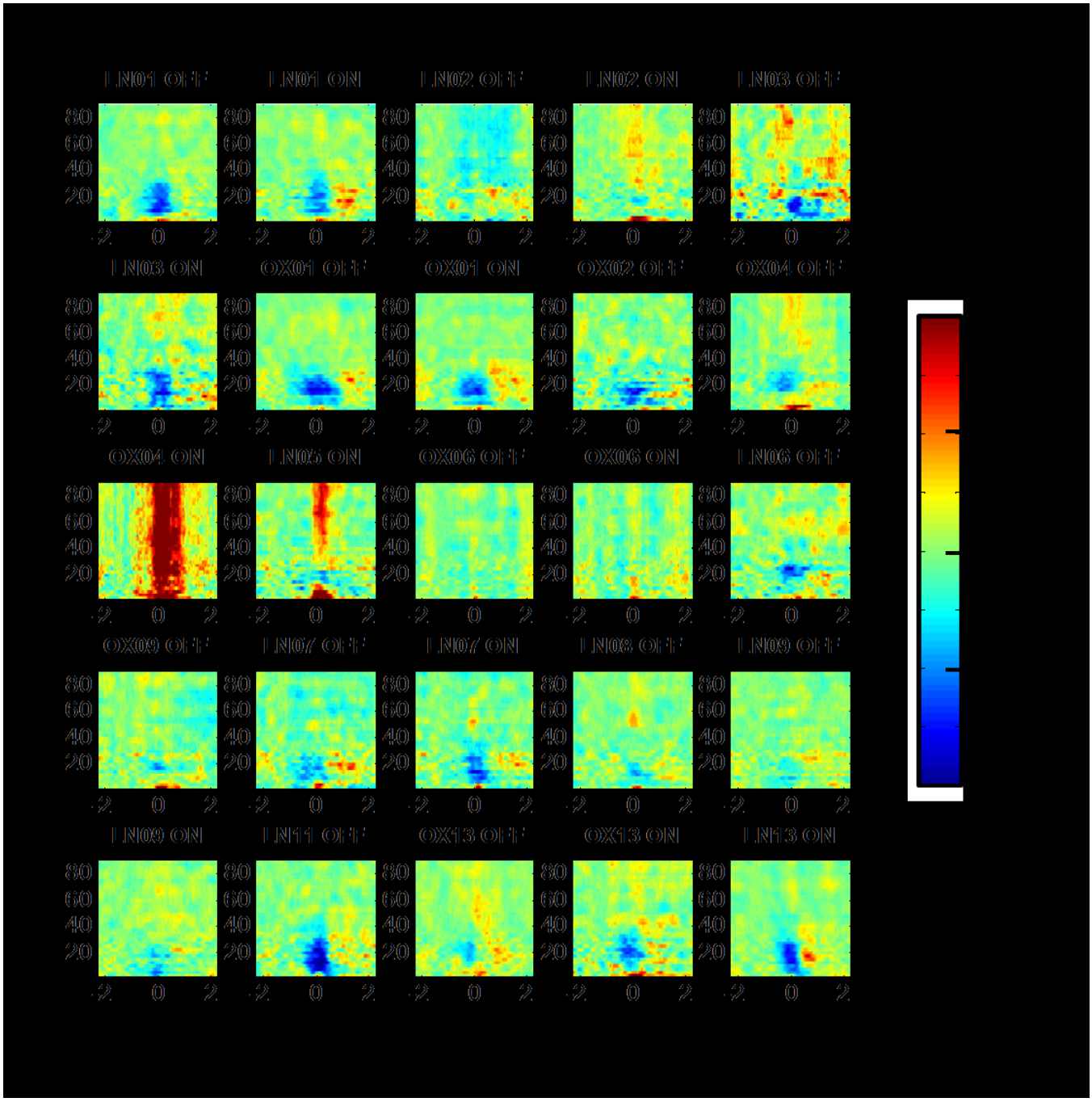

Figure 46: Individual time-frequency images of left M1 activity during a right button press. *Each subimage displays frequency (y axis, Hz) against peri-stimulus time (x axis, s).*

The button press is at t=0. Neural activity is presented as a percentage change in RMS amplitude relative to the baseline (-1.8s to 1s). The title of each image identifies the subject (e.g. LN07) and the medication condition. These images demonstrate a clear decrease in beta activity in the motor cortex during the button press, immediately followed by a beta increase. There is no clear difference in pattern between subjects recorded in Oxford ('OX') and London ('LN'). Subject OX04 may have spike artefact during the button press – seen as a broad band increase in amplitude triggered to the button press.

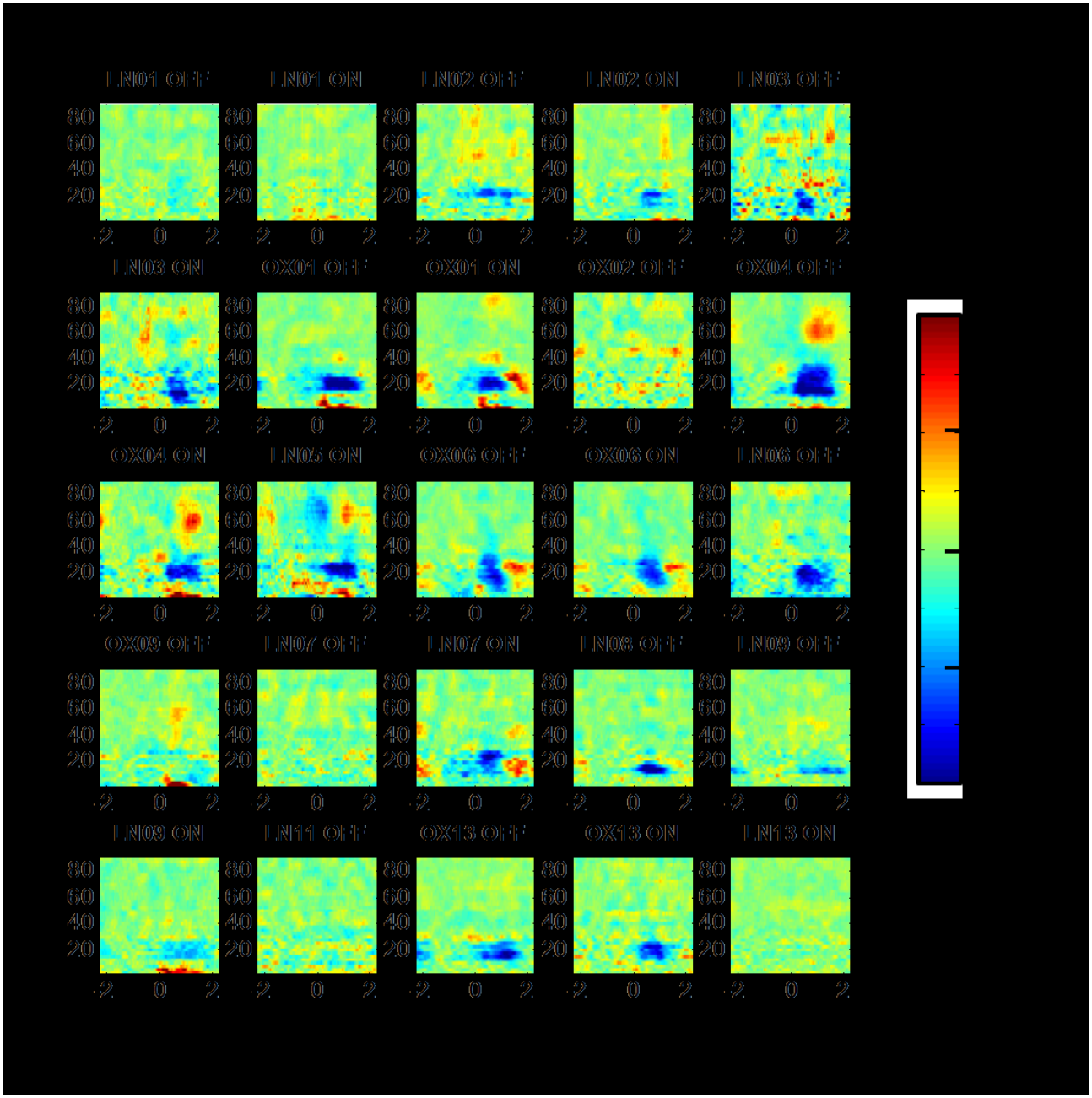

Figure 47: Individual time-frequency images of left STN activity during a right go signal. *Each subimage displays frequency (y axis, Hz) against peri-stimulus time (x axis, s). The go signal is presented at t=0. Neural activity is presented as a percentage change in RMS amplitude relative to the baseline (-1.8s to 1s). For visualisation purposes, a single STN bipolar channel is shown per subject – selected as the one with highest gamma (60-90Hz) variance. The title of each image identifies the subject (e.g. LN07) and the medication condition. These images demonstrate a clear decrease in beta activity in the motor cortex after presentation of a go signal. There is no clear difference in pattern between subjects recorded in Oxford ('OX') and London ('LN').*

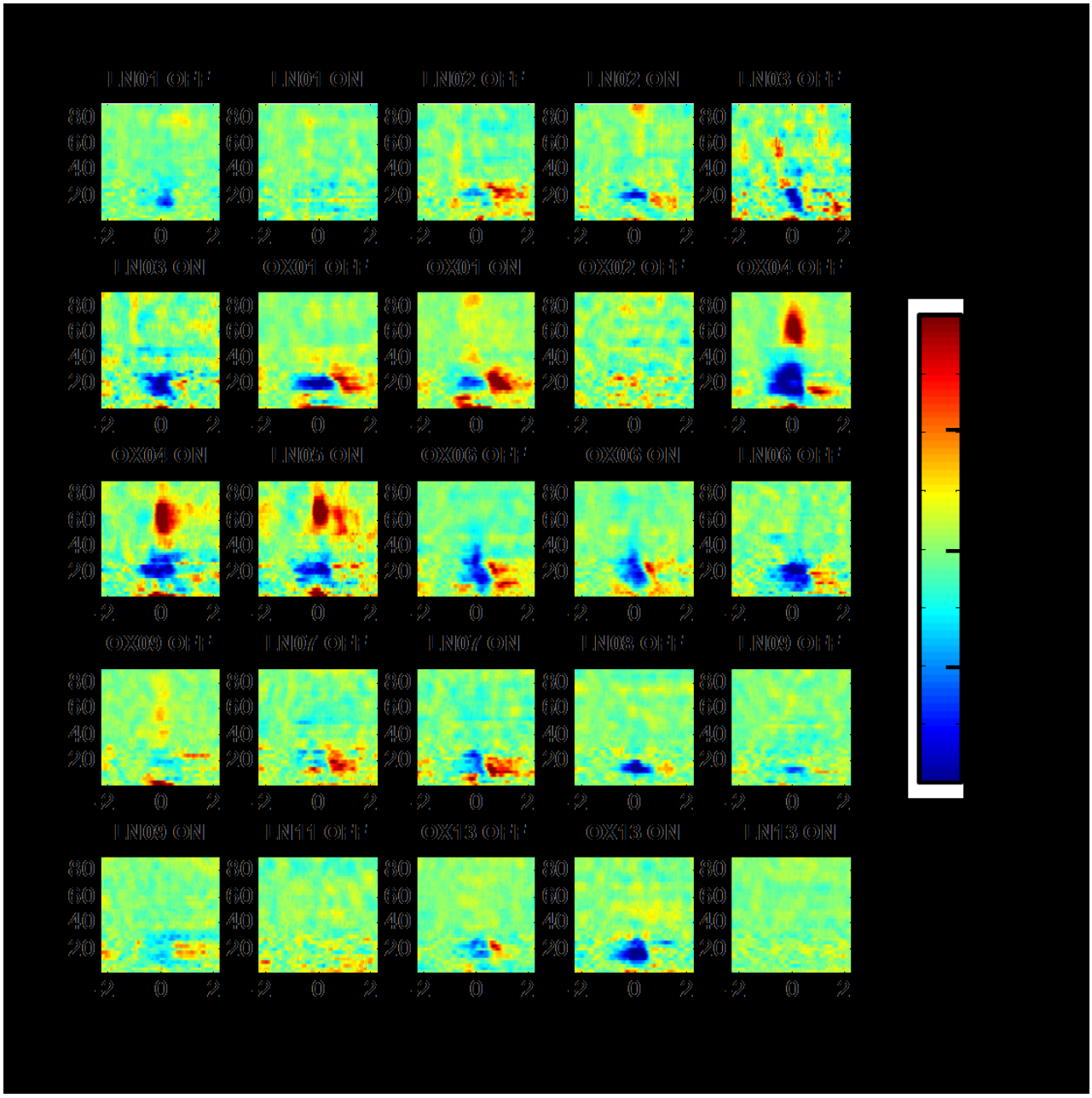

Figure 48: Individual time-frequency images of left STN activity during a right button press. *Each subimage displays frequency (y axis, Hz) against peri-stimulus time (x axis, s). The button press is at t=0. For visualisation purposes, a single STN bipolar channel is shown per subject – selected as the one with highest gamma (60-90Hz) variance. Neural activity is presented as a percentage change in RMS amplitude relative to the baseline (-1.8s to 1s). The title of each image identifies the subject (e.g. LN07) and the medication condition. These images demonstrate a clear decrease in beta activity and increase in gamma activity in the STN during the button press, immediately followed by a beta increase. There is no clear difference in pattern between subjects recorded in Oxford ('OX') and London ('LN').*

6.3.4 Group level theta and beta dynamics in the contralateral STN during a change signal

We further analysed *RMS amplitude* in the STN and the M1 by means of a novel continuous analysis GLM. In this model, the induced response to all individual events such as the go signal, change signal and button press can be estimated and disambiguated. Although cortical regions such as the rIFG and pre-SMA are implicated in changing and stopping behaviour, we focused on the STN and M1 in this provisional analysis to provide a demonstration of the principle of this technique, rather than definitive conclusions about local power changes novel to the task at hand. We used data from all available bipolar STN channels in each subject (usually 3). After estimating the individual induced responses for event type and source location we collapsed together all data from source locations contralateral to the original go signal (i.e. we collapsed left STN power during a right arrow instruction with right STN power during a left arrow instruction). We than selected the induced responses to the change signal and entered them into an ANOVA with dopamine (ON and OFF) and success (successful versus unsuccessful change) as factors. The mean response, the main effects of the experimental conditions and their interaction can be seen in **Figure 49Error! Reference source not found.** Although a transient theta response followed by a decrease in beta can be seen in the STN, there is no significant response in M1. Dopamine reduces theta activity prior to the presentation of the change signal in the STN, but has no effect on M1.

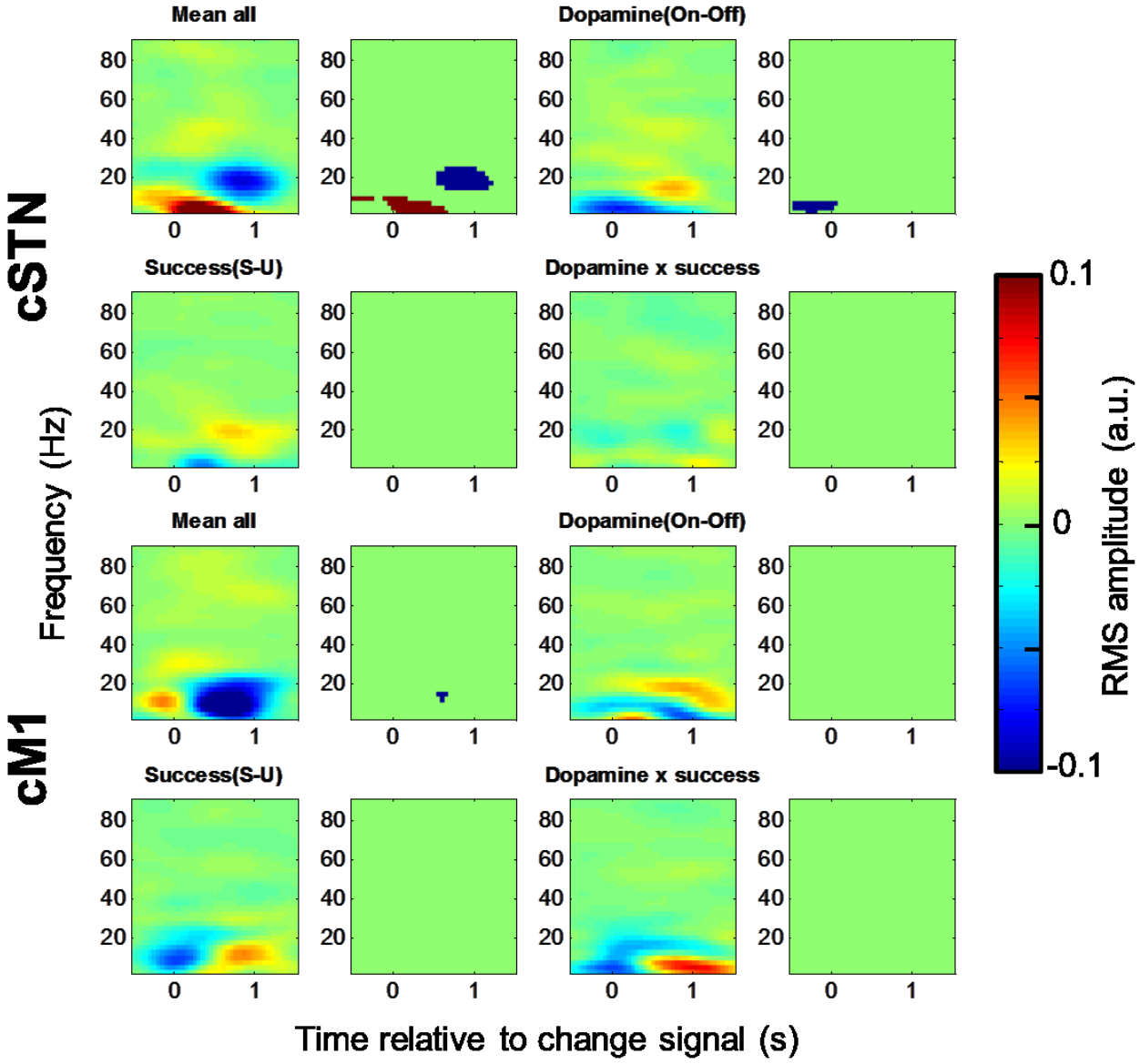

Figure 49: Experimental effects on the induced response to the change signal in STN and M1. *Induced responses to the change signal were converted to time-frequency images and entered into a within-subject ANOVA with success (successful v unsuccessful changing) and medication (ON or OFF levodopa) as factors. Each subimage displays frequency (y axis, Hz) against peri-stimulus time (x axis, s, t=0 is the time of the change signal) for a single source [top 2 rows are contralateral STN (cSTN), bottom 2 rows are contralateral M1 (cM1)], and a single experimental contrast. Each contrast image is labelled with a neighbouring statistical mask (green = no effect, blue= significant decrease in amplitude, red=significant increase in amplitude). The most marked finding is a transient theta increase during the presentation of the change signal, followed by a beta decrease. Experimental*

interventions had little effect of RMS amplitude. This demonstrates the principle of the convolution approach to RMS amplitude analysis in our cohort.

6.3.5 Coherence between the motor cortex and STN cannot be seen consistently in individual subjects.

Previous studies in a similar cohort have shown that coherence changes are rarely seen in individual subjects, and better demonstrated across the group (Litvak et al., 2012a). We examined single subject data to ensure that reasonable and comparable event-related signals could be extracted from the MEG and LFP data, in spite of prominent artefact and the use of varied recording systems. In this section we looked at coherence between left M1 and left STN during a right button press. We found that there was a detectable increase in cortico-subthalamic gamma coherence at the time of movement in only a few subjects (see ***Figure 50***).

6.3.6 Group level network coherence dynamics during the change task

Although, using robust averaging, coherence between the motor cortex and STN could not be seen at the individual level, we went on to calculate the group average of cortico-subthalamic and cortico-cortical coherence in three selected example cases. Events such as the button press and change signal may be close, but not predictably separated, in time. Therefore coherence changes cannot be definitively attributed to any particular event. Acknowledging this, in this demonstration, we have focused our interpretation of the data on coherence changes close to the triggered event (t=0), which are most likely (but not definitively) to be related to the event in question. Firstly we looked at coherence between the left motor cortex and left STN during various events in the change task (see **Figure 51**). Because we were looking at the left STN, we only included trials where the go arrow was presented to the right initially to allow ease of interpretation. The data are not all that clear, but the clearest finding triggered to an event is a relative increase in gamma coherence locked to the go signal in the ON medication condition. This is consistent with recent evidence linking increased cortico-subthalamic gamma coherence with increased motor responsiveness to dopamine in PD subjects (Litvak et al., 2012a). Next we looked at coherence between the pre-SMA and STN during the same trials and events (see **Figure 52**). Here, the most striking feature was a gamma coherence burst locked to the change signal, but only on failed change trials. Again, the significance of this is difficult to determine (see discussion). Finally, we looked at coherence between two cortical sites – the right IFG

and the pre-SMA (see **Figure 53**). Again, we found striking gamma coherence locked to both the change signal and button press. However we are unable to disambiguate whether this activity is in fact locked to one or both of these events.

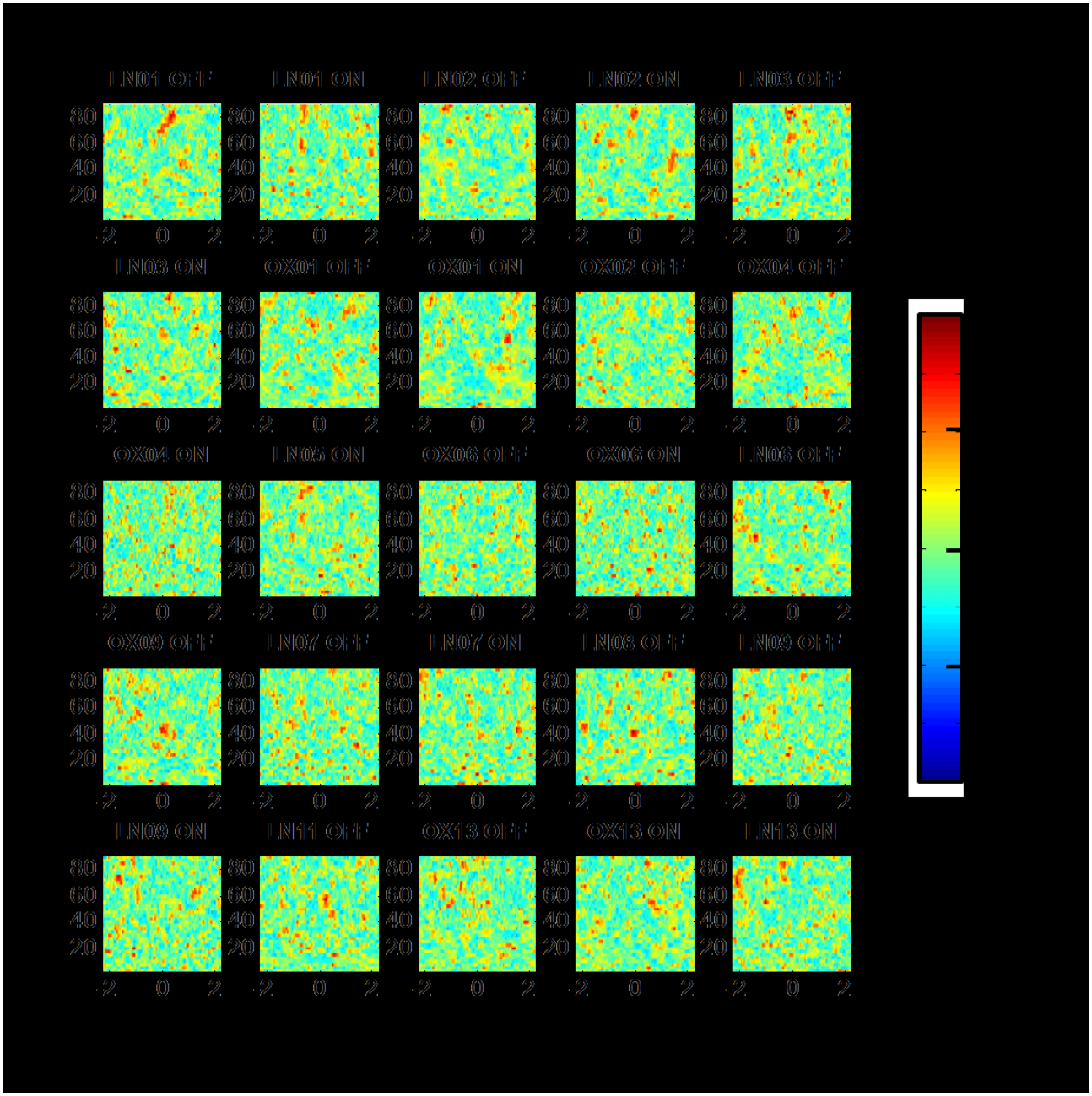

Figure 50: Coherence between the left M1 and left STN during a right button press. *Each subimage displays frequency (y axis, Hz) against peri-stimulus time (x axis, s) for a single subject per medication condition. The button press is at t=0. Coherence is presented relative to the mean of the entire time window (-2.5s to 2.5s). The title of each image identifies the subject (e.g. LN07) and the medication condition. Only some of these images suggest that there is increased gamma coherence during the button press, otherwise there are no clear signals at the individual subject level. There is no clear difference in pattern*

between subjects recorded in Oxford ('OX') and London ('LN'). Note that although subject OX04 had prominent spike artefact in the cortical amplitude signal, this artefact does not dominate the coherence signal.

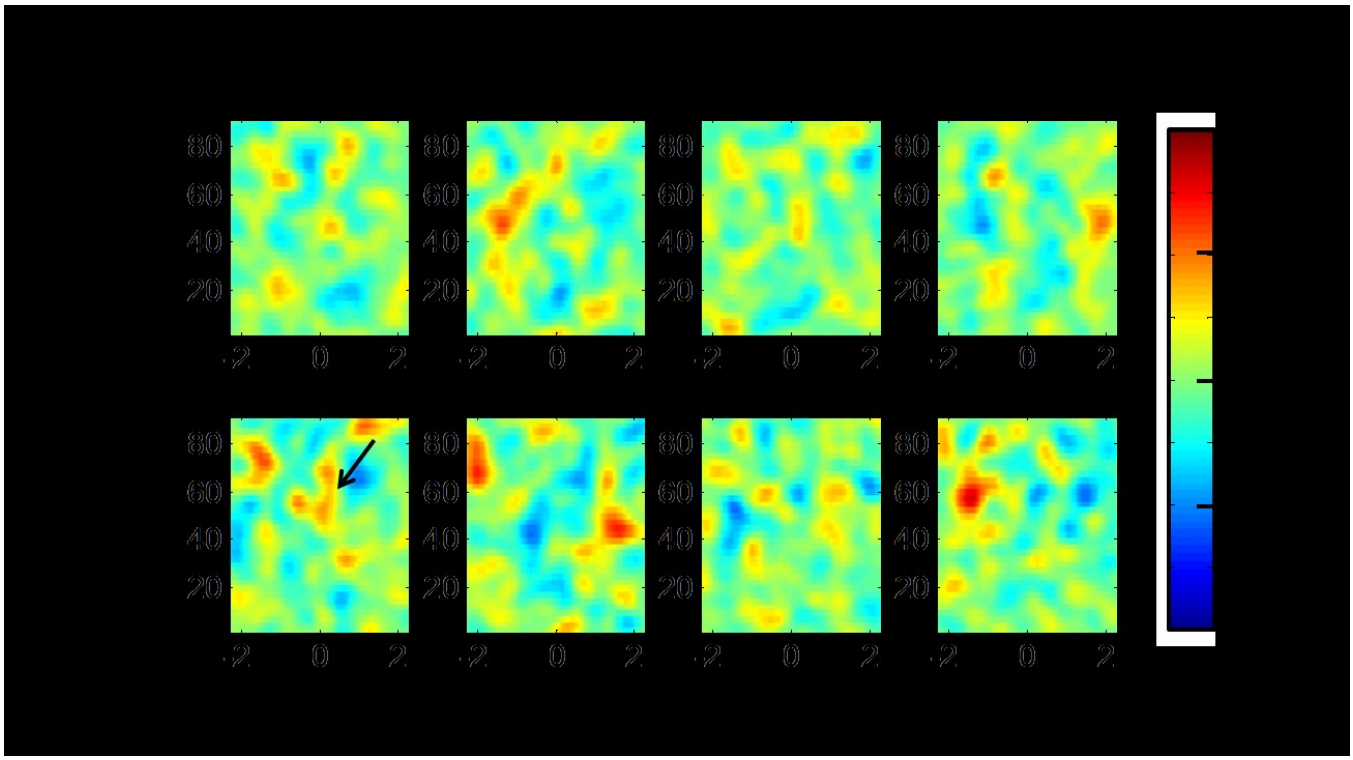

Figure 51: Average group-level coherence between the left M1 and left STN during the change task. *Only trials following presentation of a right go arrow are included for ease of interpretation. Each subimage displays frequency (y axis, Hz) against peri-stimulus time (x axis, s) for the group OFF medication (top row) and ON medication (bottom row). Individual columns represent the average of trials locked to the go signal (GO, go signal at t=0) the button press (PRESS, button press at t=0), the change signal during failed change trials (Ch-F, change signal at t=0) and change signal during successful change trials (Ch-S, change signal at t=0). The most striking feature locked to any of the trial events is a gamma increase at around the time of the go signal (black arrow) seen in the ON medication condition. Coherence is presented relative to the mean of the entire time window (-2.5s to 2.5s), and has been smoothed to aid visualisation.*

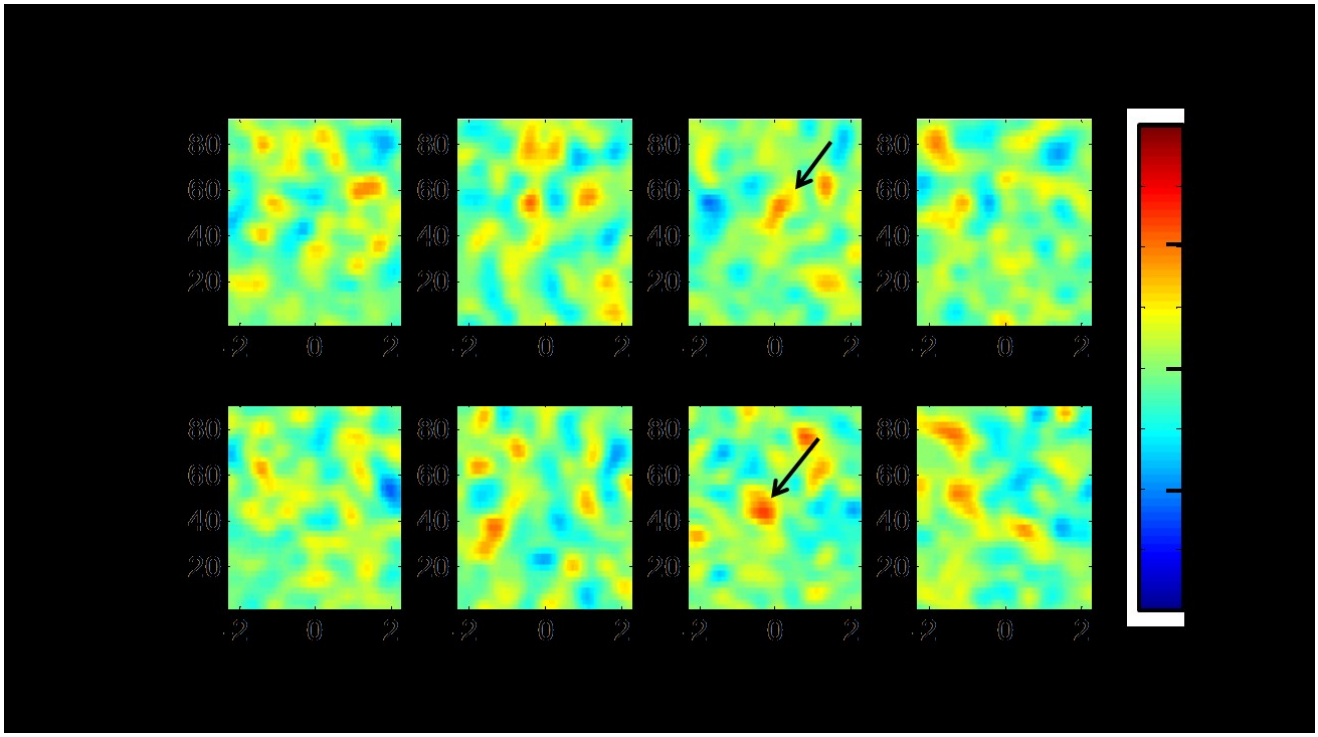

Figure 52: Average group-level coherence between the pre-SMA and left STN during the change task. *Only trials following presentation of a right go arrow are included for ease of interpretation. Each subimage displays frequency (y axis, Hz) against peri-stimulus time (x axis, s) for the group OFF medication (top row) and ON medication (bottom row). Individual columns represent the average of trials locked to the go signal (GO, go signal at t=0) the button press (PRESS, button press at t=0), the change signal during failed change trials (Ch-F, change signal at t=0) and change signal during successful change trials (Ch-S, change signal at t=0). The most striking feature is a gamma increase at around the time of the change signal – but only in the failed change condition (see black arrows). Coherence is presented relative to the mean of the entire time window (-2.5s to 2.5s), and has been smoothed to aid visualisation.*

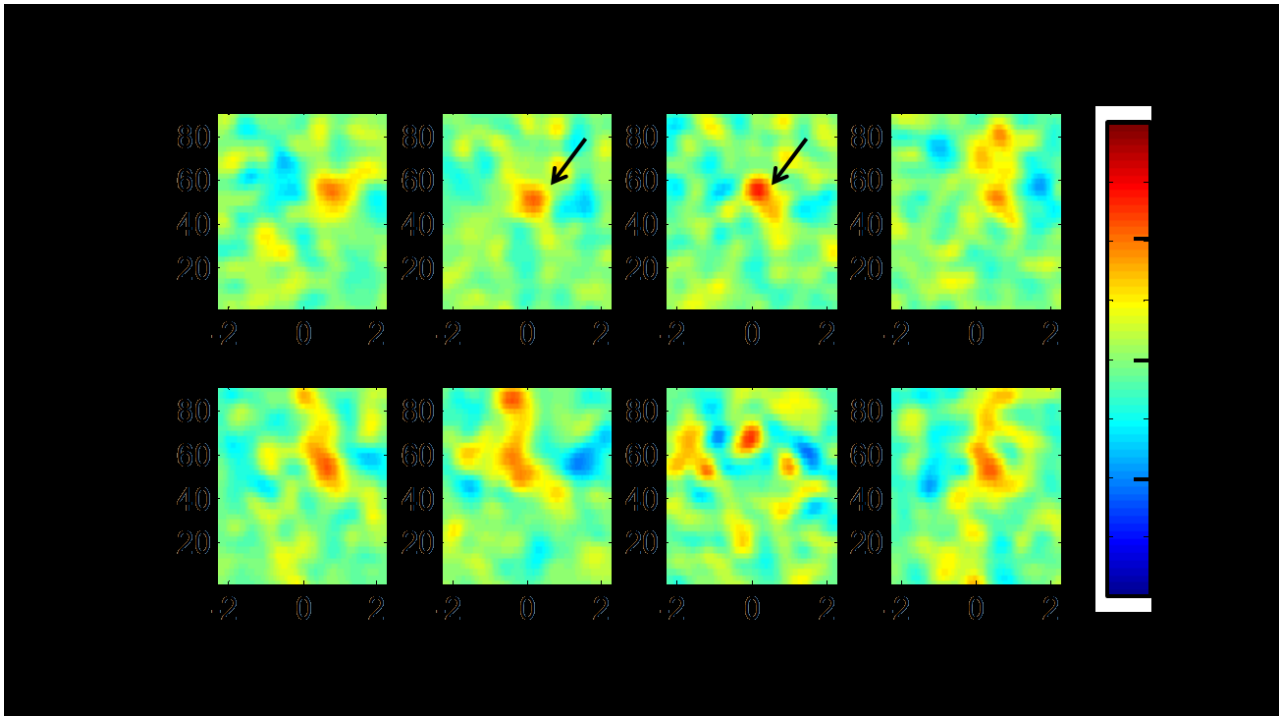

Figure 53: Average group-level coherence between the right IFG and pre-SMA during the change task. *Only trials following presentation of a right go arrow are included for ease of interpretation. Each subimage displays frequency (y axis, Hz) against peri-stimulus time (x axis, s) for the group OFF medication (top row) and ON medication (bottom row). Individual columns represent the average of trials locked to the go signal (GO, go signal at t=0) the button press (PRESS, button press at t=0), the change signal during failed change trials (Ch-F, change signal at t=0) and change signal during successful change trials (Ch-S, change signal at t=0). A clear gamma increase can be seen in most conditions, but it is unclear if this is locked to the change signal or button press (black arrows). Coherence is presented relative to the mean of the entire time window (-2.5s to 2.5s), and has been smoothed to aid visualisation.*

6.4 Discussion

This chapter provides proof-of-principle that dynamic cortico-basal ganglia activity can be measured with combined MEG and simultaneous STN-LFP recording. We demonstrated a change-signal locked theta response in the STN, similar to the cortical theta network seen in healthy controls. We have also found preliminary evidence for the role of cortico-subthalamic and cortico-cortical gamma coherence during the change task. However, although the raw data and initial analyses look promising, further more sophisticated analysis techniques are

required to make definitive biological inferences from these data – especially with regards to dynamic connectivity. In this discussion, we will therefore focus on both methodological aspects and the limited demonstration results we have presented.

6.4.1 Signal Fidelity

Standard robust averaging techniques are well suited to our data, and with minimal pre-processing, are able to provide clear induced responses to events that can even be seen individually in most subjects. This supports the notion that signal-to-noise ratio of the MEG recording is adequate in spite of the ferromagnetic artefact from the extension wires. In addition, reassuringly no systematic differences in the pattern of induced responses can be seen between subjects recorded with different MEG systems (i.e. between Oxford and London). Finally, low filter correlation coefficients suggest that source activity can be confidently extracted from the MEG data with enough resolution to separate the *a priori* regions of interest.

6.4.2 Amplitude responses of cortical and subthalamic regions during the change-of-plan task

We focused on a preliminary analysis. We found that robust averaging of induced responses confirmed a beta decrease and rebound increase, but it was unclear whether this was locked to the go signal, or also partly the button press itself. A similar pattern was found in the STN with additional gamma activity more clearly locked to the button press itself. Reassuringly these movement-related amplitude changes are similar to power changes previously reported during simple movements in other studies(Litvak et al., 2012a). However in our case, because of the nature of our cognitive task, we cannot make any further substantial inferences regarding the relationship between particular task events and brain activity changes. This is because standard averaging techniques (including robust averaging) cannot disambiguate the brain responses to closely overlapping experimental events. One approach to this problem, exemplified in chapter 5, is to use a convolution model to perform group analysis. Here, *all* individual events are modelled in the same GLM and therefore it is possible to disambiguate the response to different experimental events. Because of the increased within and between-subject variability in our patient cohort as compared to our healthy control cohort, it also becomes important to include factors such as age and UPDRS in our hierarchical model. However, due to time-constraints, we present only a provisional demonstration of the model (without including important confounds). Convolution model

analysis of the change signal revealed that, on average, there was a theta increase followed by a beta depression in the contralateral STN during a change signal. This is similar to the widespread cortical theta responses seen during a similar task in healthy controls (chapter 5). However, in this patient cohort, no such activity was seen in the motor cortex itself. There was additionally a marginal effect of dopamine on contralateral STN theta activity just before the presentation of the change signal. However more clearly defined effects may become apparent after relevant confounds are modelled out.

6.4.3 Dynamic coherence responses during the change-of-plan task

Coherence between the motor cortex and STN could not be seen clearly at the individual level, as has been noted before (Litvak et al., 2012a). In addition, coherence was derived in a fashion analogous to classical averaging, and therefore suffers from the same inferential limitations previously mentioned. However, acknowledging this, clear bursts of gamma coherence are locked to various events during the change task suggesting that gamma coherence is a fundamental message passing mechanism between pre-SMA, right IFG, primary motor cortex and the STN during the change task. Group average figures suggest that gamma coherence between the motor cortex and STN is locked to the signal to start moving, whereas gamma coherence between the pre-SMA and STN is locked to the signal to change. This is in keeping with our original hypothesis, that the pre-SMA is specifically involved in change behaviour. However, if this is the case, why then is pre-SMA to STN gamma coherence limited to *failed* change trials? This could be a genuine finding, but could also be due to unaccounted experimental confounds. Specifically, failed change trials require a different button to be pressed, than successful change trials. Therefore because the timing and nature of the motor response to the button press is different in both trials, the electromagnetic activity underlying the motor response will differentially interfere (by increasing or decreasing the change-locked coherence) with a failed and successful change event. We also demonstrated that this technique could also uncover dynamic cortico-cortical coherence between the pre-SMA and right IFG. This was in the form of a gamma coherence response which, although striking, was difficult to assign to either the button press or change signal. Cortico-cortical coherence measurement has been traditionally hampered by the presence of volume confounds. However, we have showed that the cortical sources looked at in this study are adequately separable (see section 6.3.2) using beamforming. Also, the nature of the gamma oscillatory responses are transient in time and therefore less likely to be a result of volume conduction. One way to potentially confirm this would be to ensure that the phase delay between the sources was not zero. .

So although gamma coherence may index information exchange between cortico-subthalamic and cortico-cortical hubs during dynamic motor behaviour, with our current methodology, it is difficult to disentangle what this information might mean. One approach to the inference problem is to again use a convolution model as we demonstrated with amplitude responses. This would be able to disambiguate the responses to different events and additionally account for reaction time confounds that are magnified in the patient group. However, the convolution model requires a continuous estimate of the dependent variable and unfortunately, coherence cannot be estimated continuously currently in the SPM framework. Additionally, coherence is a non-linear measure and further validation would be required before this can be modelled adequately using a GLM. However, in principle, with a continuous estimate of coherence, similar procedures found in fMRI analysis could be applied to our MEG data, to allow us to make more substantial biological inferences.

Finally we should note that there are a wide variety of other techniques that we could use to perform further analysis of these data which might enrich inferences in different ways. Firstly, coherence is only one metric of coupling between two regions. Other metrics including phase-locking value, multivariate connectivity and imaginary coherence may provide additional insight into different mechanisms of communication. Secondly, in previous chapters we have calculated *directional* connectivity using Granger-based techniques. The same method could be applied to this data in order to determine if activity in one region temporally precedes another during this task.

6.4.4 Conclusions and further directions

In conclusion, this chapter provides evidence that combined measurement of MEG and basal ganglia LFPs is a technique that is, in principle, able to test predictions about dynamic cortico-basal ganglia connectivity during cognitive tasks. Secondly, although the patients in our cohort did not perform as consistently as healthy controls, using an adapted paradigm – the change-of-plan task – and robust behavioural analysis techniques, we were able to get consistent behavioural results from this cohort. Finally, although reassuring, the analyses we have performed remain provisional. Critically, this is because currently there exists no marriage of the appropriate electrophysiological analysis techniques (continuous coherence) with the appropriate statistical techniques designed for cognitive tasks (the convolution model). Therefore, although we can demonstrate local amplitude changes in the STN and

cortex during the change-of-plan task, we cannot yet robustly infer the meaning of the changes in gamma connectivity between regions.

7. Discussion

Prior to summarising and discussing the research undertaken, we will briefly remind ourselves of the objectives of this thesis that were set out in the introduction:

1) To develop a study model and methodology to measure cortico-basal ganglia connectivity, based on simultaneous magnetoencephalographic and basal - ganglia recordings in Parkinsonian patients.

2) To determine if the cortical and subcortical spatial distribution of cortical-basal ganglia connectivity is frequency and dopamine dependent at rest.

3) To characterise the role and spectral signature of different cortical areas during the stop-signal task.

4) To characterise how activity in cortico-basal ganglia circuits changes during the performance of the stop-signal paradigm, and how these changes relate to behaviour in PD patients.

7.1 Simultaneous MEG and basal ganglia LFP recording – a new model for studying cortico-basal ganglia oscillations

The first aim of this thesis was to develop a study model by which cortico-basal ganglia interactions could be studied in humans with PD. Previous work in humans had either relied on functional MRI (fMRI) studies (e.g. (Di Martino et al., 2008)) or combined EEG and deep electrode LFP recording (e.g. (Lalo et al., 2008)). Although combined EEG and LFP recordings had sufficiently high temporal resolution to capture the spectral characteristics and directionality of cortico-basal ganglia interactions, they lacked spatial resolution at the cortex. This is primarily for two reasons. Firstly post-operative neurosurgical patients have limited access to the scalp because of the need to avoid the wounds, meaning that head coverage is not consistent. Secondly, the EEG signal is distorted by bone and scalp layers, making the accurate modelling of these distortions (i.e. a head model) particularly important. This is hampered, in this group of subjects, by the presence of burr holes, and post-operative scalp swelling. On the other hand, although fMRI studies had sufficient spatial resolution to identify distinct cortical nodes of interest, they had difficulty isolating activity from small but crucial structures such as the STN and, of course, they had poor temporal

resolution. Another approach, employed by this thesis, is to replace EEG recording with MEG recordings. In addition to increasing the number of cortical sensors (from 32 or less to over 275), the MEG signal is not distorted by bone and skin, and is therefore less sensitive to the presence of burr holes, and is less sensitive to inaccuracies in the head model. Combined with simultaneously recorded intracranial (LFPs), MEG is a promising solution but still has potential limitations – such recordings are hampered by the presence of high-amplitude artefacts in the MEG due to the presence of percutaneous extension wires made of stainless steel close to the MEG sensors. However, Litvak et al described these artefacts and showed that despite their presence, topographical mapping of coherence between bipolar LFP channels and the MEG sensors could disclose physiological patterns (Litvak et al., 2010). Furthermore, they demonstrated that beamforming effectively suppresses artefacts and thereby enables both localization of cortical sources coherent with the STN and the extraction of artefact-free virtual electrode data from these sources. In this study, we built-upon these technical advances to characterise cortico-subthalamic and cortico-pedunculopontine coherence in a cohort of PD patients. Although we have used sensor-level noise modelling (see chapter 5) to internally validate our approaches, most reassuring is that a similar study (of combined MEG and STN LFP recordings in PD patients) that used MEG compatible extension wires presented almost identical results to ours (Hirschmann et al., 2011). With increasing availability of MEG-compatible wires in the future the approaches developed in this thesis will possibly yield even better data quality.

7.1.1 Limitations

However, a couple of limitations remain. Firstly, healthy control data are necessarily limited because it would be unethical to implant electrodes into human brains for research purposes only. To militate this we have, in this thesis, limited our inferences to comparisons between conditions in the same set of subjects, rather than comparisons across different groups such as patients and controls. Additionally, as the range of indications for DBS increases, *non-parkinsonian* patients with STN electrodes may be used as controls (e.g. see (Neumann et al., 2012)). Secondly our cohort is immediately post-operative, and therefore may not be physiologically similar to typical PD patients. Perhaps the most striking demonstration of this is the so called ‘stun’ effect, where the symptoms of PD are dramatically reduced post-operatively by peri-lesional oedema from the electrode insertion (Lalo et al., 2008). However, although clinically the stun-effect may subside within days, initial STN LFP findings probably remain stable over time - even up to 7 years later (Giannicola et al., 2012).

7.2 Cortico-basal ganglia networks at rest

In chapters 3 and 4, we studied resting cortico-subthalamic and cortico-pedunculopontine networks at rest. We used coherence, a frequency dependent measure of coupling, to assess the strength of cortico-basal ganglia interactions. Remarkably we found that in both cases networks at distinct frequencies were also spatially distinct, supporting the idea that different brain regions may have different 'default' frequencies at which they synchronize together at rest (Eusebio et al., 2009). Our resting results focus on two frequency-specific networks – alpha (7-12Hz) and beta (15-35Hz). The anatomical basis for these networks is supported by recent DTI data that demonstrated connectivity between the STN and temporoparietal and medial frontal cortical hubs in PD subjects (Lambert et al., 2011).

7.2.1 The cortico-basal ganglia alpha network

Both the STN and PPNR demonstrated increased alpha frequency connectivity with other brain regions. The STN was coherent with the temporo-parietal cortex bilaterally and the brainstem, whilst the PPNR was coupled to the ipsilateral cerebellum. Additionally, a central portion of the PPNR was preferentially coupled to the inferior frontal gyrus in the alpha band.

We must acknowledge that some of these structures are deep inside the brain, where MEG sensitivity is poor. However, Parkkonen et al have recorded brainstem early auditory evoked responses with MEG (Parkkonen et al., 2009) and Schnitzler et al have suggested MEG can detect signals from the thalamus, brainstem and cerebellum (Schnitzler et al., 2009).

7.2.1.1 Potential functions of the alpha network

So can we speculate on the potential functions of the alpha network? One candidate is that the network may, in part, overlap with the previously described alpha network coherent with Parkinsonian rest tremor (Timmermann et al., 2003; Pollok et al., 2009). Although this network included brainstem areas and the cerebellum, we would not favour this explanation, because the minority of our subjects had tremor as a presenting symptom and very few had significant episodes of tremor during our recordings, as demonstrated by simultaneous EMG recordings. Changes in alpha activity in the subthalamic region have also been reported in response to emotional stimuli (Brucke et al., 2007), however, our study did not present any emotional stimuli to the patients.

We favour the hypothesis that the alpha network subserves attentional/arousal functions. Arousal can be regarded as the general state of physiological reactivity of a subject, ranging

from asleep to panicked (Coull, 1998). Such physiological states were thought to be heavily influenced by brainstem activity, particularly the activity of the reticular formation. Early neuropsychological models suggested that higher cortical and thalamic areas mediating attention were dependent on the activity of such brainstem arousal mechanisms. Attention itself, can be thought to be the allocation of awareness, or brain resources, to a particular behavioural process or thought. Indeed, attention can be described in temporal, spatial or capacity terms. Early influential models suggested that arousal and low-level attentional mechanisms (such as orienting to a stimulus) were mediated by noradrenergic and cholinergic brainstem, thalamic and parietal mechanisms, whilst higher-level functions, such as set-shifting and other executive functions, were mediated by dopamine mechanisms involving the frontal cortex (Coull, 1998).

So what is the evidence that the alpha network described here may represent an arousal and low-level attentional network? Firstly, the alpha frequency itself has been associated with modulating attention within different brain regions (Palva and Palva, 2007). Secondly, the brain structures involved in this network – temporo-parietal regions, STN, PPNR, cerebellum and brainstem – have all been implicated in studies of attention. In particular, temporo-parietal alpha/low beta (10-20Hz) has been implicated in visual attention studies and is sensitive to the levels of acetylcholine present (Bauer et al., 2012). However, the strongest support to the idea of an alpha attentional network comes from the studies on the PPNR. The PPN is considered a component of the 'reticular activating system' and may modulate states of arousal and attention (Winn, 2006). In line with such a role, PPN stimulation in patients with Parkinson's disease (PD) may increase rapid eye movement sleep (Romigi et al., 2008; Lim et al., 2009) and diurnal vigilance (Ferraye et al., 2010), and there is PPNR-cortical coherence in the alpha band during wakefulness (Androulidakis et al., 2008). In fact the brainstem region identified by the *STN* network may be the PPNR, which is directly connected with the STN (Androulidakis et al., 2007).

7.2.1.2 Clinical correlation with alpha activity

In chapter 3, we performed multiple *post hoc* correlations between local and inter-regional electrophysiological parameters and multiple clinical symptoms. After a stringent correction for multiple comparisons, no correlations remained significant. However, recent papers using a more targeted approach have correlated *local* alpha activity in the STN with maximal effort responses in patients with PD. Maximal effort has been linked to attention and arousal most strikingly by a phenomenon termed paradoxical kinesis. In such episodes, PD subjects undergoing intense stimuli (e.g. escaping from a burning house) report temporary but dramatic resolution of their motor impairment (Souques, 1921). Although the relationship

between such arousing stimuli and electrophysiological parameters is difficult to study in the laboratory, the brain responses underlying maximal effort may be related. In a study of 10 PD patients undergoing DBS surgery to the STN, Anzak et al found that both theta/alpha (5-12Hz) and broad band gamma (55- 375Hz) activity in the STN predicted approximately 70% of the inter-subject variance in maximal grip responses. This effect was relatively independent of dopamine, although the authors were unable to conclude if this effect was due to variation in arousal, attention, or the motor activity itself (Anzak et al., 2012). Furthermore, in a similar carefully parameterised motor performance study, Tan et al confirmed these findings and showed that increased STN theta/alpha activity was also associated with an ability to sustain a motor grip. Again this effect was independent of dopamine.

Previous literature has also shown attention may be especially important in those with PD and gait dysfunction, particularly freezing. A relationship between attentional control and gait performance is increasingly recognised (Yarnall et al., 2011). Gait speed reduces in healthy subjects, elderly fallers and in Parkinson's disease during the performance of a second, unrelated task ('dual tasking') (Hausdorff et al., 2003; Springer et al., 2006; Lamoth et al., 2011). Dual tasking and other processes that divert attention away from walking can all also precipitate gait freezing (Giladi and Hausdorff, 2006). In PD, attentional deficits are increased in patients that fall (Allcock et al., 2009) and freeze during gait (Amboni et al., 2008; Yogev-Seligmann et al., 2008).

Alpha networks preferentially involving the *middle* PPNR (including the caudal PPN), between 2 to 6mm below the pontomesencephalic line, may be particularly important in supporting a possible role in gait control through attentional modulation. This region demonstrates both the greatest *local* alpha synchrony, a marker that correlates with gait performance (Thevathasan et al., 2012) and clinical response to stimulation, as well as the greatest alpha synchrony with *distant* brain regions. Furthermore, just as cortical hubs of the alpha attentional network may be modulated by acetylcholine levels, acetylcholine may also have a special role in the PPNR. The middle section of the PPNR may include the caudal part of the 'pars dissipata' of the PPN (Thevathasan et al., 2012). The pars dissipata of the PPN, as defined by immunohistochemical labelling of choline-acetyltransferase in humans, extends both rostrally and caudally from the central pars compacta (Mesulam et al., 1989; Manaye et al., 1999), and has been implicated in gait and its dysfunction (Karachi et al., 2010). It should, however, be acknowledged that the pars dissipata of the PPN has indistinct boundaries, and of note, just medial to its caudal boundary is the laterodorsal tegmental nucleus which is also rich in cholinergic neurons (Manaye et al., 1999).

Can we say anything further about *inter-regional* alpha coupling? Oswal et al have re-analysed task data on the same cohort of subjects as presented in chapter 3. Using combined MEG and STN-LFP recordings they looked at activity in the temporoparietal region – a hub in the alpha network described in chapter 3 – during a button press (Oswal et al., 2012). They found that temporoparietal alpha power decreased up to 2 seconds prior to a button press, and that this remained unaffected by levodopa administration. This effect was prolonged for sequential button pressing as opposed to simultaneous pressing, suggesting that it may be related to either the increased motor activity or attentional engagement required by the more complex sequential condition. They also found a drop in temporoparietal-STN coherence immediately after a button press *regardless* of its complexity, but related to levodopa administration and the level of clinical impairment. The authors argue that the absence of a relationship with task complexity supports the notion that such coherence represents arousal or attentional modulation, as opposed to motor processing. In essence, the alpha cortico-STN network has to 'disengage' during a task to allow other (e.g. gamma) networks to be activated (Oswal et al., 2012). This is an attractive hypothesis, but further experimental studies are required to confirm whether disengagement of the alpha network represents attentional allocation, or whether it represents a different feature of motor preparation or executive function such as working memory.

In summary, although speculative, our results support the notion of an alpha cortico-basal ganglia resting network that influences attention and arousal, some components of which may also be particularly important for gait dysfunction in PD, and some for recruitment of maximal force. We would suggest that most parts of this network are sensitive to acetylcholine levels, rather than dopamine, (although see (Oswal et al., 2012)) and that future studies that extrinsically modulating acetylcholine levels may provide useful data on the role of this network.

7.2.2 The cortico-basal ganglia beta network

The second pattern of coupling was evident in the beta frequency band in which both the STN and the PPNR were coupled to medial frontal motor areas (including the primary motor cortex, sensorimotor cortex, SMA and cingulate). Overall, the STN had a larger cortical network, extending anteriorly to medial prefrontal areas and laterally to premotor areas and the lateral frontal cortex. The areas of cortical involvement suggest that this network, recorded at rest, might be engaged in setting the level of preparedness for executive functions. This would be compatible with the emerging view that beta activity may promote the status quo at the expense of action (Hammond et al., 2007; Engel and Fries, 2010;

Jenkinson and Brown, 2011). However, this remains speculative with regards to beta coherence between distant regions, rather than local beta synchronisation within a region.

7.2.2.1 Are beta networks pathological?

Do these beta networks represent physiological or pathological activity? Without the opportunity to record from the subthalamic area in healthy subjects, or at least non-Parkinsonian patients, we cannot answer this question directly. A common approach under these circumstances is to determine whether dopaminergic therapy alters the pattern of activity noted in the untreated state. The approach is based on the premise that the core deficit in PD is partially reversed by exogenous dopaminergic input, although the homology between brain states in treated PD and the healthy subject is only likely to be approximate at best. Relying on studies using this approach, it has been proposed that *local* beta synchronisation is a normal phenomenon in certain basal ganglia structures, but that this may be pathologically exaggerated in PD (Jenkinson and Brown, 2011). Hence levodopa administration reduces local beta synchronisation. But how may this apply to beta synchronisation across structures?

We found that levodopa *increased* beta coupling between the STN and a limited part of the anterior medial frontal cortex. Without a direct clinical or cognitive correlate to this change, the inference remains unclear. In fact, the limited effect of dopamine on the beta network was surprising given its consistent effect on local beta synchronisation. Similarly, Lalo et al. (2008) found little effect of medication with levodopa on the STN-cortex DTF below 35 Hz, although there was an increase in the gamma band. Williams et al. (2002) did find a suppression of beta band STN-cortex coherence at rest following medication, but this was in a much smaller sample of patients. It may be that some of the negative findings relate to stun effects in the immediate post-operative period (Lalo et al. 2008). However, the limited changes in the distributed (rather than local) networks following dopaminergic therapy might also suggest that synchronisation across structures may be at least partly physiological phenomena in patients. Further support for this is provided by recent studies of cortico – basal ganglia functional connectivity based on functional magnetic resonance imaging and positron emission tomography. Both healthy subjects (Postuma and Dagher, 2006) and PD patients (Helmich et al., 2010; Hirschmann et al., 2011) show resting connectivity between the basal ganglia and the supplementary motor area, the temporo-parietal area and parts of the prefrontal cortex.

7.2.2.2 Is there more than one beta network?

Another reason for the minimal effect of dopamine may be that local synchronisation in the STN tends to be low beta (12-20Hz), whereas we found distant synchronisation tended to be maximal around 30Hz (high beta). The implications are twofold. First, the difference in frequencies between peak subthalamic power and peak subthalamo-cortical coherence reinforces the notion that subcortico-cortical coherence is not a simple passive phenomenon, but that its pattern is dictated by the transfer characteristics of the pathways involved. Second, the difference in frequencies adds weight to the argument that subthalamic activities in the lower and upper ranges of the beta frequency band may have somewhat different functional significance (Williams et al., 2002; Priori et al., 2004; Fogelson et al., 2006). Activity in the upper beta band seems to be more strongly coupled with cortical activity, and relatively less modulated by dopaminergic therapy.

7.2.3 Directionality within the resting networks

In both resting studies, we used variants of Granger causality to explore the direction of coupling between either the STN or PPNR and other brain structures identified within either the alpha or beta networks. Such techniques identify which signal leads in time, in so far as one signal is able to predict the other over time. The most parsimonious explanation for such a relationship between two coherent population activities is that the leading population drives the lagging population. However, this may not be the only explanation. Driving may be direct or indirect, via one or more unrecorded structures, or activity in both recorded structures may be driven by a third unrecorded structure (Sharott et al., 2005a). Given this, we use the term ‘effective direction of coupling’ (distinct from effective connectivity (Friston et al., 2012)) to describe a pattern of temporal relationships rather than a measure of direct coupling.

7.2.3.1 The STN

The clearest finding was that cortical regions temporally led the activity of the STN in the alpha and beta bands, regardless of the frequency of the network or the dopaminergic state of the patient. Similar apparent driving of LFP activity in the STN region in the beta band by cortex in PD patients has been noted using linear regression of phase (P Brown et al. 2001; Noa Fogelson et al. 2006; D Williams et al. 2002b) and the DTF (Elodie Lalo et al. 2008). This has been further replicated in animal models of PD (N. Mallet et al. 2008b; Andrew Sharott et al. 2005). These observations are compatible with the recent demonstration in a rodent model of PD that it is sufficient to stimulate the afferents to the subthalamic nucleus at

high frequency, rather than the local neurons themselves, to overcome Parkinsonism (Gradinaru et al., 2009). However, although the direction of information flow is relatively clear from our data, further modelling would be required to determine whether the cortico-subthalamic coupling identified reflects a mono-(hyperdirect) or polysynaptic (direct and indirect) pathway, or a mixture of the two.

7.2.3.2 The PPNR

Conversely, the PPNR showed no clear overall directionality with other brain structures it was coupled to. The most interesting feature in this cohort was the effect of levodopa: to increase beta outflow from the middle PPNR to the cortex. Again, without a direct behavioural correlate, we can only speculate upon the role of this. Basal ganglia pathophysiology in PD is classically modelled as a relative overactivity of the polysynaptic indirect pathway. This potentially upregulates two sets of competing inputs to the downstream PPN: inhibitory GABAergic influences from the GPi and SNr and excitatory glutamatergic influences from the STN. Although still debated, several lines of evidence suggest that the inhibitory inputs dominate, resulting in an overall pathological inhibition of the PPN in PD (but on the other hand, see Teo 1997 & 1998). Hence acetylcholine synthesis is suppressed in the PPN in the Parkinsonian state (Gomez-Gallego et al., 2007). Reducing PPN activity, as occurs with destructive lesions, leads to a Parkinsonian-like state (Aziz *et al.*, 1998), and there is a relationship between the loss of cholinergic neurones in the PPN pars compacta and the severity of Parkinson's disease (Zweig et al., 1989). Furthermore, akinesia in MPTP treated monkeys may be reversed by the microinjection of the GABA antagonist, bicuculline, into the PPN (Nandi et al., 2002). Therefore if there is overall inhibition of the PPN in PD, one may hypothesise that treatment by levodopa may 'release' the PPN outflow. Indeed this is what we found – increased beta outflow from the middle PPNR to the cortex. However, the clinical associations of this remain unclear.

7.3 Dynamic cortico-basal ganglia activity during executive function

To understand how these spectrally and spatially distinct resting cortico-basal ganglia networks relate to function and dysfunction in PD, we assessed the behaviour of these networks during dynamic experimental paradigms. Patients with PD have slower reaction times than average, and also have difficulty with alternating and repeated motor tasks (Lees et al., 2009). In addition, they are disproportionately slow during tasks demanding greater

executive control such as changing or stopping pre-prepared movements (Gauggel et al., 2004). We decided to test the hypothesis that the beta cortico-subthalamic network was involved in executive motor processing – in particular response inhibition, which is specifically impaired in PD (Gauggel et al., 2004). In order to do this, we used variants of the stop-signal paradigm, which requires contextual motor control – to be precise, it requires the participant to stop a pre-planned movement based on the occurrence of a visual stop-signal. This task has previously been shown to activate specific prefrontal regions and the STN (see introductory review). However, the distinct roles of different prefrontal areas during response inhibition remain unknown. We investigated this in two stages: first we used MEG in healthy controls to clarify the specialised roles of different cortical areas during stopping; second we performed a simplified variant of the task in post-operative PD patients undergoing combined MEG and STN LFP recording to examine the behaviour of the cortico-subthalamic network during stopping. However, we found that analysis of event-related electromagnetic responses required a more sophisticated analysis approach. This was developed in parallel with this thesis (Litvak et al., 2012b), but unfortunately has not yet been extended to include network analysis (i.e. coherence). Therefore we can make biological inferences only about the healthy control group (chapter 5), and in chapter 6 have performed a provisional 'proof-of-principle' technically motivated analysis of network behaviour.

7.3.1 Theta activity and the cortical response to a stop-signal

In chapter 5, we performed 4 variants of the stop-signal task that dissociated the effect of conditional complexity – i.e. the initial requirement to cognitively 'set-up the rules of the experimental task' – from the later possible requirement to inhibit an ongoing movement. Because some variants of the task required motor inhibition (a stop), and others required an opposite movement (i.e. a change-of-plan), the signal was termed the stop/change signal.

In order to study the neural basis for the second component (the activity associated with stopping a movement) we looked at brain signals locked to the stop/change-signal. The most consistent response to the stop/change signal was a brief theta/alpha induced response which peaked around the same time as the average time taken to stop a response – the stop signal reaction time (SSRT). This response was relatively widespread - found in the pre-SMA, left and right IFG and SMA (but was not significant in the primary motor cortex itself) – suggesting that it causes parallel activation of multiple hubs of a stopping network. Although similar medial frontal theta has been shown to be a marker of cognitive interference (Nigbur et al., 2011) and to predict error-monitoring (Cavanagh et al., 2009), in our experiment, the

theta response was unaffected by the presence of an error (stop-fail or change-fail trial) irrespective of the stop/change stimulus cue.

So what are the specialised functions of different cortical areas during stopping? To isolate the region most closely related to executing the stop itself, we looked for the region which was most sensitive to stopping efficiency. At each cortical region, we modelled variation in the slope of the induced theta/alpha response as a function of the average time available to stop/change. We hypothesised that, in subjects and conditions where a longer than average time was available for stopping/changing, the cortical theta alpha response would be less efficient (less steep). This relationship was only significant in the right IFG, suggesting that this part of the cortical stopping network is most closely related to the actual stopping process. This is consistent with human lesion (Aron et al. 2003) and fMRI data (Aron and Poldrack 2006) which have correlated right IFG damage and blood oxygenation with another measure of stopping efficiency - SSRT. Our results have also highlighted that right, as opposed to left, IFG activity is most closely related to stopping. It remains unclear why, but this asymmetry exists regardless of the hand being used to stop (Konishi et al., 1999), and whether a hand movement or verbal response is being stopped (Xue et al., 2008), supporting the idea the right IFG operates a fundamental operation in stopping.

7.3.2 Pre-SMA gamma activity and the modulation of context

Our experiment was also able to dissociate the effect of contextual complexity from the requirement to stop during the stop-signal task variants. The neural correlate of contextual complexity was identified as an early and persistent gamma response found in the pre-SMA. Crucially, pre-SMA gamma activity increases with increasing contextual complexity on *all* trials prior to the presentation of instructional signals and does not differentiate later success or failure at stopping. This is consistent with the idea that this activity is coincident with the 'setting-up of the rules/context of the task'. This feature is also interesting because gamma responses generally represent local cortical processing (e.g. (Swettenham et al., 2009)) rather than network processing, and early gamma activity in the pre-SMA has been seen in a conditional variant of the stop-signal task in a single subject with subdural electrodes over the medial frontal wall (Swann et al., 2012). Finally, in one of the few cases of gamma synchrony *between* regions that have been described, the gamma coherence between the primary motor cortex and STN has been shown to correlate with bradykinesia in PD patients (Litvak et al., 2012a). Therefore the role of gamma coherence in our patient cohort would be particularly interesting. One would predict that increased gamma coherence between the

motor cortex and STN would correlate with reaction time, whereas increased coherence between the pre-SMA and STN would correlate with SSRT.

7.3.3 Beta changes selective to stopping only

So what differentiated between successful and unsuccessful stopping? We found significantly increased post-stop/change signal beta activity during successful stopping in the pre-SMA, and left and right IFG, but *after* the median go reaction time. This response was significantly stronger for post-stop signal responses and almost absent in the change condition. This has two implications. Firstly, the relative absence of beta changes in successfully changed trials, suggests that it is not a *necessary* cortical response for stopping. Secondly, beta activity may play a specific role when the subject requires only a stop, and not a further response. So what role does cortical beta activity play in stopping? Stop-failures were associated with reduced beta and lengthened subsequent reaction times, suggesting that a drop in beta activity may be an error-monitoring signal or a signal to update the motor plan. If an error signal, there would be no change in beta after a successful stop - this is not the case, and therefore we favour the idea that after a successful stop, the current motor set is reinforced with a corresponding increase in beta. This is in keeping with the idea that increased beta activity maintains the current motor set (Engel and Fries, 2010; Jenkinson and Brown, 2011) after a correct response whilst reduced beta favours motor-reprogramming after a failed stop response. However, we did not find similar cortical responses to explain the behaviour in the change paradigm, suggesting that post-change responses may be modulated by a different mechanism (e.g. locked to the motor response rather than the change-signal).

7.3.4 Cortico-subcortical interactions during stopping – a 'proof-of-principle'

Our secondary aim was to characterise event-related network activity in patients with PD during a variant of the stop-signal task: the change-of-plan task. We were unable to include the complete analysis in the present thesis because of technical limitations; however our provisional analysis suggests that the analysis could be performed on the dataset we acquired. Using standard robust averaging techniques we were able to see dynamic changes in local alpha, beta and gamma synchronisation during the change-of-plan task. These responses were visible in the primary motor cortex and the STN itself. Prefrontal regions were not examined in this technical analysis, so that no *a priori* bias exists when

they are analysed in the future. Importantly we found that the signal-to-noise ratio of the MEG recording is adequate in spite of the ferromagnetic artefact from the extension wires. In addition, reassuringly no systematic differences in the pattern of induced responses can be seen between subjects recorded with different MEG systems (i.e. between Oxford and London). Finally, a spatial sensitivity analysis (filter correlation coefficients) suggested that source activity can be confidently extracted from the MEG data with enough resolution to separate the *a priori* regions of interest.

However, although induced responses were clear enough to be visible on an individual subject basis, their relationship to experimental triggers remains debatable without a more formal analysis. Such an analysis can be performed using the convolution model used in chapter 5 – this model is able to disambiguate responses to distinct experimental events. We demonstrated this in principle in chapter 6, where we discovered a change-signal locked theta response in the STN, similar to the cortical theta network seen in healthy controls. However, in this clinically and behaviourally heterogeneous cohort, further careful dissection of the data must be performed before any robust inferences can be made.

Finally, we were unable to perform adequate analysis of dynamic cortico-subthalamic coherence in this context because a convolution model for coherence does not yet exist. We hope to perform such analysis in the future after the appropriate methodology is developed and tested.

7.4 Summary

In summary we have developed a novel methodology for measuring cortico-basal ganglia activity in humans with PD (Litvak et al., 2010, 2011a). Such measurements are critical to understanding the pathophysiological basis of symptoms in PD. Resting data have demonstrated that two spatially and spectrally segregated networks exist between both the cortex and STN and the cortex and PPNR. We speculated that the alpha network is attentional, whilst the beta network is related to motor executive processing (Litvak et al., 2011a). In order to test the second of these speculations, in parallel with this thesis, we developed further analytical tools to characterise brain responses during dynamic executive motor tasks (Litvak et al., 2012b). Using these new techniques, in healthy controls, we detected a global, widespread theta/alpha cortical network related to the executive ability to stop an ongoing movement. We were further able to find specialised roles for both the right IFG and pre-SMA during stopping and were able to characterise the spectral properties and temporal profiles of local cortical synchronisation within these regions. However, a complete

analysis of similar behaviour in PD, and the cortico-subcortical interactions that underlie it, remains outstanding.

So what are the potential benefits of such research? The critical advance is that we have seen some evidence of segregation of functional systems – both according to frequency and topography. Future research will continue to interrogate these systems more closely to try to understand the precise functional roles that they subserve. This is important because currently, electrical interfaces with the brain such as DBS presumably have side-effects partially because they interfere with multiple functioning and malfunctioning systems. In the future, by varying different stimulation parameters, such as stimulation frequency and electrode location, one may be able to target isolated malfunctioning systems without interfering with functioning ones – in essence to be able to optimise the efficacy of treatment without causing side-effects.

8. References

Airaksinen K, Butorina A, Pekkonen E, Nurminen J, Taulu S, Ahonen A, Schnitzler A, Mäkelä JP (2012) Somatomotor mu rhythm amplitude correlates with rigidity during deep brain stimulation in Parkinsonian patients. Clin Neurophysiol 123:2010-7.

Akkal D, Dum RP, Strick PL (2007) Supplementary motor area and presupplementary motor area: targets of basal ganglia and cerebellar output. J Neurosci 27:10659–10673.

Alam M, Schwabe K, Krauss JK (2011) The pedunculopontine nucleus area: critical evaluation of interspecies differences relevant for its use as a target for deep brain stimulation. Brain 134:11–23.

Albin RL, Young AB, Penney JB (1989) The functional anatomy of basal ganglia disorders. Trends Neurosci 12:366–375.

Alegre M, Rodriguez-Oroz MC, Valencia M, Perez-Alcazar M, Guridi J, Iriarte J, Obeso JA, Artieda J (2010) Changes in subthalamic activity during movement observation in Parkinson's disease: is the mirror system mirrored in the basal ganglia? Clin Neurophysiol 121:414–425.

Alexander GE, Crutcher MD (1990) Functional architecture of basal ganglia circuits: neural substrates of parallel processing. Trends Neurosci 13:266–271.

Alexander GE, DeLong MR, Strick PL (1986) Parallel organization of functionally segregated circuits linking basal ganglia and cortex. Ann Rev Neurosci 9:357–381.

Allam MF, Campbell MJ, Hofman A, Del Castillo AS, Fernández-Crehuet Navajas R (2004) Smoking and Parkinson's disease: systematic review of prospective studies. Mov Dis 19:614–621.

Allcock LM, Rowan EN, Steen IN, Wesnes K, Kenny RA, Burn DJ (2009) Impaired attention predicts falling in Parkinson's disease. Parkinsonism Rel Dis 15:110–115.

Alonso-Frech F, Zamarbide I, Alegre M, Rodriguez-Oroz MC, Guridi J, Manrique M, Valencia M, Artieda J, Obeso JA (2006) Slow oscillatory activity and levodopa-induced dyskinesias in Parkinson's disease. Brain 129:1748–1757.

Amboni M, Cozzolino A, Longo K, Picillo M, Barone P (2008) Freezing of gait and executive functions in patients with Parkinson's disease. Mov Disord 23:395–400.

Amirnovin R, Williams ZM, Cosgrove GR, Eskandar EN (2004) Visually guided movements suppress subthalamic oscillations in Parkinson's disease patients. J Neurosci 24:11302–11306.

Androulidakis AG, Doyle LMF, Yarrow K, Litvak V, Gilbertson TP, Brown P (2007) Anticipatory changes in beta synchrony in the human corticospinal system and associated improvements in task performance. Eur J Neurosci 25:3758–3765.

Androulidakis AG, Mazzone P, Litvak V, Penny W, Dileone M, Gaynor LMFD, Tisch S, Di Lazzaro V, Brown P (2008) Oscillatory activity in the pedunculopontine area of patients with Parkinson's disease. Exp Neurology 211:59–66.

Anzak A, Tan H, Pogosyan A, Foltynie T (2012) Subthalamic nucleus activity optimizes maximal effort motor responses in Parkinson's disease. Brain 135:2766-78.

Apaydin H (2002) Parkinson Disease Neuropathology: Later-Developing Dementia and Loss of the Levodopa Response. Arch Neurology 59:102–112.

Aravamuthan BR, Stein JF, Aziz TZ (2008) The anatomy and localization of the pedunculopontine nucleus determined using probabilistic diffusion tractography. Brit J Neurosurg 22:S25–32.

Ardouin C, Voon V, Worbe Y, Abouazar N, Czernecki V, Hosseini H, Pelissolo A, Moro E, Lhommée E, Lang AE, Agid Y, Benabid A-L, Pollak P, Mallet L, Krack P (2006) Pathological gambling in Parkinson's disease improves on chronic subthalamic nucleus stimulation. Mov Disord 21:1941–1946.

Arnulf I, Ferraye M, Fraix V, Benabid AL, Chabardès S, Goetz L, Pollak P, Debû B (2010) Sleep induced by stimulation in the human pedunculopontine nucleus area. Ann Neurology 67:546–549.

Aron A, Dowson J (2003) Methylphenidate improves response inhibition in adults with attention-deficit/hyperactivity disorder. Biol Psychiatry 15:1465-8.

Aron AR, Behrens TE, Smith S, Frank MJ, Poldrack RA (2007a) Triangulating a cognitive control network using diffusion-weighted magnetic resonance imaging (MRI) and functional MRI. J Neurosci 27:3743–3752.

Aron AR, Durston S, Eagle DM, Logan GD, Stinear CM, Stuphorn V (2007b) Converging evidence for a fronto-basal-ganglia network for inhibitory control of action and cognition. J Neurosci 27:11860–11864.

Aron AR, Fletcher PC, Bullmore ET, Sahakian BJ, Robbins TW (2003) Stop-signal inhibition disrupted by damage to right inferior frontal gyrus in humans. Nat Neurosci 6:115–116.

Aron AR, Poldrack R a (2006) Cortical and subcortical contributions to Stop signal response inhibition: role of the subthalamic nucleus. J Neurosci 26:2424–2433.

Ascherio A (2004) Coffee Consumption, Gender, and Parkinson's Disease Mortality in the Cancer Prevention Study II Cohort: The Modifying Effects of Estrogen. Am J Epidemiol 160:977–984.

Asrress KN, Carpenter RH (2001) Saccadic countermanding: a comparison of central and peripheral stop signals. Vis Res 41:2645–2651.

Aziz TZ, Davies L, Stein J, France S (1998) The role of descending basal ganglia connections to the brain stem in parkinsonian akinesia. Brit J Neurosurg 12:245–249.

Baccala LA, Sameshima K (2001) Partial directed coherence: a new concept in neural structure determination. Biol Cybern 84:463–474.

Ballanger B, Lozano AM, Moro E, Van Eimeren T, Hamani C, Chen R, Cilia R, Houle S, Poon YY, Lang AE, Strafella AP (2009) Cerebral blood flow changes induced by pedunculopontine nucleus stimulation in patients with advanced Parkinson's disease: a [(15)O] H2O PET study. Hum Brain Mapp 30:3901–3909.

Band GP, Van der Molen MW, Logan GD (2003) Horse-race model simulations of the stop-signal procedure. Acta Psychol (Amst) 112:105–142.

Band GP, Van der Molen MW, Overtoom CC, Verbaten MN (2000) The ability to activate and inhibit speeded responses: separate developmental trends. J Exp Child Psychol 75:263–290.

Bar-Gad I, Morris G, Bergman H (2003) Information processing, dimensionality reduction and reinforcement learning in the basal ganglia. Prog Neurobiol 71:439–473.

Barnes GR, Hillebrand A, Fawcett IP, Singh KD (2004) Realistic spatial sampling for MEG beamformer images. Hum Brain Mapp 23:120–127.

Bartels AL, Leenders KL (2008) Brain imaging in patients with freezing of gait. Mov Disord 23:S461–7.

Bauer M, Kluge C, Bach D, Bradbury D, Heinze HJ, Dolan RJ, Driver J (2012) Cholinergic Enhancement of Visual Attention and Neural Oscillations in the Human Brain. Curr Biol 22: 397-402

Beck AT, Steer R a., Carbin MG (1988) Psychometric properties of the Beck Depression Inventory: Twenty-five years of evaluation. Clin Psychol Rev 8:77–100.

Bejjani BP, Dormont D, Pidoux B, Yelnik J, Damier P, Arnulf I, Bonnet AM, Marsault C, Agid Y, Philippon J, Cornu P (2000) Bilateral subthalamic stimulation for Parkinson's disease by using three-dimensional stereotactic magnetic resonance imaging and electrophysiological guidance. J Neurosurg 92:615–625.

Benabid AALL, Pollak P, Louveau A, Henry S, De Rougemont J, Rougemont DJ (1987) Combined (Thalamotomy and Stimulation) Stereotactic Surgery of the VIM Thalamic Nucleus for Bilateral Parkinson Disease. Appl Neurophysiol 50:344–346.

Benar CG, Gotman J (2002) Modeling of post-surgical brain and skull defects in the EEG inverse problem with the boundary element method. Clin Neurophysiol 113:48–56.

Bergman H, Wichmann T, Karmon B, DeLong MR (1994) The primate subthalamic nucleus. II. Neuronal activity in the MPTP model of parkinsonism. J Neurophysiol 72:507–520.

Bertran-Gonzalez J, Herve D, Girault JA, Valjent E (2010) What is the Degree of Segregation between Striatonigral and Striatopallidal Projections? Front Neuroanat 7:4.

Bevan MD, Booth PA, Eaton SA, Bolam JP (1998) Selective innervation of neostriatal interneurons by a subclass of neuron in the globus pallidus of the rat. J Neurosci 18:9438–9452.

Bissett PG, Logan GD (2011) Balancing cognitive demands: control adjustments in the stop-signal paradigm. J Exp Psychol Learn Mem Cog 37:392–404.

Bland BH, Oddie SD (2001) Theta band oscillation and synchrony in the hippocampal formation and associated structures: the case for its role in sensorimotor integration. Behav Brain Res 127:119–136.

Bloem BR, Hausdorff JM, Visser JE, Giladi N (2004) Falls and freezing of gait in Parkinson's disease: a review of two interconnected, episodic phenomena. Mov Disord 19:871–884.

Boehler CN, Appelbaum LG, Krebs RM, Hopf J-M, Woldorff MG (2012) The influence of different Stop-signal response time estimation procedures on behavior-behavior and brain-behavior correlations. Behav Brain Res 229:123–130.

Boeve BF et al. (2007) Pathophysiology of REM sleep behaviour disorder and relevance to neurodegenerative disease. Brain 130:2770–2788.

Bolam JP, Hanley JJ, Booth P a, Bevan MD (2000) Synaptic organisation of the basal ganglia. J Anat 196:527–542.

Botvinick MM (2007) Conflict monitoring and decision making: reconciling two perspectives on anterior cingulate function. Cog Affect Behav Neurosci 7:356–366.

Bower JH, Maraganore DM, McDonnell SK, Rocca WA (1999) Incidence and distribution of parkinsonism in Olmsted County, Minnesota, 1976-1990. Neurology 52:1214–20.

Braak H, Del K, Rüb U, Vos RAI De, Jansen ENH, Braak E (2003) Staging of brain pathology related to sporadic Parkinson's disease. Neurobiol Aging 24:197–211.

Braak H, Rüb U, Jansen Steur ENH, Del Tredici K, De Vos RAI (2005) Cognitive status correlates with neuropathologic stage in Parkinson disease. Neurology 64:1404–1410.

Bronstein JM et al. (2011) Deep brain stimulation for Parkinson disease: an expert consensus and review of key issues. Arch Neurol 68:165.

Brovelli A, Ding M, Ledberg A, Chen Y, Nakamura R, Bressler SL (2004) Beta oscillations in a large-scale sensorimotor cortical network: directional influences revealed by Granger causality. Proc Natl Acad Sci USA 101:9849–9854.

Brown JW, Braver TS (2005) Learned predictions of error likelihood in the anterior cingulate cortex. Science 307:1118–1121.

Brown P (2007) Abnormal oscillatory synchronisation in the motor system leads to impaired movement. Curr Opin Neurobiol 17:656–664.

Brown P, Eusebio A (2008) Paradoxes of functional neurosurgery: clues from basal ganglia recordings. Mov Disord 23:12–20.

Brown P, Mazzone P, Oliviero A, Altibrandi MG, Pilato F, Tonali PA, Di Lazzaro V (2004) Effects of stimulation of the subthalamic area on oscillatory pallidal activity in Parkinson's disease. Exp Neurol 188:480–490.

Brown P, Oliviero A, Mazzone P, Insola A, Tonali P, Di Lazzaro V (2001) Dopamine dependency of oscillations between subthalamic nucleus and pallidum in Parkinson's disease. J Neurosci 21:1033–1038.

Brown P, Williams D (2005) Basal ganglia local field potential activity: character and functional significance in the human. Clin Neurophysiol 116:2510–2519.

Brucke C, Kupsch A, Schneider G-HH, Hariz MI, Nuttin B, Kopp U, Kempf F, Trottenberg T, Doyle L, Chen CC, Yarrow K, Brown P, Kuhn AA, Brücke C, Kühn a a (2007) The subthalamic region is activated during valence-related emotional processing in patients with Parkinson's disease. Eur J Neurosci 26:767–774.

Burn DJ (2002) Beyond the iron mask: towards better recognition and treatment of depression associated with Parkinson's disease. Mov Disord 17:445–454.

Buzsaki G, Draguhn A (2004) Neuronal oscillations in cortical networks. Science 304:1926–1929.

Cabel DWJ, Armstrong IT, Reingold E, Munoz DP (2000) Control of saccade initiation in a countermanding task using visual and auditory stop signals. Exp Brain Res 133:431–441.

Cai W, George JS, Verbruggen F, Chambers CD, Aron AR (2012) The role of the right pre-supplementary motor area in stopping action: two studies with event-related transcranial magnetic stimulation. J Neurophysiol 108:380–389.

Cassidy M, Brown P (2003) Spectral phase estimates in the setting of multidirectional coupling. J Neurosci Methods 127:95–103.

Cassidy M, Mazzone P, Oliviero A, Insola A, Tonali P, Di Lazzaro V, Brown P (2002) Movement-related changes in synchronization in the human basal ganglia. Brain 125:1235–1246.

Cavanagh JF, Cohen MX, Allen JJB (2009) Prelude to and resolution of an error: EEG phase synchrony reveals cognitive control dynamics during action monitoring. J Neurosci 29:98–105.

Ceravolo R, Brusa L, Galati S, Volterrani D, Peppe A, Siciliano G, Pierantozzi M, Moschella V, Bonuccelli U, Stanzione P, Stefani A (2011) Low frequency stimulation of the nucleus tegmenti pedunculopontini increases cortical metabolism in parkinsonian patients. Eur J Neurol 18:842–849.

Chamberlain S (2006) Motor inhibition and cognitive flexibility in obsessive-compulsive disorder and trichotillomania. Am J Psychiatry. 163:1282-4

Chambers CD, Bellgrove M a, Stokes MG, Henderson TR, Garavan H, Robertson IH, Morris AP, Mattingley JB (2006) Executive "brake failure" following deactivation of human frontal lobe. J Cog Neurosci 18:444–455.

Chaudhuri KR, Healy DG, Schapira AH V (2006) Non-motor symptoms of Parkinson's disease: diagnosis and management. Lancet Neurol 5:235–245.

Chen CC, Kuhn AA, Hoffmann KT, Kupsch A, Schneider GH, Trottenberg T, Krauss JK, Wohrle JC, Bardinet E, Yelnik J, Brown P (2006a) Oscillatory pallidal local field potential activity correlates with involuntary EMG in dystonia. Neurology 66:418–420.

Chen CC, Litvak V, Gilbertson T, Kuhn A, Lu CS, Lee ST, Tsai CH, Tisch S, Limousin P, Hariz M, Brown P (2007) Excessive synchronization of basal ganglia neurons at 20 Hz slows movement in Parkinson's disease. Exp Neurol 205:214–221.

Chen J, Nakamura M, Kawamura T, Takahashi T, Nakahara D (2006b) Roles of pedunculopontine tegmental cholinergic receptors in brain stimulation reward in the rat. Psychopharmacology 184:514–522.

Chen Y (2006) Frequency decomposition of conditional Granger causality and application to multivariate neural field potential data. J Neurosci Methods 150:228-37.

Classen J, Schnitzler A (2010) What does the pedunculopontine nucleus do? Neurology 75:944–945.

Coizet V, Graham JH, Moss J, Bolam JP, Savasta M, McHaffie JG, Redgrave P, Overton PG (2009) Short-latency visual input to the subthalamic nucleus is provided by the midbrain superior colliculus. J Neurosci 29:5701–5709.

Colonius H, Arndt P (2001) A two-stage model for visual-auditory interaction in saccadic latencies. Percep Psychophysics 63:126–147.

Congdon E, Mumford J a, Cohen JR, Galvan A, Canli T, Poldrack R a (2012) Measurement and reliability of response inhibition. Front Psychol 3(37):1–10.

Cooper IS (1953) Ligation of the anterior choroidal artery for involuntary movements; parkinsonism. Psychiatr Q 27:317–319.

Cooper IS (1964) Surgical Treatment of Parkinsonism. New York.

Cooper JA, Sagar HJ, Tidswell P, Jordan N (1994) Slowed central processing in simple and go/no-go reaction time tasks in Parkinson's disease. Brain 117:517–529.

Coull JT (1998) Neural correlates of attention and arousal: insights from electrophysiology, functional neuroimaging and psychopharmacology. Prog Neurobiol 55:343–361.

Coull JT, Vidal F, Nazarian B, Macar F (2004) Functional anatomy of the attentional modulation of time estimation. Science 303:1506–1508.

Craik K (1947) Theory of the human operator in control systems. Brit J Psychol Gen Sect 38:56-61.

Crottaz-Herbette S, Anagnoson RT, Menon V (2004) Modality effects in verbal working memory: differential prefrontal and parietal responses to auditory and visual stimuli. Neuroimage 21:340–351.

Damasio H, Grabowski T, Frank R, Galaburda A, Damasio A (1994) The return of Phineas Gage: clues about the brain from the skull of a famous patient. Science 264:1102–1105.

Damier P (1999) The substantia nigra of the human brain: II. Patterns of loss of dopamine-containing neurons in Parkinson's disease. Brain 122:1437–1448.

De Jong R, Coles MG, Logan GD (1995) Strategies and mechanisms in nonselective and selective inhibitory motor control. J Exp Psychol Hum Percept Perform 21:498–511.

Delgado MR (2007) Reward-related responses in the human striatum. Ann N Y Acad Sci 1104:70–88.

DeLong MR (1990) Primate models of movement disorders of basal ganglia origin. Trends Neurosci 13:281–285.

Deuschl G et al. (2006) A randomized trial of deep-brain stimulation for Parkinson's disease. N Engl J Med 355:896–908.

Di Martino a, Scheres a, Margulies DS, Kelly AMC, Uddin LQ, Shehzad Z, Biswal B, Walters JR, Castellanos FX, Milham MP (2008) Functional connectivity of human striatum: a resting state FMRI study. Cereb Cortex 18:2735–2747.

DiFiglia M, Pasik P, Pasik T (1976) A Golgi study of neuronal types in the neostriatum of monkeys. Brain Res 114:245–256.

Dimoska A, Johnstone SJ (2008) Effects of varying stop-signal probability on ERPs in the stop-signal task: do they reflect variations in inhibitory processing or simply novelty effects? Biol Psychol 77:324–336.

Djamshidian A, Averbeck BB, Lees AJ, O'Sullivan SS (2011) Clinical aspects of impulsive compulsive behaviours in Parkinson's disease. J Neurol Sci 310:183–188.

Doyle LMF, Kühn a a, Hariz M, Kupsch A, Schneider G-HH, Brown P, Kuhn AA (2005) Levodopa-induced modulation of subthalamic beta oscillations during self-paced movements in patients with Parkinson's disease. Eur J Neurosci 21:1403–1412.

Draganski B, Kherif F, Klöppel S, Cook P a, Alexander DC, Parker GJM, Deichmann R, Ashburner J, Frackowiak RSJ, Kloppel S (2008) Evidence for segregated and integrative connectivity patterns in the human Basal Ganglia. J Neurosci 28:7143–7152.

Eagle DM, Baunez C (2010) Is there an inhibitory-response-control system in the rat? Evidence from anatomical and pharmacological studies of behavioral inhibition. Neurosci Biobehav Rev 34:50–72.

Eagle DM, Baunez C, Hutcheson DM, Lehmann O, Shah AP, Robbins TW (2008) Stop-signal reaction-time task performance: role of prefrontal cortex and subthalamic nucleus. Cereb cortex 18:178–188.

Elbaz A, Bower JH, Maraganore DM, Mcdonnell SK, Peterson BJ, Ahlskog JE, Schaid DJ, Rocca WA (2002) Risk tables for parkinsonism and Parkinson's disease. J Clin Epidemiol 55:25–31.

Elbaz A, Tranchant C (2007) Epidemiologic studies of environmental exposures in Parkinson's disease. J Neurol Sci 262:37–44.

Emeric EE, Brown JW, Boucher L, Carpenter RHS, Hanes DP, Harris R, Logan GD, Mashru RN, Paré M, Pouget P, Stuphorn V, Taylor TL, Schall JD (2007) Influence of history on saccade countermanding performance in humans and macaque monkeys. Vis Res 47:35–49.

Emeric EE, Brown JW, Leslie M, Pouget P, Stuphorn V, Schall JD (2008) Performance monitoring local field potentials in the medial frontal cortex of primates: anterior cingulate cortex. J Neurophysiol 99:759–772.

Engel AK, Fries P (2010) Beta-band oscillations--signalling the status quo? Curr Opin Neurobiol 20:156–165.

Eusebio A, Chen CC, Lu CS, Lee ST, Tsai CH, Limousin P, Hariz M, Brown P (2008) Effects of low-frequency stimulation of the subthalamic nucleus on movement in Parkinson's disease. Exp Neurol 209:125–130.

Eusebio A, Pogosyan A, Wang S, Averbeck B, Gaynor LD, Cantiniaux S, Witjas T, Limousin P, Azulay JP, Brown P (2009) Resonance in subthalamo-cortical circuits in Parkinson's disease. Brain 132:2139–2150.

Eusebio A, Thevathasan W, Doyle Gaynor L, Pogosyan A, Bye E, Foltynie T, Zrinzo L, Ashkan K, Aziz T, Brown P (2010) Deep brain stimulation can suppress pathological synchronisation in parkinsonian patients. J Neurol Neurosurg Psychiatry 82:569-73.

Evans AH (2005) Relationship between impulsive sensation seeking traits, smoking, alcohol and caffeine intake, and Parkinson's disease. J Neurol Neurosurg Psychiatry 77:317–321.

Evans AH, Lees AJ (2004) Dopamine dysregulation syndrome in Parkinson's disease. Curr Opin Neurol 17:393–398.

Evans JR, Mason SL, Williams-Gray CH, Foltynie T, Brayne C, Robbins TW, Barker RA (2011) The natural history of treated Parkinson's disease in an incident, community based cohort. J Neurol, Neurosurg, Psychiatry 82:1112–1118.

Everitt BJ, Dickinson A, Robbins TW (2001) The neuropsychological basis of addictive behaviour. Brain Res Brain Res Rev 36:129–138.

Factor SA (2008) The clinical spectrum of freezing of gait in atypical parkinsonism. Mov Disord 23:S431–8.

Feger J, Bevan M, Crossman AR (1994) The projections from the parafascicular thalamic nucleus to the subthalamic nucleus and the striatum arise from separate neuronal populations: a comparison with the corticostriatal and corticosubthalamic efferents in a retrograde fluorescent double-labell. Neuroscience 60:125–132.

Ferraye MU, Debû B, Fraix V, Goetz L, Ardouin C, Yelnik J, Henry-Lagrange C, Seigneuret E, Piallat B, Krack P, Le Bas J-F, Benabid a-L, Chabardès S, Pollak P (2010) Effects of pedunculopontine nucleus area stimulation on gait disorders in Parkinson's disease. Brain 133:205–214.

Ferrier D (1876) The Functions of the Brain. New York: Putnam's Sons.

Fischer T, Langner R, Birbaumer N, Brocke B (2008) Arousal and attention: self-chosen stimulation optimizes cortical excitability and minimizes compensatory effort. J Cog Neurosci 20:1443–1453.

Florin E, Gross J, Pfeifer J, Fink GR, Timmermann L (2010) The effect of filtering on Granger causality based multivariate causality measures. Neuroimage 50:577–588.

Fogelson N, Williams D, Tijssen M, Van Bruggen G, Speelman H, Brown P (2006) Different functional loops between cerebral cortex and the subthalmic area in Parkinson's disease. Cereb Cortex 16:64–75.

Follett KA et al. (2010) Pallidal versus subthalamic deep-brain stimulation for Parkinson's disease. N Engl J Med 362:2077–2091.

Foltynie T, Hariz MI (2010) Surgical management of Parkinson's disease. Exp Rev Neurotherapeutics 10:903–914.

Foltynie T, Zrinzo L, Martinez-Torres I, Tripoliti E, Petersen E, Holl E, Aviles-Olmos I, Jahanshahi M, Hariz M, Limousin P (2010) MRI-guided STN DBS in Parkinson's disease without microelectrode recording: efficacy and safety. J Neurol Neurosurg Psychiatry 82:358-63

Foncke EM, Bour LJ, Speelman JD, Koelman JH, Tijssen MA (2007) Local field potentials and oscillatory activity of the internal globus pallidus in myoclonus-dystonia. Mov Disord 22:369–376.

Fox SH, Katzenschlager R, Lim S-Y, Ravina B, Seppi K, Coelho M, Poewe W, Rascol O, Goetz CG, Sampaio C (2011) The Movement Disorder Society Evidence-Based Medicine Review Update: Treatments for the motor symptoms of Parkinson's disease. Mov Disord 26:S2–S41.

Frank MJ, Samanta J, Moustafa A a, Sherman SJ (2007) Hold your horses: impulsivity, deep brain stimulation, and medication in parkinsonism. Science 318:1309–1312.

Fries P (2005) A mechanism for cognitive dynamics: neuronal communication through neuronal coherence. Trends Cogn Sci 9:474–480.

Friston K (2002) Beyond phrenology: what can neuroimaging tell us about distributed circuitry? Ann RevNeurosci 25:221–250.

Friston K, Moran R, Seth AK (2012) Analysing connectivity with Granger causality and dynamic causal modelling. Curr Op Neurobiol *In Press*.

Friston KJ, Frith CD, Liddle PF, Frackowiak RS (1993) Functional connectivity: the principal-component analysis of large (PET) data sets. J Cereb Blood Flow Metab 13:5–14.

Friston KJ, Holmes a. PA, Worsley KJ, Poline J-P, Frith CD, Frackowiak RSJ (1994) Statistical parametric maps in functional imaging: A general linear approach. Hum Brain Mapp 2:189–210.

Fründ, I, Haenel, NV, Wichmann F (2011) Inference for psychometric functions in the presence of nonstationary behavior. J Vis 11:1–19.

Gagnon J, Bédard M, Fantini ML, Petit D, Panisset M (2002) REM sleep behavior disorder and REM sleep without atonia in Parkinson's disease. Neurology 59:585–589.

Garavan H, Hester R, Murphy K, Fassbender C, Kelly C (2006) Individual differences in the functional neuroanatomy of inhibitory control. Brain Res 1105:130–142.

Garcia-Rill E, Garciarill E (1991) The pedunculopontine nucleus. Prog Neurobiol 36:363–389.

Garcia-Rill E, Houser CR, Skinner RD, Smith W, Woodward DJ (1987) Locomotion-inducing sites in the vicinity of the pedunculopontine nucleus. Brain Res Bull 18:731–738.

Gatev P, Darbin O, Wichmann T (2006) Oscillations in the basal ganglia under normal conditions and in movement disorders. Mov Disord 21:1566–1577.

Gauggel S, Rieger M, Feghoff TA (2004) Inhibition of ongoing responses in patients with Parkinson's disease. J Neurol 75:539–545.

Gaynor LMFD, Kühn a a, Dileone M, Litvak V, Eusebio a, Pogosyan a, Androulidakis a G, Tisch S, Limousin P, Insola a, Mazzone P, Di Lazzaro V, Brown P (2008) Suppression of beta oscillations in the subthalamic nucleus following cortical stimulation in humans. Eur J Neurosci 28:1686–1695.

Gengler S, Mallot HA, Holscher C (2005) Inactivation of the rat dorsal striatum impairs performance in spatial tasks and alters hippocampal theta in the freely moving rat. Behav Brain Res 164:73–82.

Geweke J (1982) Measurement of linear dependence and feedback between multiple time series. J Am Stat Assoc 77:304-313.

Geweke J (1984) Measures of conditional linear dependence and feedback between time series. J Am Stat Assoc 79:907-915.

Giannicola G, Marceglia S, Rossi L, Mrakic-Sposta S, Rampini P, Tamma F, Cogiamanian F, Barbieri S, Priori A (2010) The effects of levodopa and ongoing deep brain stimulation on subthalamic beta oscillations in Parkinson's disease. Exp Neurol 226:120–127.

Giannicola G, Rosa M, Servello D, Menghetti C, Carrabba G, Pacchetti C, Zangaglia R, Cogiamanian F, Scelzo E, Marceglia S, Rossi L, Priori A (2012) Subthalamic local field potentials after seven-year deep brain stimulation in Parkinson's disease. Exp Neurol 237:312–317.

Gibb WRG, Lees AJ (1988) The relevance of the Lewy body to the pathogenesis of idiopathic Parkinson's disease. J Neurol Neurosurg Psychiatry 51:745–752.

Giladi N, Hausdorff JM (2006) The role of mental function in the pathogenesis of freezing of gait in Parkinson's disease. J Neurol Sci 248:173–176.

Giladi N, McDermott MP, Fahn S, Przedborski S, Jankovic J, Stern M, Tanner C (2001) Freezing of gait in PD: prospective assessment in the DATATOP cohort. Neurology 56:1712–1721.

Giladi N, Shabtai H, Simon E, Biran S, Tal J, Korczyn A (2000) Construction of freezing of gait questionnaire for patients with Parkinsonism. Parkinsonism Rel Dis 6:165–170.

Giladi N, Tal J, Azulay T, Rascol O, Brooks DJ, Melamed E, Oertel W, Poewe WH, Stocchi F, Tolosa E (2009) Validation of the freezing of gait questionnaire in patients with Parkinson's disease. Mov Disord 24:655–661.

Gilbert SJ, Simons JS, Frith CD, Burgess PW (2006) Performance-related activity in medial rostral prefrontal cortex (area 10) during low-demand tasks. J Exp Psychol Hum Percep Perform 32:45–58.

Giovannoni G, O'Sullivan JD, Turner K, Manson AJ, Lees AJ (2000) Hedonistic homeostatic dysregulation in patients with Parkinson's disease on dopamine replacement therapies. J Neurol Neurosurg Psychiatry 68:423–428.

Goetz CG et al. (2008) Movement Disorder Society-sponsored revision of the Unified Parkinson's Disease Rating Scale (MDS-UPDRS): scale presentation and clinimetric testing results. Mov Disord 23:2129–2170

Gomez-Gallego M, Fernandez-Villalba E, Fernandez-Barreiro A, Herrero MT (2007) Changes in the neuronal activity in the pedunculopontine nucleus in chronic MPTP-treated primates: an in situ hybridization study of cytochrome oxidase subunit I, choline acetyl transferase and substance P mRNA expression. J Neural Trans 114:319–326.

Gradinaru V, Mogri M, Thompson KR, Henderson JM, Deisseroth K (2009) Optical Deconstruction of Parkinsonian Neural Circuitry. Science 324:354–359.

Granger CWJ (1969) Investigating Causal Relations by Econometric Models and Cross-Spectral Methods. Econometrica 37:424-438.

Greffard S, Verny M, Bonnet A-M, Seilhean D, Hauw J-J, Duyckaerts C (2010) A stable proportion of Lewy body bearing neurons in the substantia nigra suggests a model in which the Lewy body causes neuronal death. Neurobiol Aging 31:99–103.

Grinband J, Savitskaya J, Wager TD, Teichert T, Ferrera VP, Hirsch J (2011) The dorsal medial frontal cortex is sensitive to time on task, not response conflict or error likelihood. NeuroImage 57:303–311.

Gross J, Kujala J, Hamalainen M, Timmermann L, Schnitzler a, Salmelin R (2001) Dynamic imaging of coherent sources: Studying neural interactions in the human brain. Proc Natl Acad Sci USA 98:694–699.

Gross RE, Krack P, Rodriguez-Oroz MC, Rezai AR, Benabid A-L (2006) Electrophysiological mapping for the implantation of deep brain stimulators for Parkinson's disease and tremor. Mov Disord 21:S259–83.

Haber SN (2003) The primate basal ganglia: parallel and integrative networks. J Chem Neuroanat 26:317–330.

Halliday G, Hely M, Reid W, Morris J (2008) The progression of pathology in longitudinally followed patients with Parkinson's disease. Acta Neuropathologica 115:409–415.

Hammond C, Bergman H, Brown P (2007) Pathological synchronization in Parkinson's disease: networks, models and treatments. Trends Neurosci 30:357–364.

Hammond C, Rouzaire-Dubois B, Féger J, Jackson A, Crossman AR (1983) Anatomical and electrophysiological studies on the reciprocal projections between the subthalamic nucleus and nucleus tegmenti pedunculopontinus in the rat. Neuroscience 9:41–52.

Hanakawa T, Katsumi Y, Fukuyama H, Honda M, Hayashi T, Kimura J, Shibasaki H (1999) Mechanisms underlying gait disturbance in Parkinson's disease: a single photon emission computed tomography study. Brain 122:1271–1282.

Hanes DP, Carpenter RH (1999) Countermanding saccades in humans. Vis Res 39:2777–2791.

Hanes DP, Patterson WF, Schall JD (1998) Role of Frontal Eye Fields in Countermanding Saccades: Visual, Movement, and Fixation Activity. J Neurophysiol 79:817–834..

Hariz MI, Krack P, Melvill R, Jorgensen J V, Hamel W, Hirabayashi H, Lenders M, Wesslen N, Tengvar M, Yousry TA (2003) A quick and universal method for stereotactic visualization of the subthalamic nucleus before and after implantation of deep brain stimulation electrodes. Stereotact Funct Neurosurg 80:96–101.

Hariz MI, Rehncrona S, Quinn NP, Speelman JD, Wensing C (2008) Multicenter study on deep brain stimulation in Parkinson's disease: an independent assessment of reported adverse events at 4 years. Mov Disord 23:416–421.

Harnishfeger K (1995) The development of cognitive inhibition. In Eds Brainerd J, Dempster FN. Interference and inhibition in cognition. Academic Press, London 175:201.

Hassler R (1938) Zur Pathologie der Paralysis agitans und des postenzephalitischen Parkinsonismus. J Psychol Neurol 48:387–476.

Hassler R, Riechert T, Mundinger F, Umbach W, Ganglberger JA (1958) Physiological observations in stereotaxic. Brain 83:337-350.

Hausdorff JM, Balash J, Giladi N (2003) Effects of cognitive challenge on gait variability in patients with Parkinson's disease. J Geriatric Psychiatry Neurol 16:53–58.

Hazrati LN, Parent A (1992) Projection from the deep cerebellar nuclei to the pedunculopontine nucleus in the squirrel monkey. Brain Res 585:267–271.

Healy DG et al. (2008) Phenotype, genotype, and worldwide genetic penetrance of LRRK2-associated Parkinson's disease: a case-control study. Lancet Neurol 7:583–590.

Helmich RC, Derikx LC, Bakker M, Scheeringa R, Bloem BR, Toni I (2010) Spatial remapping of cortico-striatal connectivity in Parkinson's disease. Cereb Cortex 20:1175–1186.

Hershey T, Campbell MC, Videen TO, Lugar HM, Weaver PM, Hartlein J, Karimi M, Tabbal SD, Perlmutter JS (2010) Mapping Go-No-Go performance within the subthalamic nucleus region. Brain 133:3625–3634.

Hikosaka O, Isoda M (2010) Switching from automatic to controlled behavior: cortico-basal ganglia mechanisms. Trends Cog Sci 14:154–161.

Hirschmann J, Özkurt TE, Butz M, Homburger M, Elben S, Hartmann CJ, Vesper J, Wojtecki L, Schnitzler A (2011) Distinct oscillatory STN-cortical loops revealed by simultaneous MEG and local field potential recordings in patients with Parkinson's disease. Neuroimage 55:1159–1168.

Holland PW, Welsch RE (1977) Robust regression using iteratively reweighted least-squares. Comm Stat Theory Methods 6:813–827.

Humphries MD, Stewart RD, Gurney KN (2006) A physiologically plausible model of action selection and oscillatory activity in the basal ganglia. J Neurosci 26:12921–12942.

Hurtig HI, Trojanowski JQ, Galvin J, Ewbank D, Schmidt ML, Lee VM-Y, Clark CM, Glosser G, Stern MB, Gollomp SM, Arnold SE (2000) Alpha-synuclein cortical Lewy bodies correlate with dementia in Parkinson's disease. Neurology 54:1916–1921.

Husain M, Parton A, Hodgson TL, Mort D, Rees G (2003) Self-control during response conflict by human supplementary eye field. Nat Neurosci 6:117–118.

Inase M, Tokuno H, Nambu A, Akazawa T, Takada M (1999) Corticostriatal and corticosubthalamic input zones from the presupplementary motor area in the macaque monkey: comparison with the input zones from the supplementary motor area. Brain Res 833:191–201.

Isoda M, Hikosaka O (2007) Switching from automatic to controlled action by monkey medial frontal cortex. Nat Neurosci 10:240–248.

Isoda M, Hikosaka O (2008) Role for subthalamic nucleus neurons in switching from automatic to controlled eye movement. J Neurosci 28:7209–7218.

Ito S, Stuphorn V, Brown JW, Schall JD (2003) Performance monitoring by the anterior cingulate cortex during saccade countermanding. Science 302:120–122.

James W (1890) The Principles of Psychology. New York , Henry Holt and Co.

Jankovic J (2008) Parkinson's disease: clinical features and diagnosis. Journal of neurology, neurosurgery, and psychiatry 79:368–376.

Jellinger K a, Attems J (2008) Prevalence and impact of vascular and Alzheimer pathologies in Lewy body disease. Acta Neuropathologica 115:427–436.

Jellinger KA (1999) Post mortem studies in Parkinson's disease--is it possible to detect brain areas for specific symptoms? J Neural Transm Suppl 56:1–29.

Jenkinson N, Brown P (2011) New insights into the relationship between dopamine, beta oscillations and motor function. Trends Neurosci 34:611–618.

Jersild A (1927) Mental set and shift. Arch Psychol. 14:81-89.

Jha A, Brown P (2010) Paradoxes in Parkinson's Disease and other Movement Disorders. In Kapur N, Pascual-Leone A, Ramachandran VS, editors. The Paradoxical Brain. Cambridge University Press.

Joundi R a, Jenkinson N, Brittain J-S, Aziz TZ, Brown P (2012) Driving oscillatory activity in the human cortex enhances motor performance. Curr Biol 22:403–407.

Kalaitzakis ME, Graeber MB, Gentleman SM, Pearce RKB (2008) Controversies over the staging of alpha-synuclein pathology in Parkinson's disease. Acta neuropathologica 116:125–8.

Kaminski MJ, Blinowska KJ (1991) A new method of the description of the information flow in the brain structures. Biol Cybern 65:203–210.

Karachi C, Grabli D, Bernard FA, Tandé D, Wattiez N, Belaid H, Bardinet E, Prigent A, Nothacker H-P, Hunot S, Hartmann A, Lehéricy S, Hirsch EC, François C, Curie M, Inserm F, Cnrs F (2010) Cholinergic mesencephalic neurons are involved in gait and postural disorders in Parkinson disease. J Clin Invest 120:2745–2754.

Katzenschlager R, Head J, Schrag A, Ben-Shlomo Y, Evans A, Lees AJ (2008) Fourteen-year final report of the randomized PDRG-UK trial comparing three initial treatments in PD. Neurology 71:474–480.

Kelly C, De Zubicaray G, Di Martino A, Copland D a, Reiss PT, Klein DF, Castellanos FX, Milham MP, McMahon K (2009) L-dopa modulates functional connectivity in striatal cognitive and motor networks: a double-blind placebo-controlled study. J Neurosci 29:7364–7378.

Kemp JM, Powell TP (1971) The connexions of the striatum and globus pallidus: synthesis and speculation. Philos Trans R Soc Lond B Biol Sci 262:441–457.

Kempster PA, Hurwitz B, Lees AJ (2007) A new look at James Parkinson's Essay on the Shaking Palsy. Neurology 69:482–485.

Kilner JM, Friston KJ (2010) Topological Inference for EEG and MEG. Ann App Stat 4:1272–1290.

Kingstone A, Klein RM (1993) Visual offsets facilitate saccadic latency: does predisengagement of visuospatial attention mediate this gap effect? J Exp Psychol Hum Percep Perform 19:1251–1265.

Kita H (2001) Neostriatal and globus pallidus stimulation induced inhibitory postsynaptic potentials in entopeduncular neurons in rat brain slice preparations. Neuroscience 105:871–879.

Klein C, Ziegler A (2011) From GWAS to clinical utility in Parkinson's disease. Lancet 377:613–614.

Kleiner-Fisman G, Herzog J, Fisman DN, Tamma F, Lyons KE, Pahwa R, Lang AE, Deuschl G (2006) Subthalamic nucleus deep brain stimulation: summary and meta-analysis of outcomes. Mov Disord 21:S290–304.

Knutson B, Cooper JC (2005) Functional magnetic resonance imaging of reward prediction. Curr Opin Neurol 18:411–417.

Kok A, Ramautar JR, De Ruiter MB, Band GPH, Ridderinkhof KR (2004) ERP components associated with successful and unsuccessful stopping in a stop-signal task. Psychophysiology 41:9–20.

Konishi S, Nakajima K, Uchida I, Kikyo H, Kameyama M, Miyashita Y (1999) Common inhibitory mechanism in human inferior prefrontal cortex revealed by event-related functional MRI. Brain 122:981–991.

Korzeniewska A, Manczak M, Kaminski M, Blinowska KJ, Kasicki S (2003) Determination of information flow direction among brain structures by a modified directed transfer function (dDTF) method. J Neurosci Methods 125:195–207.

Kramer AF, Humphrey DG, Larish JF, Logan GD, Strayer DL (1994) Aging and inhibition: Beyond a unitary view of inhibitory processing in attention. Psychol Aging 9:491–512.

Kuhn AA, Doyle L, Pogosyan A, Yarrow K, Kupsch A, Schneider GH, Hariz MI, Trottenberg T, Brown P (2006a) Modulation of beta oscillations in the subthalamic area during motor imagery in Parkinson's disease. Brain 129:695–706.

Kuhn AA, Kupsch A, Schneider GH, Brown P (2006b) Reduction in subthalamic 8-35 Hz oscillatory activity correlates with clinical improvement in Parkinson's disease. Eur J Neurosci 23:1956–1960.

Kuhn AA, Trottenberg T, Kivi A, Kupsch A, Schneider G-HH, Brown P, Kühn A a (2005) The relationship between local field potential and neuronal discharge in the subthalamic nucleus of patients with Parkinson's disease. Exp Neurol 194:212–220.

Kuhn AA, Williams D, Kupsch A, Limousin P, Hariz M, Schneider GH, Yarrow K, Brown P (2004) Event-related beta desynchronization in human subthalamic nucleus correlates with motor performance. Brain 127:735–746.

Kunzle H (1975) Bilateral projections from precentral motor cortex to the putamen and other parts of the basal ganglia. An autoradiographic study in Macaca fascicularis. Brain Res 88:195–209.

Kunzle H (1978) An autoradiographic analysis of the efferent connections from premotor and adjacent prefrontal regions (areas 6 and 9) in macaca fascicularis. Brain Behav Evol 15:185–234.

Kuss M, Planck M, Cybernetics B, Jäkel F, Wichmann FA (2005) Bayesian inference for psychometric functions. J Vis 27:478–492.

Lalo E, Thobois S, Sharott A, Polo G, Mertens P, Pogosyan A, Brown P (2008) Patterns of bidirectional communication between cortex and basal ganglia during movement in patients with Parkinson disease. J Neurosci 28:3008–3016.

Lambert C, Zrinzo L, Nagy Z, Lutti A, Hariz M, Foltynie T, Draganski B, Ashburner J, Frackowiak R (2011) Confirmation of functional zones within the human subthalamic nucleus: Patterns of connectivity and sub-parcellation using diffusion weighted imaging. Neuroimage 60:83-94.

Lamoth CJ, Van Deudekom FJ, Van Campen JP, Appels BA, De Vries OJ, Pijnappels M (2011) Gait stability and variability measures show effects of impaired cognition and dual tasking in frail people. J Neuroeng Rehab 8:2.

Langston J, Ballard P, Tetrud J, Irwin I (1983) Chronic Parkinsonism in humans due to a product of meperidine-analog synthesis. Science 219:979–980.

Lappin JS, Eriksen CW (1966) Reaction-Time Response. J Exp Psychol 72:805–811.

Laufs H, Krakow K, Sterzer P, Eger E, Beyerle A, Salek-Haddadi A, Kleinschmidt A (2003) Electroencephalographic signatures of attentional and cognitive default modes in spontaneous brain activity fluctuations at rest. Proc Natl Acad Sci USA 100:11053–11058.

Lavoie B, Parent A (1994) Pedunculopontine nucleus in the squirrel monkey: projections to the basal ganglia as revealed by anterograde tract-tracing methods. J Comp Neurol 344:210–231.

Lees AJ, Hardy J, Revesz T (2009) Parkinson's disease. Lancet 373:2055–2066.

Lehericy S, Ducros M, Krainik A, Francois C, Van de Moortele PF, Ugurbil K, Kim DS (2004) 3-D diffusion tensor axonal tracking shows distinct SMA and pre-SMA projections to the human striatum. Cereb Cortex 14:1302–1309.

Lehéricy S, Ducros M, Van de Moortele P-FF, Francois C, Thivard L, Poupon C, Swindale N, Ugurbil K, Kim D-SS, Lehericy S (2004) Diffusion tensor fiber tracking shows distinct corticostriatal circuits in humans. Ann Neurol 55:522–529.

Leotti LA, Wager TD (2010) Motivational influences on response inhibition measures. J Exp Psychol Hum Percept Perform 36:430–447.

Levesque JC, Parent A (2005) GABAergic interneurons in human subthalamic nucleus. Mov Disord 20:574–584.

Levitt H (1971) Transformed up-down methods in psychoacoustics. J Acoustic Soc Am 4:467–477.

Levy R, Ashby P, Hutchison WD, Lang AE, Lozano AM, Dostrovsky JO (2002) Dependence of subthalamic nucleus oscillations on movement and dopamine in Parkinson's disease. Brain 125:1196–1209.

Levy R, Hutchison WD, Lozano AM, Dostrovsky JO (2000) High-frequency synchronization of neuronal activity in the subthalamic nucleus of parkinsonian patients with limb tremor. J Neurosci 20:7766–7775.

Lhommée E et al. (2012) Subthalamic stimulation in Parkinson's disease: restoring the balance of motivated behaviours. Brain 135:1463–1477.

Li C-SR, Huang C, Constable RT, Sinha R (2006) Gender differences in the neural correlates of response inhibition during a stop signal task. Neuroimage 32:1918–1929.

Lijffijt M, Kenemans J (2005) A meta-analytic review of stopping performance in attention-deficit/hyperactivity disorder: Deficient inhibitory motor control? J Abnorm Psychol 114:216:22.

Lim AS, Lozano AM, Moro E, Hamani C, Hutchison WD, Dostrovsky JO, Lang AE, Wennberg R a, Murray BJ (2007) Characterization of REM-sleep associated ponto-geniculo-occipital waves in the human pons. Sleep 30:823–827.

Lim AS, Moro E, Lozano AM, Hamani C, Dostrovsky JO, Hutchison WD, Lang AE, Wennberg RA, Murray BJ (2009) Selective enhancement of rapid eye movement sleep by deep brain stimulation of the human pons. Ann Neurol 66:110–114.

Limousin P, Krack P, Pollak P, Benazzouz A, Ardouin C, Hoffmann D, Benabid AL (1998) Electrical stimulation of the subthalamic nucleus in advanced Parkinson's disease. The N Engl J Med 339:1105–1111.

Limousin P, Pollak P, Benazzouz A, Hoffmann D, Broussolle E, Perret JE, Benabid AL (1995) Bilateral subthalamic nucleus stimulation for severe Parkinson's disease. Mov Disord 10:672–674.

Limousin P, Speelman JD, Gielen F, Janssens M (1999) Multicentre European study of thalamic stimulation in parkinsonian and essential tremor. J Neurol Neurosurg Psych 66:289–296.

Litvak V, Eusebio A, Jha A, Oostenveld R, Barnes G, Foltynie T, Limousin P, Zrinzo L, Hariz MI, Friston K, Brown P (2012a) Movement-related changes in local and long-range synchronization in Parkinson's disease revealed by simultaneous magnetoencephalography and intracranial recordings. J Neurosci 32:10541–10553.

Litvak V, Eusebio A, Jha A, Oostenveld R, Barnes GR, Penny WD, Zrinzo L, Hariz MI, Limousin P, Friston KJ, Brown P (2010) Optimized beamforming for simultaneous MEG and intracranial local field potential recordings in deep brain stimulation patients. Neuroimage 50:1578–1588.

Litvak V, Jha A, Eusebio A, Oostenveld R, Foltynie T, Limousin P, Zrinzo L, Hariz MI, Friston K, Brown P (2011a) Resting oscillatory cortico-subthalamic connectivity in patients with Parkinson's disease. Brain 134:359–374.

Litvak V, Jha A, Flandin G, Friston K (2012b) Convolution models for induced electromagnetic responses. Neuroimage. 64:388-98.

Litvak V, Mattout J, Kiebel S, Phillips C, Henson R, Kilner J, Barnes G, Oostenveld R, Daunizeau J, Flandin G, Penny W, Friston K (2011b) EEG and MEG data analysis in SPM8. Comp Intell Neurosci 2011:852961.

Liu X, Griffin IC, Parkin SG, Miall RC, Rowe JG, Gregory RP, Scott RB, Aziz TZ, Stein JF (2002) Involvement of the medial pallidum in focal myoclonic dystonia: A clinical and neurophysiological case study. Mov Disord 17:346–353.

Logan G (1997) Impulsivity and inhibitory control. Psychol Sci 8:60-64.

Logan G, Burkell J (1986) Dependence and independence in responding to double stimulation: A comparison of stop, change, and dual-task paradigms. J Exp Psychol 12:549–563.

Logan GD, Cowan WB (1984) On the ability to inhibit thought and action: A theory of an act of control. Psychol Rev 91:295–32.

Logan GD, Irwin DE (2000) Don't look! Don't touch! Inhibitory control of eye and hand movements. Psychonomic Bull Rev 7:107–112.

Luria A (1961) The role of speech in the regulation of normal and abnormal behavior. Liveright Oxford, England 1-148.

Magill PJ, Bolam JP, Bevan MD (2001) Dopamine regulates the impact of the cerebral cortex on the subthalamic nucleus-globus pallidus network. Neuroscience 106:313–330.

Magill PJ, Pogosyan A, Sharott A, Csicsvari J, Bolam JP, Brown P (2006a) Changes in functional connectivity within the rat striatopallidal axis during global brain activation in vivo. J Neurosci 26:6318–6329.

Magill PJ, Sharott A, Bolam JP, Brown P (2006b) Delayed synchronization of activity in cortex and subthalamic nucleus following cortical stimulation in the rat. J Physiol 574:929–946.

Mallet L, Mesnage V, Houeto J-L, Pelissolo A, Yelnik J, Behar C, Gargiulo M, Welter M-L, Bonnet A-M, Pillon B, Cornu P, Dormont D, Pidoux B, Allilaire J-F, Agid Y (2002) Compulsions, Parkinson's disease, and stimulation. Lancet 360:1302–1304.

Mallet N, Pogosyan A, Sharott A, Csicsvari J, Bolam JP, Brown P, Magill PJ (2008) Disrupted dopamine transmission and the emergence of exaggerated beta oscillations in subthalamic nucleus and cerebral cortex. J Neurosci 28:4795–4806.

Manaye KF, Zweig R, Wu D, Hersh LB, De Lacalle S, Saper CB, German DC (1999) Quantification of cholinergic and select non-cholinergic mesopontine neuronal populations in the human brain. Neuroscience 89:759–770.

Marsden CD, Obeso J a. (1994) The functions of the basal ganglia and the paradox of stereotaxic surgery in Parkinson's disease. Brain 117:877–897.

Marsden JF, Limousin-Dowsey P, Ashby P, Pollak P, Brown P (2001) Subthalamic nucleus, sensorimotor cortex and muscle interrelationships in Parkinson's disease. Brain 124:378–388.

Martinez-Gonzalez C, Bolam JP, Mena-Segovia J (2011) Topographical organization of the pedunculopontine nucleus. Front Neuroanat 5:22.

Matamales M, Bertran-Gonzalez J, Salomon L, Degos B, Deniau JM, Valjent E, Herve D, Girault JA (2009) Striatal medium-sized spiny neurons: identification by nuclear staining and study of neuronal subpopulations in BAC transgenic mice. PLoS One 4:e4770.

Matsumura M, Nambu A, Yamaji Y, Watanabe K, Imai H, Inase M, Tokuno H, Takada M (2000) Organization of somatic motor inputs from the frontal lobe to the pedunculopontine tegmental nucleus in the macaque monkey. Neuroscience 98:97–110.

Mattout J, Henson RN, Friston KJ (2007) Canonical source reconstruction for MEG. Comput Intell Neurosci 67613.

Mayka M a, Corcos DM, Leurgans SE, Vaillancourt DE (2006) Three-dimensional locations and boundaries of motor and premotor cortices as defined by functional brain imaging: a meta-analysis. Neuroimage 31:1453–1474.

Mazzone P, Lozano A, Stanzione P, Galati S, Scarnati E, Peppe A, Stefani A (2005) Implantation of human pedunculopontine nucleus: a safe and clinically relevant target in Parkinson's disease. Neuroreport 16:1877–1881.

McClure SM, Berns GS, Montague PR (2003) Temporal prediction errors in a passive learning task activate human striatum. Neuron 38:339–346.

McGarry T, Franks IM (1997) A horse race between independent processes: evidence for a phantom point of no return in preparation of a speeded motor response. J Exp Psychol Human Percept Perform 23:1533–1542.

McHaffie JG, Stanford TR, Stein BE, Coizet V, Redgrave P (2005) Subcortical loops through the basal ganglia. Trends Neurosci 28:401–407.

Mena-Segovia J, Bolam JP, Magill PJ (2004) Pedunculopontine nucleus and basal ganglia: distant relatives or part of the same family? Trends Neurosci 27:585–588.

Mesulam MM, Geula C, Bothwell MA, Hersh LB (1989) Human reticular formation: cholinergic neurons of the pedunculopontine and laterodorsal tegmental nuclei and some cytochemical comparisons to forebrain cholinergic neurons. J Comparative Neurol 283:611–633.

Meyers R (1940) Surgical proceedure for the postencephalitic tremor, with notes on the physiology of premotor fibres. Arch Neurol Psychiatry:455–457.

Middleton F a, Strick PL (1996) The temporal lobe is a target of output from the basal ganglia. Proc Natl Acad Sci USA 93:8683–8687.

Middleton F a, Strick PL (2002) Basal-ganglia "projections" to the prefrontal cortex of the primate. Cereb Cortex 12:926–935.

Mink JW (1996) The basal ganglia: focused selection and inhibition of competing motor programs. Prog Neurobiol 50:381–425.

Mirabella G, Iaconelli S, Romanelli P, Modugno N, Lena F, Manfredi M, Cantore G (2011) Deep Brain Stimulation of Subthalamic Nuclei Affects Arm Response Inhibition In Parkinson's Patients. Cerebral cortex 22:1–9.

Mirabella G, Pani P, Paré M, Ferraina S (2006) Inhibitory control of reaching movements in humans. Exp Brain Res 174:240–255.

Miwa H, Fuwa T, Nishi K, Kondo T (2001) Subthalamo-pallido-striatal axis: a feedback system in the basal ganglia. Neuroreport 12:3795–3798.

Monakow KH, Akert K, Kunzle H (1978) Projections of the precentral motor cortex and other cortical areas of the frontal lobe to the subthalamic nucleus in the monkey. Exp Brain Res 33:395–403.

Monchi O, Petrides M, Strafella AP, Worsley KJ, Doyon J (2006) Functional role of the basal ganglia in the planning and execution of actions. Ann Neurol 59:257–264.

Montaurier C, Morio B, Bannier S, Derost P, Arnaud P, Brandolini-Bunlon M, Giraudet C, Boirie Y, Durif F (2007) Mechanisms of body weight gain in patients with Parkinson's disease after subthalamic stimulation. Brain 130:1808–1818.

Morein-Zamir S, Kingstone A (2006) Fixation offset and stop signal intensity effects on saccadic countermanding: a crossmodal investigation. Exp Brain Res 175:453–462.

Morein-Zamir S, Nagelkerke P, Chua R, Franks I, Kingstone A (2004) Inhibiting prepared and ongoing responses: is there more than one kind of stopping? Psychonomic Bull Rev 11:1034–1040.

Moro E, Hamani C, Poon Y-Y, Al-Khairallah T, Dostrovsky JO, Hutchison WD, Lozano AM (2010) Unilateral pedunculopontine stimulation improves falls in Parkinson's disease. Brain 133:215–224.

Moruzzi G, Magoun HW (1949) Brain stem reticular formation and activation of the EEG. Electroencephalogr Clin Neurophysiol 1:455–473.

Mundinger F (1977) [New stereotactic treatment of spasmodic torticollis with a brain stimulation system (author's transl)]. Medizinische Klinik 72:1982–1986.

Munoz DP, Wurtz RH (1993) Fixation cells in monkey superior colliculus. I. Characteristics of cell discharge. J Neurophysiol 70:559–575.

Murer MG, Tseng KY, Kasanetz F, Belluscio M, Riquelme LA (2002) Brain oscillations, medium spiny neurons, and dopamine. Cell Mol Neurobiol 22:611–632.

Nachev P, Kennard C, Husain M (2008) Functional role of the supplementary and pre-supplementary motor areas. Nat Rev Neurosci 9:856–869.

Nachev P, Wydell H, O'neill K, Husain M, Kennard C (2007) The role of the pre-supplementary motor area in the control of action. Neuroimage 36:T155–63.

Nalls MA, Plagnol V, Hernandez DG, Sharma M, Sheerin U-M, Saad M, Simón-Sánchez J, Schulte C, Lesage S, Sveinbjörnsdóttir S, Stefánsson K, Martinez M, Hardy J, Heutink P, Brice A, Gasser T, Singleton AB, Wood NW (2011) Imputation of sequence variants for identification of genetic risks for Parkinson's disease: a meta-analysis of genome-wide association studies. Lancet 377:641–649.

Nambu A (2008) Seven problems on the basal ganglia. Curr Opin Neurobiol 18:595–604.

Nambu A (2011) Somatotopic organization of the primate Basal Ganglia. Front Neuroanat 5:26.

Nambu A, Takada M, Inase M, Tokuno H (1996) Dual somatotopical representations in the primate subthalamic nucleus: evidence for ordered but reversed body-map transformations from the primary motor cortex and the supplementary motor area. J Neurosci 16:2671–2683.

Nambu A, Tokuno H, Inase M, Takada M (1997) Corticosubthalamic input zones from forelimb representations of the dorsal and ventral divisions of the premotor cortex in the macaque monkey: comparison with the input zones from the primary motor cortex and the supplementary motor area. Neurosci Lett 239:13–16.

Nambu A, Tokuno H, Takada M (2002) Functional significance of the cortico-subthalamo-pallidal "hyperdirect" pathway. Neurosci Res 43:111–117.

Nandi D, Aziz TZ, Giladi N, Winter J, Stein JF (2002) Reversal of akinesia in experimental parkinsonism by GABA antagonist microinjections in the pedunculopontine nucleus. Brain 125:2418–2430.

Nelson MJ, Boucher L, Logan GD, Palmeri TJ, Schall JD, Oucher LEB, Ogan GODL, Almeri THJP, Chall JEDS (2010) Nonindependent and nonstationary response times in stopping and stepping saccade tasks. Attention Percept Psychophys 72:1913–1929.

Neumann W-J, Huebl J, Brücke C, Ruiz MH, Kupsch A, Schneider G-H, Kühn AA (2012) Enhanced low-frequency oscillatory activity of the subthalamic nucleus in a patient with dystonia. Mov Disord 27:1063–1066.

Nigbur R, Ivanova G, Stürmer B (2011) Theta power as a marker for cognitive interference. Clin Neurophysiol 122:2185–2194.

Nolte G, Bai O, Wheaton L, Mari Z, Vorbach S, Hallett M (2004) Identifying true brain interaction from EEG data using the imaginary part of coherency. Clin Neurophysiol 115:2292–2307.

Norton ABW, Jo YS, Clark EW, Taylor C a, Mizumori SJY (2011) Independent neural coding of reward and movement by pedunculopontine tegmental nucleus neurons in freely navigating rats. Eur J Neurosci 33:1885–1896.

Nutt JG, Bloem BR, Giladi N, Hallett M, Horak FB, Nieuwboer A (2011) Freezing of gait: moving forward on a mysterious clinical phenomenon. Lancet Neurol 10:734–744.

Obeso I, Wilkinson L, Casabona E, Bringas ML, Álvarez M, Álvarez L, Pavón N, Rodríguez-Oroz M-C, Macías R, Obeso J a, Jahanshahi M (2011a) Deficits in inhibitory control and conflict resolution on cognitive and motor tasks in Parkinson's disease. Exp Brain Res 212:371–384.

Obeso I, Wilkinson L, Jahanshahi M (2011b) Levodopa medication does not influence motor inhibition or conflict resolution in a conditional stop-signal task in Parkinson's disease. Exp Brain Res 213:435–445.

Okun MS, Fernandez HH, Wu SS, Kirsch-Darrow L, Bowers D, Bova F, Suelter M, Jacobson CE, Wang X, Gordon CW, Zeilman P, Romrell J, Martin P, Ward H, Rodriguez RL,

Foote KD (2009) Cognition and mood in Parkinson's disease in subthalamic nucleus versus globus pallidus interna deep brain stimulation: the COMPARE trial. Ann Neurol 65:586–595.

Olson EJ, Boeve BF, Silber MH (2000) Rapid eye movement sleep behaviour disorder: demographic, clinical and laboratory findings in 93 cases. Brain 123:331–339.

Olszewski J, Baxter D (1982) Cytoarchitecture of the human brainstem. 2nd Edition. Basel. Karger.

Oostenveld R, Fries P, Maris E, Schoffelen J-M (2011) FieldTrip: Open source software for advanced analysis of MEG, EEG, and invasive electrophysiological data. Comput Intell Neurosci 2011:156869.

Oostenveld R, Oostendorp TF (2002) Validating the boundary element method for forward and inverse EEG computations in the presence of a hole in the skull. Hum Brain Mapp 17:179–192.

Ossmann JM, Mulligan NW (2003) Inhibition and attention deficit hyperactivity disorder in adults. Am J Psychol 116:35–50.

Oswal A, Brown P, Litvak V (2012) Movement related dynamics of subthalmo-cortical alpha connectivity in Parkinson's Disease. Neuroimage *In Press.*

Ouchi Y, Kanno T, Okada H, Yoshikawa E, Futatsubashi M, Nobezawa S, Torizuka T, Tanaka K (2001) Changes in dopamine availability in the nigrostriatal and mesocortical dopaminergic systems by gait in Parkinson's disease. Brain 124:784–792.

Ozyurt J, Colonius H, Arndt PA (2003) Countermanding saccades: evidence against independent processing of go and stop signals. Percept Psychophys 65:420–428.

Pahapill P a. (2000) The pedunculopontine nucleus and Parkinson's disease. Brain 123:1767–1783.

Palva S, Palva JM (2007) New vistas for alpha-frequency band oscillations. Trends Neurosci 30:150–158.

Parent A, Hazrati LN (1995) Functional anatomy of the basal ganglia. II. The place of subthalamic nucleus and external pallidum in basal ganglia circuitry. Brain Res Brain Res Rev 20:128–154.

Parent M, Lévesque M, Parent A (2001) Two types of projection neurons in the internal pallidum of primates: single-axon tracing and three-dimensional reconstruction. J Comparative Neurol 439:162–175.

Parkinson J (1817) An Essay on the Shaking Palsy. London: Sherwood, Neely and Jones.

Parkkinen L, Kauppinen T, Pirttilä T, Autere JM, Alafuzoff I (2005) Alpha-synuclein pathology does not predict extrapyramidal symptoms or dementia. Ann Neurol 57:82–91.

Parkkonen L, Fujiki N, Makela JP (2009) Sources of auditory brainstem responses revisited: contribution by magnetoencephalography. Hum Brain Mapp 30:1772–1782.

Parthasarathy HB, Graybiel AM (1997) Cortically driven immediate-early gene expression reflects modular influence of sensorimotor cortex on identified striatal neurons in the squirrel monkey. J Neurosci 17:2477–2491.

Paré M, Hanes DP (2003) Controlled movement processing: superior colliculus activity associated with countermanded saccades. J Neurosci 23:6480–6489.

Penades R, Catalan R, Rubia K (2007) Impaired response inhibition in obsessive compulsive disorder. Eur Psychiatry 22:404-10.

Penny WD, Roberts SJ (2002) Bayesian multivariate autoregressive models with structured priors. IEEE Proc Vis Image Signal Proc 149:33–41.

Pereira EA, Muthusamy KA, De Pennington N, Joint CA, Aziz TZ (2008) Deep brain stimulation of the pedunculopontine nucleus in Parkinson's disease. Preliminary experience at Oxford. Brit J Neurosurg 22:S41–4.

Plaha P, Gill SS (2005) Bilateral deep brain stimulation of the pedunculopontine nucleus for Parkinson's disease. Neuroreport 16:1883–1887.

Pogosyan A, Gaynor LD, Eusebio A, Brown P (2009) Boosting cortical activity at Beta-band frequencies slows movement in humans. Curr Biol 19:1637–1641.

Pogosyan A, Yoshida F, Chen CC, Martinez-Torres I, Foltynie T, Limousin P, Zrinzo L, Hariz MI, Brown P (2010) Parkinsonian impairment correlates with spatially extensive subthalamic oscillatory synchronization. Neuroscience 171:245–257.

Pollok B, Makhloufi H, Butz M, Gross J, Timmermann L, Wojtecki L, Schnitzler A (2009) Levodopa affects functional brain networks in Parkinsonian resting tremor. Mov Disord 24:91–98.

Ponsen MM, Stoffers D, Booij J, Van Eck-Smit BLF, Wolters EC, Berendse HW (2004) Idiopathic hyposmia as a preclinical sign of Parkinson's disease. Ann Neurol 56:173–181.

Portas CM, Rees G, Howseman AM, Josephs O, Turner R, Frith CD (1998) A specific role for the thalamus in mediating the interaction of attention and arousal in humans. J Neurosci 18:8979–8989.

Postle BR, D'Esposito M (2003) Spatial working memory activity of the caudate nucleus is sensitive to frame of reference. Cogn Affect Behav Neurosci 3:133–144.

Postuma RB, Dagher A (2006) Basal ganglia functional connectivity based on a meta-analysis of 126 positron emission tomography and functional magnetic resonance imaging publications. Cereb Cortex 16:1508–1521.

Postuma RB, Gagnon JF, Montplaisir J (2010) Clinical prediction of Parkinson's disease: planning for the age of neuroprotection. J Neurol Neurosurg Psychiatry 81:1008–1013.

Poulopoulos M, Levy O a, Alcalay RN (2012) The neuropathology of genetic Parkinson's disease. Mov Disord 27:831–842.

Priori A, Foffani G, Pesenti A, Tamma F, Bianchi AM, Pellegrini M, Locatelli M, Moxon KA, Villani RM (2004) Rhythm-specific pharmacological modulation of subthalamic activity in Parkinson's disease. Exp Neurol 189:369–379.

Priyadarshi a, Khuder S a, Schaub E a, Priyadarshi SS (2001) Environmental risk factors and Parkinson's disease: a metaanalysis. Environmental Res 86:122–127.

Rappelsberger P, Petsche H (1988) Probability mapping: power and coherence analyses of cognitive processes. Brain Topogr 1:46–54.

Ratcliff R, Smith PL (2004) A comparison of sequential sampling models for two-choice reaction time. Psychol Rev 111:333–367.

Ray NJ, Brittain J-S, Holland P, Joundi R a, Stein J, Aziz TZ, Jenkinson N (2011) The role of the subthalamic nucleus in response inhibition: Evidence from local field potential recordings in the human subthalamic nucleus. Neuroimage 60:271–278.

Ray NJ, Jenkinson N, Brittain J, Holland P, Joint C, Nandi D, Bain PG, Yousif N, Green a, Stein JS, Aziz TZ (2009) The role of the subthalamic nucleus in response inhibition: evidence from deep brain stimulation for Parkinson's disease. Neuropsychologia 47:2828–2834.

Redgrave P, Prescott TJ, Gurney K (1999) The basal ganglia: a vertebrate solution to the selection problem? Neuroscience 89:1009–1023.

Redgrave P, Rodriguez M, Smith Y, Rodriguez-Oroz MC, Lehericy S, Bergman H, Agid Y, DeLong MR, Obeso JA (2010) Goal-directed and habitual control in the basal ganglia: implications for Parkinson's disease. Nat Rev Neurosci 11:760–772.

Reuter-Lorenz PA, Hughes HC, Fendrich R (1991) The reduction of saccadic latency by prior offset of the fixation point: an analysis of the gap effect. Percept Psychophys 49:167–175.

Rezai AR, Machado AG, Deogaonkar M, Azmi H, Kubu C, Boulis NM (2008) Surgery for movement disorders. Neurosurgery 62 809:38.

Ridderinkhof KR, Band GPH, Logan GD (1999) A study of adaptive behavior : effects of age and irrelevant information on the ability to inhibit one's actions. Acta Psychologica 101:315–337.

Rieger M, Gauggel S (1999) Inhibitory after-effects in the stop signal paradigm. Brit J Psychol 90:509–518.

Rieger M, Gauggel S, Burmeister K (2003) Inhibition of ongoing responses following frontal, nonfrontal, and basal ganglia lesions. Neuropsychology 17:272–282.

Rocca WA, Bower JH, Mcdonnell SK (2001) Time trends in the incidence of parkinsonism in Olmsted County. Neurology 57:462-7.

Rodriguez-Oroz MC, Lopez-Azcarate J, Garcia-Garcia D, Alegre M, Toledo J, Valencia M, Guridi J, Artieda J, Obeso JA, López-Azcárate J (2011) Involvement of the subthalamic nucleus in impulse control disorders associated with Parkinson's disease. Brain 134:36–49.

Romigi A, Placidi F, Peppe A, Pierantozzi M, Izzi F, Brusa L, Galati S, Moschella V, Marciani MG, Mazzone P, Stanzione P, Stefani A (2008) Pedunculopontine nucleus stimulation influences REM sleep in Parkinson's disease. Eur J Neurol 15:e64–5.

Sato F, Parent M, Levesque M, Parent A (2000) Axonal branching pattern of neurons of the subthalamic nucleus in primates. J Comp Neurol 424:142–152.

Scangos KW, Stuphorn V (2010) Medial frontal cortex motivates but does not control movement initiation in the countermanding task. J Neurosci 30:1968–1982.

Schachar RJ, Chen S, Logan GD, Ornstein TJ, Crosbie J, Ickowicz A, Pakulak A (2004) Evidence for an Error Monitoring Deficit in Attention Deficit Hyperactivity Disorder. J Abn Child Psychol 32:285–293.

Schmajuk M, Liotti M, Busse L, Woldorff MG (2006) Electrophysiological activity underlying inhibitory control processes in normal adults. Neuropsychologia 44:384–395.

Schneidman E, Berry 2nd MJ, Segev R, Bialek W (2006) Weak pairwise correlations imply strongly correlated network states in a neural population. Nature 440:1007–1012.

Schnitzler A, Munks C, Butz M, Timmermann L, Gross J (2009) Synchronized brain network associated with essential tremor as revealed by magnetoencephalography. Mov Disord 24:1629–1635.

Schofield BR, Motts SD (2009) Projections from auditory cortex to cholinergic cells in the midbrain tegmentum of guinea pigs. Brain Res Bull 80:163–170.

Schofield BR, Motts SD, Mellott JG (2011) Cholinergic cells of the pontomesencephalic tegmentum: Connections with auditory structures from cochlear nucleus to cortex. Hear Res 279:85-95.

Schrag A (2000) What contributes to quality of life in patients with Parkinson's disease? J Neurol Neurosurg Psych 69:308–312.

Schultz W (1997) Dopamine neurons and their role in reward mechanisms. Curr Opin Neurobiol 7:191–197.

Selikhova M, Williams DR, Kempster PA, Holton JL, Revesz T, Lees AJ (2009) A clinico-pathological study of subtypes in Parkinson's disease. Brain 132:2947–2957.

Semba K, Fibiger HC (1992) Afferent connections of the laterodorsal and the pedunculopontine tegmental nuclei in the rat: a retro- and antero-grade transport and immunohistochemical study. J Comparative Neurol 323:387–410.

Seppi K, Weintraub D, Coelho M, Perez-Lloret S, Fox SH, Katzenschlager R, Hametner E-M, Poewe W, Rascol O, Goetz CG, Sampaio C (2011) The Movement Disorder Society Evidence-Based Medicine Review Update: Treatments for the non-motor symptoms of Parkinson's disease. Mov Disord 26:S42–80.

Sesack SR, Deutch AY, Roth RH, Bunney BS (1989) Topographical organization of the efferent projections of the medial prefrontal cortex in the rat: an anterograde tract-tracing study with Phaseolus vulgaris leucoagglutinin. J Comparative Neurol 290:213–242.

Sharott A, Magill PJ, Bolam JP, Brown P (2005a) Directional analysis of coherent oscillatory field potentials in the cerebral cortex and basal ganglia of the rat. J Physiol 562:951–963.

Sharott A, Magill PJ, Harnack D, Kupsch A, Meissner W, Brown P (2005b) Dopamine depletion increases the power and coherence of beta-oscillations in the cerebral cortex and subthalamic nucleus of the awake rat. Eur J Neurosci 21:1413–1422.

Shen B, Nadkarni M, Zappulla RA (1999) Spectral modulation of cortical connections measured by EEG coherence in humans. Clin Neurophysiol 110:115–125.

Sherrington C (1925) Remarks on some aspects of reflex inhibition. Proc Royal Soc Lond 97:519-545.

Silberstein P, Kuhn AA, Kupsch A, Trottenberg T, Krauss JK, Wohrle JC, Mazzone P, Insola A, Di Lazzaro V, Oliviero A, Aziz T, Brown P (2003) Patterning of globus pallidus local field potentials differs between Parkinson's disease and dystonia. Brain 126:2597–2608.

Silberstein P, Pogosyan A, Kuhn AA, Hotton G, Tisch S, Kupsch A, Dowsey-Limousin P, Hariz MI, Brown P (2005) Cortico-cortical coupling in Parkinson's disease and its modulation by therapy. Brain 128:1277–1291.

Skinner RD, Kinjo N, Henderson V, Garcia-Rill E (1990) Locomotor projections from the pedunculopontine nucleus to the spinal cord. Neuroreport 1:183–186.

Smeding HMM, Goudriaan AE, Foncke EMJ, Schuurman PR, Speelman JD, Schmand B (2007) Pathological gambling after bilateral subthalamic nucleus stimulation in Parkinson disease. J Neurol Neurosurg Psychiatry 78:517–519.

Smith SM, Jenkinson M, Woolrich MW, Beckmann CF, Behrens TEJ, Johansen-Berg H, Bannister PR, De Luca M, Drobnjak I, Flitney DE, Niazy RK, Saunders J, Vickers J, Zhang Y, De Stefano N, Brady JM, Matthews PM (2004) Advances in functional and structural MR image analysis and implementation as FSL. NeuroImage 23:S208–19.

Smith Y, Bevan MD, Shink E, Bolam JP (1998) Microcircuitry of the direct and indirect pathways of the basal ganglia. Neuroscience 86:353–387.

Snijders AH, Leunissen I, Bakker M, Overeem S, Helmich RC, Bloem BR, Toni I (2011) Gait-related cerebral alterations in patients with Parkinson's disease with freezing of gait. Brain 134:59–72.

Souques M (1921) Rapport sur les syndrome parkinsoniens. Séance du 3-4 Juin 1921. Rev Neurol 1:534.

Spiegel EA, Wycis HT, Freed H (1952) Stereoencephalotomy and related proceedures. J Am Med Assoc 148:446–451.

Spillantini MG, Schmidt ML, Lee VM, Tojanowski J, Jakes R, Goedert M (1997) Alpha Synuclein in Lewy bodies. Nature 388:839–840.

Springer S, Giladi N, Peretz C, Yogev G, Simon ES, Hausdorff JM (2006) Dual-tasking effects on gait variability: the role of aging, falls, and executive function. Mov Disord 21:950–957.

St George RJ, Nutt JG, Burchiel KJ, Horak FB (2010) A meta-regression of the long-term effects of deep brain stimulation on balance and gait in PD. Neurology 75:1292–1299.

Stahl J, Gibbons H (2007) Dynamics of response-conflict monitoring and individual differences in response control and behavioral control: an electrophysiological investigation using a stop-signal task. Clin Neurophysiol 118:581–596.

Stefani a., Lozano a., Stanzione P, Mazzone P (2007a) Targeting human PPN: few patients, numerous disputes. Brain 130:e80–e80.

Stefani A, Lozano AM, Peppe A, Stanzione P, Galati S, Tropepi D, Pierantozzi M, Brusa L, Scarnati E, Mazzone P (2007b) Bilateral deep brain stimulation of the pedunculopontine and subthalamic nuclei in severe Parkinson's disease. Brain 130:1596–1607.

Stern EA, Jaeger D, Wilson CJ (1998) Membrane potential synchrony of simultaneously recorded striatal spiny neurons in vivo. Nature 394:475–478.

Swann N, Tandon N, Canolty R, Ellmore TM, McEvoy LK, Dreyer S, DiSano M, Aron AR (2009) Intracranial EEG reveals a time- and frequency-specific role for the right inferior frontal gyrus and primary motor cortex in stopping initiated responses. J Neurosci 29:12675–12685.

Swann NC, Cai W, Conner CR, Pieters TA, Claffey MP, George JS, Aron AR, Tandon N (2012) Roles for the pre-supplementary motor area and the right inferior frontal gyrus in stopping action: electrophysiological responses and functional and structural connectivity. Neuroimage 59:2860–2870.

Swettenham JB, Muthukumaraswamy SD, Singh KD (2009) Spectral properties of induced and evoked gamma oscillations in human early visual cortex to moving and stationary stimuli. J Neurophysiol 102:1241–1253.

Tang JK, Mahant N, Cunic D, Chen R, Moro E, Lang AE, Lozano AM, Hutchison WD, Dostrovsky JO (2007) Changes in cortical and pallidal oscillatory activity during the execution of a sensory trick in patients with cervical dystonia. Exp Neurol 204:845–848.

Telford C (1931) The refractory phase of voluntary and associative responses. J Exp Psychol 14:1-36.

Teo C, Rasco L, al-Mefty K, Skinner RD, Boop FA, Garcia-Rill E (1997) Decreased habituation of midlatency auditory evoked responses in Parkinson's disease. Mov Disord 12:655–664.

Teo C, Rasco L, Skinner RD, Garcia-Rill E (1998) Disinhibition of the sleep state-dependent p1 potential in Parkinson's disease-improvement after pallidotomy. Sleep Res Online 1:62–70.

Thatcher RW, Krause PJ, Hrybyk M (1986) Cortico-cortical associations and EEG coherence: a two-compartmental model. Electroencephalogr Clin Neurophysiol 64:123–143.

Thevathasan W, Gregory R (2010) Deep brain stimulation for movement disorders. Pract Neurol 10:16–26.

Thevathasan W, Pogosyan A, Hyam J a, Jenkinson N, Bogdanovic M, Coyne TJ, Silburn P a, Aziz TZ, Brown P (2011) A block to pre-prepared movement in gait freezing, relieved by pedunculopontine nucleus stimulation. Brain 134:2085–2095.

Thevathasan W, Pogosyan A, Hyam JA, Jenkinson N, Foltynie T, Limousin P, Bogdanovic M, Zrinzo L, Green AL, Aziz TZ, Brown P (2012) Alpha oscillations in the pedunculopontine nucleus correlate with gait performance in parkinsonism. Brain 135:148–160.

Thomson DJ (1982) Spectrum Estimation and Harmonic-Analysis. Proc IEEE 70:1055–1096.

Timmermann L, Gross J, Dirks M, Volkmann J, Freund HJ, Schnitzler A (2003) The cerebral oscillatory network of parkinsonian resting tremor. Brain 126:199–212.

Timmermann L, Wojtecki L, Gross J, Lehrke R, Voges J, Maarouf M, Treuer H, Sturm V, Schnitzler A (2004) Ten-Hertz stimulation of subthalamic nucleus deteriorates motor symptoms in Parkinson's disease. Mov Disord 19:1328–1333.

Tripoliti E, Zrinzo L, Martinez-Torres I, Frost E, Pinto S, Foltynie T, Holl E, Petersen E, Roughton M, Hariz MI, Limousin P (2011) Effects of subthalamic stimulation on speech of consecutive patients with Parkinson disease. Neurology 76:80–86.

Tsang EW, Hamani C, Moro E, Mazzella F, Poon YY, Lozano AM, Chen R (2010) Involvement of the human pedunculopontine nucleus region in voluntary movements. Neurology 75:950–959.

Twelves D, Perkins KSM, Counsell C (2003) Systematic review of incidence studies of Parkinson's disease. Mov Disord 18:19–31.

Tzourio-Mazoyer N, Landeau B, Papathanassiou D, Crivello F, Etard O, Delcroix N, Mazoyer B, Joliot M (2002) Automated anatomical labeling of activations in SPM using a macroscopic anatomical parcellation of the MNI MRI single-subject brain. Neuroimage 15:273–289.

Van den Wildenberg WPM, Van Boxtel GJM, Van der Molen MW, Bosch DA, Speelman JD, Brunia CHM (2006) Stimulation of the subthalamic region facilitates the selection and inhibition of motor responses in Parkinson's disease. J Cog Neurosci 18:626–636.

Van den Wildenberg WPM, Van der Molen MW (2004) Developmental trends in simple and selective inhibition of compatible and incompatible responses. J Exp Child Psychol 87:201–220.

Van der Schoot M, Licht R, Horsley TM, Sergeant J a (2003) Hemispheric differences in stop task performance. Acta psychologica 112:279–295.

Van der Schoot M, Licht R, Horsley TM, Sergeant J a (2005) Effects of stop signal modality, stop signal intensity and tracking method on inhibitory performance as determined by use of the stop signal paradigm. Scand J Psychol 46:331–341.

Van Veen BD, Van Drongelen W, Yuchtman M, Suzuki A, VanVeen BD, vanDrongelen W (1997) Localization of brain electrical activity via linearly constrained minimum variance spatial filtering. Biomedical Engineering, IEEE Trans Biomeg Eng 44:867–880.

Verbruggen F, Aron AR, Stevens MA, Chambers CD (2010) Theta burst stimulation dissociates attention and action updating in human inferior frontal cortex. Proc Natl Acas Soc USA 107:13966-71.

Verbruggen F, Liefooghe B, Vandierendonck A (2004) The interaction between stop signal inhibition and distractor interference in the flanker and Stroop task. Acta psychologica 116:21–37.

Verbruggen F, Liefooghe B, Vandierendonck A (2006) The effect of interference in the early processing stages on response inhibition in the stop signal task. Q J Exp Psychol (2006) 59:190–203.

Verbruggen F, Logan GD (2008) After-effects of goal shifting and response inhibition: A comparison of the stop-change and dual-task paradigms. Q J Exp Psychol 61:1151–1159.

Verbruggen F, Logan GD (2009a) Models of response inhibition in the stop-signal and stop-change paradigms. Neurosci Biobehav Rev 33:647–661.

Verbruggen F, Logan GD (2009b) Automaticity of cognitive control: goal priming in response-inhibition paradigms. J Exp Psychol Learn Mem Cog 35:1381–1388.

Verbruggen F, Logan GD, Liefooghe B, Vandierendonck A (2008a) Short-term aftereffects of response inhibition: repetition priming or between-trial control adjustments? Journal of experimental psychology Hum Percept Perform 34:413–426.

Verbruggen F, Schneider DW, Logan GD (2008b) How to stop and change a response: the role of goal activation in multitasking. J Exp Psychol Hum Percept Perform 34:1212–1228.

Vince M (1948) The intermittency of control movements and the psychological refractory period. Brit J Psychol Gen Sec 38:149-57.

Vlaar A, Hovestadt A, Laar T Van, Bloem BR (2011) The treatment of early Parkinson's disease: levodopa rehabilitated. Pract Neurol 11:145–152.

Voon V, Krack P, Lang AE, Lozano AM, Dujardin K, Schüpbach M, D'Ambrosia J, Thobois S, Tamma F, Herzog J, Speelman JD, Samanta J, Kubu C, Rossignol H, Poon Y-YY, Saint-Cyr JA, Ardouin C, Moro E, Schupbach M (2008) A multicentre study on suicide outcomes following subthalamic stimulation for Parkinson's disease. Brain 131:2720–2728.

Wager TD, Keller MC, Lacey SC, Jonides J (2005) Increased sensitivity in neuroimaging analyses using robust regression. Neuroimage 26:99–113.

Wang H-L, Morales M (2009) Pedunculopontine and laterodorsal tegmental nuclei contain distinct populations of cholinergic, glutamatergic and GABAergic neurons in the rat. Eur J Neurosci 29:340–358.

Weaver FM et al. (2009) Bilateral deep brain stimulation vs best medical therapy for patients with advanced Parkinson disease: a randomized controlled trial. JAMA 301:63–73.

Weinberger M, Mahant N, Hutchison WD, Lozano AM, Moro E, Hodaie M, Lang AE, Dostrovsky JO (2006) Beta oscillatory activity in the subthalamic nucleus and its relation to dopaminergic response in Parkinson's disease. J Neurophysiol 96:3248–3256.

Welford (1952) The "Psychological refractory period and the timing of high-speed performance" – a review and a theory. Brit J Psychol Gen Sect 43:2–19.

Wickremaratchi MM, Perera D, O'Loghlen C, Sastry D, Morgan E, Jones A, Edwards P, Robertson NP, Butler C, Morris HR, Ben-Shlomo Y (2009) Prevalence and age of onset of Parkinson's disease in Cardiff: a community based cross sectional study and meta-analysis. J Neurol Neurosurg Psychiatry 80:805–807.

Williams A, Gill S, Varma T, Jenkinson C, Quinn N, Mitchell R, Scott R, Ives N, Rick C, Daniels J, Patel S, Wheatley K (2010) Deep brain stimulation plus best medical therapy versus best medical therapy alone for advanced Parkinson's disease (PD SURG trial): a randomised, open-label trial. Lancet Neurol 9:581–591.

Williams BR, Ponesse JS, Schachar RJ, Logan GD, Tannock R (1999) Development of inhibitory control across the life span. Dev Psychol 35:205–213.

Williams D, Kühn A, Kupsch A, Tijssen M, Van Bruggen G, Speelman H, Hotton G, Loukas C, Brown P, Kuhn A (2005) The relationship between oscillatory activity and motor reaction time in the parkinsonian subthalamic nucleus. Eur J Neurosci 21:249–258.

Williams D, Tijssen M, Van Bruggen G, Bosch A, Insola A, Di Lazzaro V, Mazzone P, Oliviero A, Quartarone A, Speelman H, Brown P (2002) Dopamine-dependent changes in the functional connectivity between basal ganglia and cerebral cortex in humans. Brain 125:1558–1569.

Williams-Gray CH, Foltynie T, Brayne CEG, Robbins TW, Barker R a (2007) Evolution of cognitive dysfunction in an incident Parkinson's disease cohort. Brain 130:1787–1798.

Wilson CJ, Groves PM (1981) Spontaneous firing patterns of identified spiny neurons in the rat neostriatum. Brain Res 220:67–80.

Wilson SAK (1912) Progressive lenticular degeneration. A familial nervous disease associated with cirrhosis of the Liver. Brain 34:295–507.

Wilson SAK (1925) Disorders of motility and of muscle tone, with special reference to the corpus striatum. Lancet 2:1–10, 53–62, 169– 78, 215–19, 268–76.

Wingeier B, Tcheng T, Koop MM, Hill BC, Heit G, Bronte-Stewart HM (2006) Intra-operative STN DBS attenuates the prominent beta rhythm in the STN in Parkinson's disease. Exp Neurol 197:244–251.

Winn P (2006) How best to consider the structure and function of the pedunculopontine tegmental nucleus: evidence from animal studies. J Neurol Sci 248:234–250.

Witt K, Pulkowski U, Herzog J, Lorenz D, Hamel W, Deuschl G, Krack P (2004) Deep brain stimulation of the subthalamic nucleus improves cognitive flexibility but impairs response inhibition in Parkinson disease. Arch Neurol 61:697–700.

Wooten GF (2004) Are men at greater risk for Parkinson's disease than women? J Neurol Neurosurg Psych 75:637–639.

Worsley K, Evans A (1992) A three-dimensional statistical analysis for CBF activation studies in human brain. J Cereb Blood Flow Metab. 12:900-18.

Worsley K, Friston K (1995) Analysis of fMRI Time-Series Revisited—Again. Neuroimage 2:173–181.

Wu Y, Richard S, Parent A (2000) The organization of the striatal output system: a single-cell juxtacellular labeling study in the rat. Neurosci Res 38:49–62.

Xue G, Aron AR, Poldrack R a (2008) Common neural substrates for inhibition of spoken and manual responses. Cereb Cortex 18:1923–1932.

Yamaguchi M, Logan GD, Bissett PG (2011) Stopping while going! Response inhibition does not suffer dual-task interference. J Exp Psychol Hum Percept Perform 38:123–134.

Yarnall A, Rochester L, Burn DJ (2011) The interplay of cholinergic function, attention, and falls in Parkinson's disease. Mov Disord 26:2496-503.

Yeung N, Cohen JD, Botvinick MM (2011) Errors of interpretation and modeling: a reply to Grinband et al. Neuroimage 57:316–319.

Yogev-Seligmann G, Hausdorff JM, Giladi N (2008) The role of executive function and attention in gait. Mov Disord 23:329–42.

Zaidel A, Spivak A, Grieb B, Bergman H, Israel Z (2010) Subthalamic span of beta oscillations predicts deep brain stimulation efficacy for patients with Parkinson's disease. Brain 133:2007–2021.

Zetusky WJ, Jankovic J, Pirozzolo FJ (1985) prognostic implications The heterogeneity of Parkinson's disease : Clinical and prognostic implications. Neurology 1985 35:522-6.

Zrinzo L, Van Hulzen AL, Gorgulho AA, Limousin P, Staal MJ, De Salles AA, Hariz MI (2009) Avoiding the ventricle: a simple step to improve accuracy of anatomical targeting during deep brain stimulation. J Neurosurg 110:1283–1290.

Zrinzo L, Zrinzo L V, Tisch S, Limousin PD, Yousry T a, Afshar F, Hariz MI (2008) Stereotactic localization of the human pedunculopontine nucleus: atlas-based coordinates and validation of a magnetic resonance imaging protocol for direct localization. Brain 131:1588–1598.

Zweig RM, Jankel WR, Hedreen JC, Mayeux R, Price DL (1989) The pedunculopontine nucleus in Parkinson's disease. Ann Neurol 26:41–46.